UC San Diego
UC San Diego Electronic Theses and Dissertations

Title

Engineering Nanoparticle Surfaces to Target and Treat Traumatic Brain Injury

Permalink

https://escholarship.org/uc/item/3kp2h0n1

Author

Waggoner, Lauren

Publication Date

2022

Peer reviewed|Thesis/dissertation

UNIVERSITY OF CALIFORNIA SAN DIEGO

Engineering Nanoparticle Surfaces to Target and Treat Traumatic Brain Injury

A Dissertation submitted in partial satisfaction of the requirements

for the degree Doctor of Philosophy

in

Nanoengineering

by

Lauren Waggoner

Committee in charge:

Professor Ester Kwon, Chair
Professor Jesse Jokerst, Co-Chair
Professor Nisarg Shah
Professor Nicole Steinmetz
Professor Mark Tuszynski

2022

The Dissertation of Lauren Waggoner is approved, and it is acceptable in quality and form for publication on microfilm and electronically.

University of California San Diego

2022

DEDICATION

Thank you to my family and friends who loved and supported me through graduate school. This achievement would not have been possible without you.

TABLE OF CONTENTS

LIST OF FIGURES

LIST OF TABLES

ACKNOWLEDGEMENTS

2014	Bachelor of Science in Nanoengineering, University of California San Diego
2019	Master of Science in Nanoengineering, University of California San Diego
2022	Doctor of Philosophy in Nanoengineering, University of California San Diego

PUBLICATIONS

Kudryashev, J. A.; Waggoner, L. E.; Leng, H. T.; Mininni, N. H.; Kwon, E. J. An Activity-Based Nanosensor for Traumatic Brain Injury. *ACS Sens.* **2020**, *5* (3), 686–692. https://doi.org/10.1021/acssensors.9b01812.

Kandell, R. M.; Waggoner, L. E.; Kwon, E. J. Nanomedicine for Acute Brain Injuries: Insight from Decades of Cancer Nanomedicine. *Mol. Pharm.* **2021**, *18* (2), 522–538. https://doi.org/10.1021/acs.molpharmaceut.0c00287.

Waggoner, L. E.; Madias, M. I.; Hurtado, A. A.; Kwon, E. J. Pharmacokinetic Analysis of Peptide-Modified Nanoparticles with Engineered Physicochemical Properties in a Mouse Model of Traumatic Brain Injury. *AAPS J.* **2021**, *23* (5), 100. https://doi.org/10.1208/s12248-021-00626-5.

Waggoner, L. E.; Kang, J.; Zuidema, J. M.; Vijayakumar, S.; Hurtado, A. A.; Sailor, M. J.; Kwon, E. J. Porous Silicon Nanoparticles Targeted to the Extracellular Matrix for Therapeutic Protein Delivery in Traumatic Brain Injury. *Bioconjug. Chem.* **2022**, *33* (9), 1685–1697. https://doi.org/10.1021/acs.bioconjchem.2c00305.

FIELD OF STUDY

Major Field: Engineering

      Studies in Nanoengineering and Bioengineering
      Professor Ester Kwon

ABSTRACT OF THE DISSERTATION

Engineering Nanoparticle Surfaces to Target and Treat Traumatic Brain Injury

by

Lauren Waggoner

Doctor of Philosophy in Nanoengineering

University of California San Diego, 2022

Professor Ester Kwon, Chair
Professor Jesse Jokerst, Co-Chair

Many traumatic brain injury (TBI) survivors suffer cognitive impairments after injury, yet there are currently no FDA approved therapeutics that address long-term patient brain health. Development of vascularly delivered TBI therapeutics is challenging due to their poor pharmacokinetics, which reduces their accumulation and retention in the brain. Nanoparticles are promising technologies that can improve the vascular delivery of TBI therapeutics by protecting the drug payload in circulation, increasing blood half-life, and passively accumulating in injured brain tissue across the transiently permeable blood-brain barrier (BBB). Nanoparticle surfaces can be modified to change their physicochemical properties and implement targeting strategies, thereby tuning their pharmacokinetics to improve delivery. Thus, vascular delivery of nanoparticle-based TBI therapeutics can be improved by engineering the surface properties of nanoparticles.

To engineer nanoparticles that accumulate in the injured brain, we modified the surfaces of diverse nanoparticle platforms to tune their physicochemical properties and implement active targeting. First, we engineered the steric forces and hydrophobicity of lipid nanoparticles (LNP) by modifying their polyethylene glycol (PEG) layer with short and long anchor PEG-lipids. We found that vascularly delivered LNPs formulated with long anchored PEG-lipids had longer blood half-lives and extended activity in the injured brain. Next, we engineered the charge and hydrophobicity of model polystyrene nanoparticles via surface modification with peptides. We found that peptide physicochemical properties affected nanoparticle pharmacokinetics, with neutral, zwitterionic, and negatively charged nanoparticles demonstrating greater passive accumulation in the injured brain than positively charged nanoparticles. Finally, we applied these ideas to a porous silicon nanoparticle (pSiNP) drug delivery system for brain derived neurotrophic factor (BDNF) surface modified with PEG and a peptide that targets the injured brain (CAQK). After intravenous administration of pSiNP-BDNF, we observed a ~24% reduction in brain lesion volumes compared to both free BDNF and untreated controls. Understanding how engineered nanoparticle surface properties affect their pharmacokinetics in TBI models informs the design of nanoparticle-based TBI therapeutics and is broadly applicable to the design of vascularly delivered therapeutic nanoparticles.

CHAPTER 1: Nanomedicine for Acute Brain Injuries: Insight from Decades of Cancer

Nanomedicine

1.1: ABSTRACT

Acute brain injuries such as traumatic brain injury and stroke affect 85 million people a year worldwide, and many survivors suffer from long-term physical, cognitive, or psychosocial impairments. There are few FDA-approved therapies that are effective at preventing, halting, or ameliorating the state of disease in the brain after acute brain injury. To address this unmet need, one potential strategy is to leverage the unique physical and biological properties of nanomaterials. Decades of cancer nanomedicine research can serve as a blueprint for innovation in brain injury nanomedicines, both to emulate the successes, but also to avoid potential pitfalls. In this review, we discuss how shared disease physiology between cancer and acute brain injuries can inform the design of novel nanomedicines for acute brain injuries. These disease hallmarks include dysregulated vasculature, an altered microenvironment, and changes in the immune system. We discuss several nanomaterial strategies that can be engineered to exploit these disease hallmarks, for example passive accumulation, active targeting of disease-associated signals, bioresponsive designs that are 'smart', and immune interactions.

1.2: INTRODUCTION

Acute brain injuries such as traumatic brain injury (TBI) and stroke are large contributors to declines in disability-adjusted life years (DALYs) worldwide and it is estimated that approximately half the world's population will have at least one TBI in their lifetime.[1,2] In the United States, TBI and stroke affect over 3 million Americans annually, at an estimated economic cost of 110.5 billion dollars.[3,4] Although there are other causes of brain injuries such as anoxic brain injury or encephalitis, in this review we focus our discussion on TBI and stroke due to their prevalence.[5,6] The predominant causes of TBI include blunt force trauma or a penetrating wound to the head after traffic accidents, falls, sporting activities, gunshot wounds, or assault.[5,7] In stoke,

blockage of an artery (ischemic stroke) or excessive bleeding from an artery in the brain (hemorrhagic stroke) causes an interruption of blood flow to the brain.[3,5] In both TBI and stroke, initial causative injuries are followed by a secondary injury that can evolve over minutes to months, and is responsible for further deterioration of brain tissue through multiple mechanisms, including mitochondrial dysfunction, cell apoptosis, and inflammatory responses.

Although there are differences between TBI and stroke in disease initiation and the long-term pathophysiology of the subsequent secondary injury, there are a number of shared disease hallmarks. These disease hallmarks include neuronal excitotoxicity and apoptosis, vasculature dysregulation, upregulation of adhesion molecules, release of inflammatory mediators, and increased levels of reactive oxygen species (ROS) and proteases.[8–10] Current TBI treatments are merely palliative, and include life-sustaining interventions and surgery to minimize tissue damage.[11,12] Neurological assessment with the Glasgow Coma Scale (GCS) and imaging of high-risk patients is used to gauge injury severity.[12] For patients identified to have large hematomas or contusions, rapid surgical intervention is crucial in order to restore blood flow and minimize tissue damage. Corrective surgery within 4 hours of clinic admittance demonstrated shorter hospital stays and a 50% lower mortality rate in TBI patients.[13] Similarly, in stroke there is a short time window for administration of reperfusion therapies in order to restore blood flow without increasing the risk of complications like intracerebral hemorrhagic conversion.[14] Thrombolytic therapy such as tissue plasminogen activator (tPA) injection must be delivered within ~4.5 hours after injury in order to be effective.[15] Additionally, endovascular thrombectomy of large-vessel clots is the standard of care for acute ischemic stroke and is typically performed 6-24 hours after stroke onset.[16,17] While these interventions at acute time points are necessary to sustain life and mitigate tissue death in the brain, there is a need for new therapeutics that halt, attenuate, or ameliorate the pathophysiology of the secondary injury in the remaining tissue to improve the long-term disease management of acute brain injuries.

Despite the unmet clinical need, there has been a challenge to obtain approval for new therapeutics for the treatment of stroke and TBI by the food and drug administration (FDA). Although systemically administered therapeutics designed to address the secondary injury have improved biochemical and functional outcomes in preclinical animal models, they have failed to show efficacy in clinical trials. Potential factors that contribute to the failure of preclinical to clinical translation include the inability of a single drug to address the complex and heterogeneous disease sequelae that follows the primary injury, difficulty in recapitulating human disease using animal models, and the inadequate bioavailability of drug to the injured brain.[18,19] In recent efforts, progesterone, a neuroprotective steroid that showed success in multiple preclinical TBI models, failed to demonstrate clinical endpoint improvement assessed by Glasgow Outcome Scale over placebo in both ProTECT III and SyNAPSe phase III clinical trials (2010-2013) for moderate-to-severe TBI patients.[20,21] This latest trial is representative of the current landscape of clinical trials for brain injuries; 30 years of TBI clinical trials have yet to yield a single treatment that improves long-term brain health.[22] In stroke, a meta-analysis of therapeutics developed over a twenty year timespan from 1995-2015 established that only ~5% of drugs that entered the clinical trial pipeline reached the market in various countries when drugs in preclinical testing were excluded from the analysis.[23] This success rate is considerably lower compared to the estimated 13.8% worldwide success rate (2000-2015) across all therapeutics made in another analysis,[24] and is similar to the 3.4% success rate for oncology. Furthermore, the molecules under investigation predominantly target the clotting cascade (thrombolytic, anti-thrombotic or anti-platelet molecules) and therefore aim to prevent further damage and do not address the complex secondary injury brain pathophysiology.[23,25,26] The lack of clinical successes for both TBI and stroke highlights the need to innovate in therapeutic development for brain injuries.

Nanomedicines, therapeutic and/or diagnostic materials with dimensions on the nanometer length scale, have been actively developed for the treatment of cancer over the past two decades, and have yielded benefits such as decreasing off-target toxicity, improving drug

distribution, and incorporating challenging cargoes such as hydrophobic small molecules and labile macromolecules. The first FDA-approved nanomedicine, Doxil®, is a polyethylene glycol (PEG)-modified liposome encapsulating the chemotherapeutic drug, doxorubicin. [27] Doxil® improves tumor accumulation due to its longer blood half-life and reduces off-target cardiotoxicity due to the altered organ biodistribution of nanometer-sized materials or 'nanomaterials'.[28] In another example, FDA-approved Abraxane® uses albumin to formulate the hydrophobic molecule paclitaxel to improve solubility and biodistribution into target tumors.[29] The field of cancer nanomedicine has experienced significant research growth since its inception, supported by funding agencies like the National Cancer Institute's Centers of Cancer Nanotechnology Excellence program.[30,31] After the first FDA approval of Doxil® in 1995, five additional cancer nanomedicine technologies, including Abraxane®, have entered the clinical market in the United States and there are currently over thirty nanoparticle formulations are in the clinical trial pipeline.[32] Several of these nanomedicines innovate beyond passive tumor accumulation, employing technologies such as active targeting, gene delivery, and stimuli-responsive materials.[30,32,33] On the horizon, there are multiple promising nanomedicine technologies under development for application to cancer. For example, cancer vaccines require the delivery of multiple molecules to an antigen presenting cell that can educate the immune system; the supramolecular structure of nanomaterials provides technology to package cancer antigens and adjuvant into one entity and exploits the natural behavior of antigen presenting cells to phagocytose nanometer-sized materials.[34]

Nanomedicines are promising technologies to fulfill the desperate need for new therapeutics in the clinical management of acute brain injuries. Herein, we compare nanomaterial engineering as a discipline between cancer and acute brain injuries, and in particular nanomaterial design that leverages disease physiology. We also look for insight from two decades of largely empirical cancer nanomedicine research to inspire future innovation in nanomedicine design for brain injuries. Successful nanomedicine destined as a treatment for use in humans

4

requires an understanding of the complex host biology and subsequent engineering of nanomaterials to interact with that biology. As such, in this review we elaborate on the perspective that cancer and acute brain injury share major disease pathologies that can be exploited by nanomedicine design (Figure 1.1, Table 1.1).
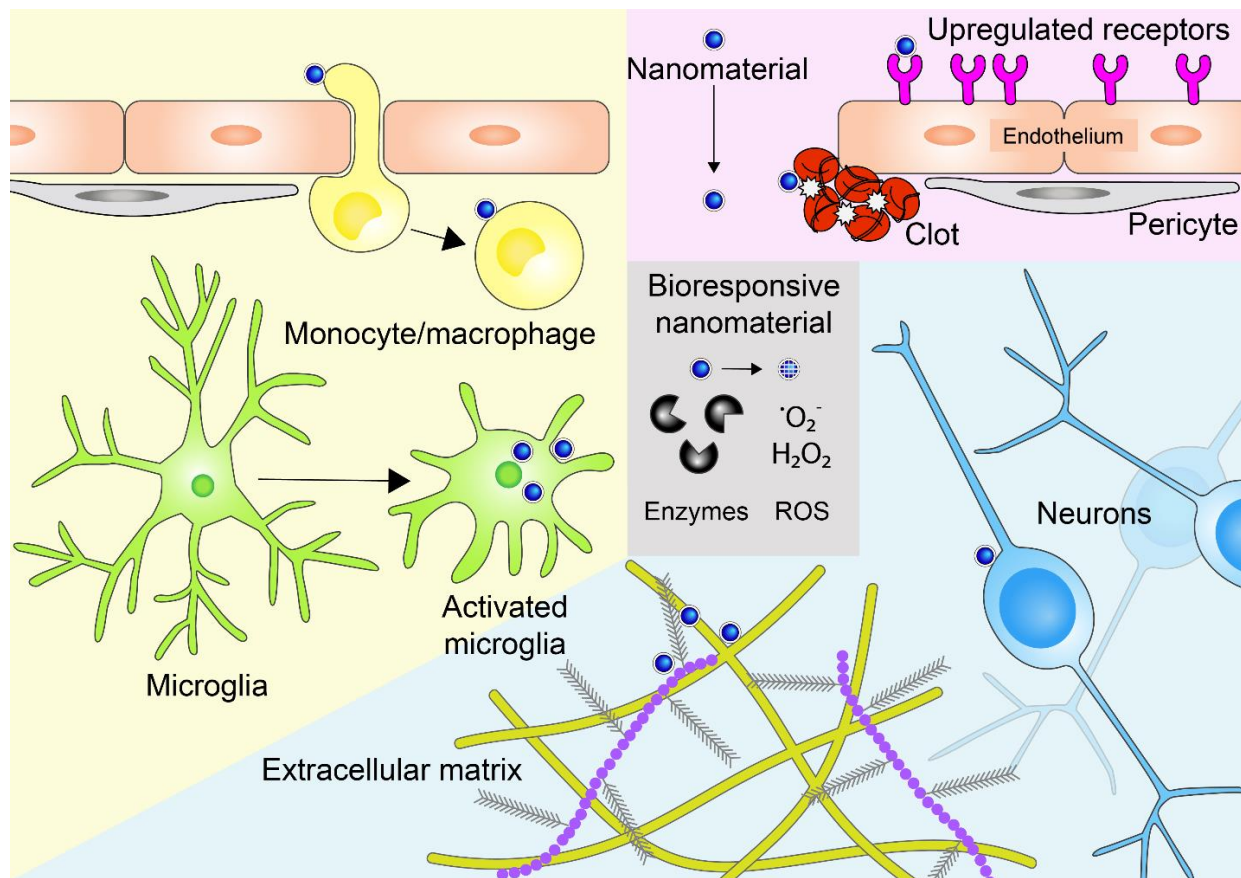
Figure 1.1: Nanomaterial paradigms in acute brain injury. Nanomaterials can be engineered to respond to disease physiology in acute brain injuries, including dysregulated vasculature (pink), an altered microenvironment (gray and blue), and changes in the immune system (yellow). Specific examples for each nanomaterial design can be found in Table 1, color-coded by quadrant.

Table 1.1: Specific examples of nanomaterial design based on pathology found in cancer and acute brain injury.

		Cancer	Acute brain injury	References
Vasculature		**Permeable vasculature**		
	Pathology	Heterogeneous, tortuous, and leaky vasculature with disorganized and reduced pericyte and smooth muscle coverage; Poorly developed lymphatic structures	Transient disruption of BBB due to injury; Increased para- and transcellular transport, pericyte migration, swelling of astrocytic endfeet.	35, 36, 37, 38
	Design	EPR effect enables passive accumulation of nanomaterials into tumors	"EPR-like" effect enables passive accumulation of nanomaterials across transiently compromised BBB	
		Coagulation		
	Pathology	Fibrin deposition in tumor stromal	Clotting cascade activation leads to fibrin deposition and clot formation	39, 40
	Design	Fibrin targeting nanomaterials	Platelet mimicking and targeting nanomaterials	
		Ectopic receptor expression		
	Pathology	Upregulation of cell adhesion molecules, such as integrins and vascular cellular adhesion molecule 1 (VCAM1)	Upregulation of receptors on the BBB such as glutathione receptor, apolipoprotein receptor, and LDLR	41, 42, 43
	Design	Active targeting of nanomaterials to upregulated cell adhesion molecules	Active targeting of nanomaterials to upregulated receptors	
Microenvironment		**Active targeting: Cell targeting**		
	Pathology	Cancer cells and stromal cells are new targets not available in healthy state	Neurons sequestered from blood-borne agents in health are transiently accessible through injured BBB	44, 45
	Design	Active targeting of nanomaterials to cancer cells and TAMs	Active targeting of nanomaterials to neurons	

Table 1.1: Specific examples of nanomaterial design based on pathology found in cancer and acute brain injury.

		Active Targeting: ECM targeting		
Microenvironment	Pathology	Upregulation of ECM (collagen, proteoglycans, and glycoproteins)	Deposition of ECM in glial scar (proteoglycans, HA, fibronectin, tenascins, and laminin) around injury site	46, 47
	Design	Active targeting of nanomaterials to tumor ECM via ligands and antibodies, such as collagen binding domains	Active targeting of nanomaterials to brain ECM, such as CAQK peptide	
		Bioresponsive materials: Reactive oxygen species		
	Pathology	Increased metabolic activity and mitochondrial dysregulation	Mitochondrial dysregulation, cell death, and neurovascular inflammation	48, 49, 50, 51
	Design	ROS-responsive and ROS-scavenging nanomaterials	ROS-responsive and ROS-scavenging nanomaterials	
		Bioresponsive materials: Protease activity		
	Pathology	Protease dysregulation (matrix metalloproteinases, peptidases, cathepsins)	Protease upregulation (matrix metalloproteinases, thrombin)	52, 53, 54
	Design	Protease-responsive therapeutic and diagnostic nanomaterials	Protease-responsive therapeutic and diagnostic nanomaterials	
		Inflammatory state		
Immune System	Pathology	Generally an immunosuppressive environment (TAM polarization to "M2-like" state, myeloid-derived suppressor cells)	Generally pro-inflammatory environment (upregulated inflammatory genes, reactive astrocytes, infiltration of bloodborne leukocytes)	55, 56, 57, 58, 59 60, 61, 62, 63
	Design	Nanomaterial accumulation in TAMs, TAM repolarization, nanovaccines, and T cell backpacking	Nanomaterial accumulation in phagocytic microglia, depletion of infiltrating leukocytes, and biomimicry of immune cells for trafficking	

Common disease pathologies include dysregulation of the vasculature, increased access to cells and extracellular matrix in the tissue microenvironment, changes in the biochemistry of the interstitial fluid (e.g., ectopic ROS and protease activity), and an activated immune system. In both diseases, pathology causes vascular damage that activates a host response such as clotting or receptor expression which can be targeted by nanomaterials. Vascular damage also leads to permeability in vasculature that presents an opportunity for nanomaterials to passively accumulate into the parenchyma.[64–66] As a consequence, in disease, nanomaterials delivered in the systemic vasculature have increased access to the cells and microenvironment of the tissue, which in health is typically sequestered.[67] After brain injury, there is a wound bed that may have an improper healing response while cancer has been described as a "wound that never heals".[68] The resulting wound microenvironment may have an extracellular matrix (ECM) composition that differs from physiologically healthy tissue, and an accumulation of disease-associated oxidative species and proteases. Nanomaterials can be engineered to respond to these changes in the microenvironment as bioresponsive materials, increasing the temporal and spatial specificity of therapeutic delivery.[69,70] Lastly, both diseases have a dysregulated immune response that could be modulated by nanomaterials to either activate or suppress the immune system in cancer and acute brain injury respectively, or take advantage of endogenous immune cell homing to deliver therapeutics to the diseased tissue.[71–73] Although the goals for therapeutic outcomes between cancer and brain injuries may diverge (i.e. tumor cell killing vs. neuro-regenerative response), there are commonalities in the pathophysiology between diseases that can be leveraged for nanomaterial design.

The goal of this review is to highlight how nanomaterials can be engineered to interact with physiological changes that occur during acute brain injury; our discussion adopts a design-centered perspective and discussion of therapeutic payloads for nanoparticles is limited. For a detailed discussion on TBI therapeutic payloads that can be carried by nanomaterials, please refer to this excellent review.[74] Several routes of administration for nanomaterials to the brain are

under investigation, such as intranasal, intrathecal, and convection-enhanced delivery (CED) [75–78] For example, intrathecal DepoCyt®, a liposomal formulation encapsulating the chemotherapeutic Cytarabine, was approved by the FDA in 2007 to treat lymphomatous meningitis caused by metastasis of non-Hodgkin lymphomas.[79] In patients with acute brain injuries, surgical intervention is often a necessary component of clinical care and creates an opportunity for direct access to the brain that circumvents many delivery barriers. While these routes of administration are promising, in this review we focus on intravenously administered nanomaterials as a minimally-invasive route of delivery commonly used in the clinical setting that is relevant in the treatment of both cancer and acute brain injury. Intravenous delivery can also be used as treatment regardless of whether patients receive surgical intervention.

1.3: ACUTE BRAIN INJURY MODELS

In order to discuss advances in acute brain injury nanomedicine, an overview of commonly utilized animal models is pertinent. Detailed discussions are available for TBI (Xiong[80], Morales[81], Wojnarowicz[82]) and stroke (Fluri[83], Herson[84], Jickling[85]). Common TBI animal models include controlled cortical impact (CCI), fluid percussion injury (FPI), weight drop, penetrating brain injury (PBI) and blast injury.[80,81] In CCI or FPI models, a craniotomy exposes the brain dura for direct focal injury via a controlled piston impact or fluid pressure pulse, respectively. In weight drop models, a guided weight falls on either an intact skull or exposed dura. CCI and FPI can be controlled and are highly reproducible but require craniotomy and therefore cannot reproduce disease physiology that includes the skull. PBI uses punctures instead of blunt trauma to simulate bullet or shrapnel wounds. Blast injuries simulate diffuse brain injury, such as injuries caused by the shock wave from military explosions, and is performed by placing the animal subject at the end of a shock tube that generates pressure waves. While maintaining the intact skull is more representative of human disease, reproducibility is difficult to control in closed skull injury models due to variability in how energy interacts with the skull. In these models, injury severity is modulated by varying injury velocity, depth, and size.[80] For ischemic stroke, the most widely used

preclinical model is the middle cerebral artery occlusion model (MCAO) where a suture or filament is tied around or inserted into the middle cerebral artery. The occlusion can be permanent (pMCAO) or transient (tMCAO). The occlusion in tMCAO is typically maintained between 60-120 minutes followed by restoration of blood flow and is a model for ischemia/reperfusion injury in the clinic.[83,86] Other models of stroke include photothrombosis and embolic stroke. In photothrombosis, light-responsive dye is injected into the brain and damages vascular structures when the skull is irradiated with light; this model is advantageous for the ability to spatially control lesion location.[87] Finally, the embolic stroke model, which best recapitulates human stroke etiology, initiates *in situ* clotting and ischemia by the injection of clotted blood, thrombin, or beads.

1.4: DYSREGULATED VASCULATURE

Vascular dysregulation and dysfunction is pathophysiology shared between acute brain injury and cancer, and can be exploited by nanomaterials (Figure 1.2). In cancer, growing tumors generate new vasculature from nearby vessels networks through secretion of angiogenic factors, such as VEGF and angiopoietin.[88] The growth of new vessels in the tumor is rapid and poorly regulated, resulting in heterogeneous and dysfunctional vessels. Whereas normal vasculature involves the coordination of multiple cell types that have a well-regulated structure, tumor vasculature is disorganized, in particular the coordination of perivascular pericytes and smooth muscle cells around endothelial cells required to regulate oxygen and blood flow.[64] This disorganization leads to endothelial fenestrae, vesicles, transcellular holes, widened endothelial junctions, and a discontinuous basal membrane.[65] The defects in the vascular unit allows the passage of multiscale materials into the tumor that are typically excluded, including proteins, macromolecules, nanomaterials, and cells.[66]

The blood-brain barrier (BBB) describes the highly selective and regulated transport of multiscale materials (ions, molecules, proteins, etc.) from the blood into the brain parenchyma. The function of the BBB is created by the neurovascular unit, a precise spatial organization of multiple cell types, notably endothelial cells, pericytes, and astrocytes, although other cells are

also observed to play a significant role.[67] In acute brain injury caused by ischemic stroke or TBI, BBB damage is a hallmark of disease and is imaged in the clinic for the purpose of diagnosis using medical imaging modalities such as MRI and CT. After acute brain injury, vasculature is severed by the physical force of the injury that can result in endothelial cell death. In addition, weakened vascular structures can lead to the rupture of blood vessels and bleeding into the brain parenchyma, which present clinically as subdural hematomas and contusions.[89] Within the neurovascular unit, tight junction proteins between endothelial cells that are major barriers of paracellular transport become downregulated in response to injury, resulting in vascular permeability. The sized-based extravasation of multiscale molecules such as Evans blue dye, horseradish peroxidase, and dextran has been used to understand the extent of BBB permeability after the primary injury.[90–92] In addition, the morphologies and functions of pericytes and astrocytes can be altered after stroke and TBI. In both stroke and TBI, pericyte migration and the swelling of astrocytic end feet further compromise the integrity of the neurovascular unit.[93–95] In stroke, pericytes contract due to oxidative stress caused by the ischemic injury leading to constricted vasculature and reduced cerebral blood flow even after removal of the occlusion.[96] These changes in cellular morphology and function contribute to the secondary injury and further increase BBB dysfunction.

BBB permeability is dynamic. In TBI, expression of tight junction proteins contribute to BBB permeability; their expression increases within hours after the injury, peaks at 24 hours, and decreases back to baseline levels 5 to 7 days after the injury occurs.[97] There have also been observations of biphasic permeability, although the evidence is conflicting. Some studies show that the permeability is highest immediately after injury followed by a second opening occurring up to 3 days later.[98] The temporal study of BBB permeability after stroke also remains inconclusive. Some studies observe increased BBB permeability for up to 30 days after ischemic injury, while others show that BBB permeability is also biphasic, with maximum permeability at 3-5 hours after injury and then again at 48 hours.[99,100] There is also evidence that vascular

dysfunction after acute brain injury extends to chronic time points, weeks to months after injury.[101,102] Conflicting accounts of permeability may be due to differences in animal models, strains of animals, and evaluation methods. Ischemic stroke also causes an increase in caveolae and vesicles in the endothelial cells of the BBB, indicating a potential increase in transcytosis after injury that could contribute to BBB permeability.[103,104] These increases in the rates of endocytosis and transcytosis have been shown as early as 6 hours after tMCAO in adult male mice.[105] Similarly in cancer, recent studies have provided evidence to support the hypothesis that transcytosis is the major mode of entry of nanoparticles into tumors.[106] While further study is required to elucidate the mechanisms, increased BBB permeability has consistently been observed within hours after injury in multiple animal models of injury.

The tortuous and leaky vasculature present in tumors is the basis of passive transport of systemically administered nanometer-sized materials across multiple cancer types.[107] Once nanomaterials enter the tumor through the leaky vasculature, they are retained due to inadequate lymphatic drainage in the tumor microenvironment. This phenomenon was first described by Maeda et al. in 1986 who coined the "enhanced permeation and retention" (EPR) effect. Although the heterogeneity of the EPR effect in human tumors have recently been challenged,[108] studies have correlated the presence of EPR (as measured by accumulation of nanoparticle MRI contrast agents) with the efficacy of nanoparticle-formulated drugs in human tumors[109,110] These recent observations support a precision medicine approach to implementing EPR effect, in which patient EPR may be measured prior to administration of nanoformulated therapeutic.[111] Nevertheless, the EPR effect is the conceptual basis of multiple FDA-approved liposome-based cancer treatments (e.g., Doxil®, DaunoXome®, Marqibo®, and Onivyde®) to increase the therapeutic window of toxic chemotherapeutics. Because passive accumulation of nanomaterials into the tumor is a function of time, these nanoformulated therapeutics benefit from increased blood circulation half-life. Accordingly, two of these formulations, Doxil® and Onivyde, are surface-

modified with PEG to increase their blood half-life by avoiding clearance by the reticuloendothelial system (RES).[112]

An EPR-like effect has been observed for nanomaterials in acute brain injury; the vascular damage caused by the injury allows nanomaterials to passively accumulate in the injured tissue. In a one-hour tMCAO model, when PEG modified liposomes were delivered intravenously between 0 and 24 hours after reperfusion, they maximally accumulated in the injured tissue when administered up to 6 hours after reperfusion.[35] Similarly, in a CCI model of TBI, passive accumulation of liposomes after vascular delivery was highest when administered at 3 or 6 hours after injury compared to uninjured controls.[36] This transient access before 6 hours was also observed when electrostatically complexed nanoparticles were applied in a penetrating brain injury model.[113] Importantly, these studies demonstrate that the accumulation of vascular delivered nanomaterials in the context of acute brain injury is local to the site of injury and not widespread throughout the brain, and therefore provides a mode to passively target the injured tissue. Another major observation is that in brain injuries, the passive targeting of vascularly delivered nanomaterials into injured brain tissue is transient. In addition, passive accumulation of nanomaterials is size-dependent in TBI, with smaller nanoparticles up to 100 nm in diameter having greater distribution into the brain, while accumulation of nanoparticles 500 nm in diameter decreases by several orders of magnitude in comparison,[101] mirroring the well-established observations of size-dependent nanoparticle accumulation in cancer.[101,114,115]

The passive accumulation of nanomaterials into the injured tissue can be exploited to improve treatment efficacies in models of brain injury. Cerebrolysin, a mixture of peptide growth factors including brain-derived neurotrophic factor (BDNF) and nerve growth factor (NGF), is used to treat neurological disorders, such as dementia and Alzheimer's disease, but its therapeutic utility is limited by a short *in vivo* half-life. Cerebrolysin was formulated into polylactic-co-glycolide (PLGA) nanoparticles to protect the labile peptide cargo, and intravenous administration between 30 minutes to 4 hours after injury to a rat model of TBI led to reduced brain edema and BBB

breakdown compared to free drug.[37] In another example, conjugates of squalenoyl lipid and the neurological therapeutic adenosine yielded an amphiphilic prodrug that can form ~120 nm nanoparticles through nanoprecipitation.[38] These nanoparticles extended the circulation half-life compared to free drug and interacted with cells of the neurovascular unit. Administration into a pMCAO mouse model 2 hours after the induction of ischemia led to decreased infarct volume by an impressive 64% compared to vehicle control and a concomitant reduction in caspase-3 activation when tissues were analyzed at 24 hours.

Beyond the initial damage of the vasculature that allows the passive accumulation of nanomaterials from the blood, the clotting cascade is initiated for hemostatic regulation of bleeding within minutes to hours after injury. A major challenge in the treatment of TBI is the clinical management of clotting; excessive clotting can lead to stroke whereas inadequate clotting can lead to brain hemorrhage.[116] A critical aspect is to manage clotting locally to the brain, an organ that is particularly vulnerable to changes in blood flow. The clotting cascade is initiated by damage to the endothelium that exposes basement membrane collagen and allows binding of the glycoprotein von Willebrand factor (vWF) present in the circulating blood.[117] The bound vWF at the damaged endothelium in turn binds and activates platelets that upregulate GPIIb/IIIa receptors (integrin $\alpha_{IIb}\beta_3$), leading to further platelet accumulation and the formation of a plug to halt bleeding at the site of injury.[117] In addition to platelet hemostasis, activation of both the intrinsic and extrinsic clotting cascades lead to processing of soluble blood fibrinogen monomers into an insoluble fibrin network surrounding the platelet thrombus.[117] Due to the rapid and robust formation of clots in response to vascular damage, the clot can be used as a beacon to recruit nanomaterials. In order to take advantage of the innate ability of platelets to incorporate into clots, iron oxide nanoparticles have been coated with platelet membranes and applied in a photothrombotic stroke model.[39] Combination of the natural platelet homing with application of a magnetic field led to maximal accumulation of materials at 6 hours post-injection and this strategy was used to deliver L-arginine for *in situ* production of nitric oxide in order to increase blood reperfusion of the ischemic tissue.

14

In another strategy to use clots as a way to target nanomaterials to the injury site, PLGA nanoparticles modified with RGD peptide was used to target glycoprotein receptors on the surface of platelets in a rodent blast injury model with polytrauma.[40] When rodents were treated with these nanoparticles encapsulating the anti-inflammatory dexamethasone, there was increased survival due to decreased internal lung hemorrhaging, improved BBB integrity, and reduced astrogliosis within the amygdala of the brain. Apart from targeting the clotting cascade to achieve greater accumulation, nanoparticles can also be engineered to interact with the clotting cascade itself to create hemostatic materials. This strategy has been pursued in peripheral injuries, and include strengthening the clot with synthetic polymers modified with clot-binding peptides[118] or homeostatic nanomaterials that release drug in response thrombin activity.[119] In the future, hemostatic technologies can be developed in the context of the specific challenges presented in acute brain injuries.[120]

The neurovascular unit itself is dysregulated hours up to months after injury and can upregulate molecules that can be targeted by nanomaterials to deliver therapeutics to the site of injury.[121] Receptors for glutathione, apolipoproteins, and low-density lipoproteins (LDL) are upregulated on the endothelium after injury, and create a potential "vascular zip code" that can be targeted by materials delivered into the blood.[122] In order to interact with LDL receptor related protein (LRP1) on the surface of the BBB for the delivery of BDNF, poloxamer 188 and BDNF were adsorbed onto the surface of 200 nm PLGA nanoparticles.[41] When these nanomaterials were injected into the weight drop model of TBI three hours after injury, the addition of poloxamer 188 significantly increased the levels of BDNF in the brain compared with nanoparticles without poloxamer 188 and free BDNF in both injured and sham injured mice. Mice treated with PLGA nanoparticles modified with BDNF and poloxamer 188 showed significant improvements in behavioral testing seven days after injury (motor, reflex, balance, and cognitive function) compared to control groups treated with nanoparticles and BDNF without poloxamer 188. Similarly, chitosan modified with the temperature-sensitive N-Isopropylacrylamide (NIPAAm) was

used to encapsulate the hydrophobic neuroprotective molecule riluzole, followed by surface coating with the surfactant Tween 80 to create 50 nm nanoparticles.[42] Intraperitoneal delivery immediately upon reperfusion after a one-hour ligation in a rat tMCAO model led to decreased infarct volume, decreased lipid peroxidation, and increased antioxidant markers. Peptides have also been used to interact with the BBB after injury. In a dual targeting strategy to sequentially cross the BBB and interact with ischemic tissue, Zhao et al. used two peptides: T7 peptide (HAIYPRH) is a ligand of the transferrin receptor on brain endothelium and SHp (CLEVSRKNC) was identified by phage display to preferentially target ischemic tissue in stroke.[43] When administered immediately after reperfusion in a two-hour tMCAO model, dual targeted ~100 nm liposomes modified with both peptides and encapsulating the small molecule inhibitor ZL006 had an increased accumulation in the ischemic injury at 6 and 24 hours after administration when compared with untargeted or singly targeted liposomes. Increased accumulation of dual targeted liposomes was consistent with decreased infarct volume and decreased neurological severity scores over free drug.
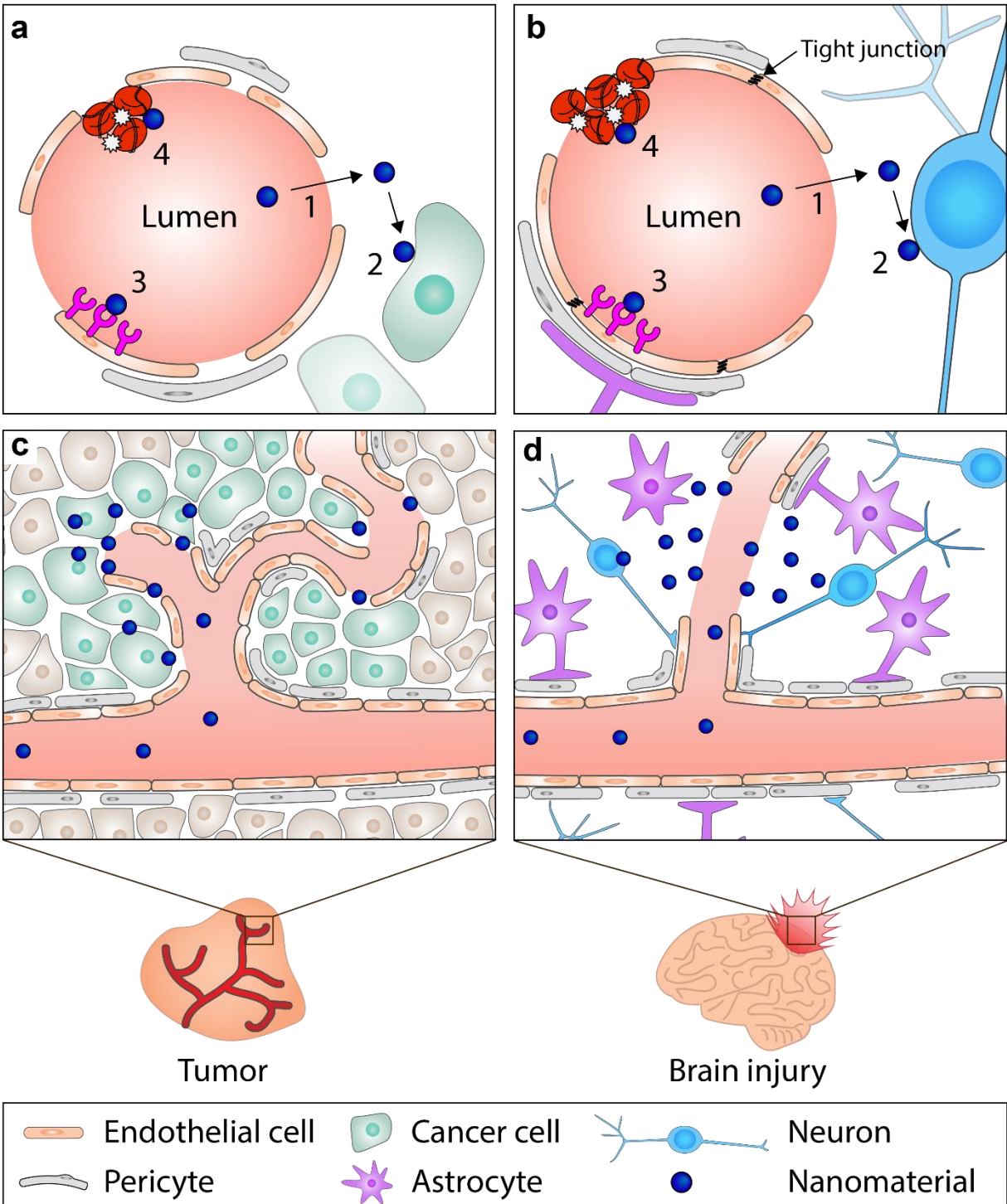
Figure 1.2: Nanomaterials that interact with vasculature in cancer and acute brain injury. a, b. In cancer and acute brain injury, nanomaterials can (1) passively accumulate into adjacent tissue, (2) actively target cells in the tissue, (3) target upregulated receptors on endothelium, and (4) target clots. c, d. Dysregulated vasculature in cancer and acute brain injury allow for passive accumulation of nanomaterials in the diseased tissue.

1.5: MICROENVIRONMENT

The cellular and non-cellular components of the microenvironment are unique to a given tissue and the homeostasis of the microenvironment is perturbed in disease.[123] In the tumor microenvironment, there is ectopic expression of receptors on stroma and tumors cells, changes in the ECM composition, and accumulation of metabolic molecules. Due to the need to penetrate deep into solid tumors for effective treatment, investigators have engineered nanomedicines that capitalize on the changes in the tumor microenvironment to increase treatment efficacy. For example, antibody-targeted liposomes or "immunoliposomes" that target cancer cells or tumor stromal cells have been extensively developed to increase anti-tumor efficacy and decrease off-target activity of chemotherapeutic treatments.[124] Doxorubicin liposomes modified with antibodies against epidermal growth factor receptor (EGFR) are currently in phase II clinical trials for treatment of triple negative EGFR-positive breast cancer (ClinicalTrials.gov identifier: NCT02833766) based on solid tumor preclinical and phase I clinical trials.[125,126] There are also major changes to the ECM in cancer,[123] creating a reservoir of disease-specific substrates for therapeutic binding. For example, polylactic acid (PLA)-PEG nanoparticles have been modified with CLT1, a peptide discovered by phage display, to bind to enriched fibronectin in gliomas, leading to increased accumulation after intravenous delivery and improvement of survival of animals when used to deliver paclitaxel.[127] In recent work, Ishihara et al. created protein engineered fusions of the anti-tumor cytokine interleukin-2 with a collagen-binding domain to bind to the collagen-rich stroma of tumors and temper the well-documented toxicity of interleukin-2.[128] In this approach, they showed reduced interleukin-2 in the blood due to enhanced tumor accumulation, attenuated tumor growth in three different tumor models, and increased populations of cytotoxic T cells over regulatory T cells.

Similarly, nanomaterials can be tailored to the specific microenvironment created after acute brain injuries. We will discuss two major modes in which nanomedicines can interact with the microenvironment of acute brain injury. The first mode is based on access; typically the brain

parenchyma is sequestered from the periphery by the selective and highly regulated BBB. In brain injuries, the passive accumulation of nanomaterials through disrupted vasculature allows access to the unique microenvironment of the brain, including cells and ECM. The second mode is based on changes that occur in the microenvironment after acute brain injuries; the disease progression during the secondary injury creates changes in the ECM composition of the brain, leads to ectopic protease activity, and generates the metabolites such as reactive oxygen species.[74,129]

1.5.1: Targeting nanomaterials to cells and molecules in the microenvironment

Cells and molecules of the brain are sequestered by the intact BBB in the healthy brain and become transiently accessible to intravenously delivered nanomaterials after acute brain injury, as discussed above. The goal of numerous therapeutic strategies is to protect neurons, identified as the major cell type responsible for functional deficits seen in patients of brain injury, but also neurodegenerative diseases. As such, nanoparticles have been modified with peptide to target neurons once they have passively accumulated into the brain. Electrostatic peptide-siRNA complexes incorporating RVG, a peptide sequence from a coat protein of rabies virus used to target neurons,[130] accumulated with 80% specificity in neurons over other cells of the brain parenchyma in a model of penetrating brain injury.[44] These nanomaterials formulated with siRNA against caspase 3, an important protein in the apoptotic cascade, were able to downregulate caspase 3 protein by ~80% in the injured brain when administered immediately after injury. These same siRNA and peptide components were able to accumulate into the injured brain and mediate silencing when they were encapsulated into the pores of an inorganic porous silicon nanoparticle using a non-covalent calcium silicate trapping chemistry.[45]

In addition to targeting cells, the ECM also presents a potential strategy to increase the retention of nanoparticles in the injured tissue due to a potential large extracellular surface area available for binding. The ECM in the healthy brain is largely composed of the glycosaminoglycan hyaluronic acid and chondroitin sulphate proteoglycans, heparin sulfate proteoglycans, and glycoproteins, with relatively low levels of collagen, fibronectin, and laminin compared to other

19

tissues.[131,132] The relative levels and spatial localization of ECM constituents is thought to change in brain pathology.[129,133] In the injury response, cells release cytokines and matrix metalloproteases to remodel the ECM. In the injured brain, ECM components including chondroitin sulfate proteoglycans (neurocan, aggrecan, NG2), heparin sulfate proteoglycans (syndecans, perlecan, agrin), fibronectin, tenascins, and laminin are deposited around the lesion site.[46,129]

In order to take advantage of this change in the ECM after acute brain injury, the Ruoslahti group used *in vivo* phage display to identify the peptide motif CAQK to bind to the injured brain tissue six hours after initiation of a penetrating brain injury model.[46] They identified the receptors of CAQK as veriscan and tenascin-R, proteoglycans known to be upregulated after injury.[129,134,135] Modification of nanomaterials with CAQK led to increased accumulation into the injured brain tissue, and CAQK-modified porous silicon nanoparticles carrying siRNA achieved efficient gene silencing. In support of the potential therapeutic translation to humans, CAQK peptide conjugated to silver nanoparticles also bound to cortical brain sections of a human TBI patient ex vivo. A separate group used CAQK in a self-assembled coiled-coil protein nanoparticle sensitive to thrombin cleavage to deliver a neuroprotective peptide, Tat-NR2B9c.[47] In the CCI model of TBI, CAQK-modified protein nanomaterials had a greater than 2-fold accumulation in the injured brain compared to untargeted nanomaterials when administered immediately after injury, and treatment led to reduced lesion volumes and improvements in behavioral testing, indicating this peptide ligand could be applied across nanoparticle platforms and to both penetrating and non-penetrating TBI. Future work remains to fully delineate the unique composition of brain ECM in health and disease, including its spatial localization near the injury and vasculature in order to fully harness its potential as a target for nanomaterials.

1.5.2: Bioresponsive Nanomaterials

Bioresponsive or 'smart' nanomaterials are designed to autonomously react to stimuli without external triggers. Bioresponsive nanomaterials have been engineered to respond to

stimuli in the tumor microenvironment, including acidic pH, increased reactive oxygen species (ROS), hypoxia, or increased proteolytic activity, as reviewed elsewhere.[136,137] These stimuli can lead to physical changes in the nanomaterials such as swelling, disassembly, degradation, or precipitation that actuate a response, such as the release of therapeutic molecules or generation of a diagnostic signal. Because the presence of the stimuli is typically restricted spatially to the microenvironment of the diseased tissue and manifests temporally with disease progression, therapeutics designed as bioresponsive nanomaterials can have increased specificity. In a diagnostic technology, Lumicell Inc. has developed a nanoscale polymer-peptide fluorescent imaging agent that is cathepsin-activated, LUM015 (clinicaltrials.gov NCT01626066), to aid resection of residual breast cancer during lumpectomy that has completed Phase 2 clinical trials.[138,139] In acute brain injuries, there are changes in the microenvironment that could be used to activate bioresponsive materials; we will focus our discussion on materials that respond to ROS and enzymes as technologies that have been the furthest developed at this point in time.

In acute brain injuries, cell death, neurovascular inflammation, and mitochondrial dysfunction initiated by the primary injury cause an increase in the concentration of ROS, including superoxide anion, hydrogen peroxide and nitric oxide.[140] Excessive ROS levels quickly deplete endogenous antioxidants within the brain microenvironment, increasing the peroxidation of lipid membranes and the oxidation of proteins that initiate apoptotic pathways in surrounding cells through inhibition of the electron transport system in mitochondria.[141] This identifies ROS as a potential therapeutic target to mitigate further damage in brain injuries and also a microenvironmental stimulus for bioresponsive nanomaterials. Core-cross-linked nanoparticles made from polysorbate 80 created a thioether core that scavenges excess ROS in the injury microenvironment.[48] These materials accumulated in the damaged brain in a CCI model of brain injury after systemic administration immediately after injury, reduced neuroinflammation in the hippocampus, and improved behavioral outcomes. Another ROS scavenging nanomaterial was created with poly(propylene sulfide) nanoparticles. These materials decreased neuroinflammation

in 17-minute tMCAO mice when administered 3 hours after reperfusion, including decreased microglial activation and reduced neutrophil infiltration, and led to reduced infarct volume compared to vehicle controls.[49] Hydrophilic ~50 nm carbon clusters have been developed as a ROS scavenging nanomaterial after acute brain injury.[51] The graphitic domains of the carbon cluster sequester ROS through covalent bonding. When carbon clusters were administered 80 minutes after injury, cerebral blood flow was restored to baseline pre-injury measurements in a rat CCI model. On a molecular level, carbon clusters were found to reduce vascular superoxide levels and normalize nitric oxide levels when measured 6 hours after treatment. These ROS-scavenging technologies have also been applied to cancer.[142] Lastly, nanomaterials can be engineered to release therapeutic in response to elevated ROS in injury. Lv et al. created a nanomaterial with a polymeric core modified with ROS-responsive boronic ester that encapsulated the neuroprotective peptide NR2B9C.[50] These cores were wrapped with a red blood cell shell modified with the stroke homing peptide SHp to form ~200 nm nanomaterials. In response to high concentration of ROS, such as found intracellularly in ischemic neurons, the boronic acid core hydrolyzes to release therapeutic cargo with an in vitro half-life of >4 hours. Application of this ROS-responsive nanomaterial immediately after reperfusion in a rat model of two-hour tMCAO model led to a significant decrease in infarct area and improvement in neurological score compared to free drug.

Proteases are important regulators of the microenvironment, and have important roles in the progression of cancer and during the immediate and chronic response after brain injuries.[143–145] In brain injuries, thrombin and the family of matrix metalloproteases (MMPs) in particular are important for regulating neuroinflammation, degradation of ECM components, and function of the BBB.[146,147] The disease-specific expression of proteases can be used to mitigate the toxic side effects common for drugs. For example, glyburide is an FDA-approved diabetes medication that blocks SUR1-TRMP4, an ion channel that is upregulated in the neurovascular unit after stroke implicated in edema and hemorrhage, but is dose restricted due to the risk of hypoglycemia.[148] In

order to increase disease-specific release in stroke, glyburide was encapsulated in micelles formed from poly-(e-caprolactone) and PEG block copolymers; the polymer blocks were linked with either a thrombin- or MMP-9-cleavable peptide.[52] The design was such that cleavage by proteases released PEG from the outer shell of the micelle, leading to a smaller diameter nanoparticle that could distribute further into the brain parenchyma. Nanomaterials made with thrombin-sensitive polymers had a 5.5-fold higher accumulation into the infarct of a 90-minute tMCAO mouse model compared to nonresponsive nanomaterials, and the delivery of glyburide using this bioresponsive shrinking nanoparticle decreased infarct size and improved neurological scores compared to the vehicle and free glyburide controls with multiple administrations of 0, 24, and 48 hours after surgery. Thrombin-reactive nanoparticles can also be used for site-specific dissociation of clots in order to prevent vessel occlusion. A sequential biomimetic approach for the dual delivery of neuroprotective and thrombolytic drugs was engineered by coating a polymeric core carrying the small molecule neuroprotective drug ZL006e with a platelet membrane that naturally accumulates at the site of clots.[53] The surface of the platelet was modified with the cell penetrating peptide Tat sterically shielded by the recombinant tissue plasminogen activator (rtPA) linked to the membrane with a thrombin-sensitive linker. In the presence of thrombin activity, the thrombolytic rtPA was released to dissociate the clot and also revealed Tat peptide on the nanomaterial surface to increase transport into the brain. When intravenously administered in a two-hour tMCAO model, this dual delivery, protease-sensitive nanomaterial decreased the ischemic area an impressive ~60% compared to no treatment and ~40% compared to animals treated with free drug or nanomaterial with linker insensitive to thrombin cleavage. Protease activity can also be used in diagnostic nanomedicines for acute brain injuries. Similar to the fluorescent cancer diagnostic material LUM015 developed by Lumicell Inc.,[138,139] a diagnostic nanomaterial responsive to TBI-associated proteases was engineered.[54] In this work, a fluorogenic substrate sensitive to calpain-1 cleavage was attached to a polymeric nanomaterial carrier in order to increase its passive accumulation into injured tissue. When

applied to a CCI model of TBI, fluorescence signal from this nanosensor was detected in the injured tissue compared to uninjured brains, indicating an increase in calpain-1 activity. Future work in bioresponsive materials for acute brain injuries can couple disease stimuli, such as ROS or protease activity, and bioresponsive therapeutic delivery for more precise treatments.

1.5.3: Nanomaterial penetration in the brain microenvironment

The abnormal vasculature, poorly developed lymphatics, high interstitial fluid pressure, dense ECM, and necrotic regions in the tumor core are obstacles to nanomaterial access throughout the entire tumor.[149] For example, liposomes 90 nm in diameter are observed to predominately accumulate in the tumor periphery near vasculature.[150] While nanomedicines such as Doxil® and Abraxane® have longer blood half-lives and reduced off-target effects, they do not exhibit significant improvements in therapeutic efficacy over free drug due to poor penetration into the tumor microenvironment.[150,151] Similarly in acute brain injury, there is a necrotic injury core surrounded by tissue that is damaged but not yet dead, called the traumatic or ischemic penumbra. Attenuating, halting, or ameliorating the secondary injury in the penumbra is the goal of many therapeutics in order to mitigate widespread tissue damage after acute brain injury. Due to BBB dysfunction that is common in secondary injury, the vasculature in the penumbra has increased permeability,[152,153] presenting a possible entry point for nanomaterials into the injured tissue. Although there have been observations that systemically delivered nanomaterials can reach the core of the injury in stroke models,[154] tissue access is likely influenced by multiple factors, including severity of injury, size of nanomaterials, and also the time delay between the injury and nanomaterial administration.[35,36,44,101] Based on the context of the injury and when materials are administered, the penetration of nanomaterials throughout the injured brain tissue is one potential obstacle to effective nanomedicines for acute brain injury.

One approach to increase distribution of nanomaterials throughout the tissue microenvironment is through engineering their physicochemical properties and surface chemistries. In our discussion of passive delivery above, we have already discussed how

nanomaterial infiltration can be size-dependent. Nance et. al. reported that nanoparticles modified with a dense PEG surface 100 nanometers and smaller can distribute widely when applied ex vivo to healthy rat and human brain samples and in vivo through direct brain injection. Through analysis of nanoparticle diffusion ex vivo, they estimated that pore sizes in the brain extracellular space are as large as 200 nm and that more than one-quarter of pores are at least 100 nm in size.[155] In this study, surface properties also affected nanoparticle diffusion within the brain; nanoparticles with a dense PEG surface exhibited significantly increased diffusion compared to the same nanoparticle cores with carboxyl surfaces. The Saltzman group observed that poly(lactic acid) nanoparticles modified with PEG or hyperbranched glycerol surfaces have decreased cellular uptake compared to nanoparticles modified with 'bio-adhesive' aldehyde surfaces when administered via convection enhanced delivery (CED) to healthy brains or glioblastoma tumors.[156] These papers establish groundwork for an early understanding of how nanomaterial properties may affect distribution and cellular interactions within the brain microenvironment, however more studies are warranted to establish systematic design rules.

Tumor-penetrating peptides are a biological approach to increase distribution of nanomaterials throughout tumors. The Ruoslahti group identified a tumor penetrating C-end-rule (CendR) sequence, consisting of a C-terminal R/KXXR/K motif, through in vivo phage display, a method for screening a large diversity of peptides in a living organism.[157,158] One tumor-penetrating CendR peptide, iRGD, combines the RGD integrin binding motif with the CendR motif.[158] After RGD binding with the primary integrin receptor, proteolytic cleavage exposes the CendR motif that can bind to the secondary receptor neuropilin-1, which mediates transcellular transport and penetration into the tissue.[158] Importantly, iRGD peptide could increase the penetration of nanomaterial both when covalently modified to the surface of nanomaterials, or when co-delivered with nanomaterials. In a model of prostate cancer that develops a thick tumor stroma, co-injection of iRGD with liposomal chemotherapeutics led to ~40% tumor shrinkage compared to co-injection with non-penetrating RGD control.[159] These penetrating peptides have

yet to be explored for nanomaterial delivery to acute brain injuries, although we note that one primary receptor for iRGD, $\alpha_v\beta_3$ integrin, is known to be expressed in wound beds and the secondary receptor, neuropilin-1, is known to be upregulated in hypoxic tissues.[160]

1.6: IMMUNOMODULATORY NANOMATERIALS IN BRAIN INJURY

Engineered nanomaterials are attractive technologies to interface with the immune system and there has been rapid development of these materials for applications in cancer. Nanomaterials are supramolecular assemblies and therefore they can deliver antigens and adjuvants (e.g., CpG oligonucleotides, imidazoquinoline, monophosphoryl lipid A, or plant virus proteins) to the same cell for the purpose of vaccination.[34] In addition, nanometer scale materials carrying diagnostic or therapeutic payloads are naturally phagocytosed by antigen presenting cells (e.g., dendritic cells and tumor-associated macrophages (TAMs). For example, maleimide-modified PEG nanoparticles have been used to capture circulating tumor antigens released after radiotherapy and subsequently be phagocytosed by dendritic cells to enhance the abscopal effect of anti-tumor immunity.[161] Nanoparticles can also mimic immune cell behavior, such as target binding, T cell activation, and tissue infiltration. Polymeric PLGA nanoparticles wrapped with neutrophil membranes used the endogenous affinity of neutrophils to bind circulating cancer cells to deliver the proteasome inhibitor carfilzomib after intravenous delivery.[162] Metal-organic framework nanoparticles, utilized for *in vivo* fluorescence imaging, were coated with a fusion of dendritic and cancer cell membranes to simultaneously mimic a dendritic antigen presenting cell and present tumor antigens to provide efficient T cell co-stimulation as a single nanomaterial.[163] In addition to direct stimulation of T cells, this material could also be phagocytosed by dendritic cells for indirect stimulation of T cells. This nanomaterial, termed a cytomembrane nanovaccine, homed to the lymph node *in vivo* after subcutaneous injection and successfully immunized 60% of mice against a tumor challenge. Lastly, immune cells can be used to increase the delivery of nanomaterials into solid tumors. Nanoparticles carrying chemotherapeutics have been attached *ex vivo* to T cells to exploit the innate infiltration of T cells for delivery of adjuvant (IL-15 super-

agonist) and chemotherapy (topoisomerase I poison SN-35) in several tumor models.[164–166] Advantages of cell-mediated therapeutic delivery include improvement in the therapeutic window due to increased biodistribution to the tumor.

The immune system in acute brain injury after TBI and stroke plays an integral role in disease progression and resolution.[72,167] Like TAMs, resident microglia and macrophages are aberrantly activated after injury. The therapeutic goal in the brain is regeneration, as opposed to cancer killing, and therefore the polarization of macrophages and microglia between pro- to anti-inflammatory states requires precise regulation during the multiple phases of injury resolution. For a detailed discussion of the immune response in stroke and TBI, see excellent reviews by Loane and Kumar,[168] Gyoneva and Ransohoff,[169] and Kawabori and Yenari.[167] In summary, the elevation of danger associated molecular patterns (DAMPs) released by apoptotic neurons bind to toll-like Receptors (TLRs) on microglia and tissue-resident macrophages.[168] TLR activation leads to transcriptional upregulation of inflammatory genes, such as interleukins and TNF-α[72,167] to polarize immune cells to an inflammatory "M1" phenotype. Inflammatory immune cells generate arachidonic acid metabolites, nitric oxide (NO), ROS, and MMPs that perpetuate the inflammatory response.[167,168] Simultaneously, astrocytes, microglia, and oligodendrocyte progenitor cells become reactive, leading to gliosis as a hypothesized mechanism to sequester tissue damage from healthy tissue.[170] Adhesion molecules, including selectins, IG, and integrins, upregulated on damaged endothelium leads to the recruitment of leukocytes from the blood.[167] The infiltrating leukocytes, mainly neutrophils and monocytes, release cytokines, ROS, and MMPs that perpetuate the inflammatory microenvironment leading to tissue damage and cell death.

Based on the destruction a sustained proinflammatory response can cause after acute injury, there has been significant effort to improve the delivery of anti-inflammatories, such as glucocorticoids, NSAIDs, TNF-α inhibitors, IL-1β inhibitors, and drugs with pleiotropic mechanisms such as statins.[171] Due to the endogenous phagocytic activity of microglia, a common goal for nanomedicines is to deliver immunomodulatory molecules to polarize microglia

to an anti-inflammatory state. The ability for nanomaterials to accumulate in microglia has been demonstrated with poly(amidoamine) (PAMAM) dendrimers after intravenous delivery in several models of brain inflammation.[172,173] In a pediatric rabbit CCI model of TBI, PAMAM dendrimer modified with a triphenylphosphonium (TPP) mitochondrial targeting moiety demonstrated accumulation in the mitochondria of microglia when delivered 6 hours post-TBI.[55]

In a different approach, nanoparticles can be used to deliver cytotoxic agents to deplete infiltrating neutrophils and monocytes in order to reduce the tissue damage, since these cells are known to exacerbate the destructive injury response.[174] In one example, albumin nanoparticles linked with cytotoxic doxorubicin through an acid-labile hydrazine bond accumulated in activated phagocytic neutrophils in the blood to induce apoptosis and prevent their infiltration into inflamed tissue.[56] The hydrazine bond was designed to be stable in circulation but degrade in the acidic endosome of neutrophils after phagocytosis. Systemic administration of these nanoparticles one hour after reperfusion in a tMCAO model depleted blood neutrophils and reduced neuroinflammation, as measured by brain levels of TNF-α, IL1β and IL-6. Depletion of monocyte infiltration into brain tissue represents another immunomodulation strategy. Highly anionic 500nm polymeric nanoparticles injected 2, 24, and 48 hours post-CCI bound to blood monocytes *in situ* via the macrophage receptor with collagenous structure (MARCO), leading to a 84.5% decrease in monocyte infiltration into the brain 3 days post-injury compared to vehicle control.[59] This decrease was concomitant with decreased lesion volume and ventricular volume, and improvements in functional behavior up to 6 months post-treatment. A similar functional outcome was reproduced when these same nanoparticles were applied to a closed head injury (CHI) model. In another study, prophylactic delivery of clondronate liposomes in a CCI model showed both beneficial (reduced ventricle enlargement) and detrimental (increased BBB permeability) outcomes with no effect on lesion volume and edema, illustrating the complicated role immune cells may have in acute injury.[57,58] Although prophylactic treatment of TBI is a clinically unrealistic treatment strategy, these preclinical data may provide clues for future research. While using

nanomaterials to deplete phagocytic immune cells is a promising strategy, further research is needed to illuminate the role of these cells in brain injury pathophysiology.

Based on the natural infiltration of innate immune cells into the brain after injury, mimicry of these cells can increase nanomaterial accumulation into the brain, where the BBB is a formidable barrier to access. In one approach, ~190 nm nanovesicles were made from a neutrophil cell line HL-60 to mimic neutrophil infiltration into the injured brain.[60] Nanovesicles loaded with the therapeutic molecule resolvin D2 maintained major surface proteins found on neutrophils (integrin β2, PECAM-1, PSGL-1, and VLA-4) and trafficked to the injured brain endothelium after intravenous injection one hour post-reperfusion in a tMCAO mouse model. The therapeutic mechanism of resolvin D2 is to reduce leukocyte-endothelium interactions, and treatment of the tMCAO model with resolvin D2 loaded neutrophil nanovesicles led to decreased neutrophil infiltration and reduced levels of inflammatory cytokines TNF-α, IL1β and IL-6 in the injured brain compared to no treatment controls.

Nanomaterials have also been used to "hitchhike" onto infiltrating immune cells, wherein nanomaterials can modify leukocytes in the blood and translocate into the brain based on the endogenous chemotaxis of these cells. For example, liposomes modified with circularized RGD targeting peptide targeted overexpressed αvβ3 integrin receptors on activated blood monocytes and neutrophils after tMCAO and become phagocytosed.[61] Liposomes labeled with dye accumulated in neutrophils and monocytes in the bloodstream, co-migrated across the BBB into the injured lesion, and transferred to neurons and microglia in the microenvironment. In related studies in models of lipopolysaccharide (LPS) induced brain inflammation, 30 nm superparamagnetic iron oxide nanoparticles with oleic acid and amphiliphilic polymer coating (SHP-30, Ocean NanoTech) were attached *ex vivo* to bone marrow-derived monocytes and intravenously injected.[62] These adoptively transferred cells carrying nanoparticles could be detected by flow cytometry in the inflamed brain 14 hours after injection. Additionally, macrophages modified with a layer-by-layer disc-shaped polymer patches 7 μm in diameter and

29

600 nm in height via an anti-CD11b antibody were able to infiltrate into brains with LPS-induced inflammation.[63] These studies demonstrate nanomaterials can modulate the natural activity of the immune system or exploit the natural trafficking of immune cells for therapeutic benefit in acute brain injuries.

1.7: PATH TO CLINICAL TRANSLATION

We have discussed preclinical research on nanomaterial designs that can intelligently interact with host biology for application to acute brain injuries. Before successful translation of these nanomaterials from preclinical studies into humans, there remain several obstacles. Many of the obstacles are attributed to the translation of therapeutics for acute brain injuries in general, for example inadequate understanding and control of the pharmacokinetics and pharmacodynamics of therapeutics (biodistribution, half-life, dose-response curve, etc.), limitations in preclinical models to represent the heterogeneity of disease phenotype, understudied biological variables such as age and sex, and lack of specific biomarkers that can predict long-term outcomes. While nanomaterials are a potential solution to these hurdles, such as improvements in the pharmacokinetic and pharmacodynamics, they also pose their own complications. For example, there are challenges associated with the scale-up and manufacture of nanomaterials and their path for FDA-approval is complicated due to their multiple components. We will focus our discussion on the obstacles to translation as they relate to nanomaterials. For a comprehensive discussion of clinical translation of therapeutics for brain injuries please see the excellent reviews by Stein,[22] Loane and Faden,[19] and Bosetti.[175] The translation of nanomaterials are discussed in reviews by Hua and Storm[176] and Anselmo and Mitragotri.[177]

One major hurdle to clinical translation of therapeutics for brain injuries is to achieve desirable pharmacokinetic profiles, most notably increased accumulation and retention in the brain and reduced accumulation in off-target organs. Formulation of drugs as nanomaterials offer potential solutions. For example, Doxil® is chemotherapeutic formulated in PEG-modified ~100 nm liposomes; the large size reduces off-target organ accumulation to mitigate toxicity and the

PEG reduces interaction with phagocytes to increase circulation times.[177] Besides passive targeting, active targeting via surface modification with peptides (RGD, RVG, CAQK) or antibodies is one avenue to increase nanomaterial selectivity to cell types and retention in brain tissue, although active targeting has yet to be implemented in clinically-approved nanomaterials.[32,177] In addition to regulating organ-level biodistribution, increasing nanoparticle penetration through biological barriers, such as the BBB and brain tissue, is another delivery challenge.[177] Further investigation is needed into the effects of nanoparticle size, charge, and other physiochemical properties on pharmacokinetics.[155,156]

Accurate quantification of therapeutic bioavailability in target organs and scaling preclinical dosage levels to humans is necessary for translation; ambiguity in effective progesterone dose and schedule has been speculated to be one reason for lack of efficacy observed in the ProTECT III and SyNAPSe III clinical trials.[22] The accurate quantification of nanomaterials which do not have intrinsic imaging properties *in vivo* is one difficulty because traditional organ collection and histology is not applicable in a clinical setting.[177] Bioresponsive nanomaterials that only release drug in the presence of stimuli are one potential solution that would alleviate the need for precise dosing, since therapeutics could be engineered to release only in the presence of disease and could therefore increase the therapeutic window. For example, self-titrating hemostatic nanoparticles are engineered to release heparin only in the presence of thrombin activity.[178]

Testing promising therapeutic candidates in preclinical animal models of brain injury is a mainstay of research and is a requirement for the FDA to support clinical trial feasibility. The utility of animal modeling is indisputable given the scientific precedence, availability, low cost, and ability to screen a multitude of therapeutic agents.[82] Using Bayesian analysis, Goodman et al. estimated that preclinical testing increases the likelihood of clinical success by several orders of magnitude.[179] Despite the value of preclinical testing for therapeutic translation and the availability of different types of injury models as discussed above, the limitation of animal models to

recapitulate human biology in response to an acute brain injury must be considered.[80,82,84,85,175]

For one, rodents have a different brain geometry and white-to-gray matter ratio, among other anatomical differences.[80,81] Several variations in innate and adaptive immune response also exist, including percentage of neutrophil populations in blood and chemokine receptor expression.[180] These biological discrepancies can result in differences in acute brain injury sequelae between humans and rodents. For example, gene expression patterns can differ in mice and humans after ischemic stroke.[85,181–186] Additional factors including the use of anesthesia and post-operative analgesia during induction of injury in animal models in compliance with animal welfare guidelines.[187] Finally, the patient population enrolled in clinical trials is typically heterogeneous and represent different ages, genders, pre-morbid conditions, injury origins and disease severity. Preclinical studies often fail to match the heterogeneous nature of the clinical patient population because the majority of experiments employ generally one optimized injury model in healthy adult rodents of the same strain and gender; rarely are geriatric, pediatric, or female mice represented in studies. More research is needed to delineate the role age plays in both TBI pathology and therapeutic response[188] given the risk of TBI is higher among children, young adults, and those over 75 years of age.[189] Variations in rodent strain,[190] age,[191,192] and sex[193] may influence measured outcomes and potentially confound results. For example, the sex hormones estrogen and progesterone may be neuroprotective after TBI in female mice compared to their male counterparts.[193,194] While biological differences between rodents and humans are intrinsic to preclinical testing, increasing awareness of the factors that are within experimental control and rigorously defining aspects of models that accurately predict disease phenotype in humans is important in future design of clinical trials based on preclinical research.[82]

A final hurdle for clinical translation stems from the complexity of acute brain injury pathology in the clinic. The most commonly utilized injury assessment metrics in the clinic, Glasgow Coma Scale (GSC) or Glasgow Outcome Scale-Extended (GOS-E) for TBI and modified Ranking Scale (mRS) for stroke, involve a series of questions to qualitatively assess neurological

deficits and quality of life in patients.[5,15] However, analysis of neurological surveys like GSC often lack sensitivity in distinguishing injury severity and stage which make monitoring patient outcomes difficult.[195] The questionnaire format of GSC, described as a "blunt instrument", can potentially miss small improvements in patient outcome.[22,175] The subjective nature of GSC, GOS-E and mRS contrast with preclinical testing which typically uses multiple quantitative and functional endpoints to assess therapeutic efficacy.[22] In addition to selection of appropriate endpoints, the complex continuum of acute and chronic secondary injury clouds determination of appropriate timelines for therapeutic intervention.[19] Matching therapeutic dose schedules gleamed from preclinical studies to timepoints in the clinic can be difficult or unrealistic.[196] For example, a significant number of preclinical studies employ prophylactic or short timepoints post-injury for therapeutic delivery, whereas it can take up to 6 hours for patients to present with TBI, provide informed consent, enroll in a clinical trial, and receive therapy.[19] In the ProTECT III and SyNAPSe III clinical trials, treatment was administered within 4 hours and 8 hours of injury, respectively.[22]

Whereas preclinical studies have provided the biological and mechanistic basis for past clinical trials, future efforts to improve the predictive accuracy of preclinical studies is a critical step to achieve success in clinical trials. Health experts aim to develop research guidelines like Stroke Therapy Academic Industry Roundtable (STAIR) recommendations to improve clinical translation.[175,197] The Federal Interagency Traumatic Brain Injury Research (FITBIR) is an informatics system built to share TBI related research across the research field. For the development of nanomaterials to treat acute brain injuries, future efforts include accurate measurement of nanomaterial pharmacokinetics in living organisms, careful selection of animal models that recapitulate specific human pathology relevant to nanomaterial design and payload, designing experiments that consider multiple biological variables, and development of technology to quantitatively measure biomarkers that can accurately predict outcomes in humans.[175,198] PAMAM dendrimers are one example of nanomaterials that were tested across species and in multiple models of brain injury.[173] Based on comprehensive preclinical studies, PAMAM dendrimer

nanomaterial drug OP-101 manufactured by Orpheris is currently undergoing Phase I clinical trials of safety, tolerability, and pharmacokinetics (clinicaltrials.gov NCT03500627).

1.8: CONCLUSION

There is an urgent need for new therapeutics to treat acute brain injuries, and engineering novel nanomedicine is one potential avenue for innovation. We drew from two decades of cancer nanomedicine in order to gain insight and inspiration to apply to the burgeoning field of nanomedicine for acute brain injuries. In particular, we focused on nanomaterials that are engineered based on disease-specific changes that occur in the vasculature, microenvironment, and the immune system. Within the current field of nanomaterials for acute brain injuries, there remain significant opportunities to innovate within the topics discussed, as well as opportunities in directions that have been largely unexplored as of yet. For example, the secondary injury after an acute brain injury is multi-factorial and the failure of single drug therapies have initiated investigations into combination therapies. While there are promising ongoing studies of combination therapies,[199] maintaining multiple drug molecules with disparate pharmacokinetics in their therapeutic windows may be a challenge. As supramolecular structures, nanomaterials can package multiple drugs for simultaneous delivery to the same tissue region or cell. In addition, nanomaterials can deliver challenging cargoes such as nucleic acids and proteins; the first FDA-approved siRNA therapy, ONPATTRO®, is a lipid nanoparticle that gained approval in 2018. Nanomaterial-mediated delivery of proteins and nucleic acids has the potential to directly translate basic biological findings from research labs into the clinic without the time-consuming development of small molecules. Lastly, many drugs, especially those designed for the brain, have poorly tolerated side effects. Future nanomaterials can be implemented as a precision medicine approach; for example, a system composed of a nanomaterial sensor that measures disease-causative protease activity paired with a homeostatic nanomaterial therapeutic that releases protease inhibitors only in response to that protease's activity.

1.9: ACKNOWLEDGEMENTS

CHAPTER 2: Analysis of Lipid Nanoparticle Pharmacokinetics and Activity in a Mouse Model of Traumatic Brain Injury

2.1: ABSTRACT

Traumatic brain injury (TBI) affects millions of people worldwide, yet there are currently no therapeutics that address the long-term impairments that develop in a large portion of survivors. Lipid nanoparticles (LNPs) are a promising and minimally invasive therapeutic strategy that may address the molecular basis of TBI pathophysiology. LNPs are the only non-viral gene delivery platform to achieve clinical success, but systemically administered formulations have only been established for targets in the liver. In this work, we evaluated the pharmacokinetics and activity of LNPs when systemically administered to a mouse model of TBI. We observed an increase in LNP accumulation and activity in the injured brain hemisphere compared to the uninjured contralateral brain hemisphere. Interestingly, transgene expression mediated by LNPs was more durable in injured brain tissue compared to off-target organs when compared between 4 and 24 hours. The polyethylene glycol (PEG)-lipid is an important component of LNP formulation necessary for the stable formation and storage of LNPs, but the PEG-lipid structure and content also has an impact on LNP function. LNP formulations containing various ratios of PEG-lipid with C18 (DSPE-PEG) and C14 (DMG-PEG) anchors displayed similar physicochemical properties, independent of the PEG-lipid compositions. As the proportion of DSPE-PEG was increased in formulations, blood circulation times of LNPs increased and the duration of expression increased. We also evaluated diffusion of LNPs after convection enhanced delivery in healthy brains and found LNPs distributed >1 mm away from the injection site, with increased spread with greater DSPE-PEG content. Understanding LNP pharmacokinetics and activity in TBI models and the impact of PEG-lipid anchor length informs the design of LNP-based therapies for TBI and is broadly applicable to LNP design for extra-hepatic targets after systemic administration.

2.2: INTRODUCTION

Traumatic brain injury (TBI) impacts millions per year globally and there are currently no clinically approved therapeutics that address long-term patient brain health,[200–202] with 43% of hospitalized TBI survivors developing long-term disabilities.[203] The primary injury initiates a number of biochemical and physiological responses that trigger progressive neurodegeneration and eventual functional impairments during the secondary injury. Gene therapy mediated by lipid nanoparticles (LNPs) is one potential therapy for TBI that could address disease pathways during the secondary injury. LNPs are the currently the most clinically advanced non-viral gene delivery vehicle, and multiple formulations have been approved by the FDA.[204–206] Patisiran, an LNP treatment for transthyretin-induced amyloidosis, was approved in 2018 and was the first LNP and siRNA therapeutic approved for clinical use.[204,207,208] In 2020, mRNA LNPs were developed as vaccines against SARS-CoV-2 and received emergency use authorization for the COVID-19 pandemic[209–211] followed by full FDA approval shortly after in the subsequent 1-2 years.[205,206] There are multiple siRNA and mRNA LNPs in the clinical pipeline as therapeutics for cancer, infections, and genetic disorders.[212–214] In this work, we evaluate the potential of LNPs for non-viral gene delivery to the injured brain in a mouse model of TBI.

The temporary dysregulation of the blood brain barrier (BBB) after TBI is an opportunity for access of nanoscale materials into injured brain tissue after systemic delivery. Our group and others have demonstrated increased transport of a variety of nanoparticle types into the injured brain exploiting this transient dysregulation.[215–218] Appreciable passive nanoparticle accumulation in the injured tissue has been reported for diameters ~100 nm in size after intravenous administration up to 24 hours after TBI.[44,219–221] The principle of nanoparticle accumulation in the injured brain is analogous to the enhanced permeation and retention (EPR) effect described in tumors.[222,223] Passive accumulation of nanoparticles in tumors and the injured brain is known to be impacted by the physicochemical properties of nanoparticles, including size,[220,224] charge,[225–227] and surface chemistry.[222,228] LNP pharmacokinetics are also impacted by their physicochemical properties. For example, increased lung, liver, and spleen LNP accumulation

have been achieved by tuning LNP charge through formulation with specific organ targeting (SORT) cationic, zwitterionic, and anionic lipids, respectively.[229] Size-based differences in organ accumulation have also been observed, with 80 nm LNPs preferentially accumulating more in the spleen compared to 45 nm and 30 nm LNPs.[230]

One aspect of nanoparticle physicochemical property is hydrophilicity, typically tuned in LNPs by the inclusion of polyethylene glycol (PEG)-lipids in the formulation. PEG has been incorporated in nanomedicine for decades in order to increase blood half-life through reducing uptake by the reticuloendothelial system (RES).[231] Generally, increased passive accumulation is observed by nanoparticles with longer blood half-lives.[225,227,231–233] For example, in a breast cancer model, the addition of PEG to paclitaxel liposomes increased blood area under the curve values ~4.5-fold, and thus increasing paclitaxel tumor accumulation ~1.5- and 4-fold at 6 and 24 hours after systemic administration.[234] Similarly, PEG-lipids are included in LNP formulations to extend their blood circulation, in addition to improving their stability during synthesis and storage.[235,236] However, PEG is also a steric barrier that hinders cellular interaction and endosomal escape, crucial steps in payload delivery.[237–240] Recent research has demonstrated that PEG mole percent (mol%),[241–243] PEG molecular weight,[244] and PEG-lipid anchor length[241,245,246] affect the activity and pharmacokinetic profiles of LNPs. Reduction in the amount of PEG-lipid in LNP formulations mediated more transfection in hepatocytes in primary cell culture and after systemic administration *in vivo* due to their increased cellular interactions.[242] In studies of LNPs formulated with different PEG-lipid anchor lengths, Mui et al. demonstrated that short C14 anchor PEG-lipids desorb quickly from LNP formulations in the blood, leading to accumulation in the liver, while LNP formulations with long C18 anchor PEG-lipids had longer blood half-lives and subsequently accumulated less in RES organs.[241] Previous research has also demonstrated that PEG-lipid anchor length affects passive accumulation into tumors after systemic administration; LNPs with longer anchor PEG-lipids demonstrate greater tumor accumulation due to their longer blood half-lives.[245]

38

In this work, our goal was to investigate PEG-lipid anchor lengths as a design parameter for passive accumulation of LNPs into the injured brain after systemic administration in a mouse model of TBI. We formulated LNPs with various ratios of DMG-PEG, a PEG-lipid with a "short" C14 anchor capable of quickly desorbing from the LNP once in circulation,[241,246] and DSPE-PEG, a PEG-lipid with a "long" C18 anchor with slower desorption kinetics.[241,245,246] When administered systemically in a mouse model of TBI, we observed greater accumulation and activity of all LNP formulations in the injured brain hemisphere compared to the uninjured contralateral brain hemisphere. In comparing how PEG-lipid composition impacts pharmacokinetics and activity, we found LNP formulations with more DSPE-PEG had longer blood half-lives and reduced activity in off-target organs 4 hours after administration. Interestingly, LNP activity in injured brain tissue remained constant or increased from 4 to 24 hours, while off-target organ LNP activity decreased ~10-fold and this phenomenon was more pronounced as DSPE-PEG content increased. We next sought to study how PEG-lipid anchor length affected LNP distribution through the brain microenvironment and found that LNPs with higher DSPE-PEG content distributed more from the injection site, but that all LNP formulations distributed at least 1 mm away from the injection site and interacted with neurons and microglia. Our results suggest that PEG-lipid anchor length is an important parameter in tuning the pharmacokinetics and activity of LNPs for application in TBI. Understanding how PEG-lipid anchor chemistry impacts pharmacokinetics and activity of LNPs can also broadly inform the design of LNPs for systemic delivery to other extra-hepatic targets.

2.3: RESULTS AND DISCUSSION

2.3.1: Characterization of LNPs Formulated with Various PEG-lipid Compositions
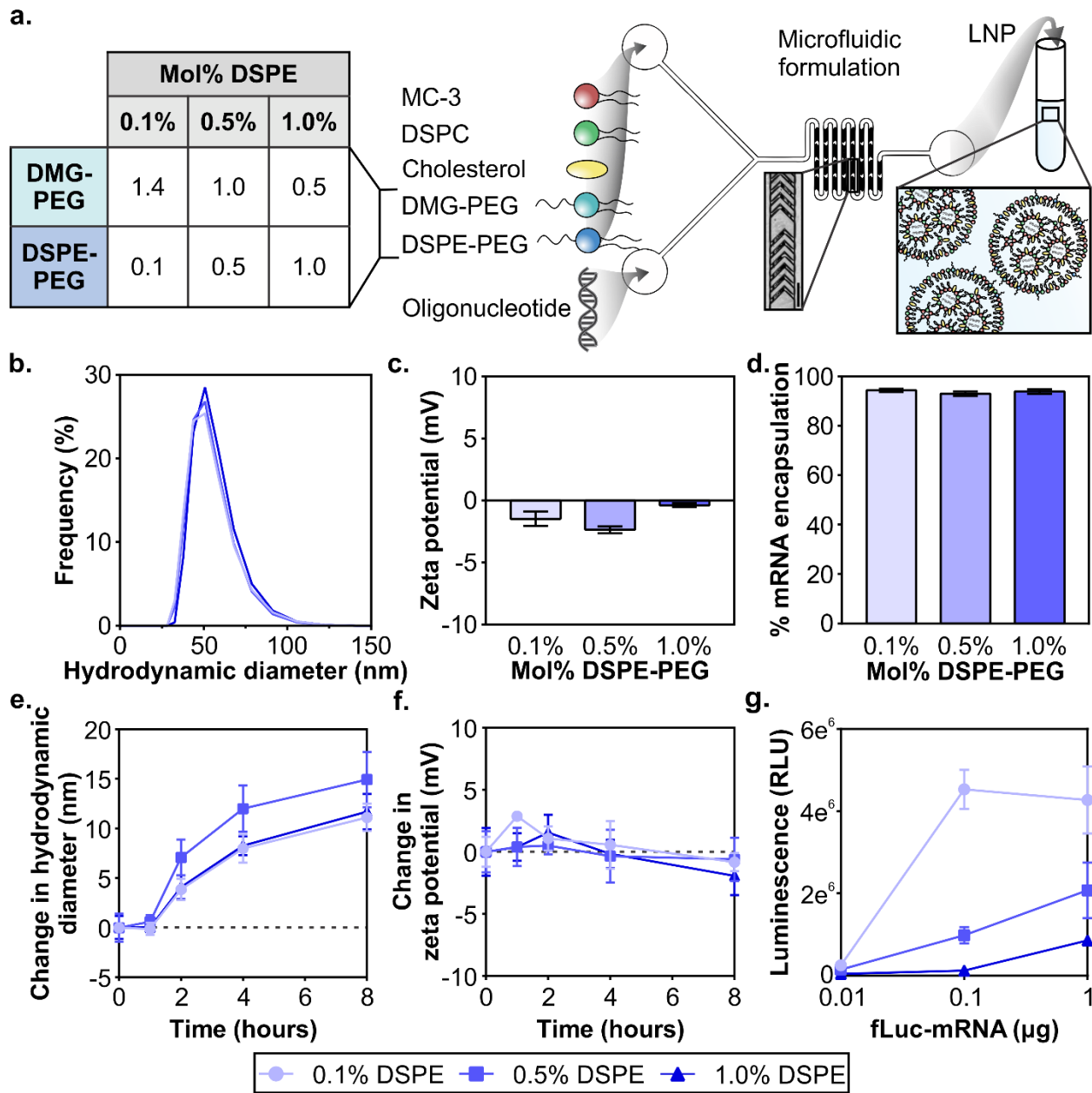
Figure 2.1: Formulation of nucleic acid LNPs with varying PEG-lipid compositions. (a) Schematic of LNP formulation and the PEG-lipid compositions evaluated. DLS analysis of (b) size distributions and (c) zeta potentials (n=2) of LNP formulations. d) Percent encapsulation of mRNA in LNPs (n=2). (e) Average sizes and (f) zeta potentials of LNPs when incubated in serum over time (n=3). (g) Luciferase activity in 293T cells after 24 hours of treatment with LNPs at various mRNA doses (n=3).

Clinical formulations have so far been applied to the liver after systemic delivery or vaccinations after intramuscular delivery and therefore LNPs were designed to desorb PEG-lipid quickly in the biological milieu to interact with target cells and tissues. The PEG-lipids used in

FDA-approved LNP formulations have two C14 alkyl chains, allowing fast desorption kinetics,[241,245,246] and include PEG$_{2000}$-C-DMG (patisiran), PEG$_{2000}$-DMG (elasomeran), and ALC-0159 (tozinameran). The only approved systemically administered LNP, patisiran, targets the liver through the desorption of PEG2000-C-DMG,[247] allowing for the adsorption of apolipoprotein E that interacts with hepatocytes through the low-density lipoprotein receptor.[248] In order to develop LNPs for non-RES targets after systemic delivery, previous studies have evaluated PEG-lipids with longer anchors to tune LNP pharmacokinetics such as extending blood half-lives and therefore increasing their accumulation in non-RES organs or tumor tissue.[245,249–251] In the present study, our objective was to analyze the effects of PEG-lipid anchor length on passive accumulation of LNPs into the injured brain after systemic administration in a model of TBI. Our LNP formulation is based on patisiran and its composition is DLin-MC3-DMA:DSPC:cholesterol:PEG-lipid at mole ratios of 50:10:38.5:1.5.[247] With the goal to study whether the PEG-lipid anchor length impacts brain accumulation and LNP pharmacokinetics, we compared LNPs formulated with a fixed total mole percent of PEG-lipid but with three ratios of DMG-PEG:DSPE-PEG (1.4:0.1, 1.0:0.5, 0.5:1.0) (Figure 2.1a). Small and uniform LNPs were formulated through nanoprecipitation in a microfluidic mixer with staggered herringbone features, as described previously (Figure 2.1a).[252,253] We established that the size and zeta potential of the LNP formulations were similar regardless of their PEG-lipid composition. All formulations were measured with dynamic light scattering (DLS) to have ~70 nm hydrodynamic diameters, low polydispersity indices under 0.06 (Figure 2.1b, S2.1), and near-neutral surface potentials (Figure 2.1c). Size and zeta potential are physicochemical measurements known to affect LNP pharmacokinetics.[229,230] The similar size and zeta potential measured for each formulation allowed us to compare LNP pharmacokinetic and activity differences based on their PEG-lipid composition. The mRNA encapsulation measured was also similar for all three formulations (Figure 2.1d), and therefore administrations matched by cargo also contained equal amounts of lipid.

In order to understand the impact of protein adsorption on the three formulations, we incubated LNPs with 55% exosome-free serum in PBS at 37℃ to recapitulate physiological protein concentrations in blood,[254] and measured their size and zeta potential at 1, 2, 4, and 8 hours. The formation of a protein corona on PEGylated and non-PEGylated nanoparticles exposed to serum is well-studied, with PEGylated nanoparticles typically adsorbing less proteins due to the steric hindrance of the PEG layer.[255–257] Over the incubation period, we observed that all LNP formulations increase in size, culminating in a 10-15 nm increase at 8 hours, suggesting the formation of a protein corona (Figure 2.1e). We also observed a slight negative shift in zeta potential for all 3 formulations at 8 hours (Figure 2.1f), consistent with the abundance of negatively charged serum proteins.[258] Increases in size up to 30 nm and negative shifts in zeta potential have been previously observed after protein corona formation on PEGylated liposomes after incubation in serum.[259]

Next, we measured the *in vitro* transfection activity of the LNP formulations. We formulated LNPs with mRNA encoding firefly luciferase (fLuc-mRNA) and transfected 293T cells in media supplemented with serum (Figure 2.1g). When cells were measured for luciferase activity at 24 hours, we observed that all formulations had measurable dose-dependent transfection efficiency. LNP formulations with the least amount of DSPE-PEG content demonstrated more luciferase expression at all tested doses, consistent with previous reports.[260–262] Prior studies have established the fast desorption kinetics of short C14 anchor PEG-lipids in the presence of plasma proteins, which reduces the steric barrier and allows LNPs to interact with the cell.[237,239,263]

2.3.2: PEG-lipid Anchor Length Impacts LNP Pharmacokinetics after Systemic Administration in a Mouse Model of TBI
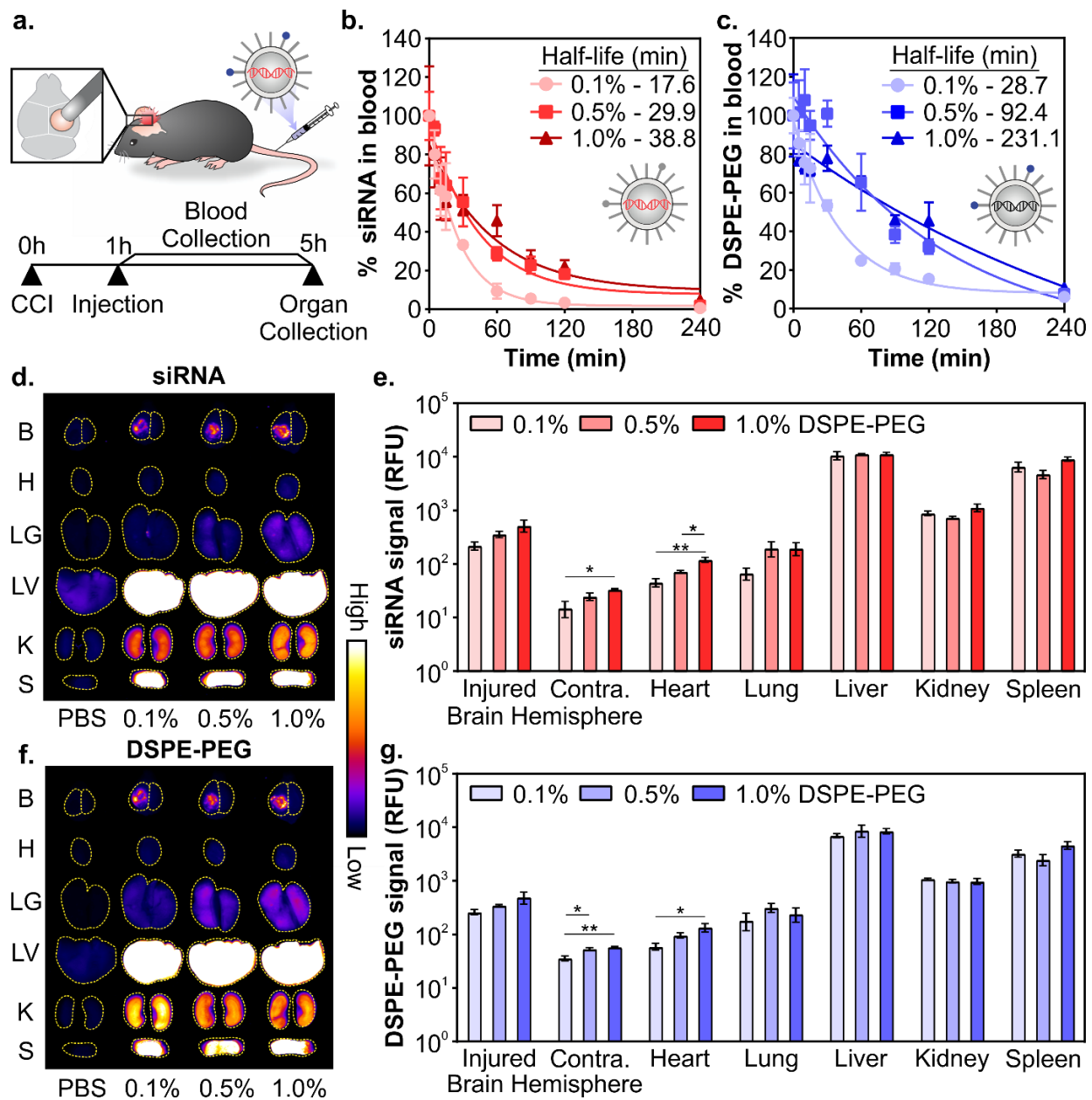
Figure 2.2: Pharmacokinetics of siRNA LNPs in a mouse model of TBI as a function of PEG-lipid composition. (a) Schematic of experiment. Blood half-lives of siRNA-LNPs as measured by fluorescently labeled (b) siRNA and (c) DSPE-PEG. Representative whole organ fluorescent surface images and their quantification measured by labeled (d, e) siRNA and (f, g) DSPE-PEG. Brains were analyzed by integrating signal from the injured vs. uninjured contralateral hemispheres. LNP organ accumulation is compared with a one-way ANOVA with Tukey's post-test within each organ type (Mean ± S.E.M., n=3, *$p < 0.05$, **$p < 0.01$).

Due to the complex interactions of nanoparticles on the whole organism level, *in vivo* activity is difficult to predict with *in vitro* measurements.[264] Therefore, in subsequent studies formulations were evaluated *in vivo*. Having confirmed that LNPs formulated with varying ratios

43

of DMG-PEG:DSPE-PEG had similar physicochemical properties (Figure 2.1), we next evaluated their pharmacokinetics after systemic administration in a mouse model of TBI. LNPs were formulated with Dy677-labeled siRNA and Cy7-labeled DSPE-PEG to monitor the distribution of both siRNA cargo and PEG-lipid. All three LNP formulations included 0.1 mol% Cy7-labeled DSPE-PEG to minimize the influence of dye molecules on the physicochemical properties of the LNPs. Controlled cortical impact (CCI) is a well-studied and reproducible model of TBI that causes transient BBB permeability due to vascular damage in the injured tissue.[216,217,265] Mice were injured on the right hemisphere of the brain with a CCI and 0.75 mg/kg of siRNA LNPs were administered via the tail-vein 1 hour post-injury (Figure 2.2a). The passive accumulation of nanoparticles into the injured brain after systemic administration 1-6 hours post-injury has previously be established for a variety of nanoparticle types.[44,220,225,266] Blood signal over 4 hours and organ biodistribution at 4 hours were measured by fluorescence of siRNA cargo and the Cy7-labeled DSPE-PEG (Figure 2.2a).

Composition of PEG-lipid anchor lengths affected the blood half-lives of LNPs when measured both by siRNA (Figure 2.2b) and the PEG-lipid (Figure 2.2c). LNPs formulated with high proportions of DSPE-PEG had longer blood half-lives, consistent with previous literature that reported that longer anchor PEG-lipids increase the circulation time of LNPs after intravenous administration.[241,245,267,268] The blood half-lives of LNPs measured by the fluorescence of the PEG-lipid (Figure 2.2c) are extended compared to the blood half-lives measured by the fluorescence of the siRNA (Figure 2.2b). Mui et al. also observed longer blood half-lives of LNPs when measured by radiolabeled PEG-lipids compared to MC3.[241] The longer blood half-lives calculated from measuring labeled PEG-lipid over cargo is likely due to the association of PEG-lipids with lipid rich and/or hydrophobic domains on extracellular vesicles, apolipoproteins, and albumin, leading to a perceived extended blood circulation.[236]

Organ biodistribution of both siRNA (Figure 2.2d,e) and PEG-lipid (Figure 2.2f,g) were evaluated by quantifying the fluorescence intensity of the organs in surface scans. Relative signal

between labeled siRNA and DSPE-PEG were largely consistent across organs. We observed that LNPs accumulate in the injured hemisphere of the brain ~10-fold over the uninjured contralateral hemisphere (Figure 2.2e,g), similar to what has been observed with the passive accumulation of other nanomaterials in the injured brain tissue after TBI due to the dysregulation of the BBB.[44,220–222] LNPs formulated with more DSPE-PEG demonstrate slightly greater accumulation in the injured brain hemisphere (Figure 2.2e,g), likely due to the longer blood half-lives of these LNP formulations (Figure 2.2b,c). Previous research has observed increased tumor[227,234,269] and injured brain[225] passive accumulation with polymeric, metallic, and lipid-based nanomaterials that have longer blood half-lives. We also observe greater LNP accumulation in the contralateral brain hemisphere and heart when they are formulated with more DSPE-PEG, likely also due to their longer blood half-lives, although these organs have the least overall accumulation compared to other organs. Lee et al. has established that PEGylated liposomes have longer blood half-lives and greater heart accumulation compared to conventional liposomes after intravenous administration,[270] supporting our observation of increased accumulation in the heart when mice were treated with LNPs with more DSPE-PEG. In line with our previous work studying the pharmacokinetics of various nanomaterials after intravenous administration in a mouse model of TBI,[225,271,272] the RES organs have greater overall LNP accumulation than the injured brain. However, there are no notable differences in accumulation between the formulations evaluated. The similarity in LNP organ distribution when measured by labeled siRNA or DSPE-PEG is likely due to the relatively slow desorption of DSPE-PEG from the LNP (0.2% desorbed per hour),[241] indicating that the accumulation of the labeled PEG-lipid in organs can be used as a proxy for intact LNPs.

Figure 2.3: Pharmacokinetics of mRNA LNPs in a mouse model of TBI as a function of PEG-lipid composition. a) Blood half-lives and b) organ biodistribution of LNPs by Cy7-labeled DSPE-PEG. LNP organ accumulation is compared with a one-way ANOVA with Tukey's post-test within each organ type (Mean ± S.E.M., n=3, *p<0.05, ***p<0.001, ****p<0.0001).
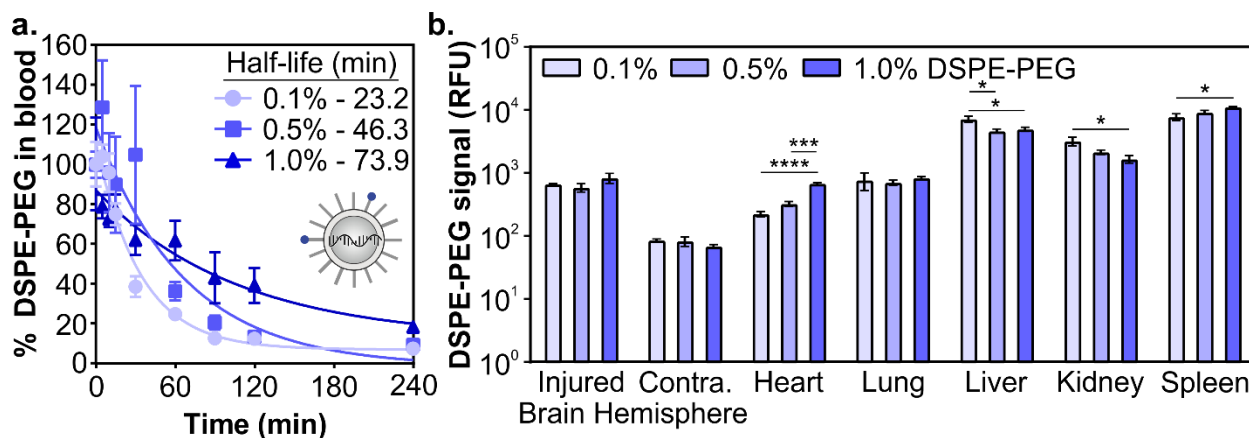
Next, we determined how the pharmacokinetic profiles of LNPs changed when formulated with mRNA cargo. siRNA and mRNA LNPs were formulated with N/P ratios of 3 and 5.6, respectively, which were chosen based on the N/P ratios of the siRNA LNP therapeutic patisiran (N/P 3) and the mRNA LNP COVID vaccines (N/P 5.6).[247,273,274] Similar to the siRNA LNPs, the mRNA LNPs were formulated with 0.1 mol% Cy7-labeled DSPE-PEG and LNP signal was measured in blood and organs using fluorescence. After intravenous administration (0.5 mg/kg) in a mouse model of TBI, we observed that mRNA LNP circulation times were longer with higher proportions of DSPE-PEG in the formulation (Figure 2.3a). Overall, mRNA LNPs exhibited shorter blood half-lives than siRNA LNPs (Figure 2.2c), like due to the higher N/P ratio of mRNA LNPs. Positively charged nanoparticles are known to have shorter blood half-lives.[227,231,275] Previous research has also demonstrated that N/P ratios impact LNP biodistribution, with lower N/P ratios leading to greater spleen accumulation and higher N/P ratios leading to greater lung accumulation.[276] We observed that the content of DSPE-PEG had more impact on mRNA LNP than siRNA LNP accumulation; modest differences were observed in the liver, kidney, and spleen (Figure 2.3b, S2.2). In the liver and kidney, the LNP formulations with less DSPE-PEG demonstrate greater accumulation, consistent with previous studies that observed higher liver

accumulation in formulations with short anchor PEG-lipids.[241,245] However, LNP accumulation in the spleen increases when formulations have more DSPE-PEG. In previous studies, PEGylation of nanoparticles has been shown to reduce uptake by the phagocytic Kupffer cells of the liver,[242] leaving a larger blood pool of nanoparticles that are available to accumulate in the spleen.[277] We similarly observed LNPs increased spleen accumulation concomitant with decreased liver accumulation.

2.3.3: PEG-lipid Anchor Length Influences mRNA LNP Activity after Systemic Administration in a Mouse Model of TBI
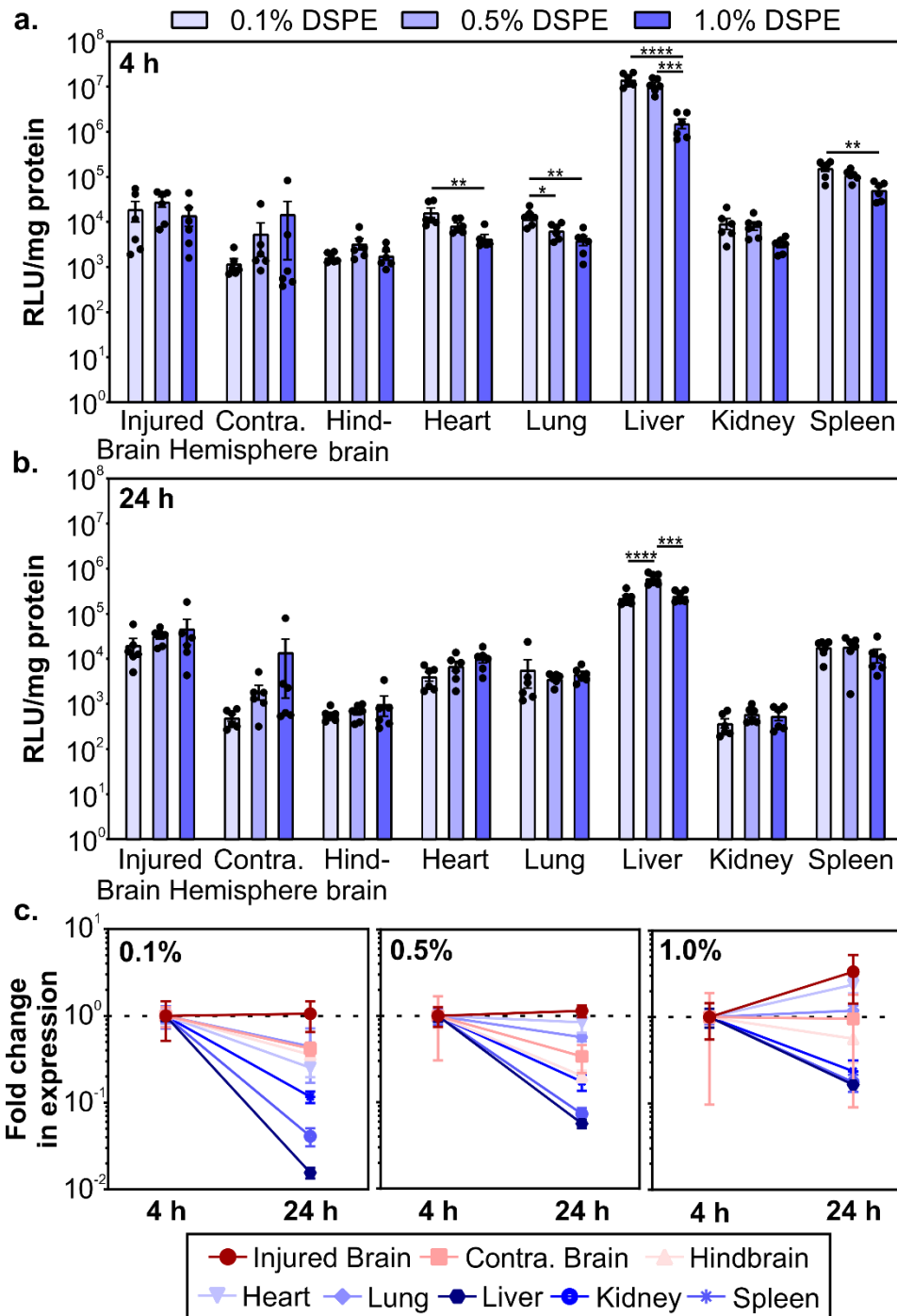
Figure 2.4: Transgene expression of mRNA LNPs in a mouse model of TBI as a function of PEG-lipid composition. Luciferase activity in organ homogenates normalized by total protein content after the injection of fLuc-mRNA LNPs at 4 (a) and 24 (b) hours post-injection. Luciferase expression in organ homogenate is compared with a one-way ANOVA with Tukey's post-test within each organ type (Mean ± S.E.M., n=6, *$p<0.05$, **$p<0.01$, ***$p<0.001$, ****$p<0.0001$). (c) Fold change in RFU/mg protein from 4 to 24 hours (normalized by the average of each organ at 4 hours) for 0.1%, 0.5%, and 1.0% DSPE-PEG LNPs (Mean ± S.E.M., n=6).

After determining how PEG-lipid anchor length affects mRNA LNP pharmacokinetics in a mouse model of TBI, we evaluated LNP activity. To do so, we used LNPs formulated with mRNA encoding firefly luciferase. We intravenously administered LNPs at 0.5 mg/kg 1 hour post-CCI and quantified the expression of luciferase at 4 and 24 hours post-administration by measuring luciferase activity in homogenized organs. LNPs mediated higher transfection efficiency in the injured brain hemisphere compared to the uninjured contralateral brain hemisphere (Figure 2.4a,b). Larger relative differences in transfection efficiency in injured vs. contralateral brain tissue were observed when LNPs were formulated with lower amounts of DSPE-PEG at both time points. In off-target organs, we observed a significant decrease in transfection efficiency in the heart, lung, liver, and spleen at 4 hours as DSPE-PEG content increased (Figure 2.4a). Transfection efficiency of LNPs in off-target organs differed from accumulation at 4 hours (Figure 2.3b); the heart and spleen had increased LNP accumulation as DSPE-PEG content increased, but transfection efficiency decreased. This may be due to the decreased cellular interaction of LNPs with more DSPE-PEG at the cellular level, which we observed in the transfection of cultured 293T cells (Figure 2.1g). Mui et al. previously established that the *in vivo* desorption rates of DMG-PEG and DSPE-PEG were 45% and 0.2% per hour respectively,[241] suggesting that the DMG-PEG is largely desorbed from LNPs while the majority of DSPE-PEG is still associated with LNPs 4 hours post-administration.

Luciferase expression could still be detected 24 hours post-administration (Figure 2.4b). Comparing the expression changes from 4 to 24 hours, we observe that luciferase expression levels in the injured brain hemisphere remain constant or increase, in contrast to the rapid loss of expression in the liver, kidney, and spleen (Figure 2.4c). Loss of expression over time in off-target organs is the most dramatic for formulations made with the lowest proportion of DSPE-PEG. Similar reductions in RES organ expression have previously been observed after the systemic administration of LNPs. Pardi et al. observed a faster reduction in liver expression over 24 hours compared to other organs and determined that the translation half-life of mRNA was 6.8 hours

49

after LNP intravenous administration, postulating that the liver turns over LNPs and/or mRNA more rapidly than other organs.[278] In mammalian cells, luciferase is known to have a short half-life of 2-3 hours,[279,280] so the expression of luciferase at 4 and 24 hours is expected to be due to active translation of mRNA from LNPs. Importantly, expression in the injured brain hemisphere has the least signal attenuation from 4 to 24 hours, indicating that LNPs could achieve greater expression duration in the brain compared to off-target organs. Tissue-dependent differences in translation half-lives after LNP administration have been demonstrated previously.[281] Interestingly, duration of expression between 4 and 24 hours improved with increasing proportions of DSPE-PEG in the LNP formulation (Figure 2.4c).

2.3.4: PEG-lipid Anchor Length Affects mRNA LNP Distribution after Convection Enhanced Delivery in a Healthy Brain
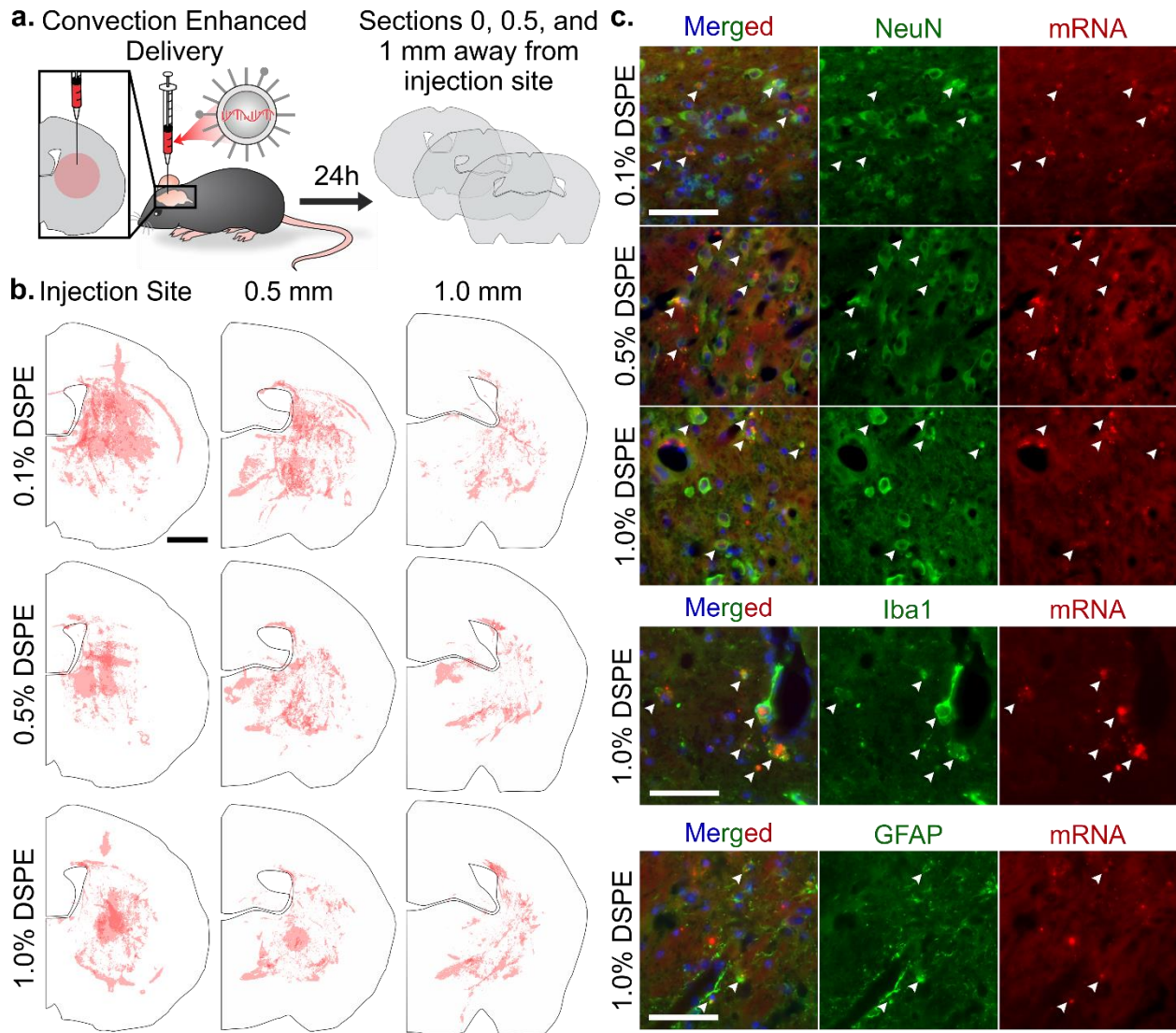
Figure 2.5: Analysis of mRNA LNP distribution and cell uptake after convection enhanced delivery. (a) Schematic of CED experiment and serial histological analysis. (b) Distribution of Cy5-labeled mRNA LNPs after CED administration in brain sections 0, 0.5, and 1 mm away from the injection site. Each hemisphere is an overlay of three injections. Scale = 1 mm. (c) Colocalization of Cy5-labeled mRNA LNPs after CED administration with neurons (NeuN), microglia (Iba1), and astrocytes (GFAP) in brain sections 0.5 mm away from the injection site. Scale = 50 μm.

Once systemically administered LNPs enter the brain across injured vasculature, they must diffuse through the tissue to transfect cells relevant to injury repair. To determine how PEG-lipid anchor length affects the diffusion and cellular interactions of LNPs in the brain microenvironment, we injected Cy5-labeled mRNA LNP formulations to the striatum of a healthy brain via convection enhanced delivery (CED) and imaged LNP distribution and cell association

in coronal brain slices collected at 0, 0.5, and 1 mm away from the injection site (Figure 2.5a). In tiled images, we detected LNPs at least 1 mm away from the injection site on the anterior-posterior axis and 1-1.5 mm away on the lateral axis (Figure 2.5b). In higher magnification images of brain slices 0.5 mm away from the injection site stained with cell type markers, we observed that all LNP formulations appeared to associate more with neurons and microglia than astrocytes (Figure 2.5c, S2.3). Consistent with our observations, Rungta et al. found that siRNA LNPs formulated with 1.5 mol% DMG-PEG associated robustly with neurons.[282] We also observed that LNPs formulated with 0.5 and 1.0 mol% DSPE-PEG distributed away from the injection site more robustly compared to 0.1% DSPE-PEG LNPs (Figure 2.5b). Consistent with our observation, Nance et al. previously established that model polystyrene nanoparticles with a dense surface modification of PEG can diffuse through the brain extracellular matrix more rapidly than unmodified polystyrene nanoparticles due to their neutral and non-interactive surface.[283] Previous work has shown that multiple properties impact nanoparticle diffusion in brain tissue, including surface chemistry.[156,225]

2.4: CONCLUSION

LNPs are a promising platform for non-viral gene therapy to treat TBI. Systemically administered LNPs offer a minimally invasive administration route for gene therapy in the injured brain tissue. Gene therapy could address pathogenic transcriptional pathways during secondary injury, such as dampening the production of pro-inflammatory cytokines[284,285] and reactive oxygen species,[286] or provide regenerative cues, such as the production of neuroprotective/neurotrophic growth factors.[287–290] Although LNP formulations have been established for delivery to the liver after systemic administration,[248] LNP design has yet to be explored for delivery in the context of the injured brain. In this study, we observed that LNPs demonstrated greater accumulation and mediated greater transgene expression in the injured brain hemisphere compared to the contralateral uninjured brain hemisphere, indicating that LNPs can passively accumulate into injured brain tissue by exploiting the temporary permeability of the BBB created by the injury. We

engineered LNPs with different compositions of DSPE(C18)-PEG and DMG(C14)-PEG and demonstrated that increasing the content of long anchor PEG-lipid extended circulation time after intravenous administration in a mouse model of TBI. Importantly, mRNA expression in injured brain tissue remained constant or increased when measured between 4 and 24 hours after administration, while off-target RES organ expression decreased ~10-fold, indicating that gene expression mediated by LNPs have greater duration in the brain compared to off-target organs. This effect was further pronounced with increasing content of DSPE-PEG in the formulation. Our work suggests that PEG-lipid anchor length is an important design parameter for LNPs and can be used to tune the pharmacokinetics and activity of LNPs in a mouse model of TBI. In future work, we plan to evaluate the levels and duration of expression that can be achieved for therapeutic proteins for the preservation and/or regeneration of brain tissue after injury.

2.5: MATERIALS AND METHODS

2.5.1: Lipid nanoparticle formulation and characterization

(6Z,9Z,28Z,31Z)-heptatriaconta-6,9,28,31-tetraen-19-yl-4-(dimethylamino) butanoate (DLin-MC3-DMA) was purchased from BioFine International Inc. 1,2-distearoyl-sn-glycero-3-phosphocholine (DSPC), 1,2-dimyristoyl-rac-glycero-3-methoxypolyethylene glycol-2000 (DMG-PEG-2000), 1,2-distearoyl-sn-glycero-3-phosphoethanolamine-N-[methoxy(polyethylene glycol)-2000] (ammonium salt) (DSPE-PEG-2000), 1,2-distearoyl-sn-glycero-3-phosphoethanolamine-N-[amino(polyethylene glycol)-2000]-N-(Cyanine 7) (DSPE PEG(2000)-N-Cy7) and cholesterol were purchased from Avanti Polar Lipids. mRNA LNPs were formulated with DLin-MC3-DMA:cholesterol:DSPC:PEG-lipid at a mole ratio of 50:38.5:10:1.5 and a lipid to RNA N/P of 5.6 (weight ratio of 20.7). siRNA LNPs were similarly formulated, with a lipid to RNA N/P of 3 (weight ratio of 11). To prepare LNPs, lipids in ethanol and oligonucleotides in 25 mM acetate buffer, pH 4.0 were combined at a flow rate of 1:3 in a PDMS staggered herringbone mixer.[94,95] Mixer channels were 200 by 100 μm, with herringbone structures 30 μm high and 50 μm wide. Immediately after formulation, 3-fold volume of PBS was added and LNPs were purified in 100

kDa MWCO centrifugal filters to less than 0.5% ethanol and sterile filtered. LNPs were stored in PBS at 4°C for up to 2 weeks or cryoprotected in 20 mM Tris with 10% sucrose (pH 7.4) and stored at -80°C for up to 1 month before use. Cryoprotectant buffer was exchanged into PBS after storage at -80 °C. LNP hydrodynamic diameter, polydispersity index, and zeta potential were measured by dynamic light scattering (Malvern NanoZS Zetasizer) in PBS and after incubation in 55% exosome free NCS in PBS at 37°C. The RNA content and percent encapsulation were measured with and without Triton X-100 using a Quant-it RiboGreen RNA Assay (Invitrogen) according to the manufacturer's protocol.

2.5.2: Lipid nanoparticle activity in 293T cell culture

293T cells (ATCC) were cultured in Dulbecco's Modified Eagle's Medium (Corning) supplemented with 10% fetal bovine serum and 2 mM GlutaMAX (Thermo Fisher Scientific) and plated at 25,000 cells/cm^2 in 96 well plates treated with 0.05 mg/mL poly-D-lysine overnight. Cells were cultured to 30-50% confluency before use in experiments. LNPs formulated with fLuc-mRNA at 1, 0.1, and 0.01 µg/mL were added to 293T cell culture through a media change and cultured for an additional 24 hours. fLuc-mRNA LNP treated cultures were lysed in Cell Lysis Reporter Reagent (Promega) and luciferase expression was quantified with the Luciferase Assay System (Promega).

2.5.3: Controlled cortical impact model of TBI

All animal experiments were approved by the University of California, San Diego Institutional Animal Care and Use Committee (IACUC). 8-week-old C57BL/6J female mice (Jackson Labs) were used in these experiments. Mice were put in a stereotaxic frame under 2.5% isoflurane anesthesia. A 5 mm diameter craniotomy was performed over the right cortex midway between lambda and bregma. The right cortex was injured with a 2 mm diameter stainless steel piston tip at a depth of 2 mm and a rate of 3 m/s using an ImpactOne (Leica Biosystems).

2.5.4: Pharmacokinetics of LNPs after systemic administration in a mouse model of TBI

One hour post-CCI, 0.75 mg/kg siRNA LNPs or 0.5 mg/kg mRNA LNPs were injected via the tail-vein and allowed to circulate for 4 hours. Blood was collected from the tail at 0, 5, 10, 15, 30, 60, 90, 120, and 240 minutes for blood half-life analysis. Four hours post-administration, mice were perfused with fixative and organs were harvested for imaging analysis. Fluorescent signals from Dy677-labeled siRNA and Cy7-labeled DSPE-PEG in the blood and organ samples were imaged with a LiCor Odyssey fluorescence scanner and quantified in ImageJ. Injured and contralateral brain signal were determined by integrating signal over the right and left brain hemispheres, respectively.

2.5.5: Expression of LNPs after systemic administration in a mouse model of TBI

One hour post-CCI, 0.5 mg/kg fLuc-mRNA LNPs were injected via the tail-vein and allowed to circulate for 4 hours or 24 hours. Organs were harvested at each experimental endpoint and the brain was separated into the injured hemisphere, contralateral hemisphere, and hindbrain. Organ tissue was lysed through 3 freeze/thaw cycles and homogenized with a Tissue-Tearor handheld homogenizer (BioSpec) in Reporter Lysis Buffer (Promega) until homogenous. Supernatants of homogenates were measured with a Luciferase Assay System (Promega) following manufacturer protocols. Protein content of supernatants was determined with a BCA assay following standard protocols.

2.5.6: Diffusion of LNPs through the healthy brain after CED administration

8-week-old female C57BL/6J mice (Jackson Labs) were secured in a stereotaxic frame under 2.5% isoflurane anesthesia. A 24-gauge needle was inserted through a 0.5 mm hole at a depth of 3 mm, 0.5 mm rostral and 1.75 mm right of bregma, and allowed to equilibrate for 1 minute. 1 µg of Cy5-labeled mRNA LNPs in 3.5 µL of PBS was injected at 0.5 µL/minute. The needle was left for 1 minute after injection to reduce backflow. 24 hours after injection, mice were perfused in 4% paraformaldehyde in PBS and brains were harvested for analysis by histology.

2.5.7: Histology

Triplicate 10 μm thick brain sections 0, 0.5, and 1 mm away from the needle tract were counterstained with Hoechst using standard protocols. Additional sections 0.5 mm from the needle tract were stained with mouse anti-NeuN (1:800, Millipore MAB377), rabbit anti-Iba1 (1:500, Wako 019-19741), and chicken anti-GFAP (1:500, Abcam ab4674) using standard protocols. Fluorescent images were obtained on a Nikon Eclipse Ti2 (Nikon Instruments Inc.).

2.5.8: Statistical Analysis

Statistical analysis was performed on GraphPad Prism 8 software, version 9.1.2. LNP accumulation and activity was analyzed by a one-way ANOVA with Tukey's post-test within each organ $p < 0.05$.

2.6 SUPPLEMENTAL INFORMATION
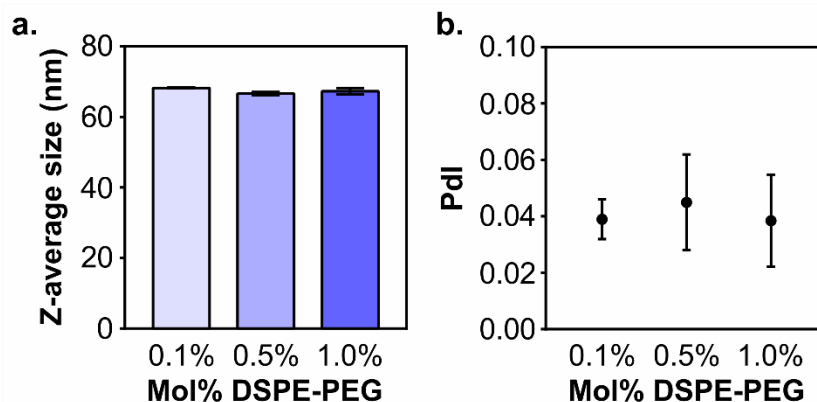
Supplemental Figure 2.1: Average size and polydispersity of nucleic acid LNPs with varying PEG-lipid compositions. DLS analysis of (a) Z-average size and (b) polydispersity (PdI) of LNP formulations used in the studies (n=2).
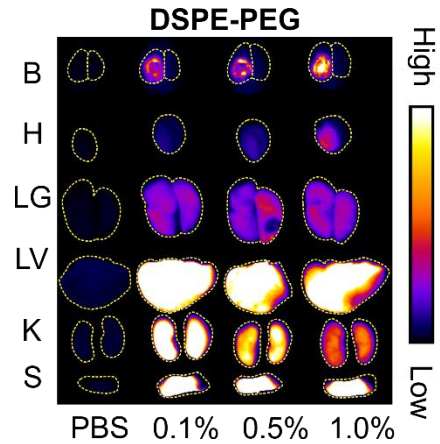
Supplemental Figure 2.2: Fluorescent surface scans of mRNA LNPs formulated with Cy7-labeled PEG-DSPE. Surface organ scan of representative organs of mRNA LNPs formulated with Cy7-labeled PEG-DSPE 4 hours post-administration in a mouse model of TBI. Triplicate scans are quantified in Figure 2.3.
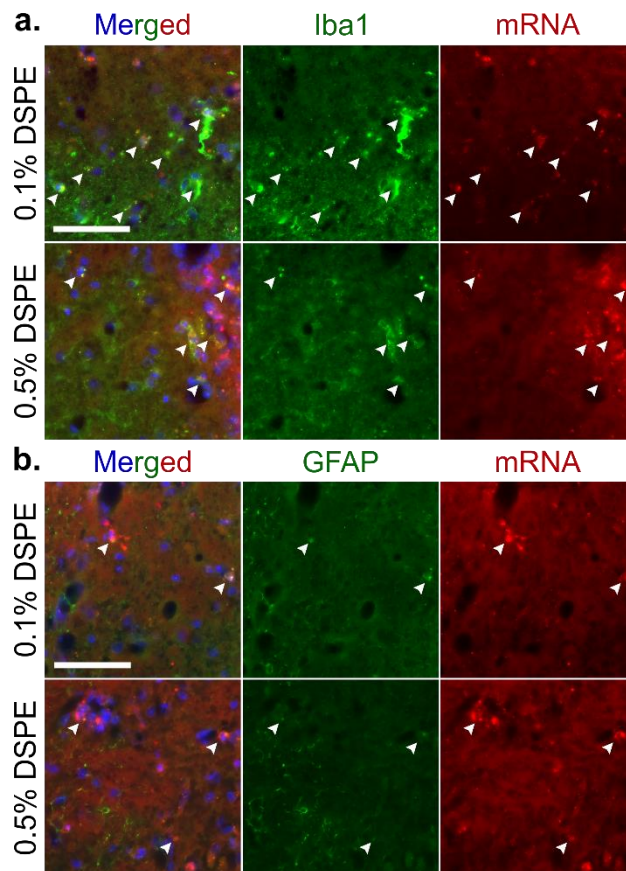
Supplemental Figure 2.3: Cell colocalization of mRNA LNPs after convection enhanced delivery. Colocalization of 0.1% and 0.5% DSPE-PEG mRNA LNPs formulated with labeled mRNA (red) with (a) microglia (Iba1) and (b) astrocytes (GFAP). Scale bar = 50 µm.

2.7 ACKNOWLEDGEMENTS

Chapter 2, in full, is currently being prepared for submission for publication of the material. Waggoner, Lauren E.; Miyazaki, Katelyn F.; Kwon, Ester J. It is coauthored with Miyazaki, Katelyn F. The dissertation author was one of the primary investigators and authors of this paper.

CHAPTER 3: Pharmacokinetic Analysis of Peptide-Modified Nanoparticles with Engineered

Physicochemical Properties in a Mouse Model of Traumatic Brain Injury

3.1: ABSTRACT

Peptides are used to control the pharmacokinetic profiles of nanoparticles due to their ability to influence tissue accumulation and cellular interactions. However, beyond the study of specific peptides, there is a lack of understanding in how peptide physicochemical properties affect nanoparticle pharmacokinetics, particularly in the context of traumatic brain injury (TBI). We engineered nanoparticle surfaces with peptides that possess a range of physicochemical properties and evaluated their distribution after two routes of administration; direct injection into a healthy mouse brain and systemic delivery in a mouse model of TBI. In both administration routes, we found that peptide-modified nanoparticle pharmacokinetics were influenced by the charge characteristics of the peptide. When peptide-modified nanoparticles are delivered directly into the brain, nanoparticles modified with positively charged peptides displayed restricted distribution from the injection site compared to nanoparticles modified with neutral, zwitterionic, or negatively charged peptides. After intravenous administration in a TBI mouse model, positively charged peptide-modified nanoparticles accumulated more in off-target organs, including the heart, lung, and kidneys, than zwitterionic, neutral, or negatively charged peptide-modified nanoparticles. The increase in off-target organ accumulation of positively charged peptide-modified nanoparticles was concomitant with a relative decrease in accumulation in the injured brain compared to zwitterionic, neutral, or negatively charged peptide-modified nanoparticles. Understanding how nanoparticle pharmacokinetics are influenced by the physicochemical properties of peptides presented on the nanoparticle surface is relevant to the development of nanoparticle-based TBI therapeutics and broadly applicable to nanotherapeutic design, including synthetic nanoparticles and viruses.

3.2: INTRODUCTION

Traumatic brain injury (TBI) affects more than 50 million people each year,[291] yet there are currently no treatments for TBI that support long-term brain health.[292,293] While the development of intravenously-delivered therapeutics for the treatment of TBI is desirable for their ease of use, their clinical translation has been challenged by the poor pharmacokinetic profiles of TBI drugs, including limited bioavailability in the brain.[200,202,294] Nanoparticle-based therapeutic systems are an attractive strategy for the delivery of drugs because as platform technologies, they have the potential to display pharmacokinetic profiles independent of their drug cargos. This independence is achieved through sequestering drug cargo in the core of the nanoparticle while controlling surface properties. Peptides are a promising class of molecules used to control nanoparticle surface properties and influence nanoparticle interactions with cells and tissues due to their biological activity and relatively small molecular size. Recent improvements in their good manufacturing practice (GMP) manufacture and chemistry to achieve long-term stability have made them tractable candidates for clinical translation.[295,296]

In the context of TBI, peptide-mediated active targeting has been used to increase tissue- and cell type-specific accumulation and retention. A clinical hallmark of TBI is damage to the vasculature, allowing for nanoparticle access to the injured brain tissue through passive accumulation across the dysregulated blood brain barrier (BBB).[113,222,297] Bharadwaj et al. investigated size-dependent passive accumulation of PEG-modified polystyrene nanoparticles 20, 40, 100, and 500 nm in diameter after systemic administration in a controlled cortical impact (CCI) model and observed a significant decrease in nanoparticle accumulation when diameters were greater than 100 nm.[220] Furthermore, nanoparticles can also be actively targeted to specific cell types or structures in the brain. For example, modification of nanoparticles with the rabies virus-derived peptide RVG[298,299] leads to neuronal tropism, as has been demonstrated for siRNA nanocomplexes and porous silicon nanoparticles delivered in mouse models of TBI.[113,300,301] Nanoparticle platforms engineered with CAQK, a targeting peptide that binds to upregulated

extracellular matrix components in the injured brain, improve delivery efficacy of siRNA and neuroprotective drug cargos to the site of injury after systemic administration.[297,302] While the pharmacokinetics of targeted nanomaterials are often compared with control materials made with biologically-inert, scrambled peptide sequences that share the same amino acid residues, and thus physicochemical properties,[297,298] beyond the study of these pairs or small groups of peptides, there is a gap in understanding how the physicochemical properties of peptides influence nanoparticle pharmacokinetics and accumulation in the injured brain after TBI.

Modifications of the engineered nanoparticle surface with polymers, proteins, and targeting moieties can impart different physicochemical properties onto the nanoparticle, such as charge and hydrophobicity, which in turn changes pharmacokinetics such as biodistribution and cell-specific interactions.[303] Recent efforts have been made to understand how the physicochemical properties of nanoparticles dictate biological interactions in the body, including the brain. In an evaluation of how engineered polymer surface properties changed nanoparticle tropism in brain cancer, Song et al. observed that nanoparticle surfaces with bio-adhesive aldehydes associated more readily with tumor cells and activated glial cells than nanoparticle surfaces with hydroxyl groups, indicating that nanoparticle surface chemistries influence their cellular interactions in the brain microenvironment.[304] In a systematic study of the effects of physicochemical properties in nanotherapeutic vaccine development, Yamankurt et. al. created a large library of ~1,000 spherical nucleic acid (SNA) nanostructures and determined that lipid core and antigen compositions with differing charges changed the efficacy of antigen release from the core nanoparticle and subsequent immune activation, demonstrating that charged components of nanoparticle therapeutics can affect their interactions with complex biological systems.[305] Biodistribution and passive tumor accumulation of micelles modified with anionic aspartic acid or cationic lysine residues mediated by the enhanced permeation and retention (EPR) effect were affected by nanoparticle charge in a mouse model of ovarian cancer.[226] Passive nanoparticle accumulation into the brain after TBI via the dysregulated BBB post-injury has been compared to

the EPR effect in solid tumors,[222,223,297,306] suggesting that the physicochemical properties of peptide-modified nanoparticles may also affect nanoparticle passive accumulation in the injured brain after TBI. To our knowledge, there has not yet been a systematic study of how the physicochemical properties of peptides displayed on nanoparticle surfaces affect the pharmacokinetics of nanoparticles in a mouse model of TBI.

In the presented work, we study how the physicochemical properties of peptide-modified nanoparticles contribute to their biodistribution *in vivo*. When nanoparticle surfaces were functionalized with PEG and reacted with peptides that display a range of physicochemical properties, we observed that nanoparticle surfaces adopted the physicochemical properties of the peptides. In order to evaluate the pharmacokinetics of these peptide-modified nanoparticles, material was directly injected into the healthy brain via convection enhanced delivery (CED) or injected intravenously in a mouse model of TBI. We observed that the biodistributions of peptide-modified nanoparticles were influenced by peptide charge in both tested models. Nanoparticles modified with basic peptides had restricted distributions in the brain after CED when compared with nanoparticles modified with acidic, zwitterionic, or neutral peptides. After systemic administration in a mouse model of TBI, nanoparticles modified with basic peptides had elevated off-target organ accumulation and short blood half-lives leading to a relative decrease in brain accumulation. Comparatively, nanoparticles modified with acidic, zwitterionic, or neutral peptides demonstrated increased blood residence and increases in relative accumulation in injured vs. uninjured brain tissue after systemic administration. Our results suggest that peptide physicochemical properties, such as charge and hydrophobicity, should be considered when engineering therapeutic nanoparticles with peptide modified surfaces. Peptides are promising tools to impart biological function onto nanoparticle therapeutics (e.g. targeting ligands, antigens for vaccines, receptor agonists) and furthering our understanding of how their physicochemical properties contribute to their biological interactions can broadly inform the design of nanoparticle-based therapeutics for pathologies such as TBI.

3.3: MATERIALS AND METHODS

3.3.1: Nanoparticle Surface Engineering and Characterization

Aminated 100 nm red or magenta fluorescent polystyrene nanoparticles (Magsphere, Inc.) were reacted with an excess of 5 kDa NHS-PEG-maleimide:NHS-PEG-methoxy (Laysan Bio, Inc.) at molar ratios 0:1, 1:10, 1:4, 1:1, and 1:0 in PBS at ~80,000 total PEG per nanoparticle for 30 minutes. PEG-modified nanoparticles were immediately purified with a Zeba Spin Desalting Column™ (Thermo Scientific™) with a 40 kDa size cut-off and reacted with cysteine-containing peptides (LifeTein, LLC) for 2-3 hours before being purified of excess peptide. FAM-labeled peptide was used for absolute quantification of peptide modification. Nanoparticles used in *in vivo* experiments were additionally reacted with a near-infrared reporter VivoTag-750® (VT-750®) (PerkinElmer) before PEG modification. Purified nanoparticles were stored at 4 °C until use.

Hydrodynamic diameters and zeta potentials were measured with a Zetasizer Nano ZS (Malvern Panalytical) in phosphate buffered saline (PBS) or after a 30-minute incubation at 37˚C in 10% exosome-free newborn calf serum (NCS) in PBS. Exosomes were removed using a 100 kDa MWCO centrifugal filter (Microcon). Zeta potential was measured using the diffusion barrier method [307]. Nanoparticle and peptide concentrations were determined via absorbance/fluorescence compared to known nanoparticle and peptide standards using a Spark Multimode Microplate Reader (Tecan Trading AG, Switzerland).

Surface charge was also evaluated with a Rose Bengal gel shift assay. Equi-volumes of 0.25 mg/mL Rose Bengal dye and 1 mg/mL nanoparticles were incubated in PBS at room temperature for 1 hour. For serum conditions, nanoparticles were incubated in 10% NCS in PBS prior to the addition of dye. Samples were run on a 2.5% agarose gel to analyze free Rose Bengal dye that did not adsorb to the nanoparticle surface. Gels were imaged on a BioRad scanner and densitometric analysis of the gels was done in ImageJ.

3.3.2: Convection Enhanced Delivery of Peptide-modified Nanoparticles

All animal experiments were approved by the University of California, San Diego Institutional Animal Care and Use Committee (IACUC). 8-week-old female C57BL/6J mice (Jackson Labs) were secured in a stereotaxic frame under 2.5% isoflurane anesthesia and a 0.5 mm hole was drilled 0.5 mm rostral and 1.75 mm right of bregma. A 24-gauge needle was inserted through the hole at a depth of 3 mm and allowed to equilibrate for 30 seconds. Mice were randomly assigned to 8 groups (n=3) and 0.25 mg of peptide-modified nanoparticles were injected in 5 µL of PBS at 0.5 µL/minute and allowed to equilibrate for 30 seconds before removal of the needle. Brains were harvested after perfusion with fixative 6 hours post-injection to allow time for nanoparticle transport and cellular association. Cellular accumulation of polymeric nanoparticles administered via CED has been previously shown to increase between 4 hours and 24 hours.[304]

3.3.3: Immunohistochemistry and Fluorescence Imaging

Brains were equilibrated in 30% w/v sucrose overnight and frozen in OCT (Tissue-Tek). 10 µm thick frozen coronal sections were taken at the site of injection and 0.5 mm and 1 mm rostral from the needle tract. Sections were counterstained with Hoechst and tiled images were acquired on a Nikon Eclipse Ti2 (Nikon Instruments Inc.). Nanoparticle fluorescence was thresholded to correct for background fluorescence with ImageJ and a map of the signal from the three replicates was overlaid and the total area quantified for each replicate.

3.3.4: Blood Clearance and Biodistribution in a Mouse Controlled Cortical Impact Model

8-week-old female C57BL/6J mice (Jackson Labs) were secured in a stereotaxic frame under 2.5% isoflurane anesthesia and a 5 mm diameter craniotomy was performed 2.0 mm caudal and 2.0 mm right of bregma. Controlled cortical impact (CCI) was performed with a 2 mm diameter stainless steel piston tip at 3 m/s to a depth of 2 mm using an ImpactOne (Leica Biosystems). Mice were randomly assigned to 8 groups (n=5 for biodistribution studies, n=3 for blood half-life studies) and 40 mg/kg of control or peptide-modified nanoparticles were delivered via a tail-vein injection 6 hours after injury. Control animals were injured and received PBS. Blood was collected from the tail-vein at 0, 5, 10, 15, 30, and 60 minutes after injection in 10 µL heparinized tubes

(Drummond™). Organs were collected after perfusion with PBS 1 hour post-injection to study nanoparticle accumulation in organs after intravenous administration. Previous studies have established organ accumulation of nanoparticles 1 hour after systemic administration in TBI models.[220,308]

3.3.5: Blood and Tissue Analysis

Tissues were homogenized at 150-250 mg tissue per mL of Laemmli buffer with 100 mM dithiothreitol (DTT) and 2 mM ethylenediaminetetraacetic acid (EDTA) with a Tissue-Tearor handheld homogenizer (BioSpec) and heated to 90°C for 10 minutes. Peptide-modified nanoparticle concentrations in tissue homogenate and blood samples were quantified based on fluorescence of VT-750® compared to known nanoparticle concentrations using a Li-Cor Odyssey (Li-Cor Biosciences). Whole tissues were scanned for surface fluorescence before being processed for tissue homogenization.

3.6.6: Statistical analysis

Statistical analysis was performed on GraphPad Prism 9.1.2 software. Biodistribution of nanoparticles in each individual organ group was analyzed by one-way ANOVA with Bonferroni post-test.

3.4: RESULTS

3.4.1: Synthesis of Peptide-modified Nanoparticles

Fluorescent polystyrene nanoparticles with aminated surfaces were used as a model nanoparticle for peptide modification based on ease of modification and fluorescence to allow for quantitative measurements of nanoparticle concentrations. Nanoparticles with 100 nm diameters were chosen based on previous studies that demonstrate nanoparticle accumulation in brain tissue after intravenous delivery in TBI animal models[219,220,222] and the similarity in size to existing FDA-approved therapeutics, such as Doxil® and ONPATTRO®.[207,309] The aminated surfaces of the nanoparticle were fully reacted with an excess of 5 kDa NHS-PEG; PEG is a polymer used in many nanoparticle applications, including Doxil® and ONPATTRO®.[207,310] The number of

peptides per nanoparticle was quantified by synthesizing nanoparticles with various feed ratios of methoxy- to maleimide-terminated PEG followed by a reaction with a cysteine-bearing, fluorescein-labeled peptide to the distal end of the maleimide-terminated PEG (Figure 3.1a). Absolute numbers of peptide modified to the nanoparticle surface were quantified by measuring the absorbance of fluorescein from resulting nanoparticles compared to peptide standards (Figure 3.1b). We observed a linear correlation between increasing proportion of maleimide-terminated PEG and number of peptides (r^2=0.96). We calculated that the resulting nanoparticles had a high PEG grafting density of 1.1 PEG/nm^2 and ~18,000 peptides per nanoparticle when 50% of PEG chains were peptide-modified. In order to create peptide-modified nanoparticles that represent a range of physicochemical properties, the following peptide sequences were conjugated to 50% peptide-modified nanoparticles and used for subsequent studies: RRRRRRRRR (R9), KKKKKKKKK (K9), EEEEEEEEE (E9), EKEKEKEKE (EK4E), GGSGGSGGS (GGS3), and GGLGGLGGL (GGL3) (Figure 3.1c). Charge and hydrophobicity are physicochemical properties that influence pharmacokinetics and interactions with cell types and can be considered as universal design parameters when engineering therapeutic nanomaterials.
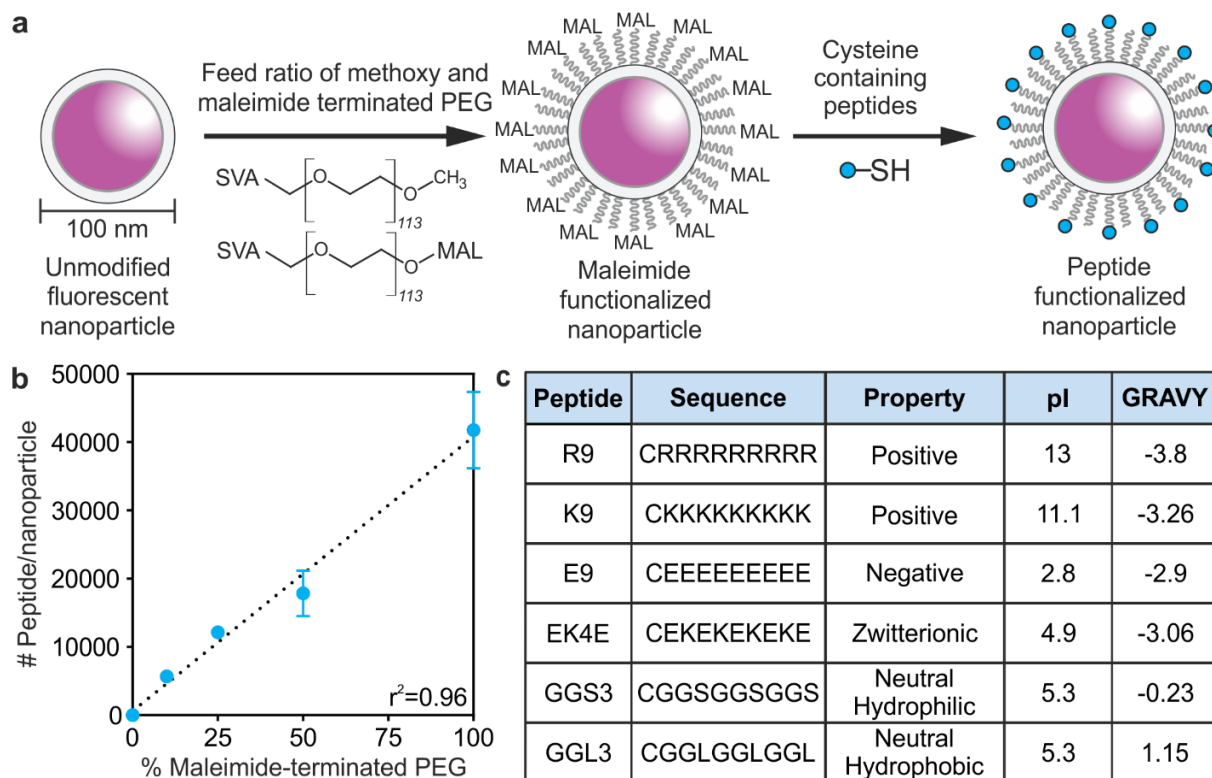
Figure 3.1: Synthesis of peptide-modified nanoparticles. (a) Schematic of nanoparticle synthesis. Aminated nanoparticles were reacted with feed ratios of NHS-PEG and NHS-PEG-maleimide to form PEG-modified nanoparticle surfaces. Linear peptides with N-terminal cysteines were conjugated to the maleimide-terminated PEG. (b) Quantification of the number of peptides conjugated to nanoparticle surfaces with 0-100% maleimide-terminated PEG (n=3, mean ± SD). (c) Peptides used in this study with their sequences, designed physicochemical properties, calculated isoelectric points and GRAVY scores.

3.4.2: Physicochemical Characterization of Peptide-modified Nanoparticles

The physicochemical properties of peptide-modified nanoparticles were characterized by dynamic light scattering (DLS) and Rose Bengal adsorption. The hydrodynamic diameter of unmodified polystyrene nanoparticles was 95 ± 1.5 nm and surface modification with PEG and peptide increased diameters ~20 nm (Figure 3.2a), consistent with the ~10 nm per molecule Flory radii of 5 kDa PEG in a brush conformation and linear peptide.[311] Peptide conjugation imparted the expected characteristic charges of each peptide onto the surface of the nanoparticle; nanoparticles modified with basic peptides R9 and K9 displayed positive zeta potentials of 3.07 and 3.52 mV respectively, and nanoparticles modified with acidic peptide E9 displayed a negative zeta potential of -2.80 mV (Figure 3.2b). Nanoparticles modified with zwitterionic EK4E peptide

also displayed a negative zeta potential of -2.09 mV, likely due to the additional terminal glutamic acid residue. Nanoparticles modified with neutral peptides GGS3 and GGL3 displayed near neutral zeta potentials of -0.44 mV and -0.99 mV, respectively. Zeta potential measurements of peptide-modified nanoparticles compared to control nanoparticles modified with PEG and no peptide (0.01 mV) and unmodified aminated polystyrene nanoparticles (14.6 mV) indicate successful PEG modification and surface potentials that reflect the properties of the respective conjugated peptides. Rose Bengal adsorption assays have been previously used to characterize nanoparticle hydrophobicity and charge.[312,313] We developed a Rose Bengal gel shift assay as an additional analysis of the peptide-modified nanoparticles. Nanoparticle interactions with Rose Bengal are largely driven by electrostatic interactions, due to the negative charge of Rose Bengal in experimental conditions.[313] R9- and K9-modified nanoparticles formed interactions with 72.0% and 63.2% of Rose Bengal dye, compared to the control nanoparticle, which interacted with 21.7% of the dye (Figure 3.2c), further confirming the basic character of R9- and K9-modified nanoparticles.

The adsorption of proteins onto nanoparticle surfaces or 'protein coronas' in biological contexts has been an active area of research due to the impact of the protein corona on the biological activity of nanoparticle.[314] Recent research has shown that the charge, hydrophobicity, size, and morphology of nanoparticles affects the composition of the protein corona.[315–319] In order to understand how protein adsorption modulates the physicochemical properties of the peptide-modified nanoparticles, we repeated characterization after incubation of nanoparticles in 10% serum for 30 minutes at 37°C. Serum adsorption caused small changes in the hydrodynamic diameter of the nanoparticles (Figure 3.2d). After serum adsorption, the zeta potential of the peptide-modified nanoparticles consistently shifted to become slightly more negative by 0.33-1.95 mV (Figure 3.2e). Additionally, serum adsorption decreased nanoparticle interactions with Rose Bengal dye, consistent with our observed decreases in zeta potential measurements (Figure 3.2f).
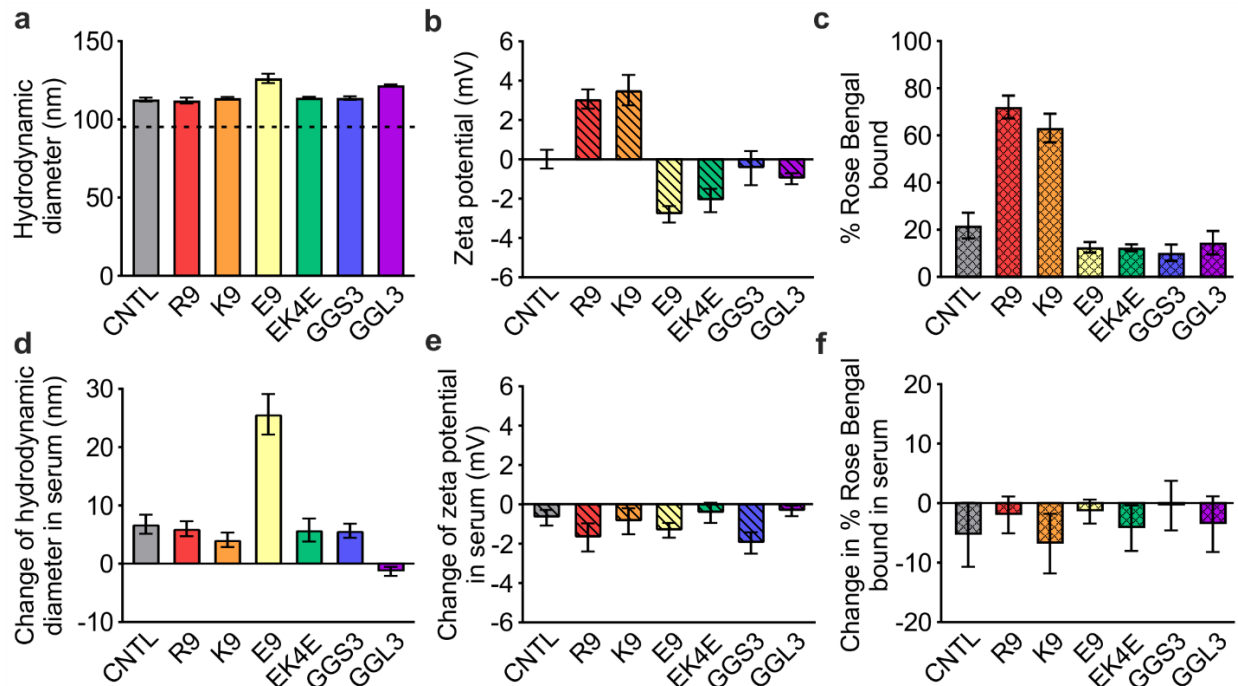
Figure 3.2: Characterization of peptide-modified nanoparticles. (a) Hydrodynamic diameter, (b) zeta potential, and (c) percent Rose Bengal interaction with peptide-modified nanoparticles measured in PBS. (d-f) Changes in hydrodynamic diameter, zeta potential, and Rose Bengal interaction after serum adsorption to nanoparticles (n=3, mean ± SD).

3.4.3: Peptide-modified Nanoparticle Distribution in the Healthy Living Brain

We next sought to understand the distribution of peptide-modified nanoparticles in the complex microenvironment of the healthy living brain. Peptide-modified nanoparticles were administered via CED directly into the striatum of a healthy mouse brain, therefore bypassing the BBB. We studied the distribution of nanoparticles away from the injection site six hours after injection to evaluate their relative mobility in the brain microenvironment. Coronal sections were taken at the injection site and 0.5 mm and 1 mm rostral from the injection site to ensure we were observing nanoparticles that had distributed away from the needle tract. We observed that R9- and K9-modified nanoparticles were not widely distributed in the analyzed brain section (Figure 3.3, S3.1), indicating that nanoparticles modified with positively charged peptides had limited mobility from the injection site. In contrast, nanoparticles modified with neutral, negative, or zwitterionic peptides distributed farther from the injection site after CED.

69
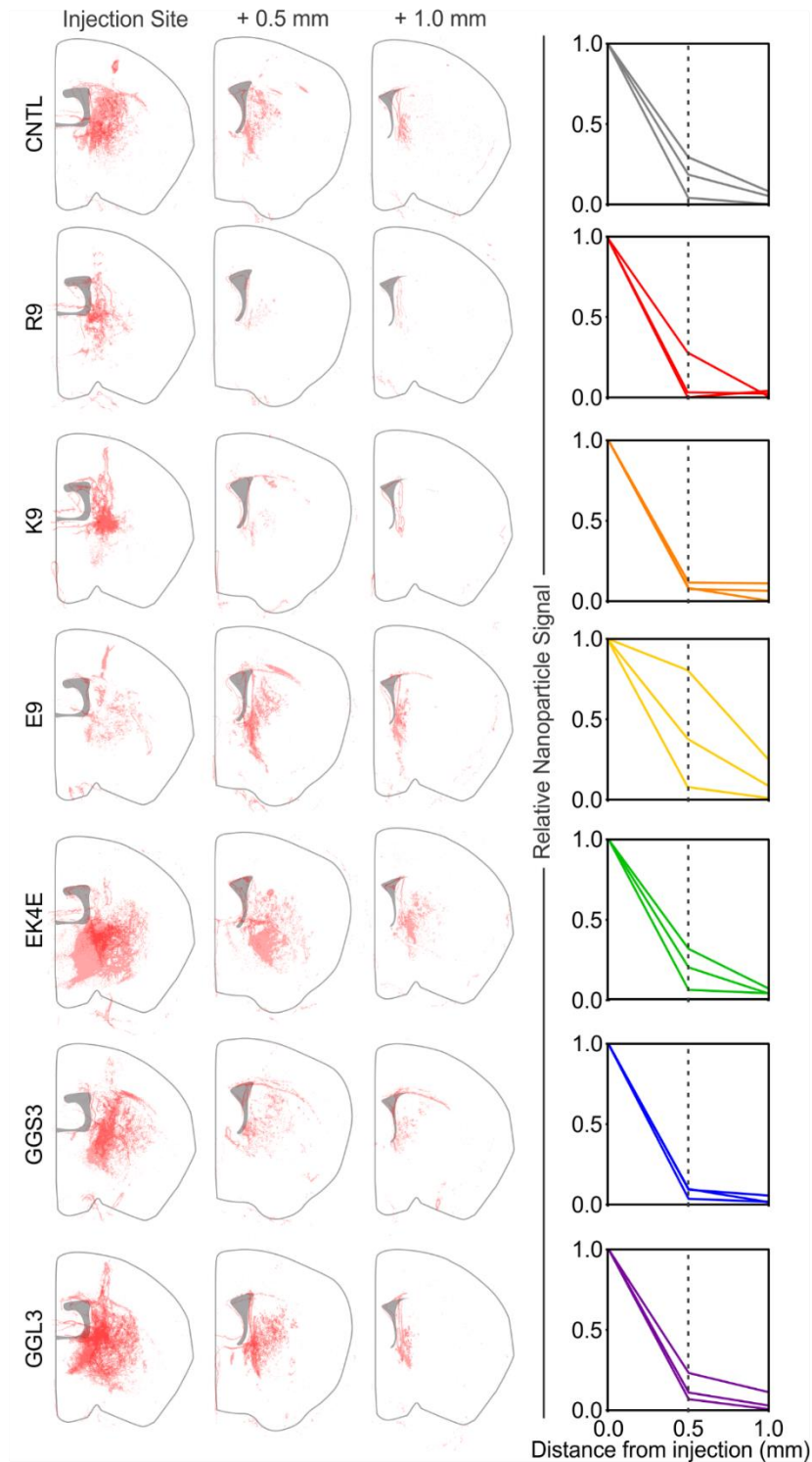
Figure 3.3: Peptide-modified nanoparticle distributions in a healthy brain. Distributions of peptide-modified nanoparticles after CED at 0, 0.5, and 1 mm away from the injection site (n=3, each replicate depicted in red at 30% opacity). Distributions are overlaid on a schematic of a brain hemisphere. Right, relative areas of detected nanoparticle signal of peptide-modified nanoparticles as a function of distance from injection.

3.4.4: Pharmacokinetics of Peptide-modified Nanoparticles in a Mouse Model of TBI

We next determined the effects of varying physicochemical properties of peptide-modified nanoparticles on nanoparticle pharmacokinetics after systemic delivery in a mouse model of TBI (Figure 3.4a). The right hemisphere of the brain was injured with a CCI and mice were administered 40 mg/kg of nanoparticles or an equivalent volume of PBS via the tail-vein 6 hours post-injury. In order to evaluate the blood half-life of the peptide-modified nanoparticles, blood samples were collected at 0, 5, 10, 15, 30, and 60 minutes after administration and nanoparticles were quantified based on their fluorescence signal (Figure 3.4b). The nanoparticles surface-modified with the zwitterionic peptide, EK4E, had the longest blood half-life of 6.1 minutes. The neutral nanoparticles, modified with GGL3 or GGS3, and the control nanoparticle had blood half-lives of 5.8, 3.3, and 3.1 minutes, respectively. Nanoparticles with the largest absolute zeta potential values (K9-, R9-, and E9-modified nanoparticles) comparatively had the shortest blood half-lives between 2.4-2.5 minutes. K9- and R9-modified nanoparticle blood concentrations rapidly reached near-zero after 15 minutes, while the zwitterionic, neutral, and negatively charged nanoparticles maintained detectable concentrations in the blood up to the 60 minutes of measurement.
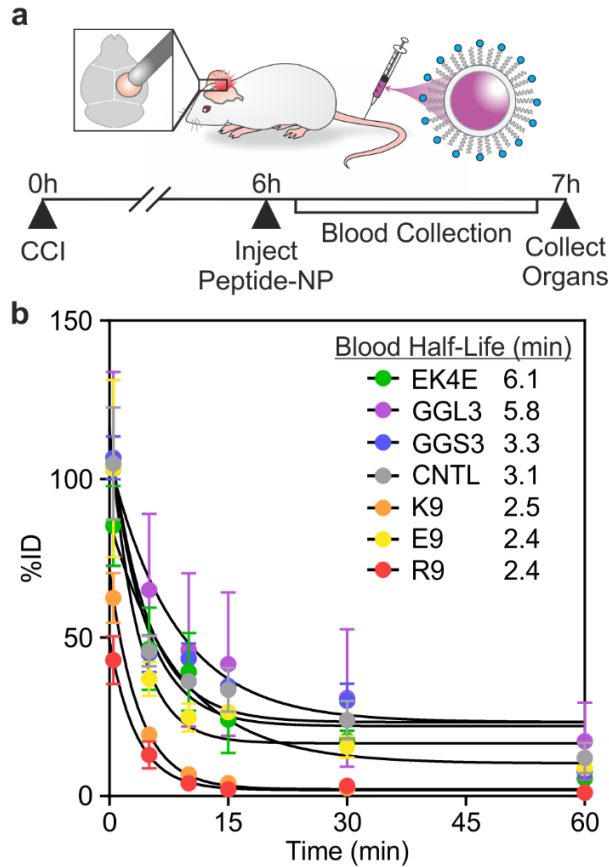
Figure 3.4: Blood half-lives of peptide-modified nanoparticles in a mouse model of TBI. (a) Schematic and timeline of CCI, systemic peptide-modified nanoparticle administration, blood collection, and organ collection. (b) Percent injected dose of peptide-modified nanoparticles remaining in the blood at 0, 5, 10, 15, 30, and 60 minutes after administration with calculated blood half-lives (n=3, mean ± SEM).

Nanoparticle biodistribution was measured in homogenized tissue samples for quantification of bulk nanoparticle accumulation (Figure 3.5). Intact organs were also imaged prior to homogenization to provide spatial information of nanoparticle distribution on the surface of organs (Figure 3.5b, c, S3.2). The majority of observed signal from the accumulated nanoparticles in the brain is localized to the injured hemisphere (Figure 3.5c-e, S3.2). Neutral, zwitterionic, and negatively charged nanoparticles demonstrate more accumulation in the injured brain than positively charged nanoparticles. Additionally, R9- and K9-modified nanoparticles demonstrated increased accumulation in off-target organs such as the heart, lung, and kidneys compared to control, neutral, zwitterionic, or negatively charged nanoparticles (Figure 3.5a). Liver accumulation was similar for all nanoparticles.
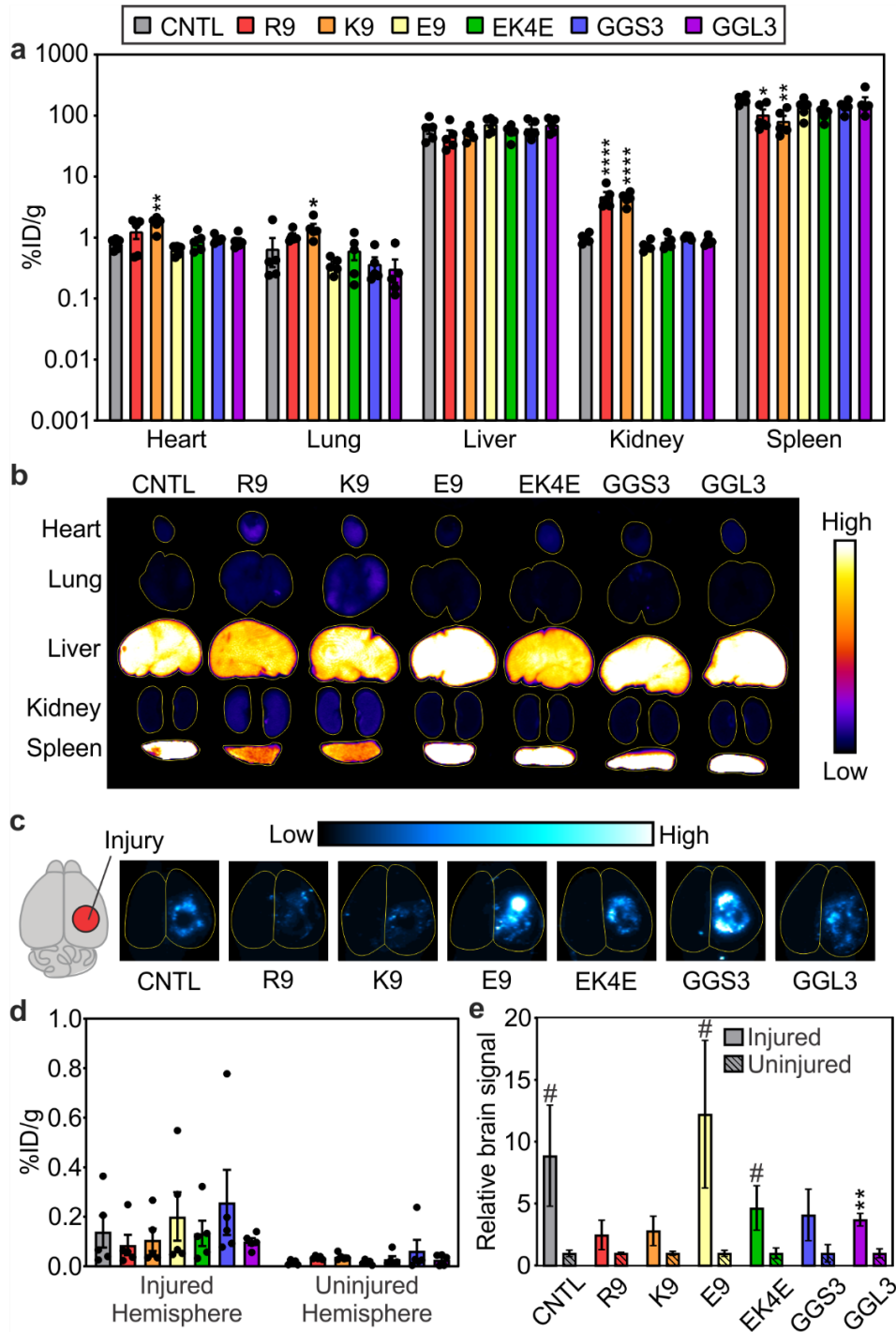
Figure 3.5: Biodistribution of peptide-modified nanoparticles in a mouse model of TBI. (a) Accumulation of peptide-modified nanoparticles in dissociated organs 1 hour after administration and (b) representative surface fluorescent images (n=5, mean ± SEM; One-way ANOVA with Bonferroni post-test compared to control nanoparticles, *p<0.05, **p<0.01, ****p<0.0001). (c) Representative surface fluorescent images and (d) accumulation of peptide-modified nanoparticles in dissociated brain tissue, separated by injured and contralateral hemispheres, 1 hour after administration. (e) Relative amounts of nanoparticle signal in the injured vs. contralateral uninjured hemisphere (n=5, mean ± SEM; two-tailed t-test between injured and uninjured groups, #p<0.1, **p<0.01).

3.5: DISCUSSION

Nanoparticle interactions with biological environments have been engineered via surface peptide modification across multiple nanoparticle platforms, such as lipid nanoparticles,[320–322] viruses,[323] polymer nanoparticles,[324,325] and porous silicon nanoparticles.[300,301] While peptides have been studied individually in these contexts, there remain gaps in understanding how the physicochemical properties of the peptides affect nanoparticle pharmacokinetics. Furthermore, to our knowledge, this study is the first analysis of peptide-modified nanoparticle pharmacokinetics based on physicochemical properties in TBI models. We synthesized PEG-modified nanoparticles displaying peptides with characteristic charge and hydrophobicity (Figure 3.1a, c). We achieved a high density of PEG grafting on the surface of the nanoparticle (1.1 PEG/ nm^2); nanoparticles with PEG grafting densities ≥0.8 PEG/nm^2 have been reported to avoid macrophage uptake *in vitro* and have increased blood half-lives *in vivo* [326] Peptide-modified nanoparticle physicochemical properties were confirmed to reflect the properties of the designed peptides when characterized by DLS and a Rose Bengal gel shift assay (Figure 3.2a, b, c). After pre-incubation with serum, peptide-modified nanoparticles had minimal increases in hydrodynamic diameter, a slight negative shift in zeta potential, and less interaction with Rose Bengal compared to their characterization in PBS (Figure 3.2d, e, f). PEG-modified nanoparticle surfaces have been shown to sterically hinder protein adsorption by repelling attachment with a hydrated shell that is formed in contact with biological fluids, leading to the formation of a minimal protein corona [327,328]. The negative shift in zeta potential after serum adsorption we observed is supported by the majority of serum proteins being negatively charged, such as albumin, immunoglobulin, fibrinogen, and lipoproteins [258]. Overall, peptide-modified nanoparticles displayed the expected physicochemical properties of their respective peptide, which were minimally affected by the adsorption of serum proteins.

Next, we studied the distribution profiles of peptide-modified nanoparticles in a healthy brain after CED to understand how the physicochemical properties of peptide surfaces affect their

interactions with brain tissue. Nance et al. previously studied the diffusion of 40-200 nm polystyrene nanoparticles surface modified with a dense layer of PEG in the extracellular space of murine and human brain tissues [283]. It was observed that nanoparticles with diameters up to 114 nm were able to diffuse through the brain, while diffusion was limited for particles 200 nm in diameter. Therefore, our objective was to understand how peptide physicochemical properties affected the transport of ~100 nm nanoparticles in the brain microenvironment. In coronal brain sections taken at the injection site and 0.5 mm and 1 mm rostral from the injection site, we observed that positively charged nanoparticles were less distributed through the brain tissue than neutral, zwitterionic, or negatively charged nanoparticles (Figure 3.3, S3.1). These observations are supported by previous findings that positive surface charge restricts liposome distribution in the brain microenvironment administered via CED compared to liposomes with negative and neutral surface charges [329]. The limited mobility of positively charged nanoparticles away from the needle tract is likely due to their interactions with cells and extracellular matrix around the injection site, as positively charged nanoparticles can interact with negatively charged cell membranes [275,330–332]. A similar phenomenon has also been described for the distribution of antibodies in a solid tumor; in the so-called "binding-site barrier", high affinity antibodies have limited mobility and penetration past the immediate cell layers adjacent to vasculature due to high affinity binding [333]. This also suggests that the reduced cellular association of neutral, zwitterionic, and negatively charged nanoparticles could contribute to increased nanoparticle distribution throughout the brain microenvironment, as their movement is less restricted by interactions with cells.[334]

In particular, we studied how peptide physicochemical properties affect pharmacokinetics of nanoparticles in an animal model of TBI. The CCI injury model is a well-characterized mouse model for TBI that results in tissue loss at the injury site and transient increase in BBB permeability caused by vascular dysregulation following the injury.[215–217] Although the extent of BBB dysregulation after injury is variable, significant nanoparticle accumulation within the brain has been previously reported for surface modified and unmodified nanoparticles up to ~120 nm in

hydrodynamic diameter when administered intravenously within 24 hours post-injury.[219,220] Peptide-modified nanoparticles were administered via the tail-vein 6 hours after CCI injury and blood samples were taken at time points over 1 hour after injection to measure nanoparticle blood half-life (Figure 3.4a). Nanoparticles with zwitterionic peptide surfaces had the longest blood-half life, followed by nanoparticles with neutral peptide surfaces and finally nanoparticles with charged peptide surfaces (Figure 3.4b). Previous studies have established that zwitterionic nanoparticles repel serum protein adsorption, increasing their blood half-life compared to charged nanoparticles.[227,335,336] Additionally, nanoparticles with greater absolute zeta potentials, E9-, K9-, and R9-modified nanoparticles, demonstrated shorter blood half-lives *in vivo* compared to more neutrally charged nanoparticles, likely due to their increased protein opsonization and subsequent macrophage uptake.[231,275,337,338]

Organ biodistribution was established by measuring the fluorescence signal of nanoparticles in dissociated tissue and the percent injected dose was calculated per gram of tissue (Figure 3.5a, d). Peptide-modified nanoparticle accumulation in the brain was more apparent in the injured hemisphere compared to the contralateral hemisphere (Figure 3.5c-e, S3.2), consistent with previous studies demonstrating that passive targeting of nanoparticles into the injured brain is localized to the site of injury.[113,220,222] Fluorescent imaging of the brains also show the localized accumulation of the peptide-modified nanoparticles proximal to the injury site, suggesting that accumulation is due to passive accumulation via the injured vasculature (Figure 3.5c, S2). Peptide modification of nanoparticles led to modest increases or reduced accumulation in the injured brain compared to the PEG-modified control nanoparticles without peptide (Figure 3.5d-e). Previous studies have demonstrated that passive accumulation of nanoparticles is dependent on reduced accumulation in off-target tissues,[231,232,339] supporting the observation that cationic peptide-modified nanoparticles have less brain accumulation. However, the use of peptides for ligand targeting is commonly implemented in nanoparticle therapeutics to actively target cell types and biomolecules in the brain. Therefore, it is important to understand how the

physicochemical properties of peptides may affect nanoparticle biodistribution and brain accumulation in models of TBI.

Positively charged peptide-modified nanoparticles have lower brain accumulation and elevated heart, lung, and kidney accumulation compared to neutral, zwitterionic, or negatively charged peptide-modified nanoparticles (Figure 3.5c-e). In previous biodistribution studies comparing charged nanoparticles, high absolute zeta potential and positive charge increased non-specific nanoparticle tissue accumulation.[226,340,341] Accumulation of positively charged peptide-modified nanoparticles in off-target organs also likely contributed to their short blood half-lives and reduced passive accumulation in the injured brain. Similar pharmacokinetic profiles were described in a previous study of cell penetrating peptides with basic character, where authors observed peptides localized to capillary-rich off-target organs, such as the liver, spleen, lung, and kidneys, and had short blood half-lives.[342] Positively charged R9- and K9-modified nanoparticles have higher non-specific accumulation in cells and tissues, and previous studies have demonstrated that positively charged nanoparticles are more cytotoxic than neutral or negatively charged nanoparticles,[343–345] indicating that nanoparticle toxicity should be carefully considered when designing nanoparticles with positively charged peptides. Although the extent of nanoparticle accumulation in injured brains exhibited a wide range due to the known variability of TBI animal models,[346] nanoparticles modified with zwitterionic, neutral, or negatively charged peptides had modest increases in injured brain accumulation compared to nanoparticles modified with cationic peptides (Figure 3.5c-e). This effect may be due to the reduced accumulation of neutral, negative, and zwitterionic peptide modified-nanoparticles in off-target organs (Figure 3.5a) and improved blood retention when compared to R9- and K9-modified nanoparticles (Figure 3.4b). Previous research supports increased nanomaterial blood half-life with increased passive injury accumulation in TBI models due to the EPR-like effect in the injured tissue.[219,222,347] Nanomaterials engineered to have long blood half-lives, such as PEG-modified materials, are

77

also well-established nanomedicine platforms in cancer research due to their greater passive accumulation in solid tumors.[231,232]

Interestingly, although the E9-modified nanoparticles have a shorter blood half-life comparable to the R9- and K9-modified nanoparticles, their brain and organ accumulation is similar to the accumulation of nanoparticles modified with zwitterionic and neutral peptides (Figure 3.4b, 3.5a, b). We observed a rapid decline in blood concentration of E9-modified nanoparticles within 10 minutes of circulation, followed by a residual blood retention that was elevated compared to R9- and K9-modified nanoparticles. At the 60-minute timepoint, E9-modified nanoparticles were comparatively 8-times more concentrated in the blood compared to basic peptide-modified nanoparticles, with 8.8% of the injected dose remaining in circulation. Interpretation of this data through a nonlinear clearance model, in which nanoparticles are sequestered from the blood by a limited number of available clearing sites, suggests that E9-modified nanoparticles may be saturating their binding sites in the reticuloendothelial system (RES) within 10 minutes, reducing nanoparticle elimination for the remaining circulation time. Similar effects have been observed in cancer research using RES blockades, in which decoy nanoparticles are injected prior to nanoparticle treatment to sequester plasma opsonins and saturate binding sites in off-target organs.[348] RES blockades have successfully increased nanoparticle blood retention and tumor accumulation for nanoparticles using active and passive targeting techniques.[348–350] Liver blockades have also been achieved by administering extremely large nanoparticle doses to saturate available binding sites while the nanoparticles are in circulation; Ouyang et al. delivered high doses of PEG-modified gold nanoparticles intravenously to elevate passive tumor accumulation and blood retention.[351] Despite rapid initial depletion of E9-modified nanoparticles from the blood, they appear to have less binding site reservoirs in the heart, lung, and kidney compared to basic peptide-modified nanoparticles (Figure 3.5a), likely leading to increased passive accumulation observed in the injured brain (Figure 3.4b).

3.6: CONCLUSION

Engineering nanotherapeutics is a promising approach for the development of TBI treatments with improved pharmacokinetics. Recent research has demonstrated that nanoparticles modified with targeting peptides, such as RVG and CAQK, improve accumulation in the injured brain after systemic delivery through a combination of active and passive targeting.[113,297,300–302] In the current study, we demonstrate that peptide charge characteristics affect peptide-modified nanoparticle pharmacokinetics after direct application to the brain with CED and intravenous administration in a TBI animal model. Our observations suggest that nanoparticles surface-modified with neutral, zwitterionic, or negatively charged peptides may have more selective delivery of therapeutic cargos in TBI, due to their reduced accumulation in off-target organs and more specific accumulation in the injured brain after systemic delivery and enhanced distribution in the brain after direct injection. Our work suggests peptide charge should be considered as a design parameter when engineering nanoparticle platforms with targeting peptides for systemic delivery of TBI therapeutics. A greater understanding of how peptide physicochemical properties on the surface of nanoparticles dictate their pharmacokinetic profiles is valuable for the engineering design of many types of therapeutic nanomaterials, including peptide-targeted synthetic materials and natural nanoparticles such as bacteriophage and viruses.

3.7: SUPPORTING INFORMATION
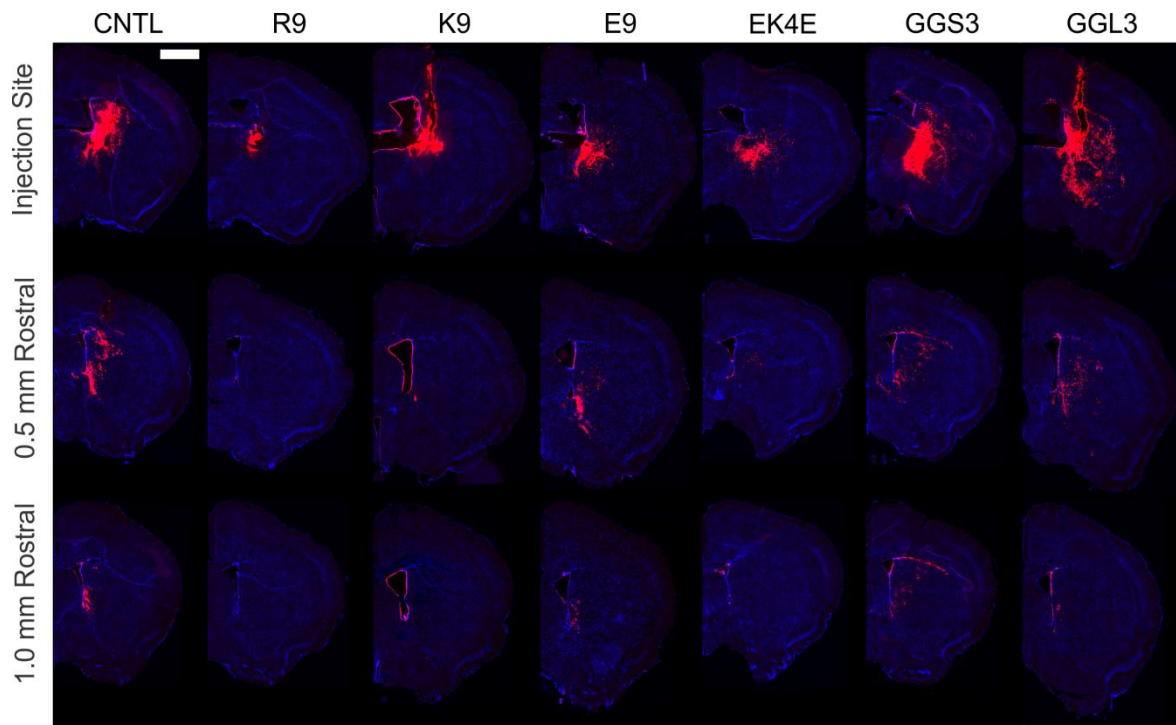
Supplemental Figure 3.1: Representative fluorescent images of peptide-modified nanoparticle distribution in a healthy brain. Representative fluorescent images of brain sections taken at the injection site, 0.5 mm, and 1 mm rostral from the injection site 6 hours post-administration into a healthy mouse brain by convection enhanced delivery (CED) for each peptide-modified nanoparticle group (n=3). Injured brain hemisphere was imaged for nanoparticles (red) and Hoechst (blue; scale bar = 1 mm).
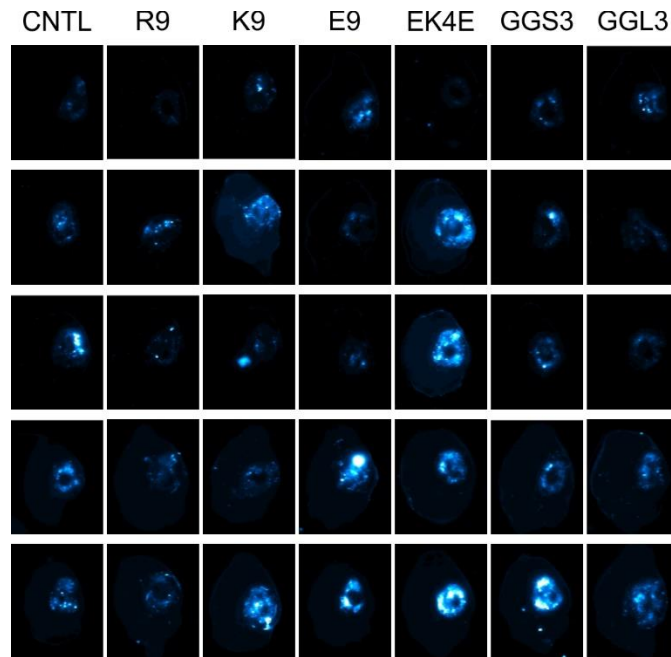
Supplemental Figure 3.2: Surface fluorescent images of peptide-modified nanoparticle brain accumulation after intravenous delivery in a mouse model of TBI. Surface fluorescent imaging of intact brains, with injured hemisphere on the right side. Peptide-modified nanoparticles were administered intravenously 6 hours after controlled cortical impact (CCI) injury and brains collected 1 hour after administration.

3.8: ACKNOWLEDGEMENTS

3.9: CONFLICT OF INTEREST

The authors have no conflict of interest to declare.

CHAPTER 4: Porous Silicon Nanoparticles Targeted to the Extracellular Matrix for Therapeutic Protein Delivery in Traumatic Brain Injury

4.1 ABSTRACT

Traumatic brain injury (TBI) is a major cause of disability and death among children and young adults in the United States, yet there are currently no treatments that improve the long-term brain health of patients. One promising therapeutic for TBI is brain-derived neurotrophic factor (BDNF), a protein that promotes neurogenesis and neuron survival. However, outstanding challenges to the systemic delivery of BDNF are its instability in blood, poor transport into the brain, and short half-life in circulation and brain tissue. Here, BDNF is encapsulated into an engineered, biodegradable porous silicon nanoparticle (pSiNP) in order to deliver bioactive BDNF to injured brain tissue after TBI. The pSiNP carrier is modified with the targeting ligand CAQK, a peptide that binds to extracellular matrix components upregulated after TBI. The protein cargo retains bioactivity after release from the pSiNP carrier, and systemic administration of the CAQK-modified pSiNPs results in effective delivery of the protein cargo to injured brain regions in a mouse model of TBI. When administered after injury, the CAQK-targeted pSiNP delivery system for BDNF reduces lesion volumes compared to free BDNF, supporting the hypothesis that pSiNPs mediate therapeutic protein delivery after systemic administration to improve outcomes in TBI.

4.2: INTRODUCTION

Traumatic brain injury (TBI) results in up to 2.8 million injury-related hospitalizations and deaths in the United States annually.[352] Currently available treatments for TBI are palliative and do not address the underlying cause of disease, leading to long-term physical, behavioral, and/or psychosocial impairments in the majority of survivors.[292,293] After the initial injury, a secondary injury progresses over a course of days to weeks and the pathophysiology involves a series of biochemical and cellular cascades, including reactive oxygen species (ROS) generation, inflammatory response, neurodegeneration, blood-brain barrier (BBB) breakdown, and cell

death.[353] While the primary injury can only be prevented, the secondary injury is an opportunity for therapeutic intervention in order to preserve brain tissue proximal to the primary injury.

Brain-derived neurotrophic factor (BDNF) is a promising neuroprotective therapeutic to mitigate the progressive deterioration of brain tissue that occurs during the secondary injury after TBI.[354] BDNF is a protein secreted from neurons and glia that promotes neuronal survival, neural plasticity, and neurogenesis[355,356] and its cognate receptor is tropomyosin receptor kinase B (TrkB).[357] TrkB activation initiates signaling cascades that regulate apoptosis, neuronal plasticity, and neurogenesis.[358] The binding of BDNF to TrkB activates pro-survival pathways and enhances expression of anti-apoptotic proteins through the phosphoinositide 3-kinase and Akt signaling pathway in neurons.[354,359] Previous studies have demonstrated that sustained BDNF levels in the brain achieved through stem cells,[360,361] genetically engineered cells,[362–367] viral gene therapy, and direct brain infusions[368] can protect brain tissue in the context of nervous system injury, neurodegenerative disease, and psychiatric disorders.[354] In a meta-analysis of available clinical data, including cohort studies and randomized controlled trials, treatment of TBI patients with cerebrolysin, a porcine-derived peptide mixture that includes BDNF,[369] led to improved outcomes in functional tests such as the Glasgow Outcome Scale and modified Rankin Scale.[370] The promise of BDNF as a potential therapeutic for neurodegenerative diseases is highlighted by the initiation of a first-in-human clinical trial to evaluate adeno-associated virus vector (AAV2)-based gene therapy of BDNF in Alzheimer's Disease patients (NCT05040217).[371]

While elevated BDNF expression, along with other neurotrophic factors, contributes to the functional preservation of injured tissue, a major barrier to the development of BDNF as a clinical therapeutic for TBI is successful delivery to the injured brain after systemic administration. Challenges to intravenous delivery of BDNF include short circulation half-life and restricted transport into the brain.[354,372,373] Nanoscale drug delivery vehicles are platform technologies with the potential to increase the bioavailability and stability of protein therapeutics; for example, vehicles can be engineered to target specific tissues to increase retention and labile cargos can

be encapsulated within the interior of vehicles to protect against degradation in the biological milieu.[373,374] In addition, the pharmacokinetic profiles of nanoscale drug delivery vehicles can be tuned independent of their therapeutic cargo, allowing for more facile formulation of a variety of cargos. However, previous efforts to encapsulate BDNF into nanoparticles have resulted in low mass loading of less than 1%.[375–377]

Porous silicon nanoparticles (pSiNPs) are an attractive candidate nano-carrier for therapeutics due to their tunable pore sizes and versatile loading chemistries, which allow for the accommodation of therapeutic cargo with a wide range of sizes and chemical properties, including small molecule drugs,[378,379] nucleic acids,[301,380,381] and peptides/proteins.[382,383] In particular, sequestration of protein-based biologics within the porous nanostructure of pSiNPs has been shown to protect them from degradation in the blood, leading to extended *in vivo* half-life and bioactivity.[378,380,382–392] In addition, pSiNPs have the advantage of linear degradation profiles, and thus can achieve linear drug release profiles, due to their anisotropic degradation mechanism.[393] This strategy has been successfully employed to encapsulate nerve growth factor (NGF) into pSiNPs, demonstrating the local release of growth factors from a polymeric scaffold.[382,386] In addition, Segal and Shefi et al. demonstrated neurotrophic factor release from nanoporous silicon microparticles after local delivery to the brain, achieved through the implantation of chips or biolistic bombardment using a pneumatic gene gun through an opening in the skull.[388] However, so far, protein delivery from pSiNPs after systemic delivery has yet to be demonstrated.

While a subset of TBI patients may undergo surgical intervention to remove blood clots and relieve intracranial pressure,[394] the brain is generally not readily accessible to therapeutics. Although intravenously delivered materials can accumulate in the injured brain through the damaged BBB that is a hallmark of TBI,[44,220,222,272,395] access to the brain is transient, with a majority of materials excluded from the brain 6 hours after injury as the BBB rapidly re-establishes.[44,222,381] This highlights the need for active targeting strategies, in order to increase penetration and retention of potential therapeutics. We recently identified a peptide ligand, CAQK,

that binds to extracellular matrix (ECM) components upregulated after brain injury.[381] CAQK-modified pSiNPs were able to deliver siRNA to brains in a penetrating TBI model after intravenous administration and mediated significant silencing of a reporter protein compared to control targeted pSiNPs.[381] This approach exploited the transient damage to the BBB caused by the injury to allow passive accumulation of the nanoparticles into brain tissue where they selectively bound to, and were retained by, accessible brain ECM.

This work combines the above two approaches for protein loading and peptide-mediated targeting of ECM in the injured brain. Here we load BDNF into pSiNPs with a loading efficiency of 13% by mass of the pSiNP-protein construct, a substantial improvement in mass loading compared to encapsulation of BDNF by other systems (<1%),[375–377] and then modify the exterior of the nanoparticles with polyethylene glycol (PEG) and the brain injury-targeting peptide CAQK. We confirm that the BDNF retains its bioactivity after loading, we track the CAQK-modified pSiNPs into injured brain tissue after systemic administration in a mouse model of TBI, and we demonstrate a substantial reduction of brain lesion volumes relative to free BDNF or PBS controls. This work therefore represents the first time chemically-targeted nanoporous silicon has achieved the delivery of protein payloads after systemic administration and improved outcomes in an animal model of TBI.

4.3: RESULTS AND DISCUSSION

4.3.1: Loading of pSiNPs with Protein Cargo and Surface Modification with Targeting Peptide

The pSiNPs used in this study were synthesized by electrochemical etching of mesopores into single crystalline silicon wafers, followed by ultrasonic fragmentation to form mesoporous nanoparticles. The electrochemical etch parameters (48% hydrofluoric acid, 46 mA/cm^2) were set to achieve a nominal pore size in the range of 10-20 nm in diameter and an average size of ~130 nm in hydrodynamic diameter (Figure 4.1).[393] The pore diameter was chosen based on previous studies to be sufficient to accommodate protein cargos.[393] The proteins were loaded into the pores of pSiNPs using an oxidative trapping method (Figure 4.1a,S4.1),[382,386] which involves partial

conversion of the Si skeleton in pSiNPs to SiO_2 by mild oxidation in deionized water. The SiO_2 shell then re-structures in the presence of the aqueous protein solution. This combination of conversion of Si to SiO_2 and aqueous restructuring of SiO_2 results in a volume expansion of the skeleton and sealing of the protein within a hydrated silicate framework, effectively trapping the protein and protecting it from degradation in the blood upon systemic delivery. We studied two protein cargoes in this work: the therapeutic protein BDNF, and the model protein lysozyme, which was labeled with Rhodamine B. Lysozyme has a molecular weight of 14.5 kDa and an isoelectric point of 11.35[396] and BDNF has a molecular weight of 13.5 kDa and an isoelectric point between 9 and 10,[397] making their size and charge properties similar at physiologic pH, which are important parameters to consider for pSiNP protein loading. Rhodamine B-labeled lysozyme provides an established functional readout of protein activity in release assays and allows tracking of the payload by image analysis in the biodistribution studies. BDNF was used in efficacy studies in SH-SY5Y cultures and the animal model of TBI. The SiO_2 shell in the pSiNPs is negatively charged at physiologic pH, with a zeta potential ranging from -24 to -28 mV,[380] which enhanced the loading of the positively charged protein cargoes *via* electrostatic interactions (pI of lysozyme = 11.35[396] and pI of BDNF ~ 9-10[397]).

In order to verify surface modification and protein loading, we analyzed the pSiNPs by Fourier-transform infrared spectroscopy (FTIR), dynamic light scattering (DLS), and transmission electron microscopy (TEM) at each stage of synthesis. After oxidation and protein loading, the FTIR spectrum revealed characteristic amide I and II bands (at 1650 cm^{-1} and 1530 cm^{-1}, respectively), denoting the presence of protein (Figure 4.1b).[398] Size measurements of unloaded pSiNPs and protein-loaded pSiNPs taken by DLS and TEM indicated that the loading process resulted in a diameter increase of ~5-10 nm, likely due to protein adsorption onto the pSiNP surface (Figure 4.1c,d,S4.2). To increase *in vivo* half-life and stability in systemic circulation,[399,400] the pSiNP surface was then aminated and modified with polyethylene glycol using NHS chemistry. PEG modification stabilized the nanoparticles, allowing them to be administered intravenously.

To increase the retention of nanoparticles in the injured brain tissue, the pendant PEG groups were then conjugated to CAQK, a peptide previously discovered to bind upregulated proteoglycan complexes in injured brain tissue.[381] CAQK was attached to the distal end of PEG by reacting the free thiol of CAQK with a maleimide on the PEG. For some of the fluorescence imaging experiments, a FAM-labeled CAQK peptide was used. The surface chemistry was confirmed by FTIR; in particular, the appearance of a C-H stretching peak (2869 cm^{-1}) confirmed successful PEG conjugation.[401] The absolute diameter of the nanoparticles increased by ~10-20 nm after PEG and CAQK surface modification, while hydrodynamic diameter measurements increased by ~20-30 nm, likely due to the size increase in the hydrated shell around the nanoparticle after PEG modification (Figure 4.1c,d,S4.2). This size increase is consistent with the ~10 nm Flory radius of 5 kDa PEG and peptide.[311] Approximate number of peptides conjugated per pSiNP was found to be ~40,000-50,000 peptides per nanoparticle, as evaluated by quantifying the amount of FAM-labeled CAQK by absorbance and estimation of nanoparticle number by Nanoparticle Tracking Analysis. The zeta potential after surface modification of the protein-loaded pSiNPs containing the pendant PEG and CAQK groups was -1 ± 1.5 mV in PBS.
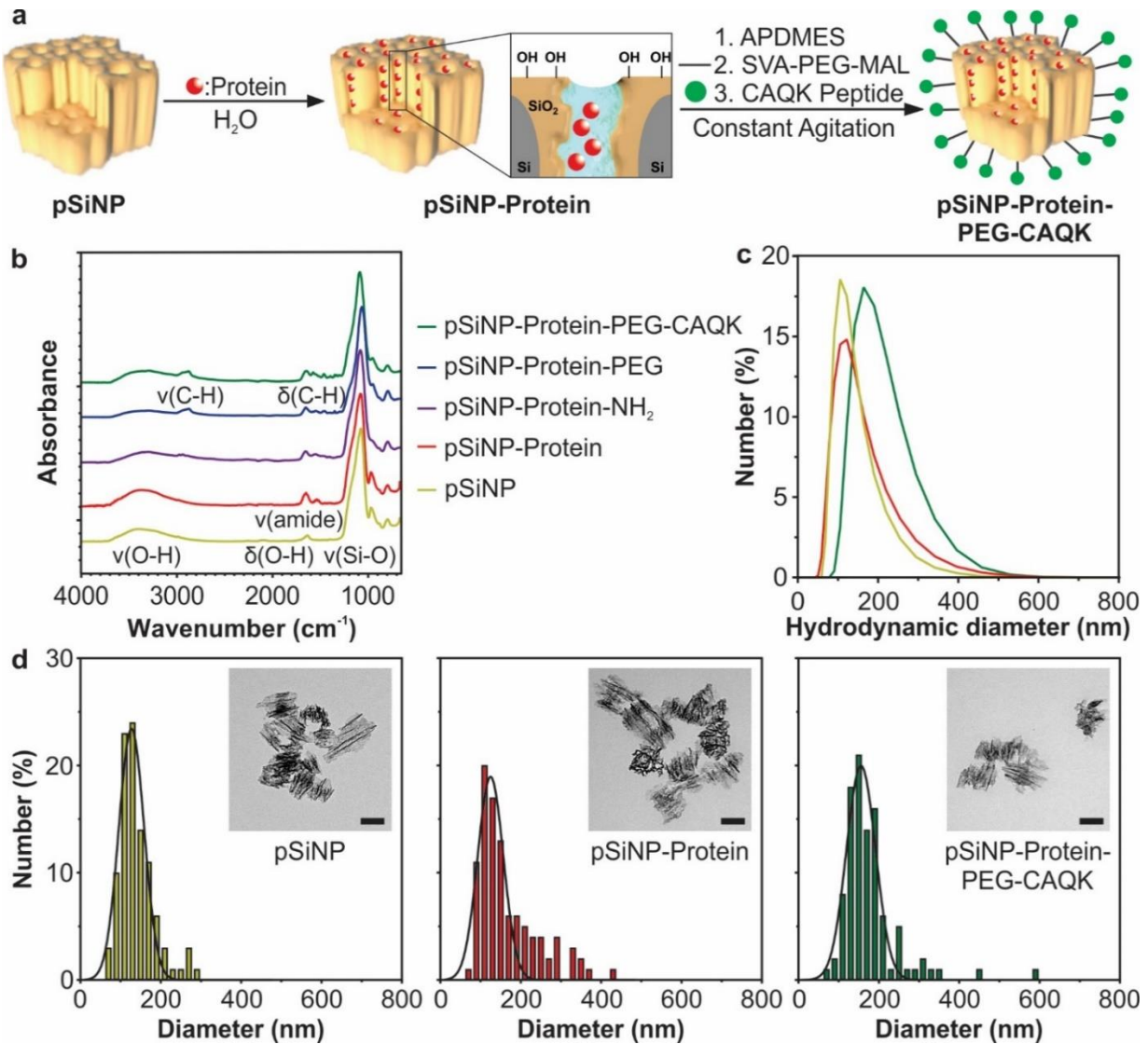
Figure 4.1: Synthesis and characterization of CAQK-targeted pSiNPs encapsulating a protein cargo. (a) Schematic of protein loading, surface modification, and CAQK-functionalization of pSiNPs. (b) FTIR analysis of pSiNPs during synthesis steps. Nanoparticle diameters as measured by (c) DLS and (d) TEM (scale bar in inset = 100 nm).

4.3.2: Model Protein Cargo is Released Linearly from pSiNPs and Retains Activity

Due to the high cost of BDNF, protein loading and performance parameters of the nanoparticle system were initially optimized using lysozyme as a model protein cargo. The degradation of pSiNPs is anisotropic due to the vertical pore orientation created by electrochemical etching that results in an increased surface area in the horizontal plane.[393] Silicon dioxide hydrolyses and dissolves in aqueous conditions to form biocompatible orthosilicic acid,

89

releasing the protein payload during this process.[393] pSiNP-Lysozyme-PEG-CAQK were degraded in PBS and imaged with TEM over 48 hours, revealing a reduction in total nanoparticle size over time (Figure 4.2a). Lysozyme loading was quantified to be 14.5% by mass relative to the pSiNP-protein construct, measured by fully degrading pSiNPs in PBS at 37°C and measuring protein content with a BCA assay (Figure 4.2b). Next, we quantified the activity of the protein released from degraded pSiNPs. Lysozyme activity after release from pSiNPs was assayed in a Micrococcus lysodeikticus cell assay (Figure 4.2c). Lysozyme hydrolyzes the cell wall of M. lysodeikticus, which can be monitored by decreased absorbance measured at 450 nm.[402] The combination of total protein measurements (Figure 4.2b) and protein activity (Figure 4.2c) confirmed that >95% of the protein released maintained its activity.
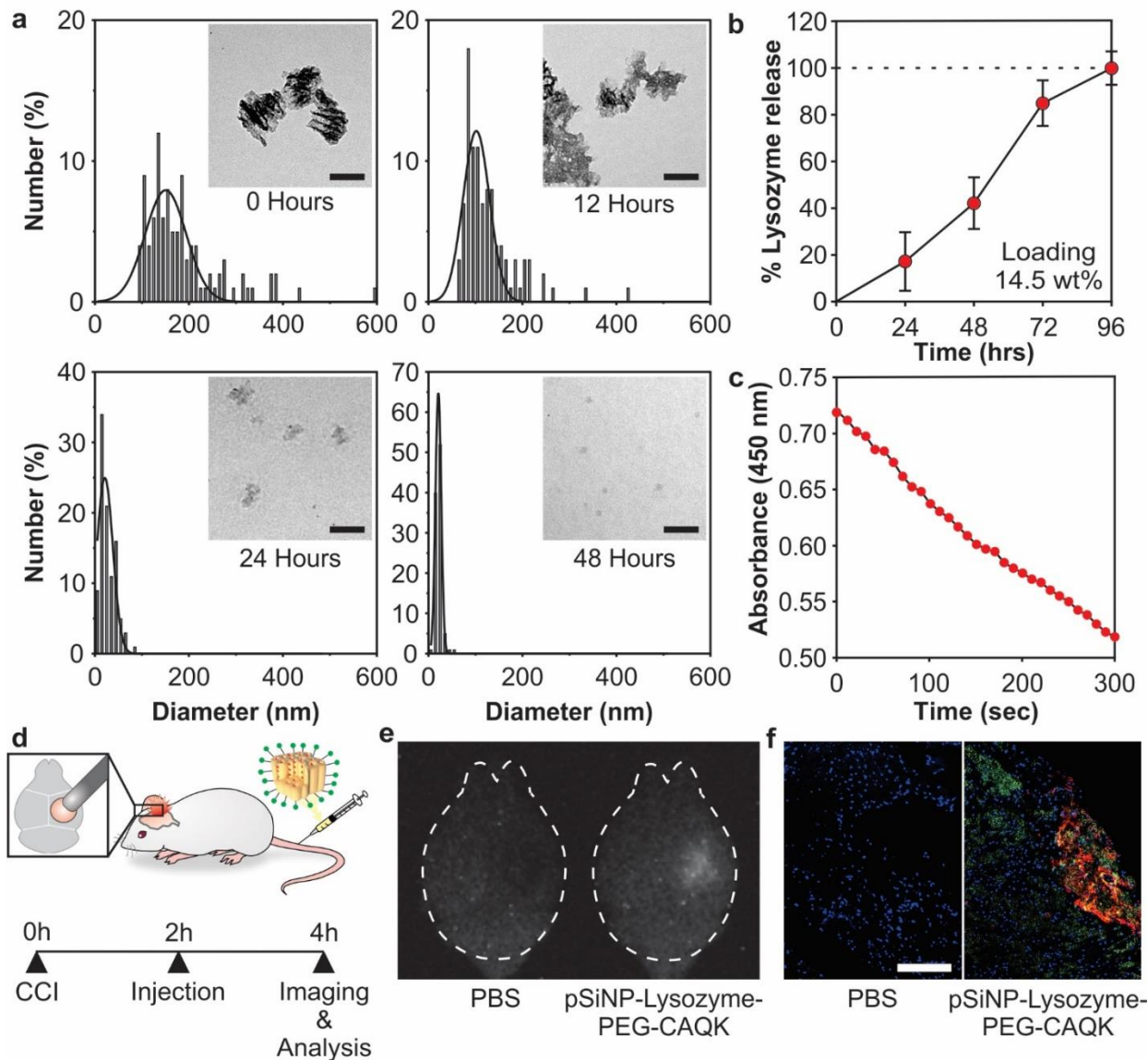
Figure 4.2: Loading and biodistribution of model protein in pSiNPs. (a) Analysis of pSiNP-Lysozyme-PEG-CAQK size by TEM image analysis after degradation in PBS at 37 °C after 0, 12, 24, and 48 hours (scale bar = 100 nm). (b) Time-dependent release of model protein lysozyme from pSiNPs in PBS at 37 °C, measured by BCA assay. The mass percentage loading of lysozyme in the pSiNP constructs was 14.5% by mass relative to the pSiNP-protein construct. (c) Activity of lysozyme after release from pSiNPs. Lysozyme activity was assayed through the hydrolysis of Micrococcus lysodeikticus, measured by loss of absorbance at 450 nm. (d) Schematic depiction of the protocol followed in the biodistribution study. The right hemisphere was injured, followed by intravenous administration of pSiNP-Lysozyme-PEG-CAQK 2 hours post-CCI, and brains collection for downstream imaging and analysis 2 hours post-injection. (e) Time-gated image of pSiNPs in whole brains and (f) confocal image of lysozyme model protein (red), CAQK (green), and nuclei (blue) from injured brain sections (scale bar = 200 µm).

4.3.3: CAQK Peptide-Targeted pSiNPs Mediate Protein Delivery into the Injured Brain after Systemic Administration

In this work we employed the peptide CAQK as a targeting ligand for the nanoparticles. CAQK has been shown to bind to the ECM upregulated in injured brain tissue, and to selectively enhance nanoparticle accumulation in the damaged regions of the mouse brain.[381] We and others have demonstrated that intravenous delivery of targeted pSiNPs successfully led to accumulation and retention of cargo in target tissues, such as siRNA against STAT3 in breast cancer tumors[403] and siRNA against peptidylprolyl isomerase B[300] or green fluorescence protein in the injured brain.[381] Concerning biodegradation of the material, prior work has demonstrated that pSiNPs accumulate mostly within the liver and spleen after intravenous administration and degrade into orthosilicic acid in organs within 1-4 weeks.[378] Orthosilicic acid is naturally found in many tissues and excreted renally.[404] Previous studies of *in vivo* degradation of pSiNPs after intravenous administration found that degradation profiles approximate zero-order release,[405,406] similar to the linear release profile we observe (Figure 4.2b). Intravenously delivered pSiNPs are well-tolerated in mice up to 20 mg/kg.[378] In the present studies, the protein-loaded pSiNP formulations were administered at 5 mg/kg of pSiNP.

Controlled cortical impact (CCI) is a well-studied model of TBI in mice and the injury is created by performing a craniotomy and impacting the exposed dura with an electromagnetically-driven piston.[265] To determine if the targeted pSiNPs could deliver a protein cargo to the injured brain tissue after CCI, pSiNPs were synthesized with the model protein, Rhodamine B-labeled lysozyme. CAQK-targeted pSiNPs carrying this payload were administered intravenously 2 hours post-injury in mice given a CCI on the right hemisphere and brains were harvested 2 hours after injection (Figure 4.2d). The intrinsic luminescence from the quantum-confined silicon domains in the pSiNPs was imaged with time-gated imaging, which highlights the long-lived (microseconds) excited state of silicon quantum dots while suppressing short-lived (nanoseconds) tissue autofluorescence.[407] The time-gated images revealed the presence of intact pSiNPs in the injured

92

hemisphere of the brain after systemic administration (Figure 4.2e). Brains were then sectioned and imaged by confocal microscopy to determine distribution of injected materials within the tissue (Figure 4.2f). We observe co-localization of fluorescent signal from Rhodamine B-labeled lysozyme and FAM-CAQK in the injured brain, surrounded by fluorescent signal from FAM-CAQK in adjacent areas. We believe that the FAM-CAQK fluorescent signal not co-localized with Rhodamine B-labeled lysozyme is due to surface degradation of pSiNPs, thus liberating FAM-CAQK that can subsequently diffuse into the surrounding tissue. These results support the hypothesis that CAQK-targeted pSiNPs can accumulate in the injured brain and deliver protein cargos after systemic administration. This result is consistent with previous studies of CAQK-targeted pSiNPs carrying siRNA cargo in a penetrating brain injury model, where CAQK- but not CGGK control-modified pSiNPs mediated gene silencing in the injured brain tissue.[381]

4.3.4: BDNF is Released Linearly from pSiNPs over 72 Hours and Maintains Activity
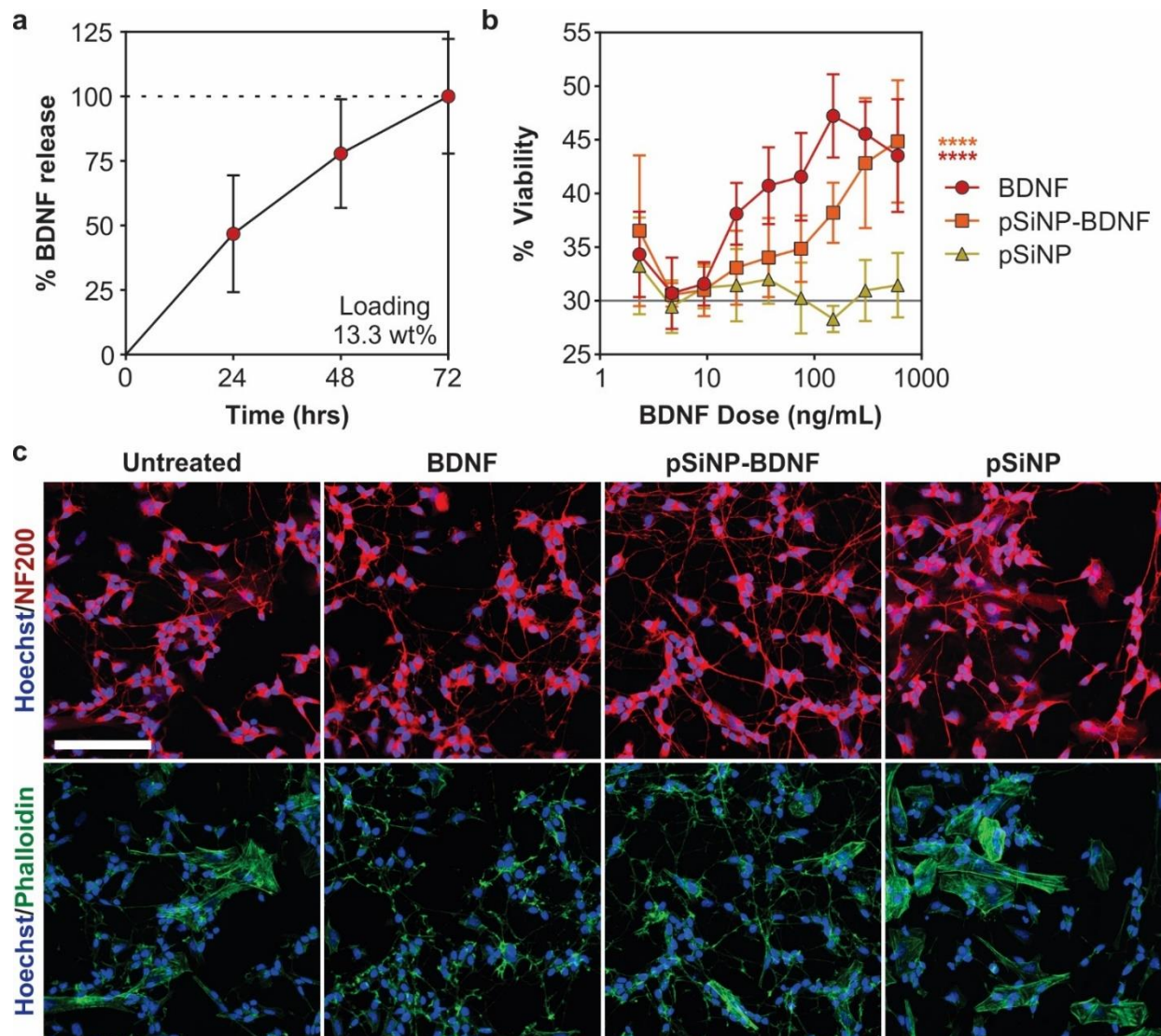
Figure 4.3: BDNF loading and activity in differentiated SH-SY5Y cultures. (a) Time-dependent release of BDNF from pSiNPs in PBS buffer at 37 °C, quantified by ELISA. The loading of BDNF in the pSiNPs was 13.3% by mass relative to the pSiNP-protein construct. (b) Cell viability in retinoic acid-differentiated SH-SY5Y cultures treated with BDNF, pSiNP, and pSiNP-BDNF. The "pSiNP" control trace corresponds to a concentration of pSiNPs that is the same amount of Si by mass as was used in the pSiNP-BDNF formulation; *i.e.*, each point in the pSiNP control trace corresponds to a mass/volume of empty pSiNPs that is ~7.5x the ng/mL value indicated on the x-axis. (Gray line represents untreated cells; n=6, mean ± SD, **** $p \leq 0.0001$ Two-way ANOVA with Dunnett's post-test compared to pSiNP control). (c) Representative images of SH-SY5Y cells treated for 72 hours with matched concentrations of 300 ng/mL BDNF and stained with NF200 (red), phalloidin (green), and Hoechst (blue) (scale bar =100 μm).

BDNF loading was determined by ELISA to be 13.3 ± 0.7% by mass relative to the total

construct and complete degradation of the pSiNP-BDNF construct occurred over 72 hours in PBS

at 37 °C (Figure 4.3a). To confirm that BDNF released from pSiNPs maintained activity, we

performed a functional assay of the pSiNP-BDNF constructs in SH-SY5Y cultures, a human neuroblastoma cell line, which were differentiated with retinoic acid to induce the expression of TrkB, the receptor for BDNF.[408,409] Improved cell viability and neurite extension are well-established responses to BDNF treatment in SH-SY5Y cultures expressing TrkB.[409–411] The pSiNP-BDNF and free BDNF-treated cultures exhibited significantly increased cell viability with treatment in a dose-dependent manner compared to untreated and empty pSiNP-treated cultures, which had no effect on cell viability even at their highest dose (Figure 4.3b). Free BDNF-treated cultures displayed higher cell viability at most doses compared to pSiNP-BDNF-treated cultures, likely due to the immediate availability of free BDNF in *in vitro* conditions (Figure 4.3a,b). Imaging of cultures for morphological changes revealed that free BDNF and pSiNP-BDNF treatments increased presence of fine and complex neurites, with multiple crossing points, and a lower density of cytoskeletal actin surrounding the nucleus compared to control and pSiNP treatments (Figure 4.3c). The similar release profiles of lysozyme and BDNF (Figure 4.2b, 4.3a) and the preservation of activity observed with the released lysozyme (Figure 4.2c) and the released BDNF (Figure 4.3b,c) support the hypothesis that the protein cargos retain their biological activity in the pSiNP formulations.

BDNF is a growth factor with pleiotropic functions known to improve neuron survival, synaptic function, and cell signaling in animal models of injury and neurodegeneration.[354] Previous studies have demonstrated that elevated BDNF concentrations in the brain achieved through stem cell engraftment increased the expression of synaptic proteins and improved neurological scores in murine models of TBI.[290,360,412,413] Due to the numerous challenges with cell therapy, alternative approaches that enable the systemic delivery of recombinant BDNF protein are desired.

The half-life of BDNF is reported to be <10 minutes in plasma[414,415] and ~3 hours in brain tissue.[416] This very short time window illustrates the challenge of developing BDNF, and protein-based biologics in general, as systemically administered therapeutics. The use of a nanoparticle

carrier in order to protect and increase bioavailability of BDNF in the brain after systemic administration has therefore been considered by several researchers as a potential solution to this problem. Of particular relevance to the present work, a previous report of nanoparticle-mediated delivery of BDNF employed poly(lactic-co-glycolic acid) (PLGA) nanoparticles.[41] This PLGA nanoparticle formulation of BDNF improved neurological behavior scores over free BDNF, supporting the potential benefit of BDNF delivered by nanoparticles.[41] In this prior work, BDNF was adsorbed onto the surface of the PLGA nanoparticles, likely due to the known challenge of maintaining protein activity when encapsulating protein drugs into the core of PLGA nanoparticles. In addition to the denaturing property of polymers and polymer surfaces, surface adsorption has a limited loading capacity, it usually displays burst release kinetics, and it leaves the biologic exposed to potential degradation by proteolytic enzymes. By comparison, the present approach preserves protein activity (Figures 4.2c, 4.3b,c), can achieve high mass loading (~13 wt%) to enhance potency, and it yields zero-order release kinetics (Figures 4.2b, 4.3a).

4.3.5: Treatment with pSiNP-BDNF Reduces Lesion Volumes in a Mouse Model of TBI

After CCI, there is progressive loss of tissue due to secondary injury mechanisms that results in a lesion,[417–419] including neuronal cell death which peaks 24-72 hours after the primary injury.[420,421] The volume of this lesion correlates with functional deficits such as motor activity and memory.[422,423] In order to evaluate the therapeutic potential of pSiNP-BDNF after systemic delivery, we administered pSiNPs *via* the tail-vein in a mouse CCI model of TBI and measured lesion volume three days post-injury (Figure 4.4a). Mice were injured on the right hemisphere of the brain with a CCI, and CAQK-targeted pSiNPs carrying BDNF were administered through the tail-vein 2 hours post-injury (5 mg/kg pSiNP and 0.65 mg/kg BDNF). Controls included animals that received PBS, empty pSiNPs with PEG-CAQK (5 mg/kg), or free BDNF (1 mg/kg). While our previous work demonstrated the improved accumulation of CAQK-targeted pSiNPs compared to control-targeted pSiNPs,[381] a limitation of the current study is that we do not evaluate the impact of CAQK-targeting on pSiNP-BDNF accumulation. Three days after injury, brains were harvested

and serial coronal sections were collected every 0.5 mm across the injury lesion (11-12 sections per brain). Lesion area was measured from each section and the lesion volume calculated by the trapezoidal rule, as described previously.[419,424,425] Nissl staining of neuronal cell bodies supported the presence of neurons in the area surrounding the injury in all groups (Figure S4.3), suggesting that any neurons that died during primary or secondary injury were included in the lesion area. We observed a 24.0% reduction in lesion volume in pSiNP-BDNF treated mice compared to the PBS treated control group (Figure 4.4b,c). In comparison, lesion volumes in free BDNF treated mice were equivalent to lesion volumes in the PBS control. We hypothesize that the reduction in lesion volume in pSiNP-BDNF treated mice is due to the ability of pSiNPs to localize to injured brain tissue (Figure 4.2e,f) and release active BDNF over a period of time (Figure 4.3) that is consistent with peak neuronal apoptosis.[82,83]
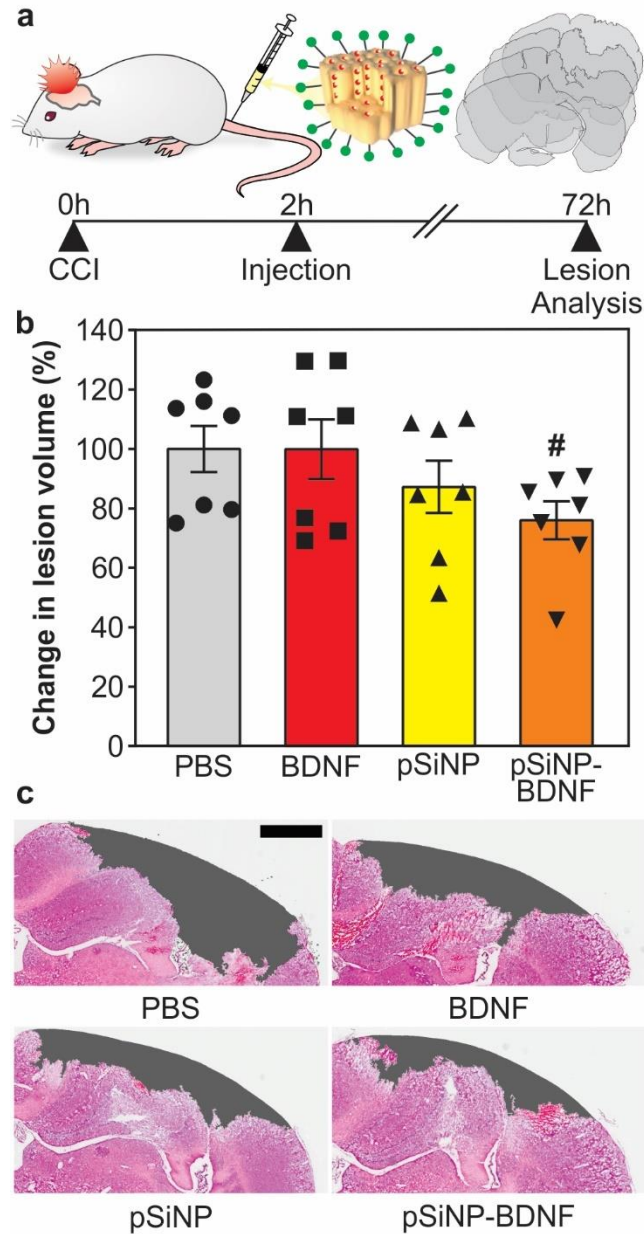
Figure 4.4: Lesion volume decreases after pSiNP-BDNF treatment. (a) Schematic and timeline of injury, treatment, and lesion volume analysis. (b) Changes in lesion volumes relative to PBS-treated controls. (n = 7 per group, mean ± SEM, # p = 0.13 One-way ANOVA with Dunnett's post-test compared to PBS control). Both pSiNP and pSiNP-BDNF formulations contained PEG-CAQK surface chemistry as described in the text. (c) Representative images of H&E-stained coronal brain sections at 1.5 mm caudal from bregma for each treatment group with measured lesion area filled in gray (scale bar = 1 mm).

Lesion volumes in mice treated with empty pSiNPs (CAQK-targeted without BDNF) were reduced by 12.8% compared to the control PBS treatment (p = 0.58). pSiNPs and their degradation product silicic acid are known to interact with calcium ions, forming calcium silicate,[301]

and ROS, which catalyzes the oxidation of porous silicon during its degradation process.[406] Calcium and ROS levels are elevated in the brain microenvironment after TBI as part of the damaging biochemical pathways that make up secondary injury.[426–428] However, more extensive studies on the interaction of pSiNPs with the injured brain microenvironment are needed to be able to draw conclusions about the extent or nature of the effect observed in animals administered empty pSiNPs.

4.4: CONCLUSIONS

While therapeutic proteins are attractive candidates to address the complicated disease biology of TBI, the systemic delivery of proteins for treatment of TBI is challenging due to the instability of proteins in the blood and limited transport into the brain.[354,372,373,429] This work demonstrated a peptide-targeted pSiNP platform that addressed these challenges. We found that up to 13% by mass of the BDNF protein could be loaded into the pores of pSiNPs, and measurement of cell viability in retinoic acid differentiated SH-SY5Y cultures confirmed that BDNF subsequently released from this carrier retained its bioactivity. Accumulation of intravenously administered CAQK-targeted pSiNPs and their protein cargo in injured brain tissue was confirmed using a fluorescently tagged model protein in a CCI mouse model of TBI. When formulated with BDNF and administered systemically 2 hours post-injury, the CAQK-modified BDNF-loaded pSiNPs reduced brain lesion volumes by ~24% compared to treatment with PBS or free BDNF. This work demonstrates that ligand-targeted pSiNPs can be used to deliver a therapeutic protein cargo to injured brains after systemic administration, and that this treatment leads to phenotypic improvements in a TBI animal model.

The positive results seen in this study for treatment of TBI suggest that systemic and targeted delivery of BDNF using nanoparticles may also have potential in other central nervous system injuries. For example, BDNF is a promising therapeutic for stroke[430–433] and spinal cord injury.[366,367,434,435] Additionally, the progressive deterioration that occurs after TBI is caused by multiple disease pathways, such as ROS generation, inflammation, and vascular dysfunction.[353]

It has been hypothesized that monotherapies are insufficient to address the multi-factor disease pathology of TBI and combination therapy may be a key to overcome the decades of failed TBI clinical trials.[436] Due to their versatile chemistry and tunable pore size, pSiNPs provide a promising platform technology for multiple therapeutic cargos in combination therapies that might better address the multi-factorial causes of TBI disease pathology.

4.5: MATERIALS AND METHODS

4.5.1: Materials

CAQK peptide and fluorescein-conjugated peptide FAM-CAQK were purchased from CPC Scientific, Inc. (San Jose, CA). Highly boron-doped p-type silicon wafers, 1.2 mΩ-cm resistivity, single-side polished on the (100) face, were obtained from Virginia Semiconductor (USA). Concentrated hydrofluoric acid (HF, 48% aqueous, ACS grade) was obtained from Fisher Scientific (USA). Succinimidyl valerate-polyethylene glycol-maleimide (SVA-PEG-MAL, MW 5 kDa) was purchased from Laysan Bio (Arab, AL). Absolute ethanol, methanol, and 3-(Ethoxydimethylsilyl)propyl-amine (APDMES) were obtained from Sigma-Aldrich (St. Louis, MO). BDNF was obtained from R&D Systems (USA).

4.5.2: Synthesis of pSiNPs

The preparation followed a published "perforated etch" procedure.[437] Single-crystalline highly doped p-type silicon wafers were anodically etched in an electrolyte consisting of hydrofluoric acid (48%) and ethanol in a 3:1 ratio by volume. CAUTION: HF is highly toxic and corrosive and contact with skin should be avoided. Procedures involving HF should always be carried out in a fume hood configured to handle HF and the operator should wear appropriate protective gloves, gown, and face shield. Etching was carried out in a Teflon etch cell using a platinum coil counter electrode. Prior to preparation of the porous silicon layers, the wafer surface was cleaned using a sacrificial etch consisting of electrochemical anodization (60 sec, 46 mA/cm^2) in the HF electrolyte, followed by ethanol rinse, then dissolution of the resulting porous film with aqueous KOH (1 M). The wafer was then rinsed with water (1x) and ethanol (2x). An etching

waveform consisting of a square wave of 200 cycles, in which a lower value of current density of 46 mA/cm^2 was applied for 1.2 s, followed by an upper value of current density of 365 mA/cm^2 applied for 0.363 s (Keithley 2651A Sourcemeter power supply). The multilayered porous nanostructure was removed from the crystalline silicon substrate by application of current pulse of 3.7 mA/cm^2 for 250 s in an electrolyte consisting of 1:29 (v:v) of 48% aqueous HF:absolute ethanol. The freestanding porous silicon sheets were placed in a sealed vial containing 1 mL of deionized water per mg of porous silicon and subjected to ultrasonic fracture in an ultrasonic bath (model 97043-960, VWR International) operating at a frequency of 35KHz and power of 48 Watts with a 1.9 L capacity overnight. The resulting ~130 nm-diameter nanoparticles were collected using centrifugation (15,000 rpm, 10 min, Eppendorf Centrifuge Model 5424R) and washed 3 times with ethanol and then isolated by centrifugation. Nanoparticles prepared in this manner are mesoporous, consisting of a crystalline silicon core skeleton coated with a surface layer of silicon dioxide.

1 mg of the pSiNPs resulting from the above procedure were washed once with DI water and then suspended in 1 mL of a solution consisting of recombinant human BDNF (200 µg/mL) dissolved in DI water. The nanoparticles were incubated under constant agitation at room temperature for ~18 hours. For the experiments involving the model protein lysozyme with conjugated Rhodamine B, the protein was loaded in a similar fashion. Protein mass loading was determined by measuring protein concentrations remaining in the supernatant after centrifugation by either BCA (lysozyme) or ELISA (BDNF; BDNF DuoSet ELISA, R&D Systems). The nanoparticles were washed once in DI water (via centrifugation/resuspension) to remove any unloaded protein from the solution, and then subsequently with 70% ethanol and finally with 100% ethanol. The loaded nanoparticles were aminated by incubation in an ethanol solution containing 12 µL/mL of APDMES for 3 hours under constant agitation. The nanoparticles were washed 3 times in 100% ethanol to remove any additional APDMES and incubated for 1 hour with 5 kDa SVA-PEG-MAL (500 µg in 1 mL ethanol) with constant agitation to achieve a PEGylated surface.

After 3 more washes with 100% ethanol to remove any additional PEG, the nanoparticles were incubated with CAQK (100 µg/1 mg pSiNPs) overnight at room temperature. The nanoparticles were washed with 100% ethanol, 70% ethanol, and water and resuspended in water for characterization and use.

4.5.3: Characterization of pSiNPs

A Malvern Zetasizer Nano (Malvern Panalytical Ltd.) was used to determine the hydrodynamic diameter and zeta potential of the nanoparticles. A Thermo Scientific Nicolet 6700 FTIR instrument fitted with a Smart iTR diamond ATR fixture was used to determine the FTIR spectra of the nanoparticles. A Genesys 150 UV/VIS Spectrophotometer (Thermo Fisher Scientific, Inc.) was used to evaluate the absorbance of FAM-peptide and a NanoSight LM10-HSB/GFT14 (Malvern Panalytical Ltd.) was used to determine the concentration of pSiNPs to calculate the number of peptides conjugated per pSiNP. For degradation studies, 0.5 mg/mL of lysozyme-loaded pSiNPs surface modified with PEG and CAQK were incubated in PBS at 37 °C. At 0, 12, 24, and 48 hours, aliquots of degraded nanoparticles were removed from the stock, pelleted, and resuspended into ethanol and loaded onto 42 µm formvar/carbon 400 mesh copper grids (Ted Pella, Inc.) and dried. The stock nanoparticles were similarly pelleted at each timepoint and resuspended in fresh PBS to ensure that degradation would not be stalled by the solubility of silicic acid in the supernatant.[378] TEM images were obtained on a JEOL 1400 plus electron microscope (JEOL USA, Inc.) operated at 80KeV and equipped with a Gatan Oneview camera (Gatan, Inc.).

4.5.4: Measurement of Protein Release from pSiNPs.

0.5 mg/mL of lysozyme or BDNF-loaded pSiNPs and an equivalent concentration of control nanoparticles were incubated in PBS at 37 °C. For release assays, supernatant was collected every 24 hours for up to 4 days and evaluated for protein concentration by BCA or ELISA. The percent protein release was calculated from the total cumulative release over the experiment. Cumulative released BDNF was calculated to be 51 ± 1.3% of BDNF calculated

during loading. Lysozyme activity was determined by a Microroccus lysodeikticus cell assay as previously described with some modification.[402] Briefly, 0.5 mg/mL of lysozyme loaded pSiNP were incubated within a solution containing M. lysodeikticus cells. Lysozyme activity was evaluated by measuring the absorbance of the intact cells at 450 nm using a plate reader (Tecan) over 5 minutes.

4.5.5: Bioactivity of BDNF in Retinoic Acid Differentiated SH-SY5Y Cultures.

SH-SY5Y cells (ATCC) were plated at 32,000 cells/cm^2 in 96 well plates or at 16,000 cells/cm^2 on cover glasses coated sequentially in 0.05 mg/mL poly-D-lysine overnight and 0.05 mg/mL rat tail collagen 1 for 2 hours at 37°C. Cells were cultured in Minimum Essential Medium (MEM) supplemented with 10% fetal bovine serum (FBS) and 1% penicillin-streptomycin for 24 hours before beginning the differentiation protocol. 10 μM retinoic acid in full media was introduced to the cells through a media change starting 24 hours after plating and exchanged every 48 hours. Cells were differentiated for 5 days to induce TrkB expression before beginning BDNF bioactivity studies.[408,409] For viability studies, doses ranging from 600 ng/mL (equivalent to 4.5 μg/mL pSiNP) to 0 ng/mL of free BDNF, pSiNP-BDNF surface modified with PEG, or pSiNP vehicles surface modified with PEG in serum-free MEM were introduced to the retinoic acid treated SH-SY5Y cells through a media change after washing the cells twice in serum-free MEM. Control wells representing 100% cell viability received full media with 10 μM retinoic acid. Cells were treated for 2 days and cell viability was evaluated with a CellTiter-Glo® Assay (Promega). For morphology studies, cells were cultured with treatments at 300 ng/mL for 3 days before being fixed and stained with anti-NF200 (Sigma), FITC-phalloidin (Millipore Sigma), and Hoechst with standard protocols. Fluorescent images were obtained on a Nikon Eclipse Ti2 (Nikon Instruments Inc.) of quadruplicate cover glasses.

4.5.6: Animal Injury Model

All animal experiments were approved by the University of California, San Diego Institutional Animal Care and Use Committee (IACUC). A CCI model of TBI in mice was used for

this study. 8-week-old C57BL/6J female mice (Jackson Labs) were placed in a stereotaxic frame under 2.5% isoflurane anesthesia and a 5 mm diameter craniotomy was performed over the right cortex, adjacent to the midline of the skull and midway between lambda and bregma. The right cortex was injured at a 2 mm depth with a 2 mm diameter stainless steel piston tip at a rate of 3 m/s using an ImpactOne (Leica Biosystems).

4.5.7: Protein Delivery from pSiNPs Targeting the Injured Brain in vivo.

Lysozyme-loaded pSiNPs surface modified with PEG and CAQK were injected *via* the tail-vein 2 hours after CCI (n=3) with control groups receiving pSiNP-Lysozyme-PEG-CAQK without injury or receiving an injury with a control PBS injection. Mice were perfused and brains were harvested 2 hours after injection. Time gated imaging was performed with an iSTAR 334T CCD camera (Andor Technology Ltd.) fitted with a Nikon AF micro lens (Nikko 105 mm) with laser excitation at 410 nm and a long-pass filter at 460 nm to quantify pSiNP localization. Brains were equilibrated in 30% w/v sucrose overnight and frozen in OCT (Tissue-Tek). Coronal sections were taken from the whole brain and counterstained with Hoechst to image the presence of Rhodamine B-tagged lysozyme being released from the pSiNPs which were tagged by FAM-labeled CAQK.

For BDNF treatments, 28 mice (n=7) were divided into 4 groups; PBS treated control, pSiNP-BDNF treatment surface modified with PEG-CAQK (13 μg BDNF equivalent, 100 μg pSiNPs), free BDNF treatment (20 μg), and a vehicle-only treatment (100 μg unloaded pSiNPs surface modified with PEG-CAQK) (Figure 4.4a).[381] 2 hours after CCI, treatments were administered intravenously through a tail-vein injection. Brains were collected 72 hours post-injury after perfusion with 10% formalin and frozen in OCT for tissue processing.

4.5.8: Lesion Volume Analysis and Histology

10-μm thick coronal sections were taken every 0.5 mm from coordinates -4 mm to 1 mm from bregma for lesion analysis and processed with H&E staining to clearly visualize the lesion area with brightfield microscopy. Images of each section were blindly analyzed for lesion size by measuring the outlined lesion area using ImageJ software. Lesion volume was calculated with

the trapezoidal rule. Sections taken from the center of each injury were Nissl stained using conventional protocols. Slides were imaged automatically using a Zeiss Axio Scan.Z1 and imaged with a color camera using a Nikon Eclipse Ti2 (Nikon Instruments Inc.).

4.5.9: Statistical Analysis

Statistical analysis was performed on GraphPad Prism 8 software (9.1.2). In Figure 4.3b, cell viability was analyzed with a two-way ANOVA and Dunnett's post hoc test conducted with $p<0.05$. In Figure 4.4b, lesion volume was analyzed with a one-way ANOVA with Dunnett's post hoc test conducted with $p<0.05$.

4.6: SUPPORTING INFORMATION
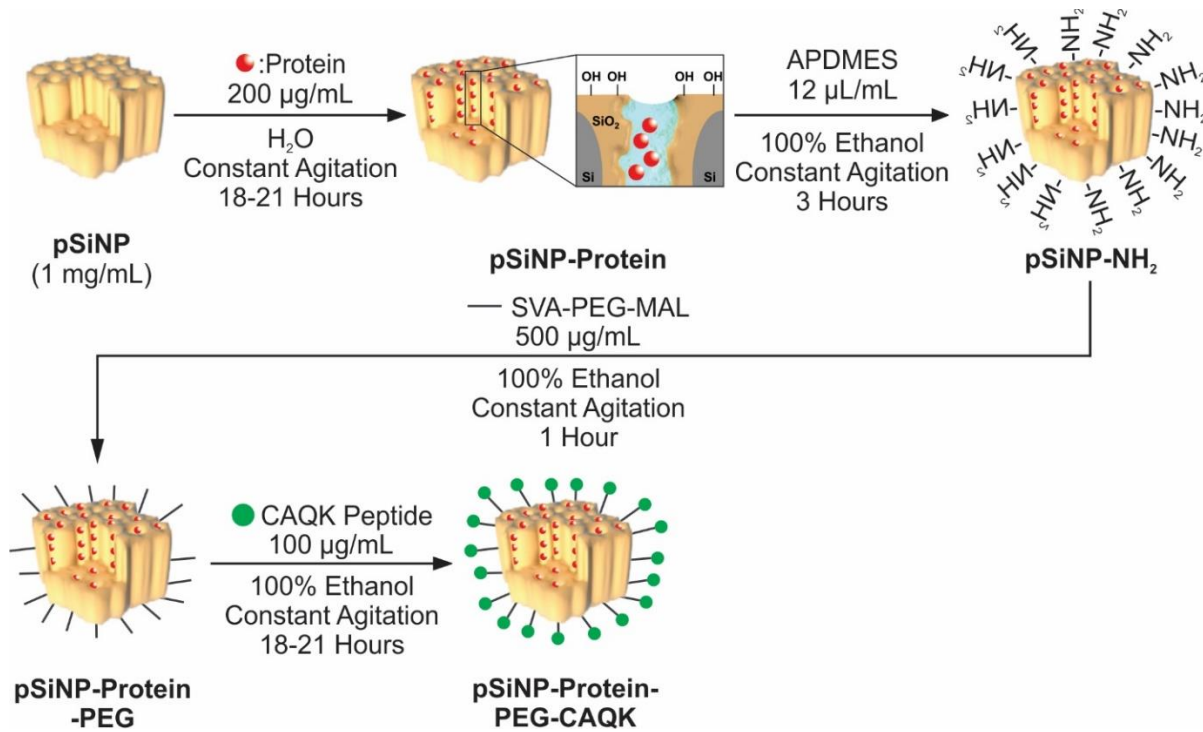
Supplemental Figure 4.1: Schematic of pSiNP-protein-PEG-CAQK synthesis. Schematic of protein loading, amination, PEG modification, and peptide modification of pSiNPs.
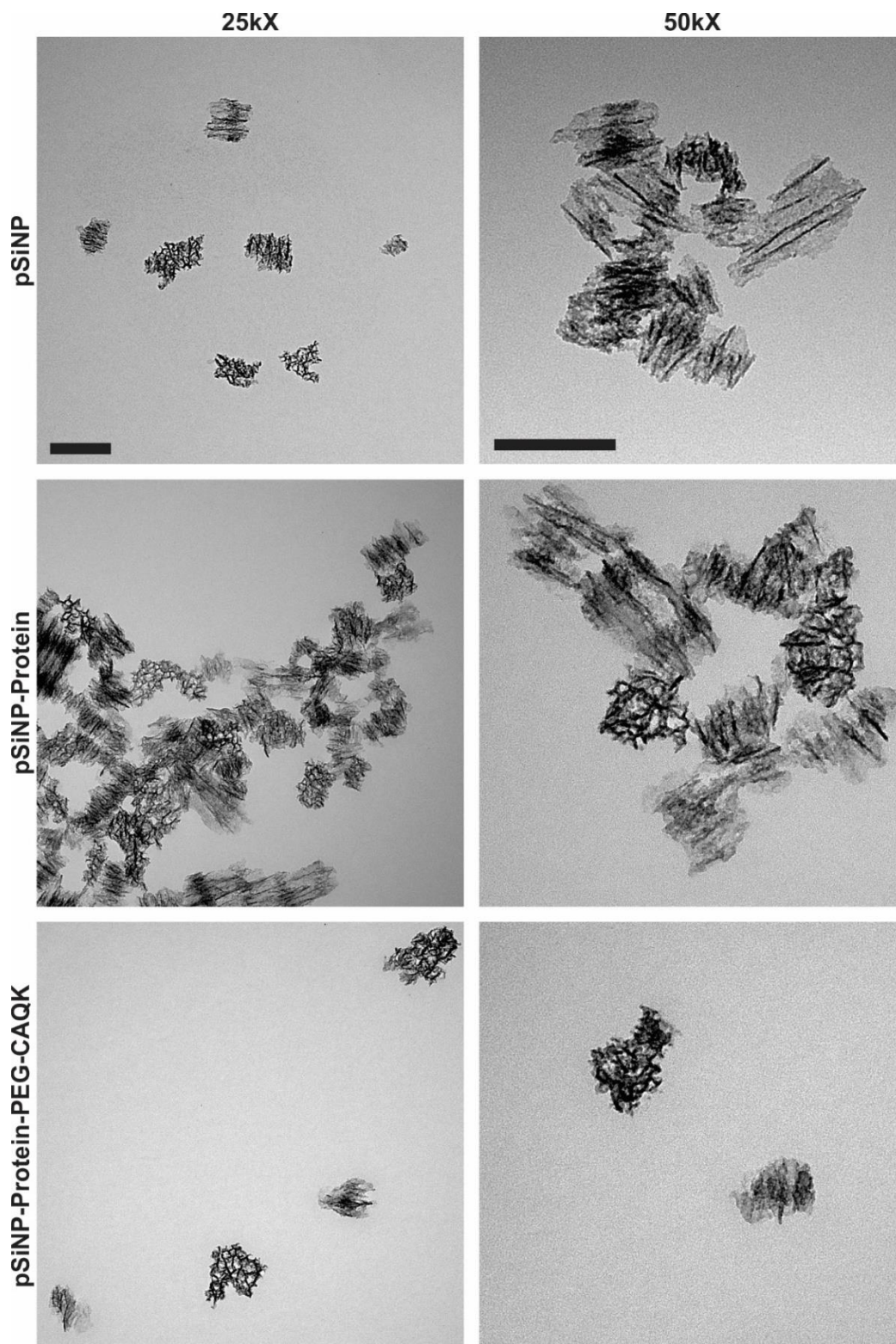
Supplemental Figure 4.2: Representative TEM images of pSiNP during synthesis. Representative TEM images at 25 kX and 50kX (scale bar = 200 nm) of pSiNPs, protein loaded pSiNPs, and protein loaded pSiNPs that are surface modified with PEG and CAQK.
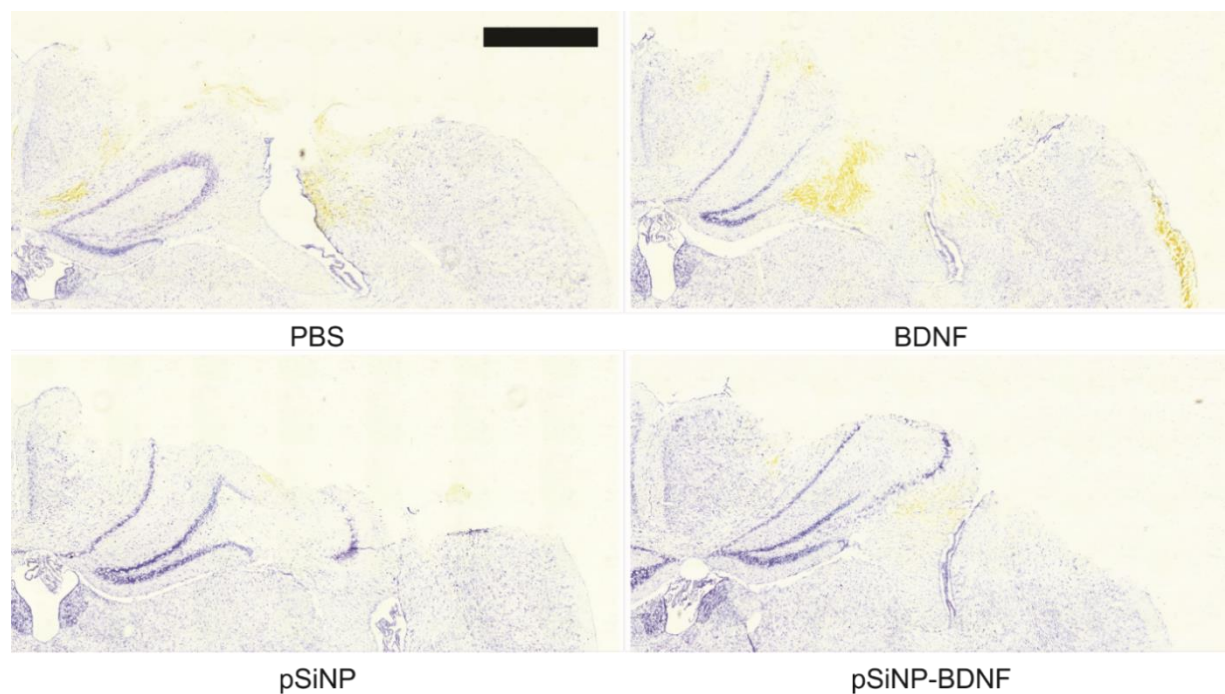
Supplemental Figure 4.3: Representative images of NISSL-stained coronal brain sections.
Representative images of NISSL-stained coronal brain section at 1.5 mm caudal from bregma for each treatment group (scale bar = 1 mm).

4.7: ACKNOWLEDGEMENTS

access and technical assistance. The UCSD-CMM-EM Core is supported in part by the NIH (Award number S10OD023527).

Chapter 4, in full, reprinted with permission from Waggoner, L. E.; Kang, J.; Zuidema, J. M.; Vijayakumar, S.; Hurtado, A. A.; Sailor, M. J.; Kwon, E. J. Porous Silicon Nanoparticles Targeted to the Extracellular Matrix for Therapeutic Protein Delivery in Traumatic Brain Injury. Bioconjug. Chem. 2022, 33 (9), 1685–1697. https://doi.org/10.1021/acs.bioconjchem.2c00305. It is coauthored with Kang, Jinyoung; Zuidema, Jonathan M. Copyright 2021 American Chemical Society. The dissertation author was one of the primary investigators and authors of this paper.

4.8 CONFLICT OF INTEREST STATEMENT

MJS is a scientific founder (SF), member of the Board of Directors (BOD), Advisory Board (AB), Scientific Advisory Board (SAB), acts as a paid consultant (PC) or has an equity interest (EI) in the following: Aivocode, Inc (AB, EI); Bejing ITEC Technologies (SAB, PC); Cend Therapeutics (SF, BOD, EI); Illumina (EI); Matrix Technologies (EI); NanoVision Bio (SAB, EI); Pacific Integrated Energy (AB, EI); Quanterix (EI); Spinnaker Biosciences, Inc. (SF, BOD, EI); TruTag Technologies (SAB, EI); and Well-Healthcare Technologies (SAB, PC). MJS is also a Guest Professor at Zhejiang University, China. Although one or more of the grants that supported this research has been identified for conflict of interest management based on the overall scope of the project and its potential benefit to the companies listed, the research findings included in this publication may not necessarily relate to their interests. The terms of these arrangements have been reviewed and approved by the University of California, San Diego in accordance with its conflict of interest policies.

REFERENCES

(1)   Maas, A. I. R.; Menon, D. K.; Adelson, P. D.; Andelic, N.; Bell, M. J.; Belli, A.; Bragge, P.;
        Brazinova, A.; Büki, A.; Chesnut, R. M.; Citerio, G.; Coburn, M.; Cooper, D. J.; Crowder,
        A. T.; Czeiter, E.; Czosnyka, M.; Diaz-arrastia, R.; Gruen, R. L.; Gupta, D.; Hartings, J. A.;
        Hill, S.; Jiang, J.; Ketharanathan, N.; Kompanje, E. J. O.; Lanyon, L.; Laureys, S.; Lecky,
        F.; Levin, H.; Lingsma, H. F.; Maegele, M.; Majdan, M.; Manley, G.; Marsteller, J.; Mascia,
        L.; Mcfadyen, C.; Mondello, S.; Newcombe, V.; Palotie, A.; Parizel, P. M.; Peul, W.;
        Piercy, J.; Polinder, S.; Puybasset, L.; Wilson, L.; Yaffe, K. The Lancet Neurology
        Commission Traumatic Brain Injury : Integrated Approaches to Improve Prevention ,
        Clinical Care , and Research. *Lancet Neurol. Comm.* **2017**, *16*.
        https://doi.org/10.1016/S1474-4422(17)30371-X.

(2)   Gorelick, P. The Global Burden of Stroke : Persistent and Disabling. *Lancet Neurol.* **2019**,
        18 (5), 417–418. https://doi.org/10.1016/S1474-4422(19)30030-4.

(3)   Benjamin, E. J.; Virani, S. S.; Callaway, C. W.; Chamberlain, A. M.; Chang, A. R.; Cheng,
        S.; Chiuve, S. E.; Cushman, M.; Delling, F. N.; Deo, R.; de Ferranti, S. D.; Ferguson, J.
        F.; Fornage, M.; Gillespie, C.; Isasi, C. R.; Jiménez, M. C.; Jordan, L. C.; Judd, S. E.;
        Lackland, D.; Lichtman, J. H.; Lisabeth, L.; Liu, S.; Longenecker, C. T.; Lutsey, P. L.;
        Mackey, J. S.; Matchar, D. B.; Matsushita, K.; Mussolino, M. E.; Nasir, K.; O'Flaherty, M.;
        Palaniappan, L. P.; Pandey, A.; Pandey, D. K.; Reeves, M. J.; Ritchey, M. D.; Rodriguez,
        C. J.; Roth, G. A.; Rosamond, W. D.; Sampson, U. K. A.; Satou, G. M.; Shah, S. H.;
        Spartano, N. L.; Tirschwell, D. L.; Tsao, C. W.; Voeks, J. H.; Willey, J. Z.; Wilkins, J. T.;
        Wu, J. HY.; Alger, H. M.; Wong, S. S.; Muntner, P. *Heart Disease and Stroke Statistics—
        2017 Update*; 2017; Vol. 135. https://doi.org/10.1161/CIR.0000000000000485.Heart.

(4)   Peterson, A.; Xu, L.; Daugherty, J.; Breiding, M. J. Surveillance Report of Traumatic Brain
        Injury-Related Emergency Department Visits, Hospitalizations, and Deaths-United States,
        2014. **2019**, 24.

(5)   Giustini, A.; Pistarini, C.; Pisoni, C. *Traumatic and Nontraumatic Brain Injury*, 1st ed.;
        Elsevier B.V., 2013; Vol. 110. https://doi.org/10.1016/B978-0-444-52901-5.00034-4.

(6)   Havakuk, O.; King, K. S.; Grazette, L.; Yoon, A. J.; Fong, M.; Bregman, N.; Elkayam, U.;
        Kloner, R. A. Heart Failure-Induced Brain Injury. *J. Am. Coll. Cardiol.* **2017**, *69* (12),
        1609–1616. https://doi.org/10.1016/j.jacc.2017.01.022.

(7)   Majdan, M.; Mauritz, W.; Brazinova, A.; Rusnak, M.; Leitgeb, J.; Janciak, I.; Wilbacher, I.
        Severity and Outcome of Traumatic Brain Injuries (TBI) with Different Causes of Injury.
        Brain Inj. **2011**, *25* (9), 797–805. https://doi.org/10.3109/02699052.2011.581642.

(8)   Werner, C.; Engelhard, K.; Gutenberg-universita, D. J. Pathophysiology of Traumatic
        Brain Injury. **2007**, *99* (1), 4–9. https://doi.org/10.1093/bja/aem131.

(9)   Woodruff, T. M.; Thundyil, J.; Tang, S.; Sobey, C. G.; Taylor, S. M.; Arumugam, T. V.
        Pathophysiology , Treatment , and Animal and Cellular Models of Human Ischemic
        Stroke. **2011**, 1–19.

(10) Aronowski, J.; Zhao, X. Molecular Pathophysiology of Cerebral Hemorrhage: Secondary Brain Injury. *Stroke* **2011**, *42* (6), 1781–1786. https://doi.org/10.1161/STROKEAHA.110.596718.Molecular.

(11) Roozenbeek, B.; Maas, A. I. R.; Menon, D. K. Changing Patterns in the Epidemiology of Traumatic Brain Injury. *Nat. Rev. Neurol.* **2013**, *9* (4), 231–236. https://doi.org/10.1038/nrneurol.2013.22.

(12) Fong, R.; Konakondla, S.; Schirmer, C. M.; Lacroix, M. Surgical Interventions for Severe Traumatic Brain Injury. *J. Emerg. Crit. Care Med.* **2017**, *1* (10), 28–28. https://doi.org/10.21037/jeccm.2017.09.03.

(13) Kim, Y. J. The Impact of Time from ED Arrival to Surgery on Mortality and Hospital Length of Stay in Patients With Traumatic Brain Injury. *J. Emerg. Nurs.* **2011**, *37* (4), 328–333. https://doi.org/10.1016/j.jen.2010.04.017.

(14) Gravanis, I. TPA as a Therapeutic Target in Stroke. *Expert Opinon Ther. Targets* **2013**, *12* (2). https://doi.org/10.1517/14728222.12.2.159.tPA.

(15) Catanese, L.; Tarsia, J.; Fisher, M. Acute Ischemic Stroke Therapy Overview. *Circ. Res.* **2017**, *120* (3), 541–558. https://doi.org/10.1161/CIRCRESAHA.116.309278.

(16) Furlan, A. J. Endovascular Therapy for Stroke — It 's about Time. *N. Engl. J. Med.* **2015**, No. 372, 2347–2349.

(17) Nogueira, R. G.; Jadhav, A. P.; Haussen, D. C.; Bonafe, A.; Budzik, R. F.; Bhuva, P.; Yavagal, D. R.; Ribo, M.; Cognard, C.; Hanel, R. A.; Sila, C. A.; Hassan, A. E.; Millan, M.; Levy, E. I.; Mitchell, P.; Chen, M.; English, J. D.; Shah, Q. A.; Silver, F. L.; Pereira, V. M.; Mehta, B. P.; Baxter, B. W.; Abraham, M. G.; Cardona, P.; Veznedaroglu, E.; Hellinger, F. R.; Feng, L.; Kirmani, J. F.; Lopes, D. K.; Jankowitz, B. T.; Frankel, M. R.; Costalat, V.; Vora, N. A.; Yoo, A. J.; Malik, A. M.; Furlan, A. J.; Rubiera, M.; Aghaebrahim, A.; Olivot, J. M.; Tekle, W. G.; Shields, R.; Graves, T.; Lewis, R. J.; Smith, W. S.; Liebeskind, D. S.; Saver, J. L.; Jovin, T. G. Thrombectomy 6 to 24 Hours after Stroke with a Mismatch between Deficit and Infarct. *N. Engl. J. Med.* **2018**, *378* (1), 11–21. https://doi.org/10.1056/NEJMoa1706442.

(18) Stocchetti, N.; Taccone, F. S.; Citerio, G.; Pepe, P. E.; Roux, P. D. Le; Oddo, M.; Polderman, K. H.; Stevens, R. D.; Barsan, W.; Maas, A. I. R.; Meyfroidt, G.; Bell, M. J.; Silbergleit, R.; Vespa, P. M.; Faden, A. I.; Helbok, R.; Tisherman, S.; Zanier, E. R. Neuroprotection in Acute Brain Injury : An up-to-Date Review. **2015**, 1–11. https://doi.org/10.1186/s13054-015-0887-8.

(19) Loane, D. J.; Faden, A. I. Neuroprotection for Traumatic Brain Injury: Translational Challenges and Emerging Therapeutic Strategies. *Trends Pharmacol Sci* **2010**, *31* (12), 596–604. https://doi.org/10.1016/j.tips.2010.09.005.Neuroprotection.

(20) Skolnick, B. E.; Maas, A. I.; Narayan, R. K.; Hoop, R. G. Van Der; Macallister, T.; Ward, J. D.; Nelson, N. R.; Stocchetti, N. A Clinical Trial of Progesterone for Severe Traumatic Brain Injury. **2014**, 2467–2476. https://doi.org/10.1056/NEJMoa1411090.

(21)   Wright, D.; Yeatts, S.; Hertzberg, V. S.; Ph, D.; Frankel, M.; Goldstein, F. C.; Ph, D.; Caveney, A. F.; Ph, D.; Howlett-smith, H.; Bengelink, E. M.; Manley, G. T.; Ph, D.; Merck, L. H.; Janis, L. S.; Ph, D.; Barsan, W. G. Very Early Administration of Progesterone for Acute Traumatic Brain Injury. *N. Engl. J. Med.* **2014**, 2457–2466. https://doi.org/10.1056/NEJMoa1404304.

(22)   Stein, D. G. Embracing Failure : What the Phase III Progesterone Studies Can Teach about TBI Clinical Trials. **2015**, *9052* (11), 1259–1272. https://doi.org/10.3109/02699052.2015.1065344.

(23)   Chen, X.; Wang, K. The Fate of Medications Evaluated for Ischemic Stroke Pharmacotherapy over the Period 1995 – 2015. *Acta Pharm. Sin. B* **2016**, *6* (6), 522–530. https://doi.org/10.1016/j.apsb.2016.06.013.

(24)   Wong, C. H.; Siah, K. W.; Lo, A. W. Estimation of Clinical Trial Success Rates and Related Parameters. *Biostatistics* **2019**, *20* (2), 273–286. https://doi.org/10.1093/biostatistics/kxx069.

(25)   Meyers, P. M.; Schumacher, H. C.; Connolly, E. S.; Heyer, E. J.; Gray, W. A.; Higashida, R. T. Current Status of Endovascular Stroke Treatment. *Circulation* **2011**, *123* (22), 2591–2601. https://doi.org/10.1161/CIRCULATIONAHA.110.971564.

(26)   Brott, T.; Bogousslavsky, J. Treatment of Acute Ischemic Stroke. *N. Engl. J. Med.* **2000**, *343*, 710–722.

(27)   Tran, S.; Degiovanni, P. J.; Piel, B.; Rai, P. Cancer Nanomedicine : A Review of Recent Success in Drug Delivery. *Clin. Transl. Med.* **2017**. https://doi.org/10.1186/s40169-017-0175-0.

(28)   Xing, M.; Yan, F.; Yu, S.; Shen, P. Efficacy and Cardiotoxicity of Liposomal Doxorubicin-Based Chemotherapy in Advanced Breast Cancer : A Meta-Analysis of Ten Randomized Controlled Trials. **2015**, 1–9. https://doi.org/10.1371/journal.pone.0133569.

(29)   Miele, E.; Spinelli, G. P.; Miele, E.; Tomao, F.; Tomao, S. Albumin-Bound Formulation of Paclitaxel (Abraxane® ABI-007) in the Treatment of Breast Cancer. *Int. J. Nanomedicine* **2009**, *4* (1), 99–105. https://doi.org/10.2147/ijn.s3061.

(30)   Shi, J.; Kantoff, P.; Wooster, R.; Farokhzad, O. C. Cancer Nanomedicine: Progress, Challenges and Opportunities. *Nat. Rev. Cancer* **2017**, *17* (1), 20–37. https://doi.org/10.1038/nrc.2016.108.

(31)   Martins, J. P.; das Neves, J.; de la Fuente, M.; Celia, C.; Florindo, H.; Günday-Türeli, N.; Popat, A.; Santos, J. L.; Sousa, F.; Schmid, R.; Wolfram, J.; Sarmento, B.; Santos, H. A. The Solid Progress of Nanomedicine. *Drug Deliv. Transl. Res.* **2020**, 9–12. https://doi.org/10.1007/s13346-020-00743-2.

(32)   Anselmo, A. C.; Mitragotri, S. Nanoparticles in the Clinic : An Update. **2019**, No. August, 1–16. https://doi.org/10.1002/btm2.10143.

(33) He, H.; Liu, L.; Morin, E. E.; Liu, M.; Schwendeman, A. Survey of Clinical Translation of Cancer Nanomedicines - Lessons Learned from Successes and Failures. *Acc. Chem. Res.* **2019**, *52* (9), 2673–2683. https://doi.org/10.1021/acs.accounts.9b00228.

(34) Kroll, A. V; Jiang, Y.; Zhou, J.; Holay, M.; Fang, R. H. Biomimetic Nanoparticle Vaccines for Cancer Therapy. *Adv. Biosyst.* **2019**, *1800219*, 1–17. https://doi.org/10.1002/adbi.201800219.

(35) Ishii, T.; Asai, T.; Oyama, D.; Fukuta, T.; Yasuda, N.; Shimizu, K.; Minamino, T.; Oku, N. Amelioration of Cerebral Ischemia-Reperfusion Injury Based on Liposomal Drug Delivery System with Asialo-Erythropoietin. *J. Controlled Release* **2012**, *160* (1), 81–87. https://doi.org/10.1016/j.jconrel.2012.02.004.

(36) Boyd, B. J.; Galle, A.; Daglas, M.; Rosenfeld, J. V.; Medcalf, R. Traumatic Brain Injury Opens Blood-Brain Barrier to Stealth Liposomes via an Enhanced Permeability and Retention (EPR)-like Effect. *J. Drug Target.* **2015**, *23* (9), 847–853. https://doi.org/10.3109/1061186X.2015.1034280.

(37) Ruozi, B.; Belletti, D.; Sharma, H. S.; Sharma, A.; Muresanu, D. F.; Mössler, H.; Forni, F.; Vandelli, M. A.; Tosi, G. PLGA Nanoparticles Loaded Cerebrolysin: Studies on Their Preparation and Investigation of the Effect of Storage and Serum Stability with Reference to Traumatic Brain Injury. *Mol. Neurobiol.* **2015**, *52* (2), 899–912. https://doi.org/10.1007/s12035-015-9235-x.

(38) Gaudin, A.; Couvreur, P. Squalenoyl Adenosine Nanoparticles Provide Neuroprotection after Stroke and Spinal Cord Injury. *Nat. Nanotechnol.* **2014**. https://doi.org/10.1038/nnano.2014.274.

(39) Li, M.; Li, J.; Chen, J.; Liu, Y.; Cheng, X.; Yang, F.; Gu, N. [ASAP] Platelet Membrane Biomimetic Magnetic Nanocarriers for Targeted Delivery and in Situ Generation of Nitric Oxide in Early Ischemic Stroke. *ACS Nano* **2020**. https://doi.org/10.1021/acsnano.9b08587.

(40) Hubbard, W. B.; Lashof-sullivan, M.; Greenberg, S.; Norris, C.; Eck, J.; Lavik, E.; Vandevord, P. Hemostatic Nanoparticles Increase Survival , Mitigate Neuropathology and Alleviate Anxiety in a Rodent Blast Trauma Model. *Sci. Rep.* **2018**, *8* (November 2017), 1–12. https://doi.org/10.1038/s41598-018-28848-2.

(41) Khalin, I.; Alyautdin, R.; Wong, T. W.; Gnanou, J.; Kocherga, G.; Kreuter, J. Brain-Derived Neurotrophic Factor Delivered to the Brain Using Poly (Lactide-Co-Glycolide) Nanoparticles Improves Neurological and Cognitive Outcome in Mice with Traumatic Brain Injury. *Drug Deliv.* **2016**, *23* (9), 3520–3528. https://doi.org/10.1080/10717544.2016.1199609.

(42) Verma, S. K.; Arora, I.; Javed, K.; Akhtar, M.; Samim, M. Enhancement in the Neuroprotective Power of Riluzole Against Cerebral Ischemia Using a Brain Targeted Drug Delivery Vehicle. *ACS Appl. Mater. Interfaces* **2016**, *8* (30), 19716–19723. https://doi.org/10.1021/acsami.6b01776.

(43) Zhao, Y.; Jiang, Y.; Lv, W.; Wang, Z.; Lv, L.; Wang, B.; Liu, X.; Liu, Y.; Hu, Q.; Sun, W.; Xu, Q.; Xin, H.; Gu, Z. Dual Targeted Nanocarrier for Brain Ischemic Stroke Treatment. *J. Controlled Release* **2016**, *233*, 64–71. https://doi.org/10.1016/j.jconrel.2016.04.038.

(44) Kwon, E. J.; Skalak, M.; Lo Bu, R.; Bhatia, S. N. Neuron-Targeted Nanoparticle for SiRNA Delivery to Traumatic Brain Injuries. *ACS Nano* **2016**, *10* (8), 7926–7933. https://doi.org/10.1021/acsnano.6b03858.

(45) Kang, J.; Joo, J.; Kwon, E. J.; Skalak, M.; Hussain, S.; She, Z.-G.; Ruoslahti, E.; Bhatia, S. N.; Sailor, M. J. Self-Sealing Porous Silicon-Calcium Silicate Core-Shell Nanoparticles for Targeted SiRNA Delivery to the Injured Brain. *Adv Mater* **2016**, *28* (36), 7962–7969. https://doi.org/10.1002/adma.201600634.Self-Sealing.

(46) Mann, A. P.; Scodeller, P.; Hussain, S.; Joo, J.; Kwon, E.; Braun, G. B.; Molder, T.; She, Z.; Kotamraju, V. R.; Ranscht, B.; Krajewski, S.; Teesalu, T.; Bhatia, S. N.; Sailor, M.; Ruoslahti, E. A Peptide for Targeted, Systemic Delivery of Imaging and Therapeutic Compounds into Acute Brain Injuries. *Nat. Commun.* **2016**, *7* (May). https://doi.org/10.1038/ncomms11980.

(47) Wu, P.; Zhao, H.; Gou, X.; Wu, X.; Zhang, S.; Deng, G.; Chen, Q. Targeted Delivery of Polypeptide Nanoparticle for Treatment of Traumatic Brain Injury. *Int. J. Nanomedicine* **2019**, *14*, 4059–4069.

(48) Yoo, D.; Magsam, A. W.; Kelly, A. M.; Stayton, P. S.; Kievit, F. M.; Convertine, A. J. Core-Cross-Linked Nanoparticles Reduce Neuroinflammation and Improve Outcome in a Mouse Model of Traumatic Brain Injury. *ACS Nano* **2017**, *11* (9), 8600–8611. https://doi.org/10.1021/acsnano.7b03426.

(49) Rajkovic, O.; Gourmel, C.; d'Arcy, R.; Wong, R.; Rajkovic, I.; Tirelli, N.; Pinteaux, E. Reactive Oxygen Species-Responsive Nanoparticles for the Treatment of Ischemic Stroke. *Adv. Ther.* **2019**, *1900038*, 1900038. https://doi.org/10.1002/adtp.201900038.

(50) Lv, W.; Xu, J.; Wang, X.; Li, X.; Xu, Q.; Xin, H. Bioengineered Boronic Ester Modified Dextran Polymer Nanoparticles as Reactive Oxygen Species Responsive Nanocarrier for Ischemic Stroke Treatment. *ACS Nano* **2018**, *12* (6), 5417–5426. https://doi.org/10.1021/acsnano.8b00477.

(51) Bitner, B. R.; Marcano, D. C.; Berlin, J. M.; Fabian, R. H.; Cherian, L.; Culver, J. C.; Dickinson, M. E.; Robertson, C. S.; Pautler, R. G.; Kent, T. A.; Tour, J. M. Antioxidant Carbon Particles Improve Cerebrovascular Dysfunction Following Traumatic Brain Injury. *ACS Nano* **2012**, *6* (9), 8007–8014. https://doi.org/10.1021/nn302615f.

(52) Guo, X.; Deng, G.; Liu, J.; Zou, P.; Du, F.; Liu, F.; Chen, A. T.; Hu, R.; Li, M.; Zhang, S.; Tang, Z.; Han, L.; Liu, J.; Sheth, K. N.; Chen, Q.; Gou, X.; Zhou, J. Thrombin-Responsive, Brain-Targeting Nanoparticles for Improved Stroke Therapy. *ACS Nano* **2018**, *12* (8), 8723–8732. https://doi.org/10.1021/acsnano.8b04787.

(53) Xu, J.; Wang, X.; Yin, H.; Cao, X.; Hu, Q.; Lv, W.; Xu, Q.; Gu, Z.; Xin, H. Sequentially Site-Specific Delivery of Thrombolytics and Neuroprotectant for Enhanced Treatment of Ischemic Stroke. *ACS Nano* **2019**, *13* (8), 8577–8588. https://doi.org/10.1021/acsnano.9b01798.

(54) Kudryashev, J. A.; Waggoner, L. E.; Leng, H. T.; Mininni, N. H.; Kwon, E. J. An Activity-Based Nanosensor for Traumatic Brain Injury. **2020**. https://doi.org/10.1021/acssensors.9b01812.

(55) Sharma, A.; Liaw, K.; Sharma, R.; Zhang, Z.; Kannan, S.; Kannan, R. M. Targeting Mitochondrial Dysfunction and Oxidative Stress in Activated Microglia Using Dendrimer-Based Therapeutics. *Theranostics* **2018**, *8* (20), 5529–5547. https://doi.org/10.7150/thno.29039.

(56) Zhang, C. Y.; Dong, X.; Gao, J.; Lin, W.; Liu, Z.; Wang, Z. Nanoparticle-Induced Neutrophil Apoptosis Increases Survival in Sepsis and Alleviates Neurological Damage in Stroke. *Sci. Adv.* **2019**, *5* (11), 1–13. https://doi.org/10.1126/sciadv.aax7964.

(57) Makinde, H. M.; Just, T. B.; Cuda, C. M.; Bertolino, N.; Procissi, D.; Schwulst, S. J. Monocyte Depletion Attenuates the Development of Posttraumatic Hydrocephalus and Preserves White Matter Integrity after Traumatic Brain Injury. *PLoS ONE* **2018**, *13* (11), 1–15. https://doi.org/10.1371/journal.pone.0202722.

(58) Aertker, B. M.; Kumar, A.; Prabhakara, K. S.; Smith, P.; Furman, N. E. T.; Hasen, X.; Cox, C. S.; Bedi, S. S. Pre-Injury Monocyte/Macrophage Depletion Results in Increased Blood–Brain Barrier Permeability after Traumatic Brain Injury. *J. Neurosci. Res.* **2019**, *97* (6), 698–707. https://doi.org/10.1002/jnr.24395.

(59) Sharma, S.; Ifergan, I.; Kurz, J. E.; Linsenmeier, R. A.; Xu, D.; Cooper, J. G.; Miller, S. D.; Kessler, J. A. Intravenous Immunomodulatory Nanoparticle Treatment for Traumatic Brain Injury. *Ann. Neurol.* **2020**, *87* (3), 442–455. https://doi.org/10.1002/ana.25675.

(60) Dong, X.; Gao, J.; Zhang, C. Y.; Hayworth, C.; Frank, M.; Wang, Z. Neutrophil Membrane-Derived Nanovesicles Alleviate Inflammation to Protect Mouse Brain Injury from Ischemic Stroke. *ACS Nano* **2019**, *13* (2), 1272–1283. https://doi.org/10.1021/acsnano.8b06572.

(61) Hou, J.; Yang, X.; Li, S.; Cheng, Z.; Wang, Y.; Zhao, J.; Zhang, C.; Li, Y.; Luo, M.; Ren, H.; Liang, J.; Wang, J.; Wang, J.; Qin, J. Accessing Neuroinflammation Sites: Monocyte/Neutrophil-Mediated Drug Delivery for Cerebral Ischemia. *Sci. Adv.* **2019**, *5* (7), 1–13. https://doi.org/10.1126/sciadv.aau8301.

(62) Tong, H.; Kang, W.; Davy, P. M. C.; Shi, Y.; Sun, S.; Allsopp, R. C. Monocyte Trafficking, Engraftment, and Delivery of Nanoparticles and an Exogenous Gene into the Acutely Inflamed Brain Tissue – Evaluations on Monocyte-Based Delivery System for the Central Nervous System. **2016**, 1–21. https://doi.org/10.1371/journal.pone.0154022.

(63) Klyachko, N. L.; Polak, R.; Haney, M. J.; Zhao, Y.; Neto, J. G.; Hill, M. C.; Kabanov, A. V; Cohen, R. E.; Rubner, F.; Batrakova, E. V; Hill, C.; State, M. V. L. M. Macrophages with Cellular Backpacks for Targeted Drug Delivery to the Brain. *Biomaterials* **2018**, *140*, 79–87. https://doi.org/10.1016/j.biomaterials.2017.06.017.Macrophages.

(64) Skinner, S. A.; Tutton, P. J. M.; O'Brien, P. E. Microvascular Architecture of Experimental Colon Tumors in the Rat. *Cancer Res.* **1990**, *50* (8), 2411–2417.

(65)   Hashizume, H.; Baluk, P.; Morikawa, S.; McLean, J. W.; Thurston, G.; Roberge, S.; Jain, R. K.; McDonald, D. M. Openings between Defective Endothelial Cells Explain Tumor Vessel Leakiness. *Am. J. Pathol.* **2000**, *156* (4), 1363–1380. https://doi.org/10.1016/S0002-9440(10)65006-7.

(66)   Maeda, H.; Wu, J.; Sawa, T.; Matsumura, Y.; Hori, K. Tumor Vascular Permeability and the EPR Effect in Macromolecular Therapeutics : A Review. **2000**, *65*, 271–284.

(67)   Ballabh, P.; Braun, A.; Nedergaard, M. The Blood-Brain Barrier: An Overview: Structure, Regulation, and Clinical Implications. *Neurobiol. Dis.* **2004**, *16* (1), 1–13. https://doi.org/10.1016/j.nbd.2003.12.016.

(68)   Dvorak, H. F. Tumors : Wounds That Do Not Heal--Redux. *Cancer Immunol Res* **2015**, *3* (1), 1–11. https://doi.org/10.1158/2326-6066.CIR-14-0209.Tumors.

(69)   Lombardo, D.; Kiselev, M. A.; Caccamo, M. T. Smart Nanoparticles for Drug Delivery Application: Development of Versatile Nanocarrier Platforms in Biotechnology and Nanomedicine. *J. Nanomater.* **2019**, *2019*. https://doi.org/10.1155/2019/3702518.

(70)   van der Meel, R.; Sulheim, E.; Shi, Y.; Kiessling, F.; Mulder, W. J. M.; Lammers, T. Smart Cancer Nanomedicine. *Nat. Nanotechnol.* **2019**, *14* (11), 1007–1017. https://doi.org/10.1038/s41565-019-0567-y.

(71)   Jiao, Q.; Li, L.; Mu, Q.; Zhang, Q. Immunomodulation of Nanoparticles in Nanomedicine Applications. *BioMed Res. Int.* **2014**, *2014*. https://doi.org/10.1155/2014/426028.

(72)   Jassam, Y. N.; Izzy, S.; Whalen, M.; McGavern, D. B.; El Khoury, J. Neuroimmunology of Traumatic Brain Injury: Time for a Paradigm Shift. *Neuron* **2017**, *95* (6), 1246–1265. https://doi.org/10.1016/j.neuron.2017.07.010.

(73)   Malone, K.; Amu, S.; Moore, A. C.; Waeber, C. Immunomodulatory Therapeutic Strategies in Stroke. *Front. Pharmacol.* **2019**, *10* (JUN), 1–21. https://doi.org/10.3389/fphar.2019.00630.

(74)   Bharadwaj, V.; Nguyen, D.; Kodibagkar, V.; Stabenfeldt, S. Nanoparticle-Based Therapeutics for Brain Injury. *Adv Heal. Mater* **2018**, *7* (1). https://doi.org/10.1016/j.physbeh.2017.03.040.

(75)   Seo, Y.-E.; Bu, T.; Saltzman, W. M. Nanomaterials for Convection-Enhanced Delivery of Agents to Treat Brain Tumors. *Curr Opin Biomed Eng* **2017**, *December* (4), 1–12. https://doi.org/10.1016/j.physbeh.2017.03.040.

(76)   Alshweiat, A.; Ambrus, R.; Csóka, Ii. Intranasal Nanoparticulate Systems as Alternative Route of Drug Delivery. *Curr. Med. Chem.* **2019**, *26* (35), 6459–6492. https://doi.org/10.2174/0929867326666190827151741.

(77)   Alavian, F.; Shams, N. Oral and Intranasal Administration of Nanoparticles in the Cerebral Ischemia Treatment; Considering the Advantages and Disadvantages. *Curr. Clin. Pharmacol.* **2019**, *14*, 20–29. https://doi.org/10.2174/1574884714666190704115345.

(78)   Calias, P.; Banks, W. A.; Begley, D.; Scarpa, M.; Dickson, P. Intrathecal Delivery of Protein Therapeutics to the Brain: A Critical Reassessment. *Pharmacol. Ther.* **2014**, *144* (2), 114–122. https://doi.org/10.1016/j.pharmthera.2014.05.009.

(79)   Pillai, G. Nanomedicines for Cancer Therapy: An Update of FDA Approved and Those under Various Stages of Development. *SOJ Pharm. Pharm. Sci.* **2014**. https://doi.org/10.15226/2374-6866/1/2/00109.

(80)   Xiong, Y.; Mahmood, A.; Choop, M. Animal Models of Traumatic Brain Injury. *Nat Rev Neurosci* **2013**, *14* (2), 128–142. https://doi.org/10.1038/nrn3407.

(81)   Morales, D. M.; Marklund, N.; Lebold, D.; Thompson, H. J.; Pitkanen, A.; Maxwell, W. L.; Longhi, L.; Laurer, H.; Maegele, M.; Neugebauer, E.; Graham, D. I.; Stocchetti, N.; McIntosh, T. K. Experimental Models of Traumatic Brain Injury: Do We Really Need to Build a Better Mousetrap? *Neuroscience* **2005**, *136* (4), 971–989. https://doi.org/10.1016/j.neuroscience.2005.08.030.

(82)   Wojnarowicz, M. W.; Fisher, A. M.; Minaeva, O.; Goldstein, L. E. Considerations for Experimental Animal Models of Concussion, Traumatic Brain Injury, and Chronic Traumatic Encephalopathy-These Matters Matter. *Front. Neurol.* **2017**, *8* (JUN), 1–14. https://doi.org/10.3389/fneur.2017.00240.

(83)   Fluri, F.; Schuhmann, M. K.; Kleinschnitz, C. Animal Models of Ischemic Stroke and Their Application in Clinical Research. *Drug Des. Devel. Ther.* **2015**, *9*, 3445–3454. https://doi.org/10.2147/DDDT.S56071.

(84)   Herson, Paco; Traystman, R. Animal Models of Stroke: Translational Potential at Present and in 2050. *Future Neurol* **2014**, *9* (5), 541–551. https://doi.org/10.2217/fnl.14.44.Animal.

(85)   Jickling, G. C.; Sharp, F. R. Improving the Translation of Animal Ischemic Stroke Studies to Humans. *Metab. Brain Dis.* **2015**, *30* (2), 461–467. https://doi.org/10.1007/s11011-014-9499-2.

(86)   Xu, W. W.; Zhang, Y. Y.; Su, J.; Liu, A. F.; Wang, K.; Li, C.; Liu, Y. E.; Zhang, Y. Q.; Lv, J.; Jiang, W. J. Ischemia Reperfusion Injury after Gradual versus Rapid Flow Restoration for Middle Cerebral Artery Occlusion Rats. *Sci. Rep.* **2018**, *8* (1), 1–9. https://doi.org/10.1038/s41598-018-20095-9.

(87)   Uzdensky, A. B. Photothrombotic Stroke as a Model of Ischemic Stroke. *Transl. Stroke Res.* **2018**, *9* (5), 437–451. https://doi.org/10.1007/s12975-017-0593-8.

(88)   Saharinen, P.; Eklund, L.; Pulkki, K.; Bono, P.; Alitalo, K. VEGF and Angiopoietin Signaling in Tumor Angiogenesis and Metastasis. *Cell Press Trends Mol. Med.* **2011**, *17* (7), 347–362. https://doi.org/10.1016/j.molmed.2011.01.015.

(89)   Chodobski, A.; Zink, B. J.; Szmydynger-Chodobska, J. Blood-Brain Barrier Pathophysiology in Traumatic Brain Injury. *Transl. Stroke Res.* **2011**, *2* (4), 492–516. https://doi.org/10.1007/s12975-011-0125-x.

(90)   Uyama, O.; Okamura, N.; Yanase, M.; Narita, M.; Kawabata, K.; Sugita, M. Quantitative Evaluation of Vascular Permeability in the Gerbil Brain after Transient Ischemia Using

Evans Blue Fluorescence. *J. Cereb. Blood Flow Metab.* **1988**, *8* (2), 282–284. https://doi.org/10.1038/jcbfm.1988.59.

(91) Chen, Y.; Constantini, S.; Trembovler, V.; Weinstock, M.; Shohami, E. An Experimental Model of Closed Head Injury in Mice: Pathophysiology, Histopathology, and Cognitive Deficits. *J. Neurotrauma* **1996**, *13* (10), 557–568. https://doi.org/10.1089/neu.1996.13.557.

(92) Mayhan, W. G.; Heistad, D. D. Permeability of Blood-Brain Barrier to Various Sized Molecules. *Am. J. Physiol. - Heart Circ. Physiol.* **1985**, *17* (5). https://doi.org/10.1152/ajpheart.1985.248.5.h712.

(93) Gonul, E.; Duz, B.; Kahraman, S.; Kayali, H.; Kubar, A.; Timurkaynak, E. Early Pericyte Response to Brain Hypoxia in Cats: An Ultrastructural Study. *Microvasc. Res.* **2002**, *64* (1), 116–119. https://doi.org/10.1006/mvre.2002.2413.

(94) Dore-Duffy, P.; Owen, C.; Balabanov, R.; Murphy, S.; Beaumont, T.; Rafols, J. A. Pericyte Migration from the Vascular Wall in Response to Traumatic Brain Injury. *Microvasc. Res.* **2000**, *60* (1), 55–69. https://doi.org/10.1006/mvre.2000.2244.

(95) Del Zoppo, G. J.; Hallenbeck, J. M. Advances in the Vascular Pathophysiology of Ischemic Stroke. *Thromb. Res.* **2000**, *98* (3), 73–81. https://doi.org/10.1016/s0049-3848(00)00218-8.

(96) Yemisci, M.; Gursoy-ozdemir, Y.; Vural, A.; Can, A.; Topalkara, K.; Dalkara, T. Pericyte Contraction Induced by Oxidative-Nitrative Stress Impairs Capillary Reflow despite Successful Opening of an Occluded Cerebral Artery. *Nat. Med.* **2009**, *1* (August), 1031–1038. https://doi.org/10.1038/nm.2022.

(97) Cunningham, T. L.; Cartagena, C. M.; Lu, X. C. M.; Konopko, M.; Dave, J. R.; Tortella, F. C.; Shear, D. A. Correlations between Blood-Brain Barrier Disruption and Neuroinflammation in an Experimental Model of Penetrating Ballistic-like Brain Injury. *J. Neurotrauma* **2014**, *31* (5), 505–514. https://doi.org/10.1089/neu.2013.2965.

(98) Başkaya, M. K.; Rao, A. M.; Doğan, A.; Donaldson, D.; Dempsey, R. J. The Biphasic Opening of the Blood-Brain Barrier in the Cortex and Hippocampus after Traumatic Brain Injury in Rats. *Neurosci. Lett.* **1997**, *226* (1), 33–36. https://doi.org/10.1016/S0304-3940(97)00239-5.

(99) Belayev, L.; Busto, R.; Zhao, W.; Ginsberg, M. D. Quantitative Evaluation of Blood-Brain Barrier Permeability Following Middle Cerebral Artery Occlusion in Rats. *Brain Res.* **1996**, *739* (1–2), 88–96. https://doi.org/10.1016/S0006-8993(96)00815-3.

(100) Strbian, D.; Durukan, A.; Pitkonen, M.; Marinkovic, I.; Tatlisumak, E.; Pedrono, E.; Abo-Ramadan, U.; Tatlisumak, T. The Blood-Brain Barrier Is Continuously Open for Several Weeks Following Transient Focal Cerebral Ischemia. *Neuroscience* **2008**, *153* (1), 175–181. https://doi.org/10.1016/j.neuroscience.2008.02.012.

(101) Bharadwaj, V. N.; Lifshitz, J.; Adelson, P. D.; Kodibagkar, V. D. Temporal Assessment of Nanoparticle Accumulation after Experimental Brain Injury : Effect of Particle Size. *Nat. Publ. Group* **2016**, No. June, 1–12. https://doi.org/10.1038/srep29988.

(102) Sashindranath, M.; Sales, E.; Daglas, M.; Freeman, R.; Samson, A. L.; Cops, E. J.; Beckham, S.; Galle, A.; McLean, C.; Morganti-Kossmann, C.; Rosenfeld, J. V.; Madani, R.; Vassalli, J. D.; Su, E. J.; Lawrence, D. A.; Medcalf, R. L. The Tissue-Type Plasminogen Activator-Plasminogen Activator Inhibitor 1 Complex Promotes Neurovascular Injury in Brain Trauma: Evidence from Mice and Humans. *Brain* **2012**, *135* (11), 3251–3264. https://doi.org/10.1093/brain/aws178.

(103) Haley, M. J.; Lawrence, C. B. The Blood-Brain Barrier after Stroke: Structural Studies and the Role of Transcytotic Vesicles. *J. Cereb. Blood Flow Metab.* **2017**, *37* (2), 456–470. https://doi.org/10.1177/0271678X16629976.

(104) Huang, Q.; Zhong, W.; Hu, Z.; Tang, X. A Review of the Role of Cav-1 in Neuropathology and Neural Recovery after Ischemic Stroke. *J. Neuroinflammation* **2018**, *15* (1), 1–16. https://doi.org/10.1186/s12974-018-1387-y.

(105) Knowland, D.; Arac, A.; Sekiguchi, K. J.; Hsu, M.; Lutz, S. E.; Perrino, J.; Steinberg, G. K.; Barres, B. A.; Nimmerjahn, A.; Agalliu, D. Stepwise Recruitment of Transcellular and Paracellular Pathways Underlies Blood-Brain Barrier Breakdown in Stroke. *Neuron* **2014**, *82* (3), 603–617. https://doi.org/10.1016/j.neuron.2014.03.003.

(106) Sindhwani, S.; Syed, A. M.; Ngai, J.; Kingston, B. R.; Maiorino, L.; Rothschild, J.; MacMillan, P.; Zhang, Y.; Rajesh, N. U.; Hoang, T.; Wu, J. L. Y.; Wilhelm, S.; Zilman, A.; Gadde, S.; Sulaiman, A.; Ouyang, B.; Lin, Z.; Wang, L.; Egeblad, M.; Chan, W. C. W. The Entry of Nanoparticles into Solid Tumours. *Nat. Mater.* **2020**. https://doi.org/10.1038/s41563-019-0566-2.

(107) Mitragotri, S.; Burke, P.; Langer, R. Overcoming the Challenges in Administering Biopharmaceutics: Formulation and Deliveyr Strategies. *Nat Rev Drug Discov* **2014**, *13* (9), 655–672. https://doi.org/10.1016/j.physbeh.2017.03.040.

(108) Wilhelm, S.; Tavares, A. J.; Dai, Q.; Ohta, S.; Audet, J.; Dvorak, H. F.; Chan, W. C. W. Analysis of Nanoparticle Delivery to Tumours. *Nat. Rev. Mater.* **2016**, *1*. https://doi.org/10.1038/natrevmats.2016.14.

(109) Danhier, F. To Exploit the Tumor Microenvironment: Since the EPR Effect Fails in the Clinic, What Is the Future of Nanomedicine? *J. Controlled Release* **2016**, *244*, 108–121. https://doi.org/10.1016/j.jconrel.2016.11.015.

(110) Fang, J.; Nakamura, H.; Maeda, H. The EPR Effect: Unique Features of Tumor Blood Vessels for Drug Delivery, Factors Involved, and Limitations and Augmentation of the Effect. *Adv. Drug Deliv. Rev.* **2011**, *63* (3), 136–151. https://doi.org/10.1016/j.addr.2010.04.009.

(111) Golombek, S. K.; May, J. N.; Theek, B.; Appold, L.; Drude, N.; Kiessling, F.; Lammers, T. Tumor Targeting via EPR: Strategies to Enhance Patient Responses. *Adv. Drug Deliv. Rev.* **2018**, *130*, 17–38. https://doi.org/10.1016/j.addr.2018.07.007.

(112) Shi, J.; Kantoff, P. W.; Wooster, R.; Farokhzad, O. C. Cancer Nanomedicine: Progress, Challenges and Opportunities. *Nat. Rev. Cancer* **2017**, *17* (1), 20–37. https://doi.org/10.1038/nrc.2016.108.

(113) Kwon, E. J.; Skalak, M.; Bu, R. L.; Bhatia, S. N. A Neuron-Targeted Nanoparticle for SiRNA Delivery to Traumatic Brain Injuries. *ACS Nano* **2016**, *10* (8), 7926–7933. https://doi.org/10.1021/acsnano.6b03858.

(114) Rosenblum, D.; Joshi, N.; Tao, W.; Karp, J. M.; Peer, D. Progress and Challenges towards Targeted Delivery of Cancer Therapeutics. *Nat. Commun.* **2018**, *9* (1). https://doi.org/10.1038/s41467-018-03705-y.

(115) Tang, L.; Yang, X.; Yin, Q.; Cai, K.; Wang, H.; Chaudhury, I.; Yao, C.; Zhou, Q.; Kwon, M.; Hartman, J. A.; Dobrucki, I. T.; Dobrucki, L. W.; Borst, L. B.; Lezmi, S.; Helferich, W. G.; Ferguson, A. L.; Fan, T. M.; Cheng, J. Investigating the Optimal Size of Anticancer Nanomedicine. *Proc. Natl. Acad. Sci. U. S. A.* **2014**, *111* (43), 15344–15349. https://doi.org/10.1073/pnas.1411499111.

(116) Laroche, M.; Kutcher, M. E.; Huang, M. C.; Cohen, M. J.; Manley, G. T. Coagulopathy after Traumatic Brain Injury. *Neurosurgery* **2012**, *70* (6), 1334–1345. https://doi.org/10.1227/NEU.0b013e31824d179b.

(117) Versteeg, H. H.; Heemskerk, J. W. M.; Levi, M.; Reitsma, P. H. New Fundamentals In Hemostasis. *Physiol Rev* **2013**, *93*, 327–358. https://doi.org/10.1152/physrev.00016.2011.

(118) Chan, L. W.-G.; Wang, X.; Wei, H.; Pun, S. H. A Synthetic Fibrin-Crosslinking Polymer for Modulating Clot Proprties and Inducing Hemostasis. *Sci. Transl. Med.* **2015**, *7* (277). https://doi.org/10.1126/scitranslmed.3010383.A.

(119) Lin, K. Y.; Lo, J. H.; Consul, N.; Kwong, G. A.; Bhatia, S. N. Self-Titrating Anticoagulant Nanocomplexes That Restore Homeostatic Regulation of the Coagulation Cascade. *ACS Nano* **2014**, *8* (9), 8776–8785. https://doi.org/10.1021/nn501129q.

(120) Brown, A. C.; Lavik, E.; Stabenfeldt, S. E. Biomimetic Strategies to Treat Traumatic Brain Injury by Leveraging Fibrinogen. *Bioconjug. Chem.* **2019**, *30* (7), 1951–1956. https://doi.org/10.1021/acs.bioconjchem.9b00360.

(121) Munji, R. N.; Soung, A. L.; Weiner, G. A.; Sohet, F.; Semple, B. D.; Trivedi, A.; Gimlin, K.; Kotoda, M.; Korai, M.; Aydin, S.; Batugal, A.; Cabangcala, A. C.; Schupp, P. G.; Oldham, M. C.; Hashimoto, T.; Noble-Haeusslein, L. J.; Daneman, R. Profiling the Mouse Brain Endothelial Transcriptome in Health and Disease Models Reveals a Core Blood–Brain Barrier Dysfunction Module. *Nat. Neurosci.* **2019**, *22* (11), 1892–1902. https://doi.org/10.1038/s41593-019-0497-x.

(122) Ruoslahti, E. Vascular Zip Codes in Angiogenesis and Metastasis. *Biochem. Soc. Trans.* **2004**, *32* (3), 397–402. https://doi.org/10.1042/BST0320397.

(123) Quail, D. F.; Joyce, J. A. The Microenvironmental Landscape of Brain Tumors. *Cancer Cell* **2017**, *31* (3), 326–341. https://doi.org/10.1016/j.ccell.2017.02.009.

(124) Merino, M.; Zalba, S.; Garrido, M. J. Immunoliposomes in Clinical Oncology: State of the Art and Future Perspectives. *J. Controlled Release* **2018**, *275* (December 2017), 162–176. https://doi.org/10.1016/j.jconrel.2018.02.015.

(125) Mamot, C.; Ritschard, R.; Wicki, A.; Stehle, G.; Dieterle, T.; Bubendorf, L.; Hilker, C.; Deuster, S.; Herrmann, R.; Rochlitz, C. Tolerability, Safety, Pharmacokinetics, and Efficacy of Doxorubicin-Loaded Anti-EGFR Immunoliposomes in Advanced Solid Tumours: A Phase 1 Dose-Escalation Study. *Lancet Oncol.* **2012**, *13* (12), 1234–1241. https://doi.org/10.1016/S1470-2045(12)70476-X.

(126) Mamot, C.; Drummond, D. C.; Noble, C. O.; Kallab, V.; Guo, Z.; Hong, K.; Kirpotin, D. B.; Park, J. W. Epidermal Growth Factor Receptor-Targeted Immunoliposomes Significantly Enhance the Efficacy of Multiple Anticancer Drugs in Vivo. *Cancer Res.* **2005**, *65* (24), 11631–11638. https://doi.org/10.1158/0008-5472.CAN-05-1093.

(127) Zhang, B.; Shen, S.; Liao, Z.; Shi, W.; Wang, Y.; Zhao, J.; Hu, Y.; Yang, J.; Chen, J.; Mei, H.; Hu, Y.; Pang, Z.; Jiang, X. Targeting Fibronectins of Glioma Extracellular Matrix by CLT1 Peptide-Conjugated Nanoparticles. *Biomaterials* **2014**, *35* (13), 4088–4098. https://doi.org/10.1016/j.biomaterials.2014.01.046.

(128) Ishihara, J.; Ishihara, A.; Sasaki, K.; Hubbell, J. A. Targeted Antibody and Cytokine Cancer Immunotherapies through Collagen Binding. *Sci Transl Med* **2019**, *11* (487). https://doi.org/10.1016/j.physbeh.2017.03.040.

(129) George, N.; Geller, H. Extracellular Matrix and Traumatic Brain Injury. *J. Neurosci.* **2018**, *96* (4), 573–588. https://doi.org/10.1002/jnr.24151.Extracellular.

(130) Kumar, P.; Wu, H.; McBride, J. L.; Jung, K. E.; Hee Kim, M.; Davidson, B. L.; Kyung Lee, S.; Shankar, P.; Manjunath, N. Transvascular Delivery of Small Interfering RNA to the Central Nervous System. *Nature* **2007**, *448* (7149), 39–43. https://doi.org/10.1038/nature05901.

(131) Bikbaev, A.; Frischknecht, R.; Heine, M. Brain Extracellular Matrix Retains Connectivity in Neuronal Networks. *Sci. Rep.* **2015**, *5*, 1–12. https://doi.org/10.1038/srep14527.

(132) Lam, D.; Enright, H. A.; Cadena, J.; Peters, S. K. G.; Sales, A. P.; Osburn, J. J.; Soscia, D. A.; Kulp, K. S.; Wheeler, E. K.; Fischer, N. O. Tissue-Specific Extracellular Matrix Accelerates the Formation of Neural Networks and Communities in a Neuron-Glia Co-Culture on a Multi-Electrode Array. *Sci. Rep.* **2019**, *9* (1), 1–15. https://doi.org/10.1038/s41598-019-40128-1.

(133) Bonneh-Barkay, D.; Wiley, C. A. Brain Extracellular Matrix in Neurodegeneration. *Brain Pathol.* **2009**, *19* (4), 573–585. https://doi.org/10.1111/j.1750-3639.2008.00195.x.

(134) Asher, R. A.; Morgenstern, D. A.; Shearer, M. C.; Adcock, K. H.; Pesheva, P.; Fawcett, J. W. Versican Is Upregulated in CNS Injury and Is a Product of Oligodendrocyte Lineage Cells. *J. Neurosci.* **2002**, *22* (6), 2225–2236. https://doi.org/10.1523/jneurosci.22-06-02225.2002.

(135) Brodkey, J. A.; Laywell, E. D.; O'Brien, T. F.; Faissner, A.; Stefansson, K.; Dorries, H. U.; Schachner, M.; Steindler, D. A. Focal Brain Injury and Upregulation of a Developmentally Regulated Extracellular Matrix Protein. *J. Neurosurg.* **1995**, *82* (1), 106–112. https://doi.org/10.3171/jns.1995.82.1.0106.

(136) Lu, Y.; Aimetti, A. A.; Langer, R.; Gu, Z. Bioresponsive Materials. *Nat. Rev. Mater.* **2016**, *2* (1). https://doi.org/10.1038/natrevmats.2016.75.

(137) Kwon, E. J.; Lo, J. H.; Bhatia, S. N. Smart Nanosystems: Bio-Inspired Technologies That Interact with the Host Environment. *Proc. Natl. Acad. Sci. U. S. A.* **2015**, *112* (47), 14460–14466. https://doi.org/10.1073/pnas.1508522112.

(138) Smith, B. L.; Gadd, M. A.; Lanahan, C. R.; Rai, U.; Tang, R.; Rice-stitt, T.; Merrill, A. L.; Strasfeld, D. B.; Ferrer, J. M.; Brachtel, E. F.; Specht, M. C. Real-Time, Intraoperative Detection of Residual Breast Cancer in Lumpectomy Cavity Walls Using a Novel Cathepsin-Activate Fluorescent Imaging System. *Breast Cancer Res Treat* **2018**, *171* (2), 413–420. https://doi.org/10.1007/s10549-018-4845-4.Real-time.

(139) Whitley, M. J.; Cardona, D. M.; Lazarides, A. L.; Spasojevic, I.; Ferrer, J. M.; Cahill, J.; Lee, C.; Snuderl, M.; Iii, D. G. B.; Hwang, S.; Greenup, R. A.; Mosca, P. J.; Mito, J. K.; Cuneo, K. C.; Larrier, N. A.; Reilly, E. K. O.; Riedel, R. F.; Eward, W. C.; David, B.; Fukumura, D.; Jain, R. K.; Lee, W. D.; Griffith, L. G.; Moungi, G.; Kirsch, D. G.; Brigman, B. E. A Mouse-Human Phase 1 Co-Clinical Trial of a Protease-Activated Fluorescent Probe for Imaging Cancer. *Sci Transl Med* **2016**, *8* (320), 1–24. https://doi.org/10.1126/scitranslmed.aad0293.A.

(140) Bains, M.; Hall, E. D. Antioxidant Therapies in Traumatic Brain and Spinal Cord Injury. *Biochim Biophys Acta* **2012**, *1822* (5), 675–684. https://doi.org/10.1038/jid.2014.371.

(141) Lewén, A.; Hillered, L. Involvement of Reactive Oxygen Species in Membrane Phospholipid Breakdown and Energy Perturbation after Traumatic Brain Injury in the Rat. *J. Neurotrauma* **1998**, *15* (7), 521–530. https://doi.org/10.1089/neu.1998.15.521.

(142) Samuel, E. L. G.; Marcano, D. C.; Berka, V.; Bitner, B. R.; Wu, G.; Potter, A.; Fabian, R. H.; Pautler, R. G.; Kent, T. A.; Tsai, A. L.; Tour, J. M. Highly Efficient Conversion of Superoxide to Oxygen Using Hydrophilic Carbon Clusters. *Proc. Natl. Acad. Sci. U. S. A.* **2015**, *112* (8), 2343–2348. https://doi.org/10.1073/pnas.1417047112.

(143) Dudani, J. S.; Warren, A. D.; Bhatia, S. N. Harnessing Protease Activity to Improve Cancer Care. *Annu. Rev. Cancer Biol.* **2018**, *2* (1), 353–376. https://doi.org/10.1146/annurev-cancerbio-030617-050549.

(144) Chen, B.; Cheng, Q.; Yang, K.; Lyden, P. D. Thrombin Mediates Severe Neurovascular Injury during Ischemia. *Stroke* **2010**, *41* (10), 2348–2352. https://doi.org/10.1161/STROKEAHA.110.584920.

(145) Zhang, S.; Kojic, L.; Tsang, M.; Grewal, P.; Liu, J.; Namjoshi, D.; Wellington, C. L.; Tetzlaff, W.; Cynader, M. S.; Jia, W. Distinct Roles for Metalloproteinases during Traumatic Brain Injury. *Neurochem. Int.* **2016**, *96*, 46–55. https://doi.org/10.1016/j.neuint.2016.02.013.

(146) Krenzlin, H.; Lorenz, V.; Danckwardt, S.; Kempski, O.; Alessandri, B. The Importance of Thrombin in Cerebral Injury and Disease. *Int. J. Mol. Sci.* **2016**, *17* (1). https://doi.org/10.3390/ijms17010084.

(147) Rosenberg, G. A. Metalloproteinases Injury. **1995**, *12* (5), 833–842.

(148) Applegate, R. L.; Chen, G.; Feng, H.; Zhang Editors, J. H. *Brain Edema XVI.*

(149) Zhang, Y.-R.; Lin, R.; Li, H. J.; He, W. ling; Du, J. Z.; Wang, J. Strategies to Improve Tumor Penetration of Nanomedicines through Nanoparticle Design. *Wiley Interdiscip. Rev. Nanomed. Nanobiotechnol.* **2019**, *11* (1), 1–12. https://doi.org/10.1002/wnan.1519.

(150) Yuan, F.; Leunig, M.; Huang, S. K.; Berk, D. A.; Papahadjopoulos, D.; Jain, R. K. Microvascular Permeability and Interstitial Penetration of Sterically Stabilized (Stealth) Liposomes in a Human Tumor Xenograft. *Cancer Res.* **1994**, *54* (13), 3352–3356.

(151) Winer, E. P.; Berry, D. A.; Woolf, S.; Duggan, D.; Kornblith, A.; Harris, L. N.; Michaelson, R. A.; Kirshner, J. A.; Fleming, G. F.; Perry, M. C.; Graham, M. L.; Sharp, S. A.; Keresztes, R.; Henderson, I. C.; Hudis, C.; Muss, H.; Norton, L. Failure of Higher-Dose Paclitaxel to Improve Outcome in Patients with Metastatic Breast Cancer: Cancer and Leukemia Group B Trial 9342. *J. Clin. Oncol.* **2004**, *22* (11), 2061–2068. https://doi.org/10.1200/JCO.2004.08.048.

(152) Wang, K.; Liu, B. Y.; Ma, J. Research Progress in Traumatic Brain Penumbra. *Chin. Med. J. (Engl.)* **2014**, *127* (10), 1964–1968. https://doi.org/10.3760/cma.j.issn.0366-6999.20120638.

(153) Lo, E. H. A New Penumbra: Transitioning from Injury into Repair after Stroke. *Nat. Med.* **2008**, *14* (5), 497–500. https://doi.org/10.1038/nm1735.

(154) Ishii, T.; Fukuta, T.; Agato, Y.; Oyama, D.; Yasuda, N.; Shimizu, K.; Kawaguchi, A. T.; Asai, T.; Oku, N. Nanoparticles Accumulate in Ischemic Core and Penumbra Region Even When Cerebral Perfusion Is Reduced. *Biochem. Biophys. Res. Commun.* **2013**, *430* (4), 1201–1205. https://doi.org/10.1016/j.bbrc.2012.12.080.

(155) Nance, E. A.; Woodworth, G. F.; Sailor, K. A.; Shih, T. Y.; Xu, Q.; Swaminathan, G.; Xiang, D.; Eberhart, C.; Hanes, J. A Dense Poly(Ethylene Glycol) Coating Improves Penetration of Large Polymeric Nanoparticles within Brain Tissue. *Sci. Transl. Med.* **2012**, *4* (149). https://doi.org/10.1126/scitranslmed.3003594.

(156) Song, E.; Gaudin, A.; King, A. R.; Seo, Y. E.; Suh, H. W.; Deng, Y.; Cui, J.; Tietjen, G. T.; Huttner, A.; Saltzman, W. M. Surface Chemistry Governs Cellular Tropism of Nanoparticles in the Brain. *Nat. Commun.* **2017**, *8* (May), 1–14. https://doi.org/10.1038/ncomms15322.

(157) Teesalu, T.; Sugahara, K. N.; Kotamraju, V. R.; Ruoslahti, E. C-End Rule Peptides Mediate Neuropilin-1-Dependent Cell, Vascular, and Tissue Penetration. *Proc. Natl. Acad. Sci. U. S. A.* **2009**, *106* (38), 16157–16162. https://doi.org/10.1073/pnas.0908201106.

(158) Sugahara, K. N.; Teesalu, T.; Karmali, P. P.; Kotamraju, V. R.; Agemy, L.; Girard, O. M.; Hanahan, D.; Mattrey, R. F.; Ruoslahti, E. Tissue-Penetrating Delivery of Compounds and Nanoparticles into Tumors. *Cancer Cell* **2009**, *16* (6), 510–520. https://doi.org/10.1016/j.ccr.2009.10.013.

(159) Sugahara, K. N.; Teesalu, T.; Karmali, P. P.; Kotamraju, V. R.; Agemy, L.; Greenwald, D.; Ruoslahti, E. Coadministration of a Tumor-Penetrating Peptide Enhances the Efficacy of

Cancer Drugs. *Science* **2010**, *328*, 1031–1035.
https://doi.org/10.1017/CBO9781107415324.004.

(160) Lange, C.; Storkebaum, E.; De Almodóvar, C. R.; Dewerchin, M.; Carmeliet, P. Vascular Endothelial Growth Factor: A Neurovascular Target in Neurological Diseases. *Nat. Rev. Neurol.* **2016**, *12* (8), 439–454. https://doi.org/10.1038/nrneurol.2016.88.

(161) Min, Y.; Roche, K. C.; Tian, S.; Eblan, M. J.; McKinnon, K. P.; Caster, J. M.; Chai, S.; Herring, L. E.; Zhang, L.; Zhang, T.; Desimone, J. M.; Tepper, J. E.; Vincent, B. G.; Serody, J. S.; Wang, A. Z. Antigen-Capturing Nanoparticles Improve the Abscopal Effect and Cancer Immunotherapy. *Nat. Nanotechnol.* **2017**, *12* (9), 877–882. https://doi.org/10.1038/nnano.2017.113.

(162) Kang, T.; Zhu, Q.; Wei, D.; Feng, J.; Yao, J.; Jiang, T.; Song, Q.; Wei, X.; Chen, H.; Gao, X.; Chen, J. Nanoparticles Coated with Neutrophil Membranes Can Effectively Treat Cancer Metastasis. *ACS Nano* **2017**, *11* (2), 1397–1411. https://doi.org/10.1021/acsnano.6b06477.

(163) Liu, W. L.; Zou, M. Z.; Liu, T.; Zeng, J. Y.; Li, X.; Yu, W. Y.; Li, C. X.; Ye, J. J.; Song, W.; Feng, J.; Zhang, X. Z. Cytomembrane Nanovaccines Show Therapeutic Effects by Mimicking Tumor Cells and Antigen Presenting Cells. *Nat. Commun.* **2019**, *10* (1), 1–12. https://doi.org/10.1038/s41467-019-11157-1.

(164) Huang, B.; Abraham, W. D.; Zheng, Y.; López, S. C. B.; Luo, S. S.; Irvine, D. J. Active Targeting of Chemotherapy to Disseminated Tumors Using Nanoparticle-Carrying T Cells. *Sci. Transl. Med.* **2015**, *7* (291).

(165) Stephan, M. T.; Moon, J. J.; Um, S. H.; Bershteyn, A.; Irvine, D. J. Therapeutic Cell Engineering Using Surface-Conjugated Synthetic Nanoparticles. *Nat. Med.* **2011**, *16* (9), 1035–1041. https://doi.org/10.1038/nm.2198.Therapeutic.

(166) Tang, L.; Zheng, Y.; Vandiera de Melo, M.; Maus, M. V.; Irvine, D. J. Enhancing T Cell Therapy through TCR Signaling-Responsive Nanoparticle Drug Delivery. *Nat. Biotechnol.* **2019**, *36* (8), 707–716. https://doi.org/10.1038/nbt.4181.Enhancing.

(167) Kawabori, M.; Yenari, M. A. Inflammatory Responses in Brain Ischemia. *Curr Med Chem* **2015**, *22* (10), 1258–1277.

(168) Loane, D. J.; Kumar, A. Microglia in the TBI Brain: The Good, The Bad, and The Dysregulated. *Exp Neurol* **2016**, *275* (0 3), 316–327. https://doi.org/10.1016/j.expneurol.2015.08.018.Microglia.

(169) Gyoneva, S.; Ransohoff, R. M. Inflammatory Reaction after Traumatic Brain Injury: Therapeutic Potential of Targeting Cell-Cell Communication by Chemokines. *Trends Pharmacol Sci* **2015**, *176* (1), 471–480. https://doi.org/10.1016/j.physbeh.2017.03.040.

(170) Burda, J.; Sofroniew, M. Reactive Gliosis and the Multicellular Response to CNS Damage and Disease. *Neuron* **2014**, *81* (2), 229–248. https://doi.org/10.1016/j.neuron.2013.12.034.Reactive.

(171) Bergold, P. J. Treatment of Traumatic Brain Injury with Anti-Inflammatory Drugs. *Exp Neurol* **2016**, *275* (3), 367–380. https://doi.org/10.1016/j.physbeh.2017.03.040.

(172) Zhang, F.; Nance, E.; Alnasser, Y.; Kannan, R.; Kannan, S. Microglial Migration and Interactions with Dendrimer Nanoparticles Are Altered in the Presence of Neuroinflammation. *J. Neuroinflammation* **2016**, *13* (1), 1–11. https://doi.org/10.1186/s12974-016-0529-3.

(173) Sharma, A.; Sharma, R.; Zhang, Z.; Liaw, K.; Kambhampati, S. P.; Porterfield, J. E.; Lin, K. C.; Deridder, L. B.; Kannan, S.; Kannan, R. M. Dense Hydroxyl Polyethylene Glycol Dendrimer Targets Activated Glia in Multiple CNS Disorders. *Sci. Adv.* **2020**, *6*, 1–15.

(174) Liu, Y.; Li, S.; Dai, S. Neutrophils in Traumatic Brain Injury (TBI): Friend or Foe ? *J. Neuroinflammation* **2018**, *15* (146), 1–18.

(175) Bosetti, F.; Koenig, J. I.; Ayata, C.; Back, S. A.; Becker, K.; Broderick, J. P.; Carmichael, S. T.; Cho, S.; Cipolla, M. J.; Corbett, D.; Corriveau, R. A.; Cramer, S. C.; Ferguson, A. R.; Finklestein, S. P.; Ford, B. D.; Furie, K. L.; Hemmen, T. M.; Iadecola, C.; Jakeman, L. B.; Janis, S.; Jauch, E. C.; Johnston, K. C.; Kochanek, P. M.; Kohn, H.; Lo, E. H.; Lyden, P. D.; Mallard, C.; Mccullough, L. D.; Mcgavern, L. M.; Meschia, J. F.; Moy, C. S.; Perez-pinzon, M. A.; Ramadan, I.; Savitz, S. I.; Schwamm, L. H.; Steinberg, G. K.; Stenzel-poore, M. P.; Tymianski, M.; Warach, S.; Wechsler, L. R.; Zhang, J. H.; Koroshetz, W. Translational Stroke Research Vision and Opportunities. *Stroke AHA J.* **2017**, *48*, 2632–2637. https://doi.org/10.1161/STROKEAHA.117.017112.

(176) Hua, S.; de Matos, M. B. C.; Metselaar, J. M.; Storm, G. Current Trends and Challenges in the Clinical Translation of Nanoparticulate Nanomedicines: Pathways for Translational Development and Commercialization. *Front. Pharmacol.* **2018**, *9* (JUL), 1–14. https://doi.org/10.3389/fphar.2018.00790.

(177) Anselmo, A. C.; Mitragotri, S. Nanoparticles in the Clinic. *Bioeng. Transl. Med.* **2016**, *1* (1), 10–29. https://doi.org/10.1002/btm2.10003.

(178) Lin, K. Y.; Kwong, G. A.; Warren, A. D.; Wood, D. K.; Bhatia, S. Nanoparticles That Sense Thrombin Activity As Synthetic Urinary Biomarkers of Thrombosis. *ACS Nano* **2013**, *7* (10), 9001–9009. https://doi.org/10.1021/nn403550c.

(179) Goodman, S. N.; Gerson, J. Mechanistic Evidence in Evidence-Based Medicine: A Conceptual Framework. **2013**, 1–121.

(180) Mestas, J.; Hughes, C. C. W. Of Mice and Not Men: Differences between Mouse and Human Immunology. *J. Immunol.* **2004**, *172* (5), 2731–2738. https://doi.org/10.4049/jimmunol.172.5.2731.

(181) Tang, Y.; Lu, A.; Aronow, B. J.; Sharp, F. R. Blood Genomic Responses Differ after Stroke, Seizures, Hypoglycemia, and Hypoxia: Blood Genomic Fingerprints of Disease. *Ann. Neurol.* **2001**, *50* (6), 699–707. https://doi.org/10.1002/ana.10042.

(182) Tang, Y.; Xu, H.; Du, X.; Lit, L.; Walker, W.; Lu, A.; Ran, R.; Gregg, J. P.; Reilly, M.; Pancioli, A.; Khoury, J. C.; Sauerbeck, L. R.; Carrozzella, J. A.; Spilker, J.; Clark, J.; Wagner, K. R.; Jauch, E. C.; Chang, D. J.; Verro, P.; Broderick, J. P.; Sharp, F. R. Gene

Expression in Blood Changes Rapidly in Neutrophils and Monocytes after Ischemic Stroke in Humans: A Microarray Study. *J. Cereb. Blood Flow Metab.* **2006**, *26* (8), 1089–1102. https://doi.org/10.1038/sj.jcbfm.9600264.

(183) Stamova, B.; Sharp, F. R. Gene Expression Profiling of Blood for the Prediction of Ischemic Stroke. *Stroke* **2010**, *41* (10), 2171–2177. https://doi.org/10.1161/STROKEAHA.110.588335.Gene.

(184) Tseveleki, V.; Rubio, R.; Vamvakas, S. S.; White, J.; Taoufik, E.; Petit, E.; Quackenbush, J.; Probert, L. Comparative Gene Expression Analysis in Mouse Models for Multiple Sclerosis, Alzheimer's Disease and Stroke for Identifying Commonly Regulated and Disease-Specific Gene Changes. *Genomics* **2010**, *96* (2), 82–91. https://doi.org/10.1016/j.ygeno.2010.04.004.

(185) Wang, Y.; Cai, Y. Obtaining Human Ischemic Stroke Gene Expression Biomarkers from Animal Models: A Cross-Species Validation Study. *Sci. Rep.* **2016**, *6* (June), 1–11. https://doi.org/10.1038/srep29693.

(186) Du, Y.; Deng, W.; Wang, Z.; Ning, M.; Zhang, W.; Zhou, Y.; Lo, E. H.; Xing, C. Differential Subnetwork of Chemokines/ Cytokines in Human, Mouse, and Rat Brain Cells after Oxygen-Glucose Deprivation. *J. Cereb. Blood Flow Metab.* **2017**, *37* (4), 1425–1434. https://doi.org/10.1177/0271678X16656199.

(187) Statler, K. D.; Alexander, H.; Vagni, V.; Dixon, C. E.; Clark, R. S. B.; Jenkins, L.; Kochanek, P. M. Comparison of Seven Anesthetic Agents on Outcome after Experimental Traumatic Brain Injury in Adult, Male Rats. *J. Neurotrauma* **2006**, *23* (1), 97–108. https://doi.org/10.1089/neu.2006.23.97.

(188) Giza, C. C.; Mink, R. B.; Madikians, A. Pediatric Traumatic Brain Injury: Not Just Little Adults. *Curr. Opin. Crit. Care* **2007**, *13* (2), 143–152. https://doi.org/10.1097/MCC.0b013e32808255dc.

(189) CDC. *CDC.gov,* 2019.

(190) Fox, G. B.; Le Vasseur, R. A.; Faden, A. Behavioral Responses of C57BL/6, FVB/N, and 129/SvEMS Mouse Strains to Traumatic Brain Injury: Implications for Gene Targeting Approaches to Neurotrauma. *Neurotrauma* **1999**, *16* (5).

(191) Sieber, M. W.; Claus, R. A.; Witte, O. W.; Frahm, C. Attenuated Inflammatory Response in Aged Mice Brains Following Stroke. *PLoS ONE* **2011**, *6* (10), 1–11. https://doi.org/10.1371/journal.pone.0026288.

(192) Kumar, A.; Stoica, B. A.; Sabirzhanov, B.; Burns, M. P.; Faden, A. I.; Loane, D. J. Traumatic Brain Injury in Aged Animals Increases Lesion Size and Chronically Alters Microglial/Macrophage Classical and Alternative Activation States. *Neurobiol. Aging* **2013**, *34* (5), 1397–1411. https://doi.org/10.1016/j.neurobiolaging.2012.11.013.

(193) Roof, R. L.; Hall, E. D. Estrogen-Related Gender Difference in Survival Rate and Cortical Blood Flow After Impact-Acceleratiaon Head Injury in Rats. *J. Neurotrauma* **2000**, *17* (12), 1155–1169.

(194) Brotfain, E.; E. Gruenbaum, S.; Boyko, M.; Kutz, R.; Zlotnik, A.; Klein, M. Neuroprotection by Estrogen and Progesterone in Traumatic Brain Injury and Spinal Cord Injury. *Curr. Neuropharmacol.* **2016**, *14* (6), 641–653. https://doi.org/10.2174/1570159x14666160309123554.

(195) Green, S. M. Cheerio, Laddie! Bidding Farewell to the Glasgow Coma Scale. *Ann. Emerg. Med.* **2011**, *58* (5), 427–430. https://doi.org/10.1016/j.annemergmed.2011.06.009.

(196) Mohamadpour, M.; Whitney, K.; Bergold, P. J.; Oliviero, A. The Importance of Therapeutic Time Window in the Treatment of Traumatic Brain Injury. **2019**, *13* (January), 1–10. https://doi.org/10.3389/fnins.2019.00007.

(197) Fisher, M.; Feuerstein, G.; Howells, D.; Hurn, P.; Kent, T.; Savitz, S.; Lo, E. H. Update of the Stroke Therapy Academic Industry Roundtable Preclinical Recommendations. *Stroke* **2009**, *40* (6), 2244–2250. https://doi.org/10.1161/STROKEAHA.108.541128.Update.

(198) Hajiaghamemar, M.; Seidi, M.; Oeur, R. A.; Margulies, S. S. Toward Development of Clinically Translatable Diagnostic and Prognostic Metrics of Traumatic Brain Injury Using Animal Models : A Review and a Look Forward. *Exp. Neurol.* **2019**, *318* (December 2018), 101–123. https://doi.org/10.1016/j.expneurol.2019.04.019.

(199) Margulies, S.; Hicks, R. Combination Therapies for Traumatic Brain Injury: Prospective Considerations. *J. Neurotrauma* **2009**, *26* (6), 925–939. https://doi.org/10.1089/neu.2008.0794.

(200) Stein, D. G. Embracing Failure: What the Phase III Progesterone Studies Can Teach about TBI Clinical Trials. *Brain Inj.* **2015**, *29* (11), 1259–1272. https://doi.org/10.3109/02699052.2015.1065344.

(201) Kabadi, S. V.; Faden, A. I. Neuroprotective Strategies for Traumatic Brain Injury: Improving Clinical Translation. *Int. J. Mol. Sci.* **2014**, *15* (1), 1216–1236. https://doi.org/10.3390/ijms15011216.

(202) Loane, D. J.; Faden, A. I. Neuroprotection for Traumatic Brain Injury: Translational Challenges and Emerging Therapeutic Strategies. *Trends Pharmacol. Sci.* **2010**, *31* (12), 596–604. https://doi.org/10.1016/j.tips.2010.09.005.

(203) Selassie, A. W.; Zaloshnja, E.; Langlois, J. A.; Miller, T.; Jones, P.; Steiner, C. Incidence of Long-Term Disability Following Traumatic Brain Injury Hospitalization, United States, 2003. *J. Head Trauma Rehabil.* **2008**, *23* (2), 123–131. https://doi.org/10.1097/01.HTR.0000314531.30401.39.

(204) Hoy, S. M. Patisiran: First Global Approval. *Drugs* **2018**, *78* (15), 1625–1631. https://doi.org/10.1007/s40265-018-0983-6.

(205) Commissioner, O. of the. *FDA Approves First COVID-19 Vaccine*. FDA. https://www.fda.gov/news-events/press-announcements/fda-approves-first-covid-19-vaccine (accessed 2022-09-19).

(206) Commissioner, O. of the. *Coronavirus (COVID-19) Update: FDA Takes Key Action by Approving Second COVID-19 Vaccine*. FDA. https://www.fda.gov/news-events/press-

announcements/coronavirus-covid-19-update-fda-takes-key-action-approving-second-covid-19-vaccine (accessed 2022-09-19).

(207) Akinc, A.; Maier, M. A.; Manoharan, M.; Fitzgerald, K.; Jayaraman, M.; Barros, S.; Ansell, S.; Du, X.; Hope, M. J.; Madden, T. D.; Mui, B. L.; Semple, S. C.; Tam, Y. K.; Ciufolini, M.; Witzigmann, D.; Kulkarni, J. A.; van der Meel, R.; Cullis, P. R. The Onpattro Story and the Clinical Translation of Nanomedicines Containing Nucleic Acid-Based Drugs. *Nat. Nanotechnol.* **2019**, *14* (12), 1084–1087. https://doi.org/10.1038/s41565-019-0591-y.

(208) Jayaraman, M.; Ansell, S. M.; Mui, B. L.; Tam, Y. K.; Chen, J.; Du, X.; Butler, D.; Eltepu, L.; Matsuda, S.; Narayanannair, J. K.; Rajeev, K. G.; Hafez, I. M.; Akinc, A.; Maier, M. A.; Tracy, M. A.; Cullis, P. R.; Madden, T. D.; Manoharan, M.; Hope, M. J. Maximizing the Potency of SiRNA Lipid Nanoparticles for Hepatic Gene Silencing In Vivo**. *Angew. Chem.* **2012**, *124* (34), 8657–8661. https://doi.org/10.1002/ange.201203263.

(209) Baden, L. R.; El Sahly, H. M.; Essink, B.; Kotloff, K.; Frey, S.; Novak, R.; Diemert, D.; Spector, S. A.; Rouphael, N.; Creech, C. B.; McGettigan, J.; Khetan, S.; Segall, N.; Solis, J.; Brosz, A.; Fierro, C.; Schwartz, H.; Neuzil, K.; Corey, L.; Gilbert, P.; Janes, H.; Follmann, D.; Marovich, M.; Mascola, J.; Polakowski, L.; Ledgerwood, J.; Graham, B. S.; Bennett, H.; Pajon, R.; Knightly, C.; Leav, B.; Deng, W.; Zhou, H.; Han, S.; Ivarsson, M.; Miller, J.; Zaks, T. Efficacy and Safety of the MRNA-1273 SARS-CoV-2 Vaccine. *N. Engl. J. Med.* **2021**, *384* (5), 403–416. https://doi.org/10.1056/NEJMoa2035389.

(210) Wang, F.; Kream, R. M.; Stefano, G. B. An Evidence Based Perspective on MRNA-SARS-CoV-2 Vaccine Development. *Med. Sci. Monit. Int. Med. J. Exp. Clin. Res.* **2020**, *26*, e924700-1-e924700-8. https://doi.org/10.12659/MSM.924700.

(211) Anderson, E. J.; Rouphael, N. G.; Widge, A. T.; Jackson, L. A.; Roberts, P. C.; Makhene, M.; Chappell, J. D.; Denison, M. R.; Stevens, L. J.; Pruijssers, A. J.; McDermott, A. B.; Flach, B.; Lin, B. C.; Doria-Rose, N. A.; O'Dell, S.; Schmidt, S. D.; Corbett, K. S.; Swanson, P. A.; Padilla, M.; Neuzil, K. M.; Bennett, H.; Leav, B.; Makowski, M.; Albert, J.; Cross, K.; Edara, V. V.; Floyd, K.; Suthar, M. S.; Martinez, D. R.; Baric, R.; Buchanan, W.; Luke, C. J.; Phadke, V. K.; Rostad, C. A.; Ledgerwood, J. E.; Graham, B. S.; Beigel, J. H. Safety and Immunogenicity of SARS-CoV-2 MRNA-1273 Vaccine in Older Adults. *N. Engl. J. Med.* **2020**, *383* (25), 2427–2438. https://doi.org/10.1056/NEJMoa2028436.

(212) Hou, X.; Zaks, T.; Langer, R.; Dong, Y. Lipid Nanoparticles for MRNA Delivery. *Nat. Rev. Mater.* **2021**, *6* (12), 1078–1094. https://doi.org/10.1038/s41578-021-00358-0.

(213) Thi, T. T. H.; Suys, E. J. A.; Lee, J. S.; Nguyen, D. H.; Park, K. D.; Truong, N. P. Lipid-Based Nanoparticles in the Clinic and Clinical Trials: From Cancer Nanomedicine to COVID-19 Vaccines. *Vaccines* **2021**, *9* (4), 359. https://doi.org/10.3390/vaccines9040359.

(214) Cullis, P. R.; Hope, M. J. Lipid Nanoparticle Systems for Enabling Gene Therapies. *Mol. Ther.* **2017**, *25* (7), 1467–1475. https://doi.org/10.1016/j.ymthe.2017.03.013.

(215) Smith, S. L.; Andrus, P. K.; Zhang, J.-R.; Hall, E. D. Direct Measurement of Hydroxyl Radicals, Lipid Peroxidation, and Blood–Brain Barrier Disruption Following Unilateral Cortical Impact Head Injury in the Rat. *J. Neurotrauma* **1994**, *11* (4), 393–404. https://doi.org/10.1089/neu.1994.11.393.

(216) Alluri, H.; Shaji, C. A.; Davis, M. L.; Tharakan, B. A Mouse Controlled Cortical Impact Model of Traumatic Brain Injury for Studying Blood–Brain Barrier Dysfunctions. In *Traumatic and Ischemic Injury: Methods and Protocols*; Tharakan, B., Ed.; Methods in Molecular Biology; Springer: New York, NY, 2018; pp 37–52. https://doi.org/10.1007/978-1-4939-7526-6_4.

(217) Whalen, M. J.; Carlos, T. M.; Kochanek, P. M.; Heineman, S. Blood-Brain Barrier Permeability, Neutrophil Accumulation and Vascular Adhesion Molecule Expression after Controlled Cortical Impact in Rats: A Preliminary Study. In *Intracranial Pressure and Neuromonitoring in Brain Injury*; Marmarou, A., Bullock, R., Avezaat, C., Baethmann, A., Becker, D., Brock, M., Hoff, J., Nagai, H., Reulen, H.-J., Teasdale, G., Eds.; Acta Neurochirurgica Supplements; Springer: Vienna, 1998; pp 212–214. https://doi.org/10.1007/978-3-7091-6475-4_61.

(218) Chodobski, A.; Zink, B. J.; Szmydynger-Chodobska, J. Blood–Brain Barrier Pathophysiology in Traumatic Brain Injury. *Transl. Stroke Res.* **2011**, *2* (4), 492–516. https://doi.org/10.1007/s12975-011-0125-x.

(219) Bharadwaj, V. N.; Nguyen, D. T.; Kodibagkar, V. D.; Stabenfeldt, S. E. Nanoparticle-Based Therapeutics for Brain Injury. *Adv. Healthc. Mater.* **2018**, *7* (1), 1700668. https://doi.org/10.1002/adhm.201700668.

(220) Bharadwaj, V. N.; Lifshitz, J.; Adelson, P. D.; Kodibagkar, V. D.; Stabenfeldt, S. E. Temporal Assessment of Nanoparticle Accumulation after Experimental Brain Injury: Effect of Particle Size. *Sci. Rep.* **2016**, *6* (1), 29988. https://doi.org/10.1038/srep29988.

(221) Bharadwaj, V. N.; Rowe, R. K.; Harrison, J.; Wu, C.; Anderson, T. R.; Lifshitz, J.; Adelson, P. D.; Kodibagkar, V. D.; Stabenfeldt, S. E. Blood–Brainbarrier Disruption Dictates Nanoparticle Accumulation Following Experimental Brain Injury. *Nanomedicine Nanotechnol. Biol. Med.* **2018**, *14* (7), 2155–2166. https://doi.org/10.1016/j.nano.2018.06.004.

(222) Boyd, B. J.; Galle, A.; Daglas, M.; Rosenfeld, J. V.; Medcalf, R. Traumatic Brain Injury Opens Blood–Brain Barrier to Stealth Liposomes via an Enhanced Permeability and Retention (EPR)-like Effect. *J. Drug Target.* **2015**, *23* (9), 847–853. https://doi.org/10.3109/1061186X.2015.1034280.

(223) Kandell, R. M.; Waggoner, L. E.; Kwon, E. J. Nanomedicine for Acute Brain Injuries: Insight from Decades of Cancer Nanomedicine. *Mol. Pharm.* **2021**, *18* (2), 522–538. https://doi.org/10.1021/acs.molpharmaceut.0c00287.

(224) Sykes, E. A.; Chen, J.; Zheng, G.; Chan, W. C. W. Investigating the Impact of Nanoparticle Size on Active and Passive Tumor Targeting Efficiency. *ACS Nano* **2014**, *8* (6), 5696–5706. https://doi.org/10.1021/nn500299p.

(225) Waggoner, L. E.; Madias, M. I.; Hurtado, A. A.; Kwon, E. J. Pharmacokinetic Analysis of Peptide-Modified Nanoparticles with Engineered Physicochemical Properties in a Mouse Model of Traumatic Brain Injury. *AAPS J.* **2021**, *23* (5), 100. https://doi.org/10.1208/s12248-021-00626-5.

(226) Xiao, K.; Li, Y.; Luo, J.; Lee, J. S.; Xiao, W.; Gonik, A. M.; Agarwal, R. G.; Lam, K. S. The Effect of Surface Charge on in Vivo Biodistribution of PEG-Oligocholic Acid Based Micellar Nanoparticles. *Biomaterials* **2011**, *32* (13), 3435–3446. https://doi.org/10.1016/j.biomaterials.2011.01.021.

(227) Arvizo, R. R.; Miranda, O. R.; Moyano, D. F.; Walden, C. A.; Giri, K.; Bhattacharya, R.; Robertson, J. D.; Rotello, V. M.; Reid, J. M.; Mukherjee, P. Modulating Pharmacokinetics, Tumor Uptake and Biodistribution by Engineered Nanoparticles. *PLOS ONE* **2011**, *6* (9), e24374. https://doi.org/10.1371/journal.pone.0024374.

(228) Perrault, S. D.; Walkey, C.; Jennings, T.; Fischer, H. C.; Chan, W. C. W. Mediating Tumor Targeting Efficiency of Nanoparticles Through Design. *Nano Lett.* **2009**, *9* (5), 1909–1915. https://doi.org/10.1021/nl900031y.

(229) Cheng, Q.; Wei, T.; Farbiak, L.; Johnson, L. T.; Dilliard, S. A.; Siegwart, D. J. Selective Organ Targeting (SORT) Nanoparticles for Tissue-Specific MRNA Delivery and CRISPR–Cas Gene Editing. *Nat. Nanotechnol.* **2020**, *15* (4), 313–320. https://doi.org/10.1038/s41565-020-0669-6.

(230) Chen, S.; Tam, Y. Y. C.; Lin, P. J. C.; Sung, M. M. H.; Tam, Y. K.; Cullis, P. R. Influence of Particle Size on the in Vivo Potency of Lipid Nanoparticle Formulations of SiRNA. *J. Controlled Release* **2016**, *235*, 236–244. https://doi.org/10.1016/j.jconrel.2016.05.059.

(231) Li, S.-D.; Huang, L. Pharmacokinetics and Biodistribution of Nanoparticles. *Mol. Pharm.* **2008**, *5* (4), 496–504. https://doi.org/10.1021/mp800049w.

(232) Maruyama, K. Intracellular Targeting Delivery of Liposomal Drugs to Solid Tumors Based on EPR Effects. *Adv. Drug Deliv. Rev.* **2011**, *63* (3), 161–169. https://doi.org/10.1016/j.addr.2010.09.003.

(233) Wilhelm, S.; Tavares, A. J.; Dai, Q.; Ohta, S.; Audet, J.; Dvorak, H. F.; Chan, W. C. W. Analysis of Nanoparticle Delivery to Tumours. *Nat. Rev. Mater.* **2016**, *1* (5). https://doi.org/10.1038/natrevmats.2016.14.

(234) Yang, T.; Cui, F.-D.; Choi, M.-K.; Cho, J.-W.; Chung, S.-J.; Shim, C.-K.; Kim, D.-D. Enhanced Solubility and Stability of PEGylated Liposomal Paclitaxel: In Vitro and in Vivo Evaluation. *Int. J. Pharm.* **2007**, *338* (1), 317–326. https://doi.org/10.1016/j.ijpharm.2007.02.011.

(235) Kulkarni, J. A.; Witzigmann, D.; Leung, J.; Tam, Y. Y. C.; Cullis, P. R. On the Role of Helper Lipids in Lipid Nanoparticle Formulations of SiRNA. *Nanoscale* **2019**, *11* (45), 21733–21739. https://doi.org/10.1039/C9NR09347H.

(236) Hald Albertsen, C.; Kulkarni, J. A.; Witzigmann, D.; Lind, M.; Petersson, K.; Simonsen, J. B. The Role of Lipid Components in Lipid Nanoparticles for Vaccines and Gene Therapy. *Adv. Drug Deliv. Rev.* **2022**, *188*, 114416. https://doi.org/10.1016/j.addr.2022.114416.

(237) Hatakeyama, H.; Akita, H.; Harashima, H. A Multifunctional Envelope Type Nano Device (MEND) for Gene Delivery to Tumours Based on the EPR Effect: A Strategy for Overcoming the PEG Dilemma. *Adv. Drug Deliv. Rev.* **2011**, *63* (3), 152–160. https://doi.org/10.1016/j.addr.2010.09.001.

(238) Mishra, S.; Webster, P.; Davis, M. E. PEGylation Significantly Affects Cellular Uptake and Intracellular Trafficking of Non-Viral Gene Delivery Particles. *Eur. J. Cell Biol.* **2004**, *83* (3), 97–111. https://doi.org/10.1078/0171-9335-00363.

(239) Remaut, K.; Lucas, B.; Braeckmans, K.; Demeester, J.; De Smedt, S. C. Pegylation of Liposomes Favours the Endosomal Degradation of the Delivered Phosphodiester Oligonucleotides. *J. Controlled Release* **2007**, *117* (2), 256–266. https://doi.org/10.1016/j.jconrel.2006.10.029.

(240) Zukancic, D.; Suys, E. J. A.; Pilkington, E. H.; Algarni, A.; Al-Wassiti, H.; Truong, N. P. The Importance of Poly(Ethylene Glycol) and Lipid Structure in Targeted Gene Delivery to Lymph Nodes by Lipid Nanoparticles. *Pharmaceutics* **2020**, *12* (11), 1068. https://doi.org/10.3390/pharmaceutics12111068.

(241) Mui, B. L.; Tam, Y. K.; Jayaraman, M.; Ansell, S. M.; Du, X.; Tam, Y. Y. C.; Lin, P. J.; Chen, S.; Narayanannair, J. K.; Rajeev, K. G.; Manoharan, M.; Akinc, A.; Maier, M. A.; Cullis, P.; Madden, T. D.; Hope, M. J. Influence of Polyethylene Glycol Lipid Desorption Rates on Pharmacokinetics and Pharmacodynamics of SiRNA Lipid Nanoparticles. *Mol. Ther. - Nucleic Acids* **2013**, *2*, e139. https://doi.org/10.1038/mtna.2013.66.

(242) Bao, Y.; Jin, Y.; Chivukula, P.; Zhang, J.; Liu, Y.; Liu, J.; Clamme, J.-P.; Mahato, R. I.; Ng, D.; Ying, W.; Wang, Y.; Yu, L. Effect of PEGylation on Biodistribution and Gene Silencing of SiRNA/Lipid Nanoparticle Complexes. *Pharm. Res.* **2013**, *30* (2), 342–351. https://doi.org/10.1007/s11095-012-0874-6.

(243) Kauffman, K. J.; Dorkin, J. R.; Yang, J. H.; Heartlein, M. W.; DeRosa, F.; Mir, F. F.; Fenton, O. S.; Anderson, D. G. Optimization of Lipid Nanoparticle Formulations for MRNA Delivery in Vivo with Fractional Factorial and Definitive Screening Designs. *Nano Lett.* **2015**, *15* (11), 7300–7306. https://doi.org/10.1021/acs.nanolett.5b02497.

(244) Pozzi, D.; Colapicchioni, V.; Caracciolo, G.; Piovesana, S.; Capriotti, A. L.; Palchetti, S.; De Grossi, S.; Riccioli, A.; Amenitsch, H.; Laganà, A. Effect of Polyethyleneglycol (PEG) Chain Length on the Bio–Nano-Interactions between PEGylated Lipid Nanoparticles and Biological Fluids: From Nanostructure to Uptake in Cancer Cells. *Nanoscale* **2014**, *6* (5), 2782. https://doi.org/10.1039/c3nr05559k.

(245) Ambegia, E.; Ansell, S.; Cullis, P.; Heyes, J.; Palmer, L.; MacLachlan, I. Stabilized Plasmid–Lipid Particles Containing PEG-Diacylglycerols Exhibit Extended Circulation Lifetimes and Tumor Selective Gene Expression. *Biochim. Biophys. Acta BBA - Biomembr.* **2005**, *1669* (2), 155–163. https://doi.org/10.1016/j.bbamem.2005.02.001.

(246) Wilson, S. C.; Baryza, J. L.; Reynolds, A. J.; Bowman, K.; Keegan, M. E.; Standley, S. M.; Gardner, N. P.; Parmar, P.; Agir, V. O.; Yadav, S.; Zunic, A.; Vargeese, C.; Lee, C. C.; Rajan, S. Real Time Measurement of PEG Shedding from Lipid Nanoparticles in Serum via NMR Spectroscopy. *Mol. Pharm.* **2015**, *12* (2), 386–392. https://doi.org/10.1021/mp500400k.

(247) Suzuki, Y.; Ishihara, H. Difference in the Lipid Nanoparticle Technology Employed in Three Approved SiRNA (Patisiran) and MRNA (COVID-19 Vaccine) Drugs. *Drug Metab. Pharmacokinet.* **2021**, *41*, 100424. https://doi.org/10.1016/j.dmpk.2021.100424.

(248) Akinc, A.; Querbes, W.; De, S.; Qin, J.; Frank-Kamenetsky, M.; Jayaprakash, K. N.; Jayaraman, M.; Rajeev, K. G.; Cantley, W. L.; Dorkin, J. R.; Butler, J. S.; Qin, L.; Racie, T.; Sprague, A.; Fava, E.; Zeigerer, A.; Hope, M. J.; Zerial, M.; Sah, D. W.; Fitzgerald, K.; Tracy, M. A.; Manoharan, M.; Koteliansky, V.; Fougerolles, A. de; Maier, M. A. Targeted Delivery of RNAi Therapeutics With Endogenous and Exogenous Ligand-Based Mechanisms. *Mol. Ther.* **2010**, *18* (7), 1357–1364. https://doi.org/10.1038/mt.2010.85.

(249) Lee, J. B.; Zhang, K.; Tam, Y. Y. C.; Tam, Y. K.; Belliveau, N. M.; Sung, V. Y. C.; Lin, P. J. C.; LeBlanc, E.; Ciufolini, M. A.; Rennie, P. S.; Cullis, P. R. Lipid Nanoparticle SiRNA Systems for Silencing the Androgen Receptor in Human Prostate Cancer in Vivo. *Int. J. Cancer* **2012**, *131* (5), E781–E790. https://doi.org/10.1002/ijc.27361.

(250) Lee, J. B.; Zhang, K.; Tam, Y. Y. C.; Quick, J.; Tam, Y. K.; Lin, P. J.; Chen, S.; Liu, Y.; Nair, J. K.; Zlatev, I.; Rajeev, K. G.; Manoharan, M.; Rennie, P. S.; Cullis, P. R. A Glu-Urea-Lys Ligand-Conjugated Lipid Nanoparticle/SiRNA System Inhibits Androgen Receptor Expression In Vivo. *Mol. Ther. - Nucleic Acids* **2016**, *5*, e348. https://doi.org/10.1038/mtna.2016.43.

(251) Yamamoto, Y.; Lin, P. J. C.; Beraldi, E.; Zhang, F.; Kawai, Y.; Leong, J.; Katsumi, H.; Fazli, L.; Fraser, R.; Cullis, P. R.; Gleave, M. SiRNA Lipid Nanoparticle Potently Silences Clusterin and Delays Progression When Combined with Androgen Receptor Cotargeting in Enzalutamide-Resistant Prostate Cancer. *Clin. Cancer Res.* **2015**, *21* (21), 4845–4855. https://doi.org/10.1158/1078-0432.CCR-15-0866.

(252) Belliveau, N. M.; Huft, J.; Lin, P. J.; Chen, S.; Leung, A. K.; Leaver, T. J.; Wild, A. W.; Lee, J. B.; Taylor, R. J.; Tam, Y. K.; Hansen, C. L.; Cullis, P. R. Microfluidic Synthesis of Highly Potent Limit-Size Lipid Nanoparticles for In Vivo Delivery of SiRNA. *Mol. Ther. Nucleic Acids* **2012**, *1* (8), e37. https://doi.org/10.1038/mtna.2012.28.

(253) Chen, D.; Love, K. T.; Chen, Y.; Eltoukhy, A. A.; Kastrup, C.; Sahay, G.; Jeon, A.; Dong, Y.; Whitehead, K. A.; Anderson, D. G. Rapid Discovery of Potent SiRNA-Containing Lipid Nanoparticles Enabled by Controlled Microfluidic Formulation. *J. Am. Chem. Soc.* **2012**, *134* (16), 6948–6951. https://doi.org/10.1021/ja301621z.

(254) Aylward, L. L. Biomarkers of Environmental Exposures in Blood. In *Encyclopedia of Environmental Health (Second Edition)*; Nriagu, J., Ed.; Elsevier: Oxford, 2019; pp 376–385. https://doi.org/10.1016/B978-0-12-409548-9.10658-X.

(255) Partikel, K.; Korte, R.; Stein, N. C.; Mulac, D.; Herrmann, F. C.; Humpf, H.-U.; Langer, K. Effect of Nanoparticle Size and PEGylation on the Protein Corona of PLGA Nanoparticles. *Eur. J. Pharm. Biopharm.* **2019**, *141*, 70–80. https://doi.org/10.1016/j.ejpb.2019.05.006.

(256) Gref, R.; Lück, M.; Quellec, P.; Marchand, M.; Dellacherie, E.; Harnisch, S.; Blunk, T.; Müller, R. H. 'Stealth' Corona-Core Nanoparticles Surface Modified by Polyethylene Glycol (PEG): Influences of the Corona (PEG Chain Length and Surface Density) and of the Core Composition on Phagocytic Uptake and Plasma Protein Adsorption. *Colloids Surf. B Biointerfaces* **2000**, *18* (3), 301–313. https://doi.org/10.1016/S0927-7765(99)00156-3.

(257) Li, H.; Wang, Y.; Tang, Q.; Yin, D.; Tang, C.; He, E.; Zou, L.; Peng, Q. The Protein Corona and Its Effects on Nanoparticle-Based Drug Delivery Systems. *Acta Biomater.* **2021**, *129*, 57–72. https://doi.org/10.1016/j.actbio.2021.05.019.

(258) Busher, J. T. Serum Albumin and Globulin. In *Clinical Methods: The History, Physical, and Laboratory Examinations*; Walker, H. K., Hall, W. D., Hurst, J. W., Eds.; Butterworths: Boston, 1990.

(259) Palchetti, S.; Colapicchioni, V.; Digiacomo, L.; Caracciolo, G.; Pozzi, D.; Capriotti, A. L.; La Barbera, G.; Laganà, A. The Protein Corona of Circulating PEGylated Liposomes. *Biochim. Biophys. Acta BBA - Biomembr.* **2016**, *1858* (2), 189–196. https://doi.org/10.1016/j.bbamem.2015.11.012.

(260) Mok, K. W. C.; Lam, A. M. I.; Cullis, P. R. Stabilized Plasmid-Lipid Particles: Factors Influencing Plasmid Entrapment and Transfection Properties. *Biochim. Biophys. Acta BBA - Biomembr.* **1999**, *1419* (2), 137–150. https://doi.org/10.1016/S0005-2736(99)00059-0.

(261) Sarode, A.; Fan, Y.; E. Byrnes, A.; Hammel, M.; L. Hura, G.; Fu, Y.; Kou, P.; Hu, C.; I. Hinz, F.; Roberts, J.; G. Koenig, S.; Nagapudi, K.; C. Hoogenraad, C.; Chen, T.; Leung, D.; Yen, C.-W. Predictive High-Throughput Screening of PEGylated Lipids in Oligonucleotide-Loaded Lipid Nanoparticles for Neuronal Gene Silencing. *Nanoscale Adv.* **2022**, *4* (9), 2107–2123. https://doi.org/10.1039/D1NA00712B.

(262) Song, L. Y.; Ahkong, Q. F.; Rong, Q.; Wang, Z.; Ansell, S.; Hope, M. J.; Mui, B. Characterization of the Inhibitory Effect of PEG-Lipid Conjugates on the Intracellular Delivery of Plasmid and Antisense DNA Mediated by Cationic Lipid Liposomes. *Biochim. Biophys. Acta BBA - Biomembr.* **2002**, *1558* (1), 1–13. https://doi.org/10.1016/S0005-2736(01)00399-6.

(263) Wheeler, J. J.; Palmer, L.; Ossanlou, M.; MacLachlan, I.; Graham, R. W.; Zhang, Y. P.; Hope, M. J.; Scherrer, P.; Cullis, P. R. Stabilized Plasmid-Lipid Particles: Construction and Characterization. *Gene Ther.* **1999**, *6* (2), 271–281. https://doi.org/10.1038/sj.gt.3300821.

(264) Zhu, Y.; Shen, R.; Vuong, I.; Reynolds, R. A.; Shears, M. J.; Yao, Z.-C.; Hu, Y.; Cho, W. J.; Kong, J.; Reddy, S. K.; Murphy, S. C.; Mao, H.-Q. Multi-Step Screening of DNA/Lipid Nanoparticles and Co-Delivery with SiRNA to Enhance and Prolong Gene Expression. *Nat. Commun.* **2022**, *13* (1), 4282. https://doi.org/10.1038/s41467-022-31993-y.

(265) Xiong, Y.; Mahmood, A.; Chopp, M. Animal Models of Traumatic Brain Injury. *Nat. Rev. Neurosci.* **2013**, *14* (2), 128–142. https://doi.org/10.1038/nrn3407.

(266) Waggoner, L. E.; Kang, J.; Zuidema, J. M.; Vijayakumar, S.; Hurtado, A. A.; Sailor, M. J.; Kwon, E. J. Porous Silicon Nanoparticles Targeted to the Extracellular Matrix for Therapeutic Protein Delivery in Traumatic Brain Injury. *Bioconjug. Chem.* **2022**, *33* (9), 1685–1697. https://doi.org/10.1021/acs.bioconjchem.2c00305.

(267) Xu, Y.; Ou, M.; Keough, E.; Roberts, J.; Koeplinger, K.; Lyman, M.; Fauty, S.; Carlini, E.; Stern, M.; Zhang, R.; Yeh, S.; Mahan, E.; Wang, Y.; Slaughter, D.; Gindy, M.; Raab, C.; Thompson, C.; Hochman, J. Quantitation of Physiological and Biochemical Barriers to

SiRNA Liver Delivery via Lipid Nanoparticle Platform. *Mol. Pharm.* **2014**, *11* (5), 1424–1434. https://doi.org/10.1021/mp400584h.

(268) Monck, M. A.; Mori, A.; Lee, D.; Tam, P.; Wheeler, J. J.; Cullis, P. R.; Scherrer, P. Stabilized Plasmid–Lipid Particles: Pharmacokinetics and Plasmid Delivery to Distal Tumors Following Intravenous Injection. *J. Drug Target.* **2000**, *7* (6), 439–452. https://doi.org/10.3109/10611860009102218.

(269) Yao, C.; Wang, P.; Zhou, L.; Wang, R.; Li, X.; Zhao, D.; Zhang, F. Highly Biocompatible Zwitterionic Phospholipids Coated Upconversion Nanoparticles for Efficient Bioimaging. *Anal. Chem.* **2014**, *86* (19), 9749–9757. https://doi.org/10.1021/ac5023259.

(270) Lee, C.-M.; Choi, Y.; Huh, E. J.; Lee, K. Y.; Song, H.-C.; Sun, M. J.; Jeong, H.-J.; Cho, C.-S.; Bom, H.-S. Polyethylene Glycol (PEG) Modified 99mTc-HMPAOLiposome for Improving Blood Circulation and Biodistribution: The Effect of the Extent of PEGylation. *Cancer Biother. Radiopharm.* **2005**, *20* (6), 620–628. https://doi.org/10.1089/cbr.2005.20.620.

(271) Kandell, R. M.; Kudryashev, J. A.; Kwon, E. J. Targeting the Extracellular Matrix in Traumatic Brain Injury Increases Signal Generation from an Activity-Based Nanosensor. *ACS Nano* **2021**, *15* (12), 20504–20516. https://doi.org/10.1021/acsnano.1c09064.

(272) Kudryashev, J. A.; Waggoner, L. E.; Leng, H. T.; Mininni, N. H.; Kwon, E. J. An Activity-Based Nanosensor for Traumatic Brain Injury. *ACS Sens.* **2020**, *5* (3), 686–692. https://doi.org/10.1021/acssensors.9b01812.

(273) Hassett, K. J.; Benenato, K. E.; Jacquinet, E.; Lee, A.; Woods, A.; Yuzhakov, O.; Himansu, S.; Deterling, J.; Geilich, B. M.; Ketova, T.; Mihai, C.; Lynn, A.; McFadyen, I.; Moore, M. J.; Senn, J. J.; Stanton, M. G.; Almarsson, Ö.; Ciaramella, G.; Brito, L. A. Optimization of Lipid Nanoparticles for Intramuscular Administration of MRNA Vaccines. *Mol. Ther. - Nucleic Acids* **2019**, *15*, 1–11. https://doi.org/10.1016/j.omtn.2019.01.013.

(274) Schoenmaker, L.; Witzigmann, D.; Kulkarni, J. A.; Verbeke, R.; Kersten, G.; Jiskoot, W.; Crommelin, D. J. A. MRNA-Lipid Nanoparticle COVID-19 Vaccines: Structure and Stability. *Int. J. Pharm.* **2021**, *601*, 120586. https://doi.org/10.1016/j.ijpharm.2021.120586.

(275) He, C.; Hu, Y.; Yin, L.; Tang, C.; Yin, C. Effects of Particle Size and Surface Charge on Cellular Uptake and Biodistribution of Polymeric Nanoparticles. *Biomaterials* **2010**, *31* (13), 3657–3666. https://doi.org/10.1016/j.biomaterials.2010.01.065.

(276) Kranz, L. M.; Diken, M.; Haas, H.; Kreiter, S.; Loquai, C.; Reuter, K. C.; Meng, M.; Fritz, D.; Vascotto, F.; Hefesha, H.; Grunwitz, C.; Vormehr, M.; Hüsemann, Y.; Selmi, A.; Kuhn, A. N.; Buck, J.; Derhovanessian, E.; Rae, R.; Attig, S.; Diekmann, J.; Jabulowsky, R. A.; Heesch, S.; Hassel, J.; Langguth, P.; Grabbe, S.; Huber, C.; Türeci, Ö.; Sahin, U. Systemic RNA Delivery to Dendritic Cells Exploits Antiviral Defence for Cancer Immunotherapy. *Nature* **2016**, *534* (7607), 396–401. https://doi.org/10.1038/nature18300.

(277) Khalil, I. A.; Younis, M. A.; Kimura, S.; Harashima, H. Lipid Nanoparticles for Cell-Specific *in Vivo* Targeted Delivery of Nucleic Acids. *Biol. Pharm. Bull.* **2020**, *43* (4), 584–595. https://doi.org/10.1248/bpb.b19-00743.

(278) Pardi, N.; Tuyishime, S.; Muramatsu, H.; Kariko, K.; Mui, B. L.; Tam, Y. K.; Madden, T. D.; Hope, M. J.; Weissman, D. Expression Kinetics of Nucleoside-Modified MRNA Delivered in Lipid Nanoparticles to Mice by Various Routes. *J. Control. Release Off. J. Control. Release Soc.* **2015**, *217*, 345–351. https://doi.org/10.1016/j.jconrel.2015.08.007.

(279) Thompson, J. F.; Hayes, L. S.; Lloyd, D. B. Modulation of Firefly Luciferase Stability and Impact on Studies of Gene Regulation. *Gene* **1991**, *103* (2), 171–177. https://doi.org/10.1016/0378-1119(91)90270-l.

(280) Ignowski, J. M.; Schaffer, D. V. Kinetic Analysis and Modeling of Firefly Luciferase as a Quantitative Reporter Gene in Live Mammalian Cells. *Biotechnol. Bioeng.* **2004**, *86* (7), 827–834. https://doi.org/10.1002/bit.20059.

(281) Di, J.; Du, Z.; Wu, K.; Jin, S.; Wang, X.; Li, T.; Xu, Y. Biodistribution and Non-Linear Gene Expression of MRNA LNPs Affected by Delivery Route and Particle Size. *Pharm. Res.* **2022**, *39* (1), 105–114. https://doi.org/10.1007/s11095-022-03166-5.

(282) Rungta, R. L.; Choi, H. B.; Lin, P. J.; Ko, R. W.; Ashby, D.; Nair, J.; Manoharan, M.; Cullis, P. R.; MacVicar, B. A. Lipid Nanoparticle Delivery of SiRNA to Silence Neuronal Gene Expression in the Brain. *Mol. Ther. Nucleic Acids* **2013**, *2* (12), e136. https://doi.org/10.1038/mtna.2013.65.

(283) Nance, E. A.; Woodworth, G. F.; Sailor, K. A.; Shih, T.-Y.; Xu, Q.; Swaminathan, G.; Xiang, D.; Eberhart, C.; Hanes, J. A Dense Poly(Ethylene Glycol) Coating Improves Penetration of Large Polymeric Nanoparticles Within Brain Tissue. *Sci. Transl. Med.* **2012**, *4* (149), 149ra119-149ra119. https://doi.org/10.1126/scitranslmed.3003594.

(284) Block, M. L.; Hong, J.-S. Microglia and Inflammation-Mediated Neurodegeneration: Multiple Triggers with a Common Mechanism. *Prog. Neurobiol.* **2005**, *76* (2), 77–98. https://doi.org/10.1016/j.pneurobio.2005.06.004.

(285) Kalra, S.; Malik, R.; Singh, G.; Bhatia, S.; Al-Harrasi, A.; Mohan, S.; Albratty, M.; Albarrati, A.; Tambuwala, M. M. Pathogenesis and Management of Traumatic Brain Injury (TBI): Role of Neuroinflammation and Anti-Inflammatory Drugs. *Inflammopharmacology* **2022**, *30* (4), 1153–1166. https://doi.org/10.1007/s10787-022-01017-8.

(286) Boone, D. R.; Leek, J. M.; Falduto, M. T.; Torres, K. E. O.; Sell, S. L.; Parsley, M. A.; Cowart, J. C.; Uchida, T.; Micci, M.-A.; DeWitt, D. S.; Prough, D. S.; Hellmich, H. L. Effects of AAV-Mediated Knockdown of NNOS and GPx-1 Gene Expression in Rat Hippocampus after Traumatic Brain Injury. *PLOS ONE* **2017**, *12* (10), e0185943. https://doi.org/10.1371/journal.pone.0185943.

(287) Longhi, L.; Watson, D. J.; Saatman, K. E.; Thompson, H. J.; Zhang, C.; Fujimoto, S.; Royo, N.; Castelbuono, D.; Raghupathi, R.; Trojanowski, J. Q.; Lee, V. M.-Y.; Wolfe, J. H.; Stocchetti, N.; McIntosh, T. K. Ex Vivo Gene Therapy Using Targeted Engraftment of NGF-Expressing Human NT2N Neurons Attenuates Cognitive Deficits Following Traumatic Brain Injury in Mice. *J. Neurotrauma* **2004**, *21* (12), 1723–1736. https://doi.org/10.1089/neu.2004.21.1723.

(288) Zou, L. L.; Huang, L.; Hayes, R. L.; Black, C.; Qiu, Y. H.; Perez-Polo, J. R.; Le, W.; Clifton, G. L.; Yang, K. Liposome-Mediated NGF Gene Transfection Following Neuronal

Injury: Potential Therapeutic Applications. *Gene Ther.* **1999**, *6* (6), 994–1005. https://doi.org/10.1038/sj.gt.3300936.

(289) Philips, M. F.; Mattiasson, G.; Wieloch, T.; Björklund, A.; Johansson, B. B.; Tomasevic, G.; Martínez-Serrano, A.; Lenzlinger, P. M.; Sinson, G.; Grady, M. S.; McIntosh, T. K. Neuroprotective and Behavioral Efficacy of Nerve Growth Factor—Transfected Hippocampal Progenitor Cell Transplants after Experimental Traumatic Brain Injury. *J. Neurosurg.* **2001**, *94* (5), 765–774. https://doi.org/10.3171/jns.2001.94.5.0765.

(290) Ma, H.; Yu, B.; Kong, L.; Zhang, Y.; Shi, Y. Neural Stem Cells Over-Expressing Brain-Derived Neurotrophic Factor (BDNF) Stimulate Synaptic Protein Expression and Promote Functional Recovery Following Transplantation in Rat Model of Traumatic Brain Injury. *Neurochem. Res.* **2012**, *37* (1), 69–83. https://doi.org/10.1007/s11064-011-0584-1.

(291) Maas, A. I. R.; Menon, D. K.; Adelson, P. D.; Andelic, N.; Bell, M. J.; Belli, A.; Bragge, P.; Brazinova, A.; Büki, A.; Chesnut, R. M.; Citerio, G.; Coburn, M.; Cooper, D. J.; Crowder, A. T.; Czeiter, E.; Czosnyka, M.; Diaz-Arrastia, R.; Dreier, J. P.; Duhaime, A.-C.; Ercole, A.; Essen, T. A. van; Feigin, V. L.; Gao, G.; Giacino, J.; Gonzalez-Lara, L. E.; Gruen, R. L.; Gupta, D.; Hartings, J. A.; Hill, S.; Jiang, J.; Ketharanathan, N.; Kompanje, E. J. O.; Lanyon, L.; Laureys, S.; Lecky, F.; Levin, H.; Lingsma, H. F.; Maegele, M.; Majdan, M.; Manley, G.; Marsteller, J.; Mascia, L.; McFadyen, C.; Mondello, S.; Newcombe, V.; Palotie, A.; Parizel, P. M.; Peul, W.; Piercy, J.; Polinder, S.; Puybasset, L.; Rasmussen, T. E.; Rossaint, R.; Smielewski, P.; Söderberg, J.; Stanworth, S. J.; Stein, M. B.; Steinbüchel, N. von; Stewart, W.; Steyerberg, E. W.; Stocchetti, N.; Synnot, A.; Ao, B. T.; Tenovuo, O.; Theadom, A.; Tibboel, D.; Videtta, W.; Wang, K. K. W.; Williams, W. H.; Wilson, L.; Yaffe, K.; Adams, H.; Agnoletti, V.; Allanson, J.; Amrein, K.; Andaluz, N.; Anke, A.; Antoni, A.; As, A. B. van; Audibert, G.; Azaševac, A.; Azouvi, P.; Azzolini, M. L.; Baciu, C.; Badenes, R.; Barlow, K. M.; Bartels, R.; Bauerfeind, U.; Beauchamp, M.; Beer, D.; Beer, R.; Belda, F. J.; Bellander, B.-M.; Bellier, R.; Benali, H.; Benard, T.; Beqiri, V.; Beretta, L.; Bernard, F.; Bertolini, G.; Bilotta, F.; Blaabjerg, M.; Boogert, H. den; Boutis, K.; Bouzat, P.; Brooks, B.; Brorsson, C.; Bullinger, M.; Burns, E.; Calappi, E.; Cameron, P.; Carise, E.; Castaño-León, A. M.; Causin, F.; Chevallard, G.; Chieregato, A.; Christie, B.; Cnossen, M.; Coles, J.; Collett, J.; Corte, F. D.; Craig, W.; Csato, G.; Csomos, A.; Curry, N.; Dahyot-Fizelier, C.; Dawes, H.; DeMatteo, C.; Depreitere, B.; Dewey, D.; Dijck, J. van; Đilvesi, Đ.; Dippel, D.; Dizdarevic, K.; Donoghue, E.; Duek, O.; Dulière, G.-L.; Dzeko, A.; Eapen, G.; Emery, C. A.; English, S.; Esser, P.; Ezer, E.; Fabricius, M.; Feng, J.; Fergusson, D.; Figaji, A.; Fleming, J.; Foks, K.; Francony, G.; Freedman, S.; Freo, U.; Frisvold, S. K.; Gagnon, I.; Galanaud, D.; Gantner, D.; Giraud, B.; Glocker, B.; Golubovic, J.; López, P. A. G.; Gordon, W. A.; Gradisek, P.; Gravel, J.; Griesdale, D.; Grossi, F.; Haagsma, J. A.; Håberg, A. K.; Haitsma, I.; Hecke, W. V.; Helbok, R.; Helseth, E.; Heugten, C. van; Hoedemaekers, C.; Höfer, S.; Horton, L.; Hui, J.; Huijben, J. A.; Hutchinson, P. J.; Jacobs, B.; Jagt, M. van der; Jankowski, S.; Janssens, K.; Jelaca, B.; Jones, K. M.; Kamnitsas, K.; Kaps, R.; Karan, M.; Katila, A.; Kaukonen, K.-M.; Keyser, V. D.; Kivisaari, R.; Kolias, A. G.; Kolumbán, B.; Kolundžija, K.; Kondziella, D.; Koskinen, L.-O.; Kovács, N.; Kramer, A.; Kutsogiannis, D.; Kyprianou, T.; Lagares, A.; Lamontagne, F.; Latini, R.; Lauzier, F.; Lazar, I.; Ledig, C.; Lefering, R.; Legrand, V.; Levi, L.; Lightfoot, R.; Lozano, A.; MacDonald, S.; Major, S.; Manara, A.; Manhes, P.; Maréchal, H.; Martino, C.; Masala, A.; Masson, S.; Mattern, J.; McFadyen, B.; McMahon, C.; Meade, M.; Melegh, B.; Menovsky, T.; Moore, L.; Correia, M. M.; Morganti-Kossmann, M. C.; Muehlan, H.; Mukherjee, P.; Murray, L.; Naalt, J. van der; Negru, A.; Nelson, D.; Nieboer, D.; Noirhomme, Q.; Nyirádi, J.; Oddo, M.; Okonkwo, D. O.; Oldenbeuving, A. W.; Ortolano,

F.; Osmond, M.; Payen, J.-F.; Perlbarg, V.; Persona, P.; Pichon, N.; Piippo-Karjalainen, A.; Pili-Floury, S.; Pirinen, M.; Ple, H.; Poca, M. A.; Posti, J.; Praag, D. V.; Ptito, A.; Radoi, A.; Ragauskas, A.; Raj, R.; Real, R. G. L.; Reed, N.; Rhodes, J.; Robertson, C.; Rocka, S.; Røe, C.; Røise, O.; Roks, G.; Rosand, J.; Rosenfeld, J. V.; Rosenlund, C.; Rosenthal, G.; Rossi, S.; Rueckert, D.; Ruiter, G. C. W. de; Sacchi, M.; Sahakian, B. J.; Sahuquillo, J.; Sakowitz, O.; Salvato, G.; Sánchez-Porras, R.; Sándor, J.; Sangha, G.; Schäfer, N.; Schmidt, S.; Schneider, K. J.; Schnyer, D.; Schöhl, H.; Schoonman, G. G.; Schou, R. F.; Sir, Ö.; Skandsen, T.; Smeets, D.; Sorinola, A.; Stamatakis, E.; Stevanovic, A.; Stevens, R. D.; Sundström, N.; Taccone, F. S.; Takala, R.; Tanskanen, P.; Taylor, M. S.; Telgmann, R.; Temkin, N.; Teodorani, G.; Thomas, M.; Tolias, C. M.; Trapani, T.; Turgeon, A.; Vajkoczy, P.; Valadka, A. B.; Valeinis, E.; Vallance, S.; Vámos, Z.; Vargiolu, A.; Vega, E.; Verheyden, J.; Vik, A.; Vilcinis, R.; Vleggeert-Lankamp, C.; Vogt, L.; Volovici, V.; Voormolen, D. C.; Vulekovic, P.; Vyvere, T. V.; Waesberghe, J. V.; Wessels, L.; Wildschut, E.; Williams, G.; Winkler, M. K. L.; Wolf, S.; Wood, G.; Xirouchaki, N.; Younsi, A.; Zaaroor, M.; Zelinkova, V.; Zemek, R.; Zumbo, F. Traumatic Brain Injury: Integrated Approaches to Improve Prevention, Clinical Care, and Research. *Lancet Neurol.* **2017**, *16* (12), 987–1048. https://doi.org/10.1016/S1474-4422(17)30371-X.

(292) Dean, P. J. A.; Sterr, A. Long-Term Effects of Mild Traumatic Brain Injury on Cognitive Performance. *Front. Hum. Neurosci.* **2013**, *7*. https://doi.org/10.3389/fnhum.2013.00030.

(293) Vanderploeg, R. D.; Curtiss, G.; Belanger, H. G. Long-Term Neuropsychological Outcomes Following Mild Traumatic Brain Injury. *J. Int. Neuropsychol. Soc.* **2005**, *11* (3), 228–236. https://doi.org/10.1017/S1355617705050289.

(294) Skolnick, B. E.; Maas, A. I.; Narayan, R. K.; van der Hoop, R. G.; MacAllister, T.; Ward, J. D.; Nelson, N. R.; Stocchetti, N. A Clinical Trial of Progesterone for Severe Traumatic Brain Injury. *N. Engl. J. Med.* **2014**, *371* (26), 2467–2476. https://doi.org/10.1056/NEJMoa1411090.

(295) Krag, D. N.; Shukla, G. S.; Shen, G.-P.; Pero, S.; Ashikaga, T.; Fuller, S.; Weaver, D. L.; Burdette-Radoux, S.; Thomas, C. Selection of Tumor-Binding Ligands in Cancer Patients with Phage Display Libraries. *Cancer Res.* **2006**, *66* (15), 7724–7733. https://doi.org/10.1158/0008-5472.CAN-05-4441.

(296) R, B.; Jk, P.; Ni, G. Identification of Cancer Targets and Therapeutics Using Phage Display. *Curr. Opin. Drug Discov. Devel.* **2006**, *9* (3), 363–369.

(297) Mann, A. P.; Scodeller, P.; Hussain, S.; Joo, J.; Kwon, E.; Braun, G. B.; Mölder, T.; She, Z. G.; Kotamraju, V. R.; Ranscht, B.; Krajewski, S.; Teesalu, T.; Bhatia, S.; Sailor, M. J.; Ruoslahti, E. A Peptide for Targeted, Systemic Delivery of Imaging and Therapeutic Compounds into Acute Brain Injuries. *Nat. Commun.* **2016**, *7* (11980). https://doi.org/10.1038/ncomms11980.

(298) Kumar, P.; Wu, H.; McBride, J. L.; Jung, K.-E.; Hee Kim, M.; Davidson, B. L.; Kyung Lee, S.; Shankar, P.; Manjunath, N. Transvascular Delivery of Small Interfering RNA to the Central Nervous System. *Nature* **2007**, *448* (7149), 39–43. https://doi.org/10.1038/nature05901.

(299) Alvarez-Erviti, L.; Seow, Y.; Yin, H.; Betts, C.; Lakhal, S.; Wood, M. J. A. Delivery of SiRNA to the Mouse Brain by Systemic Injection of Targeted Exosomes. *Nat. Biotechnol.* **2011**, *29* (4), 341–345. https://doi.org/10.1038/nbt.1807.

(300) Joo, J.; J. Kwon, E.; Kang, J.; Skalak, M.; J. Anglin, E.; P. Mann, A.; Ruoslahti, E.; N. Bhatia, S.; J. Sailor, M. Porous Silicon–Graphene Oxide Core–Shell Nanoparticles for Targeted Delivery of SiRNA to the Injured Brain. *Nanoscale Horiz.* **2016**, *1* (5), 407–414. https://doi.org/10.1039/C6NH00082G.

(301) Kang, J.; Joo, J.; Kwon, E. J.; Skalak, M.; Hussain, S.; She, Z.-G.; Ruoslahti, E.; Bhatia, S. N.; Sailor, M. J. Self-Sealing Porous Silicon-Calcium Silicate Core–Shell Nanoparticles for Targeted SiRNA Delivery to the Injured Brain. *Adv. Mater.* **2016**, *28* (36), 7962–7969. https://doi.org/10.1002/adma.201600634.

(302) Wu, P.; Zhao, H.; Gou, X.; Wu, X.; Zhang, S.; Deng, G.; Chen, Q. Targeted Delivery of Polypeptide Nanoparticle for Treatment of Traumatic Brain Injury. *Int. J. Nanomedicine* **2019**, *14*, 4059–4069. https://doi.org/10.2147/IJN.S202353.

(303) Nel, A. E.; Mädler, L.; Velegol, D.; Xia, T.; Hoek, E. M. V.; Somasundaran, P.; Klaessig, F.; Castranova, V.; Thompson, M. Understanding Biophysicochemical Interactions at the Nano–Bio Interface. *Nat. Mater.* **2009**, *8* (7), 543–557. https://doi.org/10.1038/nmat2442.

(304) Song, E.; Gaudin, A.; King, A. R.; Seo, Y. E.; Suh, H. W.; Deng, Y.; Cui, J.; Tietjen, G. T.; Huttner, A.; Saltzman, W. M. Surface Chemistry Governs Cellular Tropism of Nanoparticles in the Brain. *Nat. Commun.* **2017**, *8*. https://doi.org/10.1038/ncomms15322.

(305) Yamankurt, G.; Berns, E. J.; Xue, A.; Lee, A.; Bagheri, N.; Mrksich, M.; Mirkin, C. A. Exploration of the Nanomedicine-Design Space with High-Throughput Screening and Machine Learning. *Nat. Biomed. Eng.* **2019**, *3* (4), 318–327. https://doi.org/10.1038/s41551-019-0351-1.

(306) Maeda, H.; Wu, J.; Sawa, T.; Matsumura, Y.; Hori, K. Tumor Vascular Permeability and the EPR Effect in Macromolecular Therapeutics: A Review. *J. Controlled Release* **2000**, *65* (1), 271–284. https://doi.org/10.1016/S0168-3659(99)00248-5.

(307) Corbett, J.; Connah, M.; Mattison, K. Advances in the Measurement of Protein Mobility Using Laser Doppler Electrophoresis—The Diffusion Barrier Technique. *Electrophoresis* **2011**, *32*, 1787–1794. https://doi.org/10.1002/elps.201100108.

(308) Cruz, L. J.; Stammes, M. A.; Que, I.; van Beek, E. R.; Knol-Blankevoort, V. T.; Snoeks, T. J. A.; Chan, A.; Kaijzel, E. L.; Löwik, C. W. G. M. Effect of PLGA NP Size on Efficiency to Target Traumatic Brain Injury. *J. Controlled Release* **2016**, *223*, 31–41. https://doi.org/10.1016/j.jconrel.2015.12.029.

(309) Barenholz, Y. (Chezy). Doxil® — The First FDA-Approved Nano-Drug: Lessons Learned. *J. Controlled Release* **2012**, *160* (2), 117–134. https://doi.org/10.1016/j.jconrel.2012.03.020.

(310) Bobo, D.; Robinson, K. J.; Islam, J.; Thurecht, K. J.; Corrie, S. R. Nanoparticle-Based Medicines: A Review of FDA-Approved Materials and Clinical Trials to Date. *Pharm. Res.* **2016**, *33* (10), 2373–2387. https://doi.org/10.1007/s11095-016-1958-5.

(311) Jokerst, J. V.; Lobovkina, T.; Zare, R. N.; Gambhir, S. S. Nanoparticle PEGylation for Imaging and Therapy. *Nanomed.* **2011**, *6* (4), 715–728. https://doi.org/10.2217/nnm.11.19.

(312) Doktorovova, S.; Shegokar, R.; Martins-Lopes, P.; Silva, A. M.; Lopes, C. M.; Müller, R. H.; Souto, E. B. Modified Rose Bengal Assay for Surface Hydrophobicity Evaluation of Cationic Solid Lipid Nanoparticles (CSLN). *Eur. J. Pharm. Sci.* **2012**, *45* (5), 606–612. https://doi.org/10.1016/j.ejps.2011.12.016.

(313) Xiao, Y.; Wiesner, M. R. Characterization of Surface Hydrophobicity of Engineered Nanoparticles. *J. Hazard. Mater.* **2012**, *215–216*, 146–151. https://doi.org/10.1016/j.jhazmat.2012.02.043.

(314) Tenzer, S.; Docter, D.; Kuharev, J.; Musyanovych, A.; Fetz, V.; Hecht, R.; Schlenk, F.; Fischer, D.; Kiouptsi, K.; Reinhardt, C.; Landfester, K.; Schild, H.; Maskos, M.; Knauer, S. K.; Stauber, R. H. Rapid Formation of Plasma Protein Corona Critically Affects Nanoparticle Pathophysiology. *Nat. Nanotechnol.* **2013**, *8* (10), 772–781. https://doi.org/10.1038/nnano.2013.181.

(315) Lundqvist, M.; Stigler, J.; Elia, G.; Lynch, I.; Cedervall, T.; Dawson, K. A. Nanoparticle Size and Surface Properties Determine the Protein Corona with Possible Implications for Biological Impacts. *PNAS* **2008**, *105* (38), 14265–14270.

(316) Monopoli, M. P.; Åberg, C.; Salvati, A.; Dawson, K. A. Biomolecular Coronas Provide the Biological Identity of Nanosized Materials. *Nat. Nanotechnol.* **2012**, *7* (12), 779–786. https://doi.org/10.1038/nnano.2012.207.

(317) Gunawan, C.; Lim, M.; P. Marquis, C.; Amal, R. Nanoparticle–Protein Corona Complexes Govern the Biological Fates and Functions of Nanoparticles. *J. Mater. Chem. B* **2014**, *2* (15), 2060–2083. https://doi.org/10.1039/C3TB21526A.

(318) Khan, S.; Gupta, A.; Nandi, C. K. Controlling the Fate of Protein Corona by Tuning Surface Properties of Nanoparticles. *J. Phys. Chem. Lett.* **2013**, *4* (21), 3747–3752. https://doi.org/10.1021/jz401874u.

(319) Lu, X.; Xu, P.; Ding, H.-M.; Yu, Y.-S.; Huo, D.; Ma, Y.-Q. Tailoring the Component of Protein Corona via Simple Chemistry. *Nat. Commun.* **2019**, *10* (1), 1–14. https://doi.org/10.1038/s41467-019-12470-5.

(320) Du, H.; Cui, C.; Wang, L.; Liu, H.; Cui, G. Novel Tetrapeptide, RGDF, Mediated Tumor Specific Liposomal Doxorubicin (DOX) Preparations. *Mol. Pharm.* **2011**, *8* (4), 1224–1232. https://doi.org/10.1021/mp200039s.

(321) Kuai, R.; Yuan, W.; Li, W.; Qin, Y.; Tang, J.; Yuan, M.; Fu, L.; Ran, R.; Zhang, Z.; He, Q. Targeted Delivery of Cargoes into a Murine Solid Tumor by a Cell-Penetrating Peptide and Cleavable Poly(Ethylene Glycol) Comodified Liposomal Delivery System via Systemic Administration. *Mol. Pharm.* **2011**, *8* (6), 2151–2161. https://doi.org/10.1021/mp200100f.

(322) Accardo, A.; Mansi, R.; Morisco, A.; Mangiapia, G.; Paduano, L.; Tesauro, D.; Radulescu, A.; Aurilio, M.; Aloj, L.; Arra, C.; Morelli, G. Peptide Modified Nanocarriers for Selective

Targeting of Bombesin Receptors. *Mol. Biosyst.* **2010**, *6* (5), 878–887. https://doi.org/10.1039/B923147A.

(323) Rohovie, M. J.; Nagasawa, M.; Swartz, J. R. Virus-like Particles: Next-generation Nanoparticles for Targeted Therapeutic Delivery. *Bioeng. Transl. Med.* **2017**, *2* (1), 43–57. https://doi.org/10.1002/btm2.10049.

(324) Gupta, M.; Chashoo, G.; Sharma, P. R.; Saxena, A. K.; Gupta, P. N.; Agrawal, G. P.; Vyas, S. P. Dual Targeted Polymeric Nanoparticles Based on Tumor Endothelium and Tumor Cells for Enhanced Antitumor Drug Delivery. *Mol. Pharm.* **2014**, *11* (3), 697–715. https://doi.org/10.1021/mp400404p.

(325) Jadia, R.; Kydd, J.; Rai, P. Remotely Phototriggered, Transferrin-Targeted Polymeric Nanoparticles for the Treatment of Breast Cancer. *Photochem. Photobiol.* **2018**, *94* (4), 765–774. https://doi.org/10.1111/php.12903.

(326) Yang, Q.; Jones, S. W.; Parker, C. L.; Zamboni, W. C.; Bear, J. E.; Lai, S. K. Evading Immune Cell Uptake and Clearance Requires PEG Grafting at Densities Substantially Exceeding the Minimum for Brush Conformation. *Mol. Pharm.* **2014**, *11* (4), 1250–1258. https://doi.org/10.1021/mp400703d.

(327) Harris, J. M. *Poly(Ethylene Glycol) Chemistry: Biotechnical and Biomedical Applications*; Springer Science & Business Media, 1992.

(328) Gref, R.; Domb, A.; Quellec, P.; Blunk, T.; Müller, R. H.; Verbavatz, J. M.; Langer, R. The Controlled Intravenous Delivery of Drugs Using PEG-Coated Sterically Stabilized Nanospheres. *Adv. Drug Deliv. Rev.* **1995**, *16* (2), 215–233. https://doi.org/10.1016/0169-409X(95)00026-4.

(329) MacKay, J. A.; Deen, D. F.; Szoka, F. C. Distribution in Brain of Liposomes after Convection Enhanced Delivery; Modulation by Particle Charge, Particle Diameter, and Presence of Steric Coating. *Brain Res.* **2005**, *1035* (2), 139–153. https://doi.org/10.1016/j.brainres.2004.12.007.

(330) Yue, Z.-G.; Wei, W.; Lv, P.-P.; Yue, H.; Wang, L.-Y.; Su, Z.-G.; Ma, G.-H. Surface Charge Affects Cellular Uptake and Intracellular Trafficking of Chitosan-Based Nanoparticles. *Biomacromolecules* **2011**, *12* (7), 2440–2446. https://doi.org/10.1021/bm101482r.

(331) Ferrari, R.; Lupi, M.; Colombo, C.; Morbidelli, M.; D'Incalci, M.; Moscatelli, D. Investigation of Size, Surface Charge, PEGylation Degree and Concentration on the Cellular Uptake of Polymer Nanoparticles. *Colloids Surf. B Biointerfaces* **2014**, *123*, 639–647. https://doi.org/10.1016/j.colsurfb.2014.10.003.

(332) Arvizo, R. R.; Miranda, O. R.; Thompson, M. A.; Pabelick, C. M.; Bhattacharya, R.; Robertson, J. D.; Rotello, V. M.; Prakash, Y. S.; Mukherjee, P. Effect of Nanoparticle Surface Charge at the Plasma Membrane and Beyond. *Nano Lett.* **2010**, *10* (7), 2543–2548. https://doi.org/10.1021/nl101140t.

(333) Wittrup, K. D.; Thurber, G. M.; Schmidt, M. M.; Rhoden, J. J. Practical Theoretic Guidance for the Design of Tumor-Targeting Agents. In *Methods in Enzymology*; Elsevier, 2012; Vol. 503, pp 255–268. https://doi.org/10.1016/B978-0-12-396962-0.00010-0.

(334) Jo, D. H.; Kim, J. H.; Lee, T. G.; Kim, J. H. Size, Surface Charge, and Shape Determine Therapeutic Effects of Nanoparticles on Brain and Retinal Diseases. *Nanomedicine Nanotechnol. Biol. Med.* **2015**, *11* (7), 1603–1611. https://doi.org/10.1016/j.nano.2015.04.015.

(335) Jiang, S.; Cao, Z. Ultralow-Fouling, Functionalizable, and Hydrolyzable Zwitterionic Materials and Their Derivatives for Biological Applications. *Adv. Mater.* **2010**, *22* (9), 920–932. https://doi.org/10.1002/adma.200901407.

(336) Ladd, J.; Zhang, Z.; Chen, S.; Hower, J. C.; Jiang, S. Zwitterionic Polymers Exhibiting High Resistance to Nonspecific Protein Adsorption from Human Serum and Plasma. *Biomacromolecules* **2008**, *9* (5), 1357–1361. https://doi.org/10.1021/bm701301s.

(337) Zahr, A. S.; Davis, C. A.; Pishko, M. V. Macrophage Uptake of Core−Shell Nanoparticles Surface Modified with Poly(Ethylene Glycol). *Langmuir* **2006**, *22* (19), 8178–8185. https://doi.org/10.1021/la060951b.

(338) Xu, F.; Yuan, Y.; Shan, X.; Liu, C.; Tao, X.; Sheng, Y.; Zhou, H. Long-Circulation of Hemoglobin-Loaded Polymeric Nanoparticles as Oxygen Carriers with Modulated Surface Charges. *Int. J. Pharm.* **2009**, *377* (1), 199–206. https://doi.org/10.1016/j.ijpharm.2009.05.015.

(339) Wilhelm, S.; Tavares, A. J.; Dai, Q.; Ohta, S.; Audet, J.; Dvorak, H. F.; Chan, W. C. W. Analysis of Nanoparticle Delivery to Tumours. *Nat. Rev. Mater.* **2016**, *1* (5), 1–12. https://doi.org/10.1038/natrevmats.2016.14.

(340) Yamamoto, Y.; Nagasaki, Y.; Kato, Y.; Sugiyama, Y.; Kataoka, K. Long-Circulating Poly(Ethylene Glycol)–Poly(d,l-Lactide) Block Copolymer Micelles with Modulated Surface Charge. *J. Controlled Release* **2001**, *77* (1), 27–38. https://doi.org/10.1016/S0168-3659(01)00451-5.

(341) Feng, Q.; Liu, Y.; Huang, J.; Chen, K.; Huang, J.; Xiao, K. Uptake, Distribution, Clearance, and Toxicity of Iron Oxide Nanoparticles with Different Sizes and Coatings. *Sci. Rep.* **2018**, *8* (1), 2082. https://doi.org/10.1038/s41598-018-19628-z.

(342) Sarko, D.; Beijer, B.; Garcia Boy, R.; Nothelfer, E.-M.; Leotta, K.; Eisenhut, M.; Altmann, A.; Haberkorn, U.; Mier, W. The Pharmacokinetics of Cell-Penetrating Peptides. *Mol. Pharm.* **2010**, *7* (6), 2224–2231. https://doi.org/10.1021/mp100223d.

(343) Sukhanova, A.; Bozrova, S.; Sokolov, P.; Berestovoy, M.; Karaulov, A.; Nabiev, I. Dependence of Nanoparticle Toxicity on Their Physical and Chemical Properties. *Nanoscale Res. Lett.* **2018**, *13*. https://doi.org/10.1186/s11671-018-2457-x.

(344) Hühn, D.; Kantner, K.; Geidel, C.; Brandholt, S.; De Cock, I.; Soenen, S. J. H.; Rivera_Gil, P.; Montenegro, J.-M.; Braeckmans, K.; Müllen, K.; Nienhaus, G. U.; Klapper, M.; Parak, W. J. Polymer-Coated Nanoparticles Interacting with Proteins and Cells: Focusing on the Sign of the Net Charge. *ACS Nano* **2013**, *7* (4), 3253–3263. https://doi.org/10.1021/nn3059295.

(345) Liu, Y.; Li, W.; Lao, F.; Liu, Y.; Wang, L.; Bai, R.; Zhao, Y.; Chen, C. Intracellular Dynamics of Cationic and Anionic Polystyrene Nanoparticles without Direct Interaction

with Mitotic Spindle and Chromosomes. *Biomaterials* **2011**, *32* (32), 8291–8303. https://doi.org/10.1016/j.biomaterials.2011.07.037.

(346) Sellappan, P.; Cote, J.; Kreth, P. A.; Schepkin, V. D.; Darkazalli, A.; Morris, D. R.; Alvi, F. S.; Levenson, C. W. Variability and Uncertainty in the Rodent Controlled Cortical Impact Model of Traumatic Brain Injury. *J. Neurosci. Methods* **2019**, *312*, 37–42. https://doi.org/10.1016/j.jneumeth.2018.10.027.

(347) Miller, H. A.; Magsam, A. W.; Tarudji, A. W.; Romanova, S.; Weber, L.; Gee, C. C.; Madsen, G. L.; Bronich, T. K.; Kievit, F. M. Evaluating Differential Nanoparticle Accumulation and Retention Kinetics in a Mouse Model of Traumatic Brain Injury via K Trans Mapping with MRI. *Sci. Rep.* **2019**, *9* (1), 16099. https://doi.org/10.1038/s41598-019-52622-7.

(348) Liu, T.; Choi, H.; Zhou, R.; Chen, I.-W. RES Blockade: A Strategy for Boosting Efficiency of Nanoparticle Drug. *Nano Today* **2015**, *10* (1), 11–21. https://doi.org/10.1016/j.nantod.2014.12.003.

(349) Simberg, D.; Duza, T.; Park, J. H.; Essler, M.; Pilch, J.; Zhang, L.; Derfus, A. M.; Yang, M.; Hoffman, R. M.; Bhatia, S.; Sailor, M. J.; Ruoslahti, E. Biomimetic Amplification of Nanoparticle Homing to Tumors. *Proc. Natl. Acad. Sci.* **2007**, *104* (3), 932–936. https://doi.org/10.1073/pnas.0610298104.

(350) Sun, X.; Yan, X.; Jacobson, O.; Sun, W.; Wang, Z.; Tong, X.; Xia, Y.; Ling, D.; Chen, X. Improved Tumor Uptake by Optimizing Liposome Based RES Blockade Strategy. *Theranostics* **2017**, *7* (2), 319–328. https://doi.org/10.7150/thno.18078.

(351) Ouyang, B.; Poon, W.; Zhang, Y.-N.; Lin, Z. P.; Kingston, B. R.; Tavares, A. J.; Zhang, Y.; Chen, J.; Valic, M. S.; Syed, A. M.; MacMillan, P.; Couture-Senécal, J.; Zheng, G.; Chan, W. C. W. The Dose Threshold for Nanoparticle Tumour Delivery. *Nat. Mater.* **2020**, *19* (12), 1362–1371. https://doi.org/10.1038/s41563-020-0755-z.

(352) Surveillance Report of Traumatic Brain Injury-Related Emergency Department Visits, Hospitalizations, and Deaths.

(353) Werner, C.; Engelhard, K. Pathophysiology of Traumatic Brain Injury. *Br. J. Anaesth.* **2007**, *99* (1), 4–9. https://doi.org/10.1093/bja/aem131.

(354) Nagahara, A. H.; Tuszynski, M. H. Potential Therapeutic Uses of BDNF in Neurological and Psychiatric Disorders. *Nat. Rev. Drug Discov.* **2011**, *10* (3), 209–219. https://doi.org/10.1038/nrd3366.

(355) Huang, E. J.; Reichardt, L. F. Neurotrophins: Roles in Neuronal Development and Function. *Annu. Rev. Neurosci.* **2001**, *24*, 677–736. https://doi.org/10.1146/annurev.neuro.24.1.677.

(356) Wurzelmann, M.; Romeika, J.; Sun, D. Therapeutic Potential of Brain-Derived Neurotrophic Factor (BDNF) and a Small Molecular Mimics of BDNF for Traumatic Brain Injury. *Neural Regen. Res.* **2017**, *12* (1), 7–12. https://doi.org/10.4103/1673-5374.198964.

(357) Klein, R.; Martin-Zanca, D.; Acid, M. B.; Parada, L. F. Expression of the Tyrosine Kinase Receptor Gene TrkB Is Confined to the Murine Embryonic and Adult Nervous System. 10.

(358) Huang, E. J.; Reichardt, L. F. Trk Receptors: Roles in Neuronal Signal Transduction. *Annu. Rev. Biochem.* **2003**, *72* (1), 609–642. https://doi.org/10.1146/annurev.biochem.72.121801.161629.

(359) Kaplan, D. R.; Miller, F. D. Neurotrophin Signal Transduction in the Nervous System. *Curr. Opin. Neurobiol.* **2000**, *10* (3), 381–391. https://doi.org/10.1016/s0959-4388(00)00092-1.

(360) Xiong, L.-L.; Hu, Y.; Zhang, P.; Zhang, Z.; Li, L.-H.; Gao, G.-D.; Zhou, X.-F.; Wang, T.-H. Neural Stem Cell Transplantation Promotes Functional Recovery from Traumatic Brain Injury via Brain Derived Neurotrophic Factor-Mediated Neuroplasticity. *Mol. Neurobiol.* **2018**, *55* (3), 2696–2711. https://doi.org/10.1007/s12035-017-0551-1.

(361) Lu, P.; Jones, L. L.; Snyder, E. Y.; Tuszynski, M. H. Neural Stem Cells Constitutively Secrete Neurotrophic Factors and Promote Extensive Host Axonal Growth after Spinal Cord Injury. *Exp. Neurol.* **2003**, *181* (2), 115–129. https://doi.org/10.1016/S0014-4886(03)00037-2.

(362) Blurton-Jones, M.; Kitazawa, M.; Martinez-Coria, H.; Castello, N. A.; Muller, F.-J.; Loring, J. F.; Yamasaki, T. R.; Poon, W. W.; Green, K. N.; LaFerla, F. M. Neural Stem Cells Improve Cognition via BDNF in a Transgenic Model of Alzheimer Disease. *Proc. Natl. Acad. Sci.* **2009**, *106* (32), 13594–13599. https://doi.org/10.1073/pnas.0901402106.

(363) Fink, K. D.; Deng, P.; Torrest, A.; Stewart, H.; Pollock, K.; Gruenloh, W.; Annett, G.; Tempkin, T.; Wheelock, V.; Nolta, J. A. Developing Stem Cell Therapies for Juvenile and Adult-Onset Huntington's Disease. *Regen. Med.* **2015**, *10* (5), 623–646. https://doi.org/10.2217/rme.15.25.

(364) Frim, D. M.; Uhler, T. A.; Galpern, W. R.; Beal, M. F.; Breakefield, X. O.; Isacson, O. Implanted Fibroblasts Genetically Engineered to Produce Brain-Derived Neurotrophic Factor Prevent 1-Methyl-4-Phenylpyridinium Toxicity to Dopaminergic Neurons in the Rat. *Proc. Natl. Acad. Sci. U. S. A.* **1994**, *91* (11), 5104–5108.

(365) Pollock, K.; Dahlenburg, H.; Nelson, H.; Fink, K. D.; Cary, W.; Hendrix, K.; Annett, G.; Torrest, A.; Deng, P.; Gutierrez, J.; Nacey, C.; Pepper, K.; Kalomoiris, S.; Anderson, J. D.; McGee, J.; Gruenloh, W.; Fury, B.; Bauer, G.; Duffy, A.; Tempkin, T.; Wheelock, V.; Nolta, J. A. Human Mesenchymal Stem Cells Genetically Engineered to Overexpress Brain-Derived Neurotrophic Factor Improve Outcomes in Huntington's Disease Mouse Models. *Mol. Ther.* **2016**, *24* (5), 965–977. https://doi.org/10.1038/mt.2016.12.

(366) Tobias, C. A.; Shumsky, J. S.; Shibata, M.; Tuszynski, M. H.; Fischer, I.; Tessler, A.; Murray, M. Delayed Grafting of BDNF and NT-3 Producing Fibroblasts into the Injured Spinal Cord Stimulates Sprouting, Partially Rescues Axotomized Red Nucleus Neurons from Loss and Atrophy, and Provides Limited Regeneration. *Exp. Neurol.* **2003**, *184* (1), 97–113. https://doi.org/10.1016/S0014-4886(03)00394-7.

(367) Blesch, A.; Tuszynski, M. H. Transient Growth Factor Delivery Sustains Regenerated Axons after Spinal Cord Injury. *J. Neurosci.* **2007**, *27* (39), 10535–10545. https://doi.org/10.1523/JNEUROSCI.1903-07.2007.

(368) Nagahara, A. H.; Merrill, D. A.; Coppola, G.; Tsukada, S.; Schroeder, B. E.; Shaked, G. M.; Wang, L.; Blesch, A.; Kim, A.; Conner, J. M.; Rockenstein, E.; Chao, M. V.; Koo, E. H.; Geschwind, D.; Masliah, E.; Chiba, A. A.; Tuszynski, M. H. Neuroprotective Effects of Brain-Derived Neurotrophic Factor in Rodent and Primate Models of Alzheimer's Disease. *Nat. Med.* **2009**, *15* (3), 331–337. https://doi.org/10.1038/nm.1912.

(369) Preeti Kumaran Menon; Dafin Fior Muresanu; Aruna Sharma; Herbert Mossler; Hari Shanker Sharma. Cerebrolysin, a Mixture of Neurotrophic Factors Induces Marked Neuroprotection in Spinal Cord Injury Following Intoxication of Engineered Nanoparticles from Metals. *CNS Neurol. Disord. - Drug Targets* **2012**, *11* (1), 40–49. https://doi.org/10.2174/187152712799960781.

(370) Ghaffarpasand, F.; Torabi, S.; Rasti, A.; Niakan, M. H.; Aghabaklou, S.; Pakzad, F.; Beheshtian, M. S.; Tabrizi, R. Effects of Cerebrolysin on Functional Outcome of Patients with Traumatic Brain Injury: A Systematic Review and Meta-Analysis. *Neuropsychiatr. Dis. Treat.* **2018**, *15*, 127–135. https://doi.org/10.2147/NDT.S186865.

(371) *First-in-Human Clinical Trial to Assess Gene Therapy for Alzheimer's Disease*. https://ucsdnews.ucsd.edu/pressrelease/first-in-human-clinical-trial-to-assess-gene-therapy-for-alzheimers-disease (accessed 2021-04-16).

(372) Price, R.; Milne, S.; Sharkey, J.; Matsuoka, N. Advances in Small Molecules Promoting Neurotrophic Function. *Pharmacol. Ther.* **2007**, *115* (2), 292–306. https://doi.org/10.1016/j.pharmthera.2007.03.005.

(373) Géral, C.; Angelova, A.; Lesieur, S. From Molecular to Nanotechnology Strategies for Delivery of Neurotrophins: Emphasis on Brain-Derived Neurotrophic Factor (BDNF). *Pharmaceutics* **2013**, *5* (1), 127–167. https://doi.org/10.3390/pharmaceutics5010127.

(374) Emerich, D. F.; Thanos, C. G. The Pinpoint Promise of Nanoparticle-Based Drug Delivery and Molecular Diagnosis. *Biomol. Eng.* **2006**, *23* (4), 171–184. https://doi.org/10.1016/j.bioeng.2006.05.026.

(375) Lampe, K. J.; Kern, D. S.; Mahoney, M. J.; Bjugstad, K. B. The Administration of BDNF and GDNF to the Brain via PLGA Microparticles Patterned within a Degradable PEG-Based Hydrogel: Protein Distribution and the Glial Response. *J. Biomed. Mater. Res. A* **2011**, *96A* (3), 595–607. https://doi.org/10.1002/jbm.a.33011.

(376) Bertram, J. P.; Rauch, M. F.; Chang, K.; Lavik, E. B. Using Polymer Chemistry to Modulate the Delivery of Neurotrophic Factors from Degradable Microspheres: Delivery of BDNF. *Pharm. Res.* **2010**, *27* (1), 82–91. https://doi.org/10.1007/s11095-009-0009-x.

(377) Wang, Y.; Wei, Y. T.; Zu, Z. H.; Ju, R. K.; Guo, M. Y.; Wang, X. M.; Xu, Q. Y.; Cui, F. Z. Combination of Hyaluronic Acid Hydrogel Scaffold and PLGA Microspheres for Supporting Survival of Neural Stem Cells. *Pharm. Res.* **2011**, *28* (6), 1406. https://doi.org/10.1007/s11095-011-0452-3.

(378) Park, J.-H.; Gu, L.; von Maltzahn, G.; Ruoslahti, E.; Bhatia, S. N.; Sailor, M. J. Biodegradable Luminescent Porous Silicon Nanoparticles for in Vivo Applications. *Nat. Mater.* **2009**, *8* (4), 331–336. https://doi.org/10.1038/nmat2398.

(379) Foraker, A. B.; Walczak, R. J.; Cohen, M. H.; Boiarski, T. A.; Grove, C. F.; Swaan, P. W. Microfabricated Porous Silicon Particles Enhance Paracellular Delivery of Insulin Across Intestinal Caco-2 Cell Monolayers. 7.

(380) Kim, D.; Zuidema, J. M.; Kang, J.; Pan, Y.; Wu, L.; Warther, D.; Arkles, B.; Sailor, M. J. Facile Surface Modification of Hydroxylated Silicon Nanostructures Using Heterocyclic Silanes. *J. Am. Chem. Soc.* **2016**, *138* (46), 15106–15109. https://doi.org/10.1021/jacs.6b08614.

(381) Mann, A. P.; Scodeller, P.; Hussain, S.; Joo, J.; Kwon, E.; Braun, G. B.; Mölder, T.; She, Z.-G.; Kotamraju, V. R.; Ranscht, B.; Krajewski, S.; Teesalu, T.; Bhatia, S.; Sailor, M. J.; Ruoslahti, E. A Peptide for Targeted, Systemic Delivery of Imaging and Therapeutic Compounds into Acute Brain Injuries. *Nat. Commun.* **2016**, *7* (1), 11980. https://doi.org/10.1038/ncomms11980.

(382) Zuidema, J. M.; Kumeria, T.; Kim, D.; Kang, J.; Wang, J.; Hollett, G.; Zhang, X.; Roberts, D. S.; Chan, N.; Dowling, C.; Blanco-Suarez, E.; Allen, N. J.; Tuszynski, M. H.; Sailor, M. J. Oriented Nanofibrous Polymer Scaffolds Containing Protein-Loaded Porous Silicon Generated by Spray Nebulization. *Adv. Mater.* **2018**, *30* (12), 1706785. https://doi.org/10.1002/adma.201706785.

(383) Kwon, E. J.; Skalak, M.; Bertucci, A.; Braun, G.; Ricci, F.; Ruoslahti, E.; Sailor, M. J.; Bhatia, S. N. Porous Silicon Nanoparticle Delivery of Tandem Peptide Anti-Infectives for the Treatment of Pseudomonas Aeruginosa Lung Infections. *Adv. Mater.* **2017**, *29* (35), 1701527. https://doi.org/10.1002/adma.201701527.

(384) Li, W.; Liu, Z.; Fontana, F.; Ding, Y.; Liu, D.; Hirvonen, J. T.; Santos, H. A. Tailoring Porous Silicon for Biomedical Applications: From Drug Delivery to Cancer Immunotherapy. *Adv. Mater.* **2018**, *30* (24), 1703740. https://doi.org/10.1002/adma.201703740.

(385) Bertucci, A.; Kim, K.-H.; Kang, J.; Zuidema, J. M.; Lee, S. H.; Kwon, E. J.; Kim, D.; Howell, S. B.; Ricci, F.; Ruoslahti, E.; Jang, H.-J.; Sailor, M. J. Tumor-Targeting, MicroRNA-Silencing Porous Silicon Nanoparticles for Ovarian Cancer Therapy. *ACS Appl. Mater. Interfaces* **2019**, *11* (27), 23926–23937. https://doi.org/10.1021/acsami.9b07980.

(386) Zuidema, J. M.; Dumont, C. M.; Wang, J.; Batchelor, W. M.; Lu, Y.-S.; Kang, J.; Bertucci, A.; Ziebarth, N. M.; Shea, L. D.; Sailor, M. J. Porous Silicon Nanoparticles Embedded in Poly(Lactic-Co-Glycolic Acid) Nanofiber Scaffolds Deliver Neurotrophic Payloads to Enhance Neuronal Growth. *Adv. Funct. Mater.* **2020**, *30* (25), 2002560. https://doi.org/10.1002/adfm.202002560.

(387) Kumeria, T.; Wang, J.; Kim, B.; Park, J.-H.; Zuidema, J. M.; Klempner, M.; Cavacini, L.; Wang, Y.; Sailor, M. J. Enteric Polymer-Coated Porous Silicon Nanoparticles for Site-Specific Oral Delivery of IgA Antibody. *ACS Biomater. Sci. Eng.* **2020**. https://doi.org/10.1021/acsbiomaterials.0c01313.

(388) Zilony-Hanin, N.; Rosenberg, M.; Richman, M.; Yehuda, R.; Schori, H.; Motiei, M.; Rahimipour, S.; Groisman, A.; Segal, E.; Shefi, O. Neuroprotective Effect of Nerve Growth Factor Loaded in Porous Silicon Nanostructures in an Alzheimer's Disease Model and Potential Delivery to the Brain. *Small* **2019**, *15* (45), 1904203. https://doi.org/10.1002/smll.201904203.

(389) Rosenberg, M.; Zilony, N.; Shefi, O.; Segal, E. Designing Porous Silicon Films as Carriers of Nerve Growth Factor. *JoVE J. Vis. Exp.* **2019**, No. 143, e58982. https://doi.org/10.3791/58982.

(390) Wu, C.-C.; Hu, Y.; Miller, M.; Aroian, R. V.; Sailor, M. J. Protection and Delivery of Anthelmintic Protein Cry5B to Nematodes Using Mesoporous Silicon Particles. *ACS Nano* **2015**, *9* (6), 6158–6167. https://doi.org/10.1021/acsnano.5b01426.

(391) Henstock, J. R.; Canham, L. T.; Anderson, S. I. Silicon: The Evolution of Its Use in Biomaterials. *Acta Biomater.* **2015**, *11*, 17–26. https://doi.org/10.1016/j.actbio.2014.09.025.

(392) Andrew, J. S.; Anglin, E. J.; Wu, E. C.; Chen, M. Y.; Cheng, L.; Freeman, W. R.; Sailor, M. J. Sustained Release of a Monoclonal Antibody from Electrochemically Prepared Mesoporous Silicon Oxide. *Adv. Funct. Mater.* **2010**, *20* (23), 4168–4174. https://doi.org/10.1002/adfm.201000907.

(393) Wang, J.; Kumeria, T.; Bezem, M. T.; Wang, J.; Sailor, M. J. Self-Reporting Photoluminescent Porous Silicon Microparticles for Drug Delivery. *ACS Appl. Mater. Interfaces* **2018**, *10* (4), 3200–3209. https://doi.org/10.1021/acsami.7b09071.

(394) Fong, R.; Konakondla, S.; Schirmer, C. M.; Lacroix, M. Surgical Interventions for Severe Traumatic Brain Injury. *J. Emerg. Crit. Care Med.* **2017**, *1* (10). https://doi.org/10.21037/jeccm.2017.09.03.

(395) Cunningham, T. L.; Cartagena, C. M.; Lu, X.-C. M.; Konopko, M.; Dave, J. R.; Tortella, F. C.; Shear, D. A. Correlations between Blood–Brain Barrier Disruption and Neuroinflammation in an Experimental Model of Penetrating Ballistic-Like Brain Injury. *J. Neurotrauma* **2014**, *31* (5), 505–514. https://doi.org/10.1089/neu.2013.2965.

(396) Wetter, L. R.; Deutsch, H. F. Immunological Studies on Egg White Proteins Iv. Immunochemical and Physical Studies of Lysozyme. *J. Biol. Chem.* **1951**, *192* (1), 237–242.

(397) Hempstead, B. L. Brain-Derived Neurotrophic Factor: Three Ligands, Many Actions. *Trans. Am. Clin. Climatol. Assoc.* **2015**, *126*, 9.

(398) Gole, A.; Thakar, J.; Sastry, M. Protein Diffusion into Thermally Evaporated Lipid Films: Role of Protein Charge/Mass Ratio. *Colloids Surf. B Biointerfaces* **2003**, *28* (2–3), 209–214. https://doi.org/10.1016/S0927-7765(02)00141-8.

(399) Harris, J. M.; Martin, N. E.; Modi, M. Pegylation. *Clin. Pharmacokinet.* **2001**, *40* (7), 539–551. https://doi.org/10.2165/00003088-200140070-00005.

(400) Harris, J. M.; Chess, R. B. Effect of Pegylation on Pharmaceuticals. *Nat. Rev. Drug Discov.* **2003**, *2* (3), 214–221. https://doi.org/10.1038/nrd1033.

(401) Chieng, B.; Ibrahim, N.; Yunus, W.; Hussein, M. Poly(Lactic Acid)/Poly(Ethylene Glycol) Polymer Nanocomposites: Effects of Graphene Nanoplatelets. *Polymers* **2013**, *6* (1), 93–104. https://doi.org/10.3390/polym6010093.

(402) Jiang, Z.-L.; Huang, G.-X. Resonance Scattering Spectra of Micrococcus Lysodeikticus and Its Application to Assay of Lysozyme Activity. *Clin. Chim. Acta* **2007**, *376* (1), 136–141. https://doi.org/10.1016/j.cca.2006.08.005.

(403) Shen, J.; Xu, R.; Mai, J.; Kim, H.-C.; Guo, X.; Qin, G.; Yang, Y.; Wolfram, J.; Mu, C.; Xia, X.; Gu, J.; Liu, X.; Mao, Z.-W.; Ferrari, M.; Shen, H. High Capacity Nanoporous Silicon Carrier for Systemic Delivery of Gene Silencing Therapeutics. *ACS Nano* **2013**, *7* (11), 9867–9880. https://doi.org/10.1021/nn4035316.

(404) Popplewell, J. F.; King, S. J.; Day, J. P.; Ackrill, P.; Fifield, L. K.; Cresswell, R. G.; di Tada, M. L.; Liu, K. Kinetics of Uptake and Elimination of Silicic Acid by a Human Subject: A Novel Application of 32Si and Accelerator Mass Spectrometry. *J. Inorg. Biochem.* **1998**, *69* (3), 177–180. https://doi.org/10.1016/S0162-0134(97)10016-2.

(405) Jin, Y.; Kim, D.; Roh, H.; Kim, S.; Hussain, S.; Kang, J.; Pack, C.-G.; Kim, J. K.; Myung, S.-J.; Ruoslahti, E.; Sailor, M. J.; Kim, S. C.; Joo, J. Tracking the Fate of Porous Silicon Nanoparticles Delivering a Peptide Payload by Intrinsic Photoluminescence Lifetime. *Adv. Mater.* **2018**, *30* (35), 1802878. https://doi.org/10.1002/adma.201802878.

(406) Tzur-Balter, A.; Shatsberg, Z.; Beckerman, M.; Segal, E.; Artzi, N. Mechanism of Erosion of Nanostructured Porous Silicon Drug Carriers in Neoplastic Tissues. *Nat. Commun.* **2015**, *6* (1), 6208. https://doi.org/10.1038/ncomms7208.

(407) Joo, J.; Liu, X.; Kotamraju, V. R.; Ruoslahti, E.; Nam, Y.; Sailor, M. J. Gated Luminescence Imaging of Silicon Nanoparticles. *ACS Nano* **2015**, *9* (6), 6233–6241. https://doi.org/10.1021/acsnano.5b01594.

(408) Kaplan, D. R.; Matsumoto, K.; Lucarelli, E.; Thielet, C. J. Induction of TrkB by Retinoic Acid Mediates Biologic Responsiveness to BDNF and Differentiation of Human Neuroblastoma Cells. *Neuron* **1993**, *11* (2), 321–331. https://doi.org/10.1016/0896-6273(93)90187-V.

(409) Encinas, M.; Iglesias, M.; Liu, Y.; Wang, H.; Muhaisen, A.; Ceña, V.; Gallego, C.; Comella, J. X. Sequential Treatment of SH-SY5Y Cells with Retinoic Acid and Brain-Derived Neurotrophic Factor Gives Rise to Fully Differentiated, Neurotrophic Factor-Dependent, Human Neuron-Like Cells. *J. Neurochem.* **2000**, *75* (3), 991–1003. https://doi.org/10.1046/j.1471-4159.2000.0750991.x.

(410) Dedoni, S.; Olianas, M. C.; Ingianni, A.; Onali, P. Type I Interferons Impair BDNF-Induced Cell Signaling and Neurotrophic Activity in Differentiated Human SH-SY5Y Neuroblastoma Cells and Mouse Primary Cortical Neurons. *J. Neurochem.* **2012**, *122* (1), 58–71. https://doi.org/10.1111/j.1471-4159.2012.07766.x.

(411) Encinas, M.; Iglesias, M.; Llecha, N.; Comella, J. X. Extracellular-Regulated Kinases and Phosphatidylinositol 3-Kinase Are Involved in Brain-Derived Neurotrophic Factor-Mediated Survival and Neuritogenesis of the Neuroblastoma Cell Line SH-SY5Y. *J. Neurochem.* **1999**, *73* (4), 1409–1421. https://doi.org/10.1046/j.1471-4159.1999.0731409.x.

(412) Kim, H.-J.; Lee, J.-H.; Kim, S.-H. Therapeutic Effects of Human Mesenchymal Stem Cells on Traumatic Brain Injury in Rats: Secretion of Neurotrophic Factors and Inhibition of Apoptosis. *J. Neurotrauma* **2009**, *27* (1), 131–138. https://doi.org/10.1089/neu.2008.0818.

(413) Wang, Z.; Yao, W.; Deng, Q.; Zhang, X.; Zhang, J. Protective Effects of BDNF Overexpression Bone Marrow Stromal Cell Transplantation in Rat Models of Traumatic Brain Injury. *J. Mol. Neurosci.* **2013**, *49* (2), 409–416. https://doi.org/10.1007/s12031-012-9908-0.

(414) Sakane, T.; Pardridge, W. M. Carboxyl-Directed Pegylation of Brain-Derived Neurotrophic Factor Markedly Reduces Systemic Clearance with Minimal Loss of Biologic Activity. *Pharm. Res.* **1997**, *14* (8), 1085–1091. https://doi.org/10.1023/A:1012117815460.

(415) Poduslo, J. F.; Curran, G. L. Permeability at the Blood-Brain and Blood-Nerve Barriers of the Neurotrophic Factors: NGF, CNTF, NT-3, BDNF. *Mol. Brain Res.* **1996**, *36* (2), 280–286. https://doi.org/10.1016/0169-328X(95)00250-V.

(416) Fukumitsu, H.; Ohtsuka, M.; Murai, R.; Nakamura, H.; Itoh, K.; Furukawa, S. Brain-Derived Neurotrophic Factor Participates in Determination of Neuronal Laminar Fate in the Developing Mouse Cerebral Cortex. *J. Neurosci.* **2006**, *26* (51), 13218–13230. https://doi.org/10.1523/JNEUROSCI.4251-06.2006.

(417) Turtzo, L. C.; Budde, M. D.; Gold, E. M.; Lewis, B. K.; Janes, L.; Yarnell, A.; Grunberg, N. E.; Watson, W.; Frank, J. A. The Evolution of Traumatic Brain Injury in a Rat Focal Contusion Model. *NMR Biomed.* **2013**, *26* (4), 468–479. https://doi.org/10.1002/nbm.2886.

(418) Gennarelli, T. A.; Spielman, G. M.; Langfitt, T. W.; Gildenberg, P. L.; Harrington, T.; Jane, J. A.; Marshall, L. F.; Miller, J. D.; Pitts, L. H. Influence of the Type of Intracranial Lesion on Outcome from Severe Head Injury: A Multicenter Study Using a New Classification System. *J. Neurosurg.* **1982**, *56* (1), 26–32. https://doi.org/10.3171/jns.1982.56.1.0026.

(419) Kenne, E.; Erlandsson, A.; Lindbom, L.; Hillered, L.; Clausen, F. Neutrophil Depletion Reduces Edema Formation and Tissue Loss Following Traumatic Brain Injury in Mice. *J. Neuroinflammation* **2012**, *9* (1), 17. https://doi.org/10.1186/1742-2094-9-17.

(420) Zhou, H.; Chen, L.; Gao, X.; Luo, B.; Chen, J. Moderate Traumatic Brain Injury Triggers Rapid Necrotic Death of Immature Neurons in the Hippocampus. *J. Neuropathol. Exp. Neurol.* **2012**, *71* (4), 348–359. https://doi.org/10.1097/NEN.0b013e31824ea078.

(421) Hall, E. D.; Sullivan, P. G.; Gibson, T. R.; Pavel, K. M.; Thompson, B. M.; Scheff, S. W. Spatial and Temporal Characteristics of Neurodegeneration after Controlled Cortical Impact in Mice: More than a Focal Brain Injury. *J. Neurotrauma* **2005**, *22* (2), 252–265. https://doi.org/10.1089/neu.2005.22.252.

(422) Villapol, S.; Yaszemski, A. K.; Logan, T. T.; Sánchez-Lemus, E.; Saavedra, J. M.; Symes, A. J. Candesartan, an Angiotensin II AT 1 -Receptor Blocker and PPAR-γ Agonist, Reduces Lesion Volume and Improves Motor and Memory Function After Traumatic Brain Injury in Mice. *Neuropsychopharmacology* **2012**, *37* (13), 2817–2829. https://doi.org/10.1038/npp.2012.152.

(423) Wu, Y.; Wang, J.; Shi, Y.; Pu, H.; Leak, R. K.; Liou, A. K. F.; Badylak, S. F.; Liu, Z.; Zhang, J.; Chen, J.; Chen, L. Implantation of Brain-Derived Extracellular Matrix Enhances Neurological Recovery after Traumatic Brain Injury. *Cell Transplant.* **2017**, *26* (7), 1224–1234. https://doi.org/10.1177/0963689717714090.

(424) Gu, Y.; Zhang, J.; Zhao, Y.; Su, Y.; Zhang, Y. Potassium Aspartate Attenuates Brain Injury Induced by Controlled Cortical Impact in Rats Through Increasing Adenosine Triphosphate (ATP) Levels, Na+/K+-ATPase Activity and Reducing Brain Edema. *Med. Sci. Monit.* **2016**, *22*, 4894–4901. https://doi.org/10.12659/MSM.898185.

(425) Park, H.-J.; Machado, A. G.; Cooperrider, J.; Truong, H.; Johnson, M.; Krishna, V.; Chen, Z.; Gale, J. T. Semi-Automated Method for Estimating Lesion Volumes. *J. Neurosci. Methods* **2013**, *213* (1), 76–83. https://doi.org/10.1016/j.jneumeth.2012.12.010.

(426) Weber, J. T. Altered Calcium Signaling Following Traumatic Brain Injury. *Front. Pharmacol.* **2012**, *3*. https://doi.org/10.3389/fphar.2012.00060.

(427) Kabu, S.; Jaffer, H.; Petro, M.; Dudzinski, D.; Stewart, D.; Courtney, A.; Courtney, M.; Labhasetwar, V. Blast-Associated Shock Waves Result in Increased Brain Vascular Leakage and Elevated ROS Levels in a Rat Model of Traumatic Brain Injury. *PLOS ONE* **2015**, *10* (5), e0127971. https://doi.org/10.1371/journal.pone.0127971.

(428) Xie, B.-S.; Wang, Y.-Q.; Lin, Y.; Mao, Q.; Feng, J.-F.; Gao, G.-Y.; Jiang, J.-Y. Inhibition of Ferroptosis Attenuates Tissue Damage and Improves Long-Term Outcomes after Traumatic Brain Injury in Mice. *CNS Neurosci. Ther.* **2019**, *25* (4), 465–475. https://doi.org/10.1111/cns.13069.

(429) Oyesiku, N. M.; Evans, C.-O.; Houston, S.; Darrell, R. S.; Smith, J. S.; Fulop, Z. L.; Dixon, C. E.; Stein, D. G. Regional Changes in the Expression of Neurotrophic Factors and Their Receptors Following Acute Traumatic Brain Injury in the Adult Rat Brain. *Brain Res.* **1999**, *833* (2), 161–172. https://doi.org/10.1016/S0006-8993(99)01501-2.

(430) van Velthoven Cindy T.J.; Sheldon R. Ann; Kavelaars Annemieke; Derugin Nikita; Vexler Zinaida S.; Willemen Hanneke L.D.M.; Maas Mirjam; Heijnen Cobi J.; Ferriero Donna M. Mesenchymal Stem Cell Transplantation Attenuates Brain Injury After Neonatal Stroke. *Stroke* **2013**, *44* (5), 1426–1432. https://doi.org/10.1161/STROKEAHA.111.000326.

(431) Schäbitz W.-R.; Berger C.; Kollmar R.; Seitz M.; Tanay E.; Kiessling M.; Schwab S.; Sommer C. Effect of Brain-Derived Neurotrophic Factor Treatment and Forced Arm Use on Functional Motor Recovery After Small Cortical Ischemia. *Stroke* **2004**, *35* (4), 992–997. https://doi.org/10.1161/01.STR.0000119754.85848.0D.

(432) Yu, S.-J.; Tseng, K.-Y.; Shen, H.; Harvey, B. K.; Airavaara, M.; Wang, Y. Local Administration of AAV-BDNF to Subventricular Zone Induces Functional Recovery in

Stroke Rats. *PLOS ONE* **2013**, *8* (12), e81750. https://doi.org/10.1371/journal.pone.0081750.

(433) Ferrer, I.; Krupinski, J.; Goutan, E.; Martí, E.; Ambrosio, S.; Arenas, E. Brain-Derived Neurotrophic Factor Reduces Cortical Cell Death by Ischemia after Middle Cerebral Artery Occlusion in the Rat. *Acta Neuropathol. (Berl.)* **2001**, *101* (3), 229–238. https://doi.org/10.1007/s004010000268.

(434) Lu, P.; Blesch, A.; Tuszynski, M. H. Neurotrophism without Neurotropism: BDNF Promotes Survival but Not Growth of Lesioned Corticospinal Neurons. *J. Comp. Neurol.* **2001**, *436* (4), 456–470. https://doi.org/10.1002/cne.1080.

(435) Stokols, S.; Tuszynski, M. H. Freeze-Dried Agarose Scaffolds with Uniaxial Channels Stimulate and Guide Linear Axonal Growth Following Spinal Cord Injury. *Biomaterials* **2006**, *27* (3), 443–451. https://doi.org/10.1016/j.biomaterials.2005.06.039.

(436) Margulies, S.; Hicks, R. Combination Therapies for Traumatic Brain Injury: Prospective Considerations. 16.

(437) Qin, Z.; Joo, J.; Gu, L.; Sailor, M. J. Porous Films: Size Control of Porous Silicon Nanoparticles by Electrochemical Perforation Etching (Part. Part. Syst. Charact. 2/2014). *Part. Part. Syst. Charact.* **2014**, *31* (2), 171–171. https://doi.org/10.1002/ppsc.201470007.